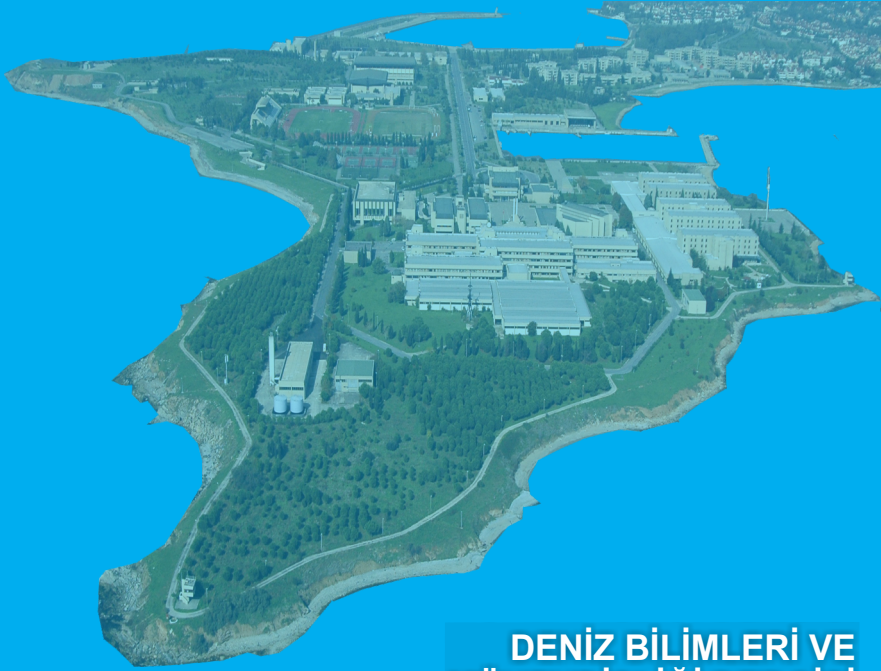




**MİLLÎ SAVUNMA ÜNİVERSİTESİ  
DENİZ HARP OKULU DEKANLIĞI**

**JOURNAL OF NAVAL SCIENCES AND ENGINEERING**

VOLUME:18 NUMBER:2 NOVEMBER 2022 ISSN:1304-2025



**DENİZ BİLİMLERİ VE  
MÜHENDİSLİĞİ DERGİSİ**

**CİLT : 18 SAYI : 2 KASIM 2022**

**DENİZ HARP OKULU MATBAASI - İSTANBUL**



# Journal of Naval Sciences and Engineering

Deniz Bilimleri ve Mühendisliği Dergisi

National Defence University

Milli Savunma Üniversitesi

Deniz Harp Okulu Dekanlığı

Turkish Naval Academy

Volume/Cilt:18

Number/Sayı:2

November/2022

## PRINTED BY / BASKI

National Defence University Turkish Naval Academy Printing House / Milli Savunma Üniversitesi Deniz Harp Okulu Matbaası

## CORRESPONDENCE AND COMMUNICATION ADDRESS / YAZIŞMA VE HABERLEŞME ADRESİ

Milli Savunma Üniversitesi  
Deniz Harp Okulu Dekanlığı 34940  
Tuzla/İstanbul/Türkiye

**Phone/Telefon** : +90 216 395 26 30  
**E-mail/E-posta** : [jnse@dho.edu.tr](mailto:jnse@dho.edu.tr)  
**Web** : <https://dergipark.org.tr/tr/pub/jnse>

**NATIONAL DEFENCE UNIVERSITY  
TURKISH NAVAL ACADEMY  
JOURNAL OF NAVAL SCIENCES AND ENGINEERING**

**MİLLİ SAVUNMA ÜNİVERSİTESİ  
DENİZ HARP OKULU DEKANLIĞI  
DENİZ BİLİMLERİ VE MÜHENDİSLİĞİ DERGİSİ**

Volume/Cilt: 18

Number/Sayı: 2

November/Kasım 2022

ISSN: 1304-2025

**Owner on Behalf of the Turkish Naval Academy  
Deniz Harp Okulu Dekanlığı Adına Sahibi ve Sorumlusu  
Prof.Dr. Cemalettin ŞAHİN**

Journal of Naval Sciences and Engineering (JNSE) is a peer reviewed, international, inter-disciplinary journal in science and technology, which is published semi-annually in April and November since 2003. It publishes full research articles, review articles, technical notes, short communications, book reviews, letters to the editor and extended versions of conference papers. Topics of interest include the technological and scientific aspects of the following areas: **Computer Science and Engineering, Electrical and Electronics Engineering, Naval/Mechanical Engineering, Naval Architecture and Marine Engineering, Industrial Engineering** and **Basic/Social Sciences**. The journal aims to provide a scientific contribution to the theory and applications of naval sciences and engineering, and share knowledge in relevant fields. The papers in the journal are published in English.

Following Open Access Model of Publishing, Journal of Naval Sciences and Engineering presents a variety of scientific viewpoints. The authors are responsible for the scientific, contextual and linguistic aspects of the articles published in the journal. The views expressed or implied in this publication, unless otherwise noted, should not be interpreted as official positions of the Turkish Naval Academy.

Our journal uses “double-blind review”, which means that both the reviewer and author identities are concealed from the reviewers, and vice versa, throughout the review process. The articles submitted to JNSE to be published are free of article submission, processing and publication charges. The accepted articles are published free-of-charge as online from the journal website and printed.

**DATABASES INDEXING OUR JOURNAL / TARANDIĞIMIZ VERİ TABANLARI**

Open Academic Journals Index (OAJI) (13.03.2016)

Sobiad Citation Index (31.01.2018)

Scientific Indexing Services (SIS) (28.02.2018)

Arastirmax Scientific Publication Index (13.03.2018)

CiteFactor Academic Scientific Journals (14.05.2018)

Asian Digital Library (03.09.2018)

Idealonline (05.09.2018)

ULAKBİM TR Index (14.05.2020)

Deniz Bilimleri ve Mühendisliği Dergisi (DBMD); uluslararası düzeyde, hakemli, çok disiplinli, Nisan ve Kasım aylarında olmak üzere 2003 yılından bu yana yılda iki kez yayımlanan, bilim ve teknoloji dergisidir. Dergide; **Bilgisayar, Makine, Gemi İnşa, Elektrik/Elektronik, Endüstri Mühendisliği** ile **Temel/Sosyal Bilimler** alanlarında bilimsel nitelikli araştırma makaleleri, derlemeler, teknik notlar, kitap incelemeleri, editöre mektuplar ile konferans ve toplantıların genişletilmiş raporlarına yer verilmektedir. Dergi, deniz bilimleri ve mühendisliğinin teori ve uygulamalarına bilimsel katkı sağlamayı ve ilgili alanlarda bilgi paylaşımını amaçlamaktadır. Dergide yer alan makaleler İngilizce olarak yayımlanmaktadır.

Açık erişimli yayım politikası izleyen Deniz Bilimleri ve Mühendisliği Dergisi değişik bilimsel bakış açılarını okuyucularına sunmaktadır. Dergide yayınlanan makalelerin bilim, içerik ve dil bakımından sorumluluğu yazarlarına aittir. Doğrudan veya dolaylı olarak ifade edilen görüşler Deniz Harp Okulu'nun resmi görüşleri olarak görülmemelidir.

Dergimiz, makale değerlendirme sürecinde “çift-kör hakemlik” sistemini kullanmaktadır. DBMD'ye yayımlanmak üzere gönderilen makaleler; makale gönderim, işlem ve yayım ücretinden muafır. Kabul edilen makaleler, ücretsiz olarak basılı şekilde ve dergi web sayfasından çevrimiçi (on-line) olarak yayınlanmaktadır.

© 2022 Copyright by Turkish Naval Academy  
Her hakkı saklıdır.

**NATIONAL DEFENCE UNIVERSITY  
TURKISH NAVAL ACADEMY  
JOURNAL OF NAVAL SCIENCES AND ENGINEERING**

**MİLLİ SAVUNMA ÜNİVERSİTESİ  
DENİZ HARP OKULU DEKANLIĞI  
DENİZ BİLİMLERİ VE MÜHENDİSLİĞİ DERGİSİ**

Volume/Cilt: 18

Number/Sayı: 2

November/Kasım 2022

ISSN: 1304-2025

**EDITOR-IN-CHIEF / BAŞ EDITÖR**

Associate Prof.Dr. Fatih ERDEN, National Defence University

**ASSISTANT EDITOR / YARDIMCI EDITÖR**

Assistant Prof.Dr. Onur USTA, National Defence University

**EDITORIAL BOARD / YAYIN KURULU**

Assoc.Prof.Dr. Dođuş ÖZKAN, National Defence U.  
Assoc.Prof.Dr. Erkan KAPLANOđLU, University of Tennessee  
Assoc.Prof.Dr. Ertan YAKICI, National Defence U.  
Assoc.Prof.Dr. Levent ERİŞKİN, National Defence U.  
Assoc.Prof.Dr. Mariya S. ANTYUFEYEVA, Newcastle University  
Prof.Dr. Mustafa TÜRKMEN, Erciyes University  
Assoc.Prof.Dr. Mümtaz KARATAŞ, National Defence U.  
Assoc.Prof.Dr. Okan ERKAYMAZ, National Defence U.  
Prof.Dr. Rumen KISHEV, Bulgarian Academy of Sciences  
Assoc.Prof.Dr. Muhammet DEVECİ, National Defence U.

**ADVISORY BOARD / DANIŞMA KURULU**

Prof.Dr. Ahmet Arif ERGİN, Yeditepe University  
Prof.Dr. Alexander NOSICH, Inst. of Radiophysics, Kharkiv  
Prof.Dr. Alper ERTÜRK, Australian University - Kuwait  
Prof.Dr. Atilla İNCEKİK, University of Strathclyde  
Prof.Dr. Bettar O. el MOCTAR, University of Duisburg  
Prof.Dr. Cem ERSOY, Bogazici University  
Prof.Dr. Cemal ZEHİR, Yıldız Technical University  
Prof.Dr. Cengiz KAHRAMAN, İstanbul Technical University  
Prof.Dr. Drazan KOZAK, University of Osijek  
Prof.Dr. Ertuđrul KARAÇUHA, İstanbul Technical University  
Prof.Dr. Hakan TEMELTAŞ, İstanbul Technical University  
Prof.Dr. Gennady S. ZALEVSKY, Kharkiv National University  
Prof.Dr. Nafiz ARICA, Piri Reis University  
Prof.Dr. Nurettin ACIR, National Defence U.  
Prof.Dr. Osman TURAN, University of Strathclyde  
Prof.Dr. Özlem ÖZKANLI, Ankara University  
Prof.Dr. Serdar PİRTİNİ, Marmara University  
Prof.Dr. Serdar SALMAN, National Defence U.  
Prof.Dr. Sergej HLOCH, Technical University of Kosice  
Prof.Dr. Süleyman ÖZKAYNAK, Piri Reis University  
Prof.Dr. Yahya KARSLIĞİL, Yıldız Technical University

**REFEREES FOR THIS ISSUE / SAYI HAKEMLERİ**

Ahmet Ziya SAYDAM  
Ali ÇALHAN  
Cem GAZİOđLU  
Deniz ÖZENLİ  
Engin Ufuk ERGÜL  
Erdiñ KOÇ  
Hüsne ALTİOK  
Mahmut Ođuz SELBESOđLU  
Mehmet KAYA  
Murtaza CİCİOđLU

Musa Nurullah YAZAR  
Müge EREL ÖZÇEVİK  
Onur USTA  
Selçuk ATASOY  
Serkan AKSOY  
Sultan ALDIRMAZ ÇOLAK  
Sultan N. TURHAN  
Süleyman ERSÖZ  
Yasin ÇELİK

**TECHNICAL EDITOR / TEKNİK EDITÖR**

Rıza KAYA, National Defence U.

**LAYOUT EDITOR & SECRETARIAT / MİZANPAJ EDITÖRÜ & SEKRETERYA**

Kürşat Alp ARPACI, National Defence U.  
Özgür ÇOBAN, National Defence U.

NATIONAL DEFENCE UNIVERSITY  
TURKISH NAVAL ACADEMY  
JOURNAL OF NAVAL SCIENCES AND ENGINEERING

VOLUME: 18 NUMBER: 2 NOVEMBER 2022 ISSN: 1304-2025

---

CONTENTS / İÇİNDEKİLER

*EDITORIAL*

**Foreword (Önsöz)** 155-157  
*Fatih ERDEN*

*Electrical-Electronics Engineering / Elektrik-Elektronik Mühendisliği*

*RESEARCH ARTICLE*

**A New Receiver Design for Spatial Modulation Systems** 159-178  
(Uzaysal Modülasyon Sistemleri için Yeni Bir Alıcı Tasarımı)  
*Gökhan ALTIN*

*Electrical-Electronics Engineering / Elektrik-Elektronik Mühendisliği*

*RESEARCH ARTICLE*

**Mechanical Gyroscope-based Roll Motion Reduction of Marine Vehicles:  
An Educational Setup** 179-204  
(Mekanik Jiroskop ile Deniz Araçlarında Yalpa Hareketinin Sönümlendirilmesi:  
Bir Eğitim Seti Tasarımı)  
*Şefik CİNAL, İlyas EMİNOĞLU*

*Electrical-Electronics Engineering / Elektrik-Elektronik Mühendisliği*

*RESEARCH ARTICLE*

**The Effect of FOV Angle on a RSSI-based Visible Light Positioning System** 205-230  
(Bir RSSI Tabanlı Görünür Işık Konum Belirleme Sistemi Üzerine FOV Açısının Etkisi)  
*Özlem AKGÜN*

*Electrical-Electronics Engineering / Elektrik-Elektronik Mühendisliği*

*RESEARCH & REVIEW ARTICLE*

**An Extension of the Last Work of Oleg A. Tretyakov:  
A Novel Format of the Wave Equation in SI Units** 231-250  
(Oleg A. Tretyakov'un Son Çalışmasının Bir Uzantısı:  
SI Birim Sisteminde Yeni Bir Dalga Denklemi Formatı)  
*Fatih ERDEN, Ahmet Arda ÇOŞAN*

---

MİLLİ SAVUNMA ÜNİVERSİTESİ  
DENİZ HARP OKULU DEKANLIĞI  
DENİZ BİLİMLERİ VE MÜHENDİSLİĞİ DERGİSİ

CİLT: 18 SAYI: 2 KASIM 2022 ISSN: 1304-2025

NATIONAL DEFENCE UNIVERSITY  
TURKISH NAVAL ACADEMY  
JOURNAL OF NAVAL SCIENCES AND ENGINEERING

VOLUME: 18      NUMBER: 2      NOVEMBER 2022      ISSN: 1304-2025

---

CONTENTS / İÇİNDEKİLER

<i>Naval Architecture and Marine Engineering / Gemi İnşaatı ve Gemi Makineleri Mühendisliği</i> <i>RESEARCH ARTICLE</i>	
<b>Investigation of the Effect of the Flow Regulators on the Flow Around a Generic Submarine Sail</b>	251-279
(Akış Düzenleyicilerin Bir Jenerik Denizaltı Yelkeni Etrafındaki Akışa Etkisinin İncelenmesi) <i>Gökay SEVGİ, Barış BARLAS, Uğur Oral ÜNAL</i>	
<i>Oceanography and Hydrography / Oşinografi ve Hidrografi</i> <i>RESEARCH ARTICLE</i>	
<b>Bathymetric Analysis of Lystad Bay, Horseshoe Island by Using High Resolution Multibeam Echosounder Data</b>	281-303
(Yüksek Çözünürlüklü Çok Bimli İskandil Verileri ile Horseshoe Adası, Lystad Körfezi'nin Batimetrik Analizi) <i>Emre TÜKENMEZ, Emre GÜLHER, Özgür KAYA, H. Fatih POLAT</i>	
<i>Computer Engineering / Bilgisayar Mühendisliği</i> <i>RESEARCH ARTICLE</i>	
<b>An Evaluation on Weapon Target Assignment Problem</b>	305-332
(Silah Hedef Atama Problemi Üzerine Bir Değerlendirme) <i>Tolga ÖNEL, Elif BOZKAYA</i>	
<i>Computer Engineering / Bilgisayar Mühendisliği</i> <i>RESEARCH ARTICLE</i>	
<b>Machine and Deep Learning-based Intrusion Detection and Comparison in Internet of Things</b>	333-361
(Makine ve Derin Öğrenme Yöntemleri ile Nesnelerin İnterneti için Saldırı Tespitinin Karşılaştırılması) <i>Siham AMAROUCHE, Kerem KÜÇÜK</i>	
<i>Industrial Engineering / Endüstri Mühendisliği</i> <i>RESEARCH ARTICLE</i>	
<b>Project Planning with CPM and PERT Methods: Example of Defence Industry</b>	363-385
(CPM ve PERT Yöntemleriyle Proje Planlama: Savunma Sanayi Örneği) <i>Beste DESTİCİOĞLU TAŞDEMİR</i>	

---

MİLLİ SAVUNMA ÜNİVERSİTESİ  
DENİZ HARP OKULU DEKANLIĞI  
DENİZ BİLİMLERİ VE MÜHENDİSLİĞİ DERGİSİ

CİLT: 18      SAYI: 2      KASIM 2022      ISSN: 1304-2025

## **FOREWORD**

The year 2023 represents a milestone for our country, our academy, and for our journal. The Republic of Türkiye will celebrate its centennial, the Turkish Naval Academy (TNA) will celebrate its quarter-millennial, and the Journal of Naval Sciences and Engineering (JNSE) will celebrate its vicennial in 2023. Undoubtedly, the historical intersection is a source of praise and pride for our academy and for our journal.

Founded in 1773, the Imperial School of Naval Engineering (Mühendishane-i Bahr-i Hümayûn), considered the first engineering school of the Empire, became the foundation of both the TNA and the Istanbul Technical University (ITU). TNA and ITU have special positions in terms of Turkish modernization history as the institutions where engineering and technical education have continued since the Ottoman period with their 249 years of distinguished history. 2023 will mark these exceptional institutions' 250th anniversary.

2023 will also mark the 20th anniversary of the JNSE. The journal, which has published 18 volumes and 36 issues under the ownership of the Naval Sciences and Engineering Institute since its first issue in 2003, has aimed to provide a scientific contribution to the theory and applications of naval sciences and engineering and share knowledge in relevant fields.

As we are entering this historically significant year, by virtue of the restructuring of the Institutes affiliated with the National Defence University, the journal has been transferred from the Barbaros Naval Sciences and Engineering Institute to the ownership of the Turkish Naval Academy Deanery starting with this issue.

*Fatih ERDEN*

As an Editorial Board Member of the JNSE since 2013, as well as an Editor in both 2018 and 2019, and as an Administrative Board Member of the Naval Sciences and Engineering Institute from 2013 to 2022, it has been encouraging to see JNSE's continued improvement. The role of Editor-in-Chief (EIC) has been passed to me at a special time when our journal has been included within the scope of the ULAKBIM TR Index.

The journal must, first and foremost, continue to provide a contribution to science and engineering in fields aligned with the areas of interest of the JNSE, e.g., electrical and electronics engineering, naval/mechanical engineering, naval architecture and marine engineering, industrial engineering, computer science and engineering, and basic/social sciences. In the meantime, we will do our best to make our journal ready to be a candidate to be indexed in Science Citation Indexes. Raising the quality of the accepted papers by introducing strict review criteria will be instrumental in achieving this goal by increasing the impact of the journal.

To this end, we recently applied to join Crossref as a member under the sponsorship of TÜBİTAK ULAKBİM DergiPark, and consequently, we are entitled to provide a DOI (Digital Object Identifier) for the papers accepted after September 1, 2022. The editorial processes of the articles sent after the specified date are carried out by the new editorial board.

With the new structure of JNSE's Editorial Board, when a manuscript is submitted, the EIC assigns it to the appropriate Editorial Board Member based on the main topic area of the manuscript. The assigned Member should assign a minimum of two reviewers to evaluate the manuscript. He/she is expected to make his/her own independent review of the manuscript and, once the reviewers have completed their evaluation, he/she submits a recommendation to the EIC. The EIC checks for consistency among the recommendations, typically accepts the recommendation of the assigned Editorial Board Member and then communicates to the corresponding author the final decision together with the comments of the reviewers.



## Foreword

We are therefore starting with a smaller, more flexible, and resourceful Editorial Board, dedicated to this purpose. I hope that with the other editors, we can push JNSE to a more competitive position within the field; a position that it rightly deserves.

The success of any journal is built on the support of the contributors, the reviewers, the editors, and the publication staff. We look forward to receiving your ideas for making JNSE more valuable for our community.

We welcome your original contributions to our issues that will be published in this historical year of 2023.

Fatih ERDEN , PhD  
Editor-in-Chief

*\*An ethical committee approval and/or legal/special permission has not been required within the scope of this study.*

**A NEW RECEIVER DESIGN FOR SPATIAL MODULATION SYSTEMS\***

**Gökhan ALTIN**<sup>ID</sup>

*National Defence University, Turkish Air Force Academy, Department of  
Electronics Engineering, Istanbul, Turkey,  
galtin@msu.hho.edu.tr*

**Received: 13.06.2022**

**Accepted: 05.09.2022**

**ABSTRACT**

*In this study, spatial modulation (SM), which is an interesting and new approach for 5G and beyond communication systems, and deep neural network (DNN), which have also received great attention recently, are discussed, and a DNN-based receiver architecture for SM systems is proposed. Since the DNN will not be retrained until the channel change after training, it requires less processing, so it will be a potential receiver architecture for next-generation wireless communication and therefore SM systems. In this paper, a new DNN-based SM receiver is proposed to detect the transmitted symbols and the activated antenna index at the same time, and its performance is examined. As can be seen from the computer simulations, the DNN-based receiver offers low error performance with a small number of hidden layers and a low number of neurons in these layers. At the same time, even when the data rate is increased, the same DNN structure (without increasing the processing load) shows better/same performance than the receivers in the literature.*

**Keywords:** *MIMO, Spatial Modulation, Deep Learning, Deep Neural Network.*

Gökhan ALTIN

## UZAYSAL MODÜLASYON SİSTEMLERİ İÇİN YENİ BİR ALICI TASARIMI

### ÖZ

*Bu makalede, 5G ve ötesi iletişim sistemleri için ilgi çekici ve yeni bir yaklaşım olan uzaysal modülasyon (Spatial Modulation (SM)) ile yine son zamanlarda büyük ilgi gören derin sinir ağları (Deep Neural Network (DNN)) konuları ele alınmış ve SM sistemleri için DNN tabanlı alıcı mimarisi önerilmiştir. DNN, eğitim sonrası kanal değişene kadar yeniden eğitilmeyeceğinden daha az işlem gerektirir, bu nedenle yeni nesil kablosuz iletişim ve dolayısıyla SM sistemleri için potansiyel bir alıcı mimarisi olacaktır. Bu çalışmada, aktif edilmiş anten indisi ile iletilen sembolleri ortaklaşa algılamak için tam bağlantılı (fully connected) DNN tabanlı yeni bir SM sezici önerilmiş ve performansı analiz edilmiştir. Bilgisayar benzetimlerinden de görüldüğü gibi DNN tabanlı alıcı az sayıda gizli katman ve bu katmanlardaki yine az sayıdaki nöron sayısı ile düşük hata performansı sunmaktadır. Aynı zamanda veri hızı artırıldığında bile aynı DNN yapısı (işlem yükü artmadan) literatürdeki alıcılardan daha iyi/aynı performansı göstermektedir.*

**Anahtar Kelimeler:** MIMO, Uzaysal Modülasyon, Derin Öğrenme, Derin Sinir Ağları

## **1. INTRODUCTION**

Today, access to information quickly and accurately has become an indispensable need. Therefore, multiple-input multiple-output (MIMO) systems are currently one of the most effective methods in increasing the reliability of information. MIMO systems aim to increase the capacity of the radio link with the multipath obtained by using multiple transmit and receive antennas (Telatar, 1999). MIMO has been a fundamental element used in new generation communication standards such as IEEE 802.11n (Wi-fi 4), IEEE 802.11ac (Wi-fi 5) (IEEE, 2020), WiMAX, Long Term Evolution (LTE) (IEEE, 2017). The two main MIMO transmission techniques in the literature are space-time block code (STBC) (Tarokh et al., 1999) and spatial multiplexing (SMX) (Tse & Viswanath, 2005). The first of these techniques extends the traditional two-dimensional signal constellation set to space and time dimensions, providing transmission diversity, and increasing signal reliability. However, an orthogonal STBC per channel use provides the full symbol rate for two transmit antennas, while for more than two transmit antennas, it is a maximum of 3/4 symbols. The latter can achieve higher data rates. The best-known applications of SMX are Bell Labs layered space time (BLAST) techniques. In one of the BLAST techniques, Vertical-BLAST (V-BLAST) (Wolniansky et al., 1998), the capacity is increased by sending multiple symbols from multiple transmit antennas. However, since these systems have simultaneous transmission over all antennas, a pricy radio frequency (RF) stage is needed for whole antennas and a high rate of inter-channel interference (ICI) occurs, which adds additional complexity to the receiver.

Spatial modulation (SM) (Mesleh et al., 2008), which carries information in both antenna domain and classical symbol set, has started to attract increasing attention in recent years and has become a new alternative to STBC and SMX. In an SM system where  $N_t$  is the number of transmit antennas and  $M$  is the size of the constellation set for conventional phase shift keying (PSK)/quadrature amplitude modulation (QAM) modulations,  $\log_2(N_t M)$  information bits are assigned to an SM symbol. The first  $\log_2(N_t)$  bit of the total  $\log_2(N_t M)$  bit defines the transmit antenna, while the remaining bits are reserved for  $M$ -PSK/QAM modulation. Since a single

transmit antenna is activated during each symbol transmission, a single RF stage is adequate in SM systems and ICI is eliminated.

As a result of the popularity of SM, special cases of SM such as space shift keying (SSK) (Jeganathan et al., 2009), generalized spatial modulation (GSM) (Younis et al., 2010), quadrature SM (QSM) (Mesleh, Ikki & Aggoune, 2015), receive SM (RSM) (Yang, 2011), etc. has been proposed. In SSK, information is carried only in antenna domain where symbol domain is not used. In the GSM system, multiple transmit antennas are enabled rather than a single antenna for increasing the data rate. In QSM, on the other hand, PSK/QAM symbols are divided into real and imaginary parts and sent over activated antennas. In RSM, the receive antenna indices convey messages with the help of precoding in the transmitter. An extensive study of SM systems can be found at (Wen et al., 2019).

Artificial neural networks (ANNs) are parallel and distributed computing structures that are designed with inspiration from the human brain, and are formed with interconnecting nodes, each of which operates with weighting and biasing (Hassoun, 2003). In other words, they are computer programs that emulate biological neural networks. Deep neural networks (DNN) are defined as versions of ANNs that are structurally "deep" by increasing the number of hidden layers and neurons in these layers. In recent years, DNN has been used in many fields from health to medicine, engineering applications to architecture, finance to weather forecasts, biology to chemistry, etc. Three main techniques are generally used in DNN applications, namely: Fully connected neural network (FCNN), convolutional neural network (CNN) and recurrent neural network (RNN). Detailed information on these techniques can be found in (Hassoun, 2003), (Bishop, 2006).

The use of ANNs in wireless communication has attracted great interest and there has been a great increase in studies on the subject in recent years. Studies on the use of DNN in wireless communication can be found in (Dai et al., 2020) and its references. This interest in DNN has started to be seen in SM and other variants (SSK, GSM, etc.) and various studies have emerged. Transmit antenna selection and power allocation for SM systems using machine learning methods are investigated in (Yang et al., 2019). A GSM system in which the transmitted symbols and antenna indices are

determined by separate DNN structures is given in (Shamasundar & Chockhalingam, 2020). Unlike (Shamasundar & Chockhalingam, 2020), the GSM system, which uses a Block-DNN structure that decodes both active antenna indices and modulated symbols together, is studied in (Albinsaid et al. 2020). In (Luong et al., 2019), the OFDM frames are decoded by FCNN technique in index modulated OFDM (OFDM-IM) structure. In (Kim, Ro & Park, 2021), an architecture that decodes active antenna indices with CNN and transmitted PSK/QAM symbols with FCNN is proposed for dual-mode OFDM-IM. (Altın, 2022) develops a new detection technique for MIMO-OFDM-IM using deep learning (DL) methods.

To the best of the authors' knowledge, a receiver design using the DNN method for the SM system (only for SM, not for other variants of SM) has never been considered. In this study, a new SM receiver using FCNN is constituted to decode SM symbols. The main contributions of this article are listed below:

- Since the complexness of the optimum receiver for SM systems increases exponentially due to the number of transmit and receive antennas, and constellation size, using a DNN-based receiver will be a more convenient solution due to its near-optimal performance and lower complexity.
- As far as is known, DNN-based receiver structures have been studied for other types of SM in the literature, but no study has been done in this direction for SM. In these studies, antenna indices and modulated symbols is determined separately. However, since the correct decoding of both dimensions at the same time in SM is very important for performance, a DNN receiver is designed in this paper that jointly detects both the antenna index and the transmitted symbol.
- In order to increase the performance, some studies in the literature process the received signal in another layer and give it to the DNN input. However, this complicates the receiver even more and brings extra costs. In our study, there is no preprocessing before DNN.

The remainder of the paper is composed as follows. The classical SM scheme and optimal decoding for the SM are re-examined in Section 2. In Section 3, the architecture, training and testing phases of the DNN for the

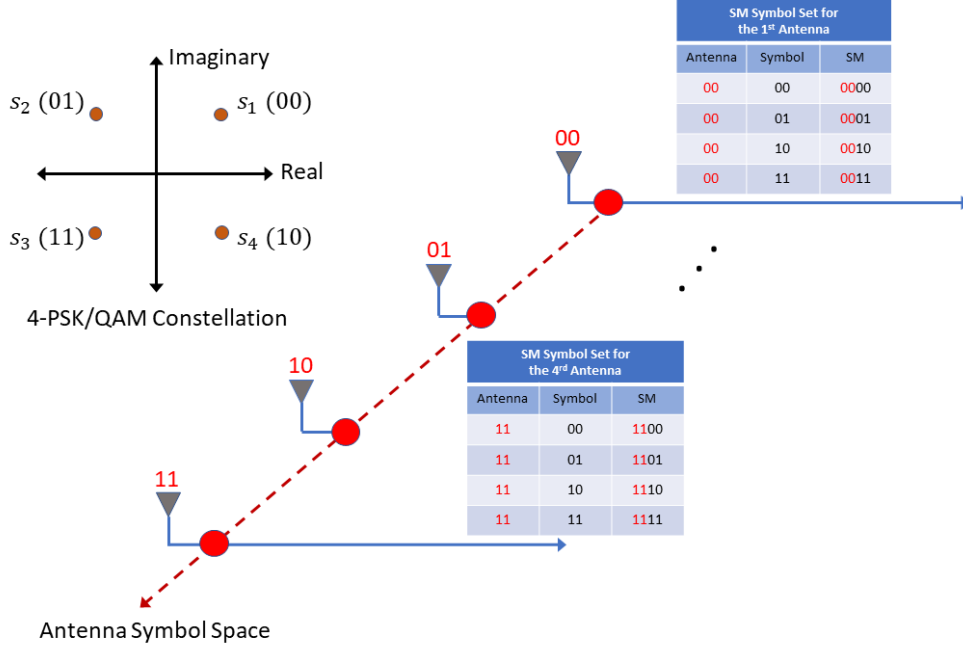


**Figure 1.** SM constellation for  $N_t = 4$  and 4-PSK/QAM modulation.

SM receiver are proposed in Section 3. The computer simulations for the proposed scheme are given in Section 4 and Section 5 concludes the work.

**Notation:** A scalar is represented by lowercase and uppercase italics. A vector is in bold, lowercase and a matrix is in bold, uppercase letters.  $(.)^T$  and  $(.)^H$  denote transpose and Hermitian transpose, respectively.  $\|\cdot\|$  corresponds to the Euclidean/Frobenius.  $\mathbf{I}_N$ , is the  $N \times N$  unitary matrix.  $diag(\cdot)$  shows the diagonal of a matrix and  $vek(\mathbf{A})$  is the vectorization operator by writing consecutive columns of matrix  $\mathbf{A}$ .  $\mathbb{C}^{n \times m}$  shows the dimensions of a complex matrix. Expectation operation is denoted by  $E\{\cdot\}$ .  $\mathcal{CN}(0, \sigma^2)$  describes a circularly symmetric, zero-mean complex Gaussian distribution with  $\sigma^2$  variance. Binomial coefficient and floor operator can be given as  $\binom{\cdot}{\cdot}$  and  $\lfloor \cdot \rfloor$ , respectively.  $\Re\{\cdot\}$  is the real part and  $\Im\{\cdot\}$  is the imaginary part of a complex number.

## 2. CLASSICAL SM SCHEME

As mentioned before, it can be thought that the antenna index is added as a third dimension to the two-dimensional signal set to transmit information in the SM method. Thus, the SM symbol is selected from the set of symbols, an example of which is shown in Figure 1. So, an SM symbol with unit energy,  $E\{\mathbf{s}^H \mathbf{s}\} = 1$ , can be given as  $\mathbf{s} = \left[ \underbrace{0 \dots 0}_{i-1} \quad s_q \quad \underbrace{0 \dots 0}_{N_t-i} \right]^T$  where  $i$  is the activated antenna index and  $s_q$  is the  $M$ -PSK/QAM symbol. For the channel matrix  $\mathbf{H}$ , which consists of independent and identically distributed (i.i.d.) random variables with  $\mathcal{CN}(0,1)$  distribution, and the noise vector  $\mathbf{n}$ , which consists of i.i.d. random variables with double-sided noise spectral density  $N_0$  and  $\mathcal{CN}(0, N_0)$  distribution, the received signal vector will be

$$\begin{aligned} \mathbf{r} &= \mathbf{H}\mathbf{s} + \mathbf{n} \\ &= \mathbf{h}_i s_q + \mathbf{n}. \end{aligned} \quad (1)$$

Here,  $\mathbf{h}_i$  represents the  $i^{\text{th}}$  column of the matrix  $\mathbf{H}$ .

Under the assumption that the channel state information (CSI) is known at the receiver, when the maximum likelihood (ML) method, which is the optimum detection technique, is used, the antenna index and the transmitted signal is decided with

$$[\hat{i}, s_{\hat{q}}] = \arg \min_{i,q} \|\mathbf{r} - \mathbf{h}_i s_q\|^2 \quad (2)$$

(Jeganathan et al., 2008). The receiver complexity of the ML method given in (2) increases with the size of the symbol set,  $M$ , and the number of transmit and receive antennas. For this reason, many studies have been carried out in the literature to reduce the complexity of ML. Some of these works are presented in (Al Nahhal et al., 2019; Liu et al., 2019; Jiang et al., 2015; Men & Jin, 2014; Rajashekar et al., 2014; Tang et al., 2013; Wang, Jia & Song, 2012; Pillay & Xu, 2013; Zhang & Yin, 2014). However, these studies have generally been developed by arranging and applying known algorithms, and as far as we know, heuristic methods have never been applied for the SM technique.



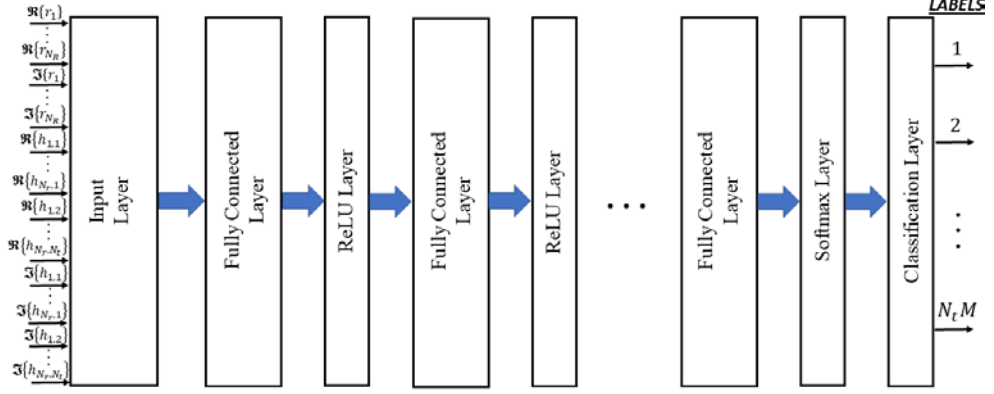


Figure 2. Proposed DNN-based SM receiver.

### 3. A NEW RECEIVER DESIGN FOR SM SYSTEMS

#### 3.1. DNN-based Receiver Architecture

SM receiver architecture with a single DNN-based decoder is presented in Figure 2. This architecture has no preprocessing, which further increases the receiver's processing load, so the received signal and channel parameters are given to the input of the proposed DNN, as they are, assuming that CSI is present at the receiver (as in ML). At the same time, since the DNN method is inspired by the human brain, generally the input information is real numbers. Therefore, in our study, the inputs are expressed in real terms as well. As a result, the input (feature) vector for the receiver can be written as

$$\mathbf{v} = \left[ (\Re(\mathbf{r}))^T (\Im(\mathbf{r}))^T (\Re(\text{vek}(\mathbf{H})))^T (\Im(\text{vek}(\mathbf{H})))^T \right]^T. \quad (3)$$

As seen in Figure 2, the proposed DNN receiver consists of multiple fully connected (FC) layers and a classification layer. FC layers transmit the output of the previous layer to the next layer by multiplying it with a weighting matrix and summing it with a bias vector. Furthermore, the rectified linear unit (ReLU) function, which makes the negative input 0 and determines the positive input as itself, is used to activate the neurons, i.e.  $f(z) = \max(0, z)$ . The softmax function, which shows the probabilities of the results, is selected for the output layer as  $\sigma(\mathbf{x})_i = \frac{e^{x_i}}{\sum_{j=1}^Z e^{x_j}}, i = 1, 2, \dots, Z$

for an arbitrary vector  $\mathbf{x} = [x_1 \ x_2 \ \dots \ x_Z] \in \mathbb{R}^Z$ . Therefore, the most probable outcome will correspond to the index of that symbol inside the SM symbol set. Since there are possible  $N_t M$  SM symbols to be classified, the number of neurons for the classification layer will also be  $N_t M$ .

### 3.2. Training and Testing Phases

The received signal and the channel parameters are needed to train the DNN. At this phase, no channel estimation is needed since the DNN will be trained offline, and the received signal,  $\mathbf{r}$ , and the corresponding channel parameters,  $\mathbf{H}$ , which are artificially generated using (1), help to train the DNN. The noise vector in (1) can be randomly generated based on a given SNR value.

At the training stage, labels are given to each of the SM symbols produced in the transmitter and known in the receiver, and the DNN is expected to make the right decision on these labels at the end of the training process. The labels that will correspond to the SM symbols to be formed for the proposed DNN is given in Table 1.

**Table 1.** Labelling for training sequence.

SM Symbol	Label
$[s_1 \ 0 \ \dots \ 0 \ 0]^T$	1
$[s_2 \ 0 \ \dots \ 0 \ 0]^T$	2
$\vdots$	$\vdots$
$[0 \ \dots \ 0 \ \underbrace{s_q}_i \ 0 \ \dots \ 0]^T$	$i_q$
$\vdots$	$\vdots$
$[0 \ 0 \ \dots \ 0 \ s_M]^T$	$N_t M$

For a good performance in the training phase, the number of dataset is selected at least  $10^7$ . In addition, 20% of the produced data is reserved for

testing/validating of the proposed network. Dataset generation at the training stage is given in Algorithm 1. If the dataset is very large, it can be divided into smaller sets, which is called mini batches, to increase processing speed.

**Algorithm 1.** Data generation for DNN.

---

**Input:**  $N_t, N_r, M,$

**Initialization:** Number of Dataset, SNR

- 1 **for**  $i \leftarrow$  Number of Dataset **do**
- 2     Generate randomly  $N_r \times N_t$  channel matrix,  $\mathbf{H}$ , and  $N_r \times 1$  AWGN noise vector,  $\mathbf{n}$ , based on fixed SNR value.
- 3     Generate known GSM symbols corresponding to the  $\log_2(N_t M)$  bit and give each a label according to Table 1.  
 $\mathbf{l} = [l^{(1)}, l^{(2)}, \dots, l^{(i)}]^T, \quad l \in \{1, 2, \dots, N_t M\}$
- 4      $\mathbf{r} = \mathbf{h}_i s_q + \mathbf{n}$
- 5      $\mathbf{v}^{(i)} = [(\Re(\mathbf{r}))^T (\Im(\mathbf{r}))^T (\Re(\text{vek}(\mathbf{H})))^T (\Im(\text{vek}(\mathbf{H})))^T]^T$
- 6 **end**
- 7 Allocate 20% of the generated dataset for validation of the network (test).

**Output:**  $\mathbf{v}^{(training)}, \mathbf{v}^{(test)}, \mathbf{l}^{(training)}, \mathbf{l}^{(test)}$

---

#### 4. SIMULATION RESULTS

In this section, computer simulations are depicted for the proposed DNN-based SM receiver on a standalone PC with an AMD Ryzen 5 3600 @3.60 GHz CPU, NVIDIA GeForce GTX 1650 GPU, and 16 GB RAM. These computer simulations include finding the best SNR value and BER results made accordingly. At the same time, the comparisons of the proposed

structure according to the BER results with other studies (Wang, Jia & Song, 2012), (Pillay & Xu, 2013) and (Mesleh et al., 2006) are also presented. For DNN simulations, the mini batch size is set as 4096, and step-based learning schedule is selected to scan the first steps quickly and to investigate the next steps in more detail. In here, the initial learning rate is chosen as 0.01 and is reduced by 10% in every 2 epochs.

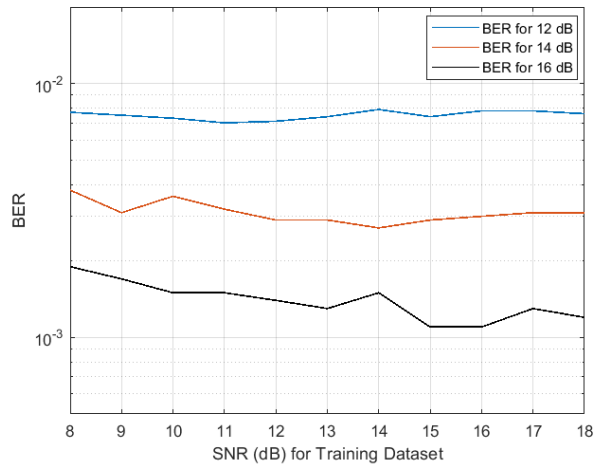


**Figure 3.** Bit error probabilities for  $N_t = 2$ ,  $N_r = 4$  and 16-QAM according to SNR values to be used to determine noise levels in training dataset.

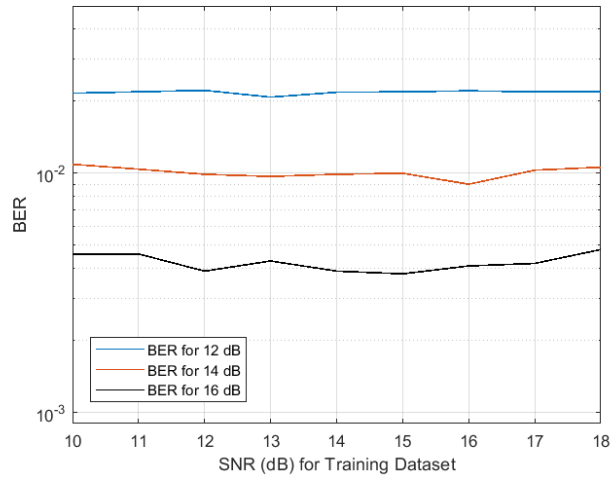
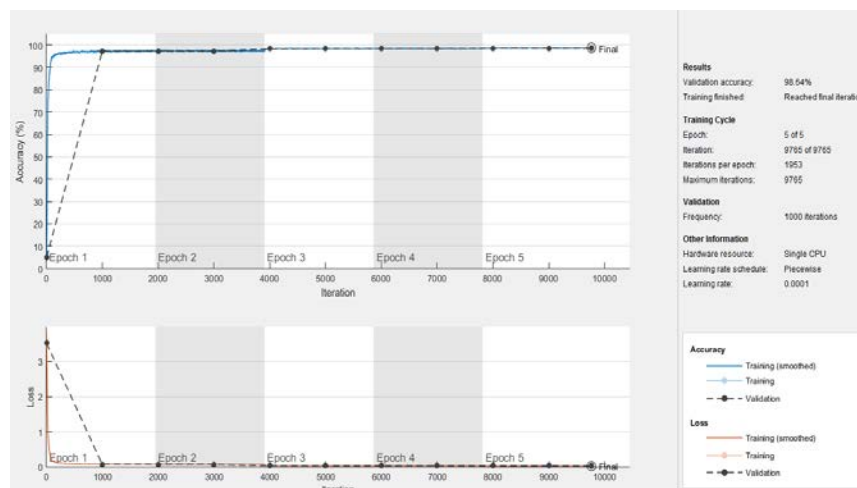


**Figure 4.** Bit error probabilities for  $N_t = 2$ ,  $N_r = 4$  and 32-QAM according to SNR values to be used to determine noise levels in training dataset.

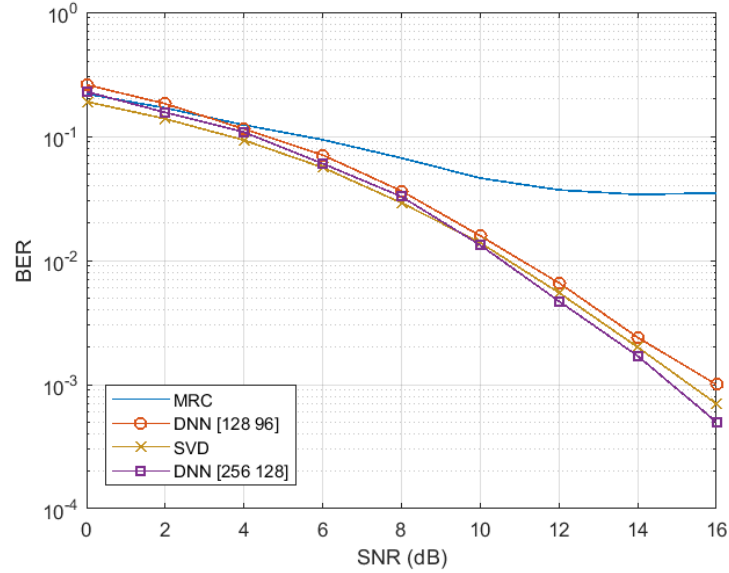
On the other hand, the signal-to-noise ratio (SNR) is applied as the received SNR seen at the receiver front end. The performance of a DNN receiver is closely related to how well it is trained. For this reason, the noise level to be used in the dataset gains importance. Thus, a trained DNN according to an appropriate SNR will give optimal error performance at all SNR levels. In Figures 3 and 4, bit error probabilities (BER) are given according to the SNR values to be used in determining the noise level in the training dataset for the data rate  $R=5 \text{ bits/second/Hz}$  and  $R=6 \text{ bits/second/Hz}$ , respectively. In Figure 3, the BER performances of the SM system at 12 dB, 14 dB, and 16 dB show that they jointly perform at the lowest when the training is realized at an SNR of 13 dB. Again, with the same method, if the DNN structure suggested for  $R=6 \text{ bits/second/Hz}$  is trained with a 15 dB SNR level, the BER performance of the whole system will be at the optimum level as in Figure 4.

Figure 5 shows the accuracy level during training of the proposed DNN structure with 128 and 96 neurons in the first and second hidden layers, respectively ([128 96]) and the reduction of the loss function according to each iteration. As can be seen from the figure, the proposed DNN architecture reaches a very high level of accuracy in the first iterations and reaches its highest level in the 3<sup>rd</sup> epoch. This shows that there is no need for long epochs to train the DNN. Likewise, the loss function reaches its minimum value in low iteration numbers.

Figure 6 shows the error performance curves of DNN structures in various configurations and MRC and SVD detectors in the literature for a data rate of  $R=5 \text{ bits/second/Hz}$ .



**Figure 5.** Accuracy level and loss function during training of [128 96] DNN.



**Figure 6.** BER performance comparison for R=5 bits/second/Hz.

For the training dataset in DNN, SNR = 13 dB and the number of epochs is chosen as 5. As can be seen from the BER curves presented for the MIMO system structure with  $N_t = 2$ ,  $N_r = 4$  and 16-QAM, the [256, 128] DNN receiver gives much better results than the MRC detector, and it provides 0.5 dB SNR gain at  $10^{-3}$  error probability with respect to SVD detector. Moreover, if it is desired to train the DNN faster and reduce the processing load, the number of neurons in the FC layers can be reduced. As can be seen from Figure 6, although the [128, 96] DNN receiver has lower neuron numbers, it gives better results than the MRC algorithm and offers similar performance to the SVD algorithm.

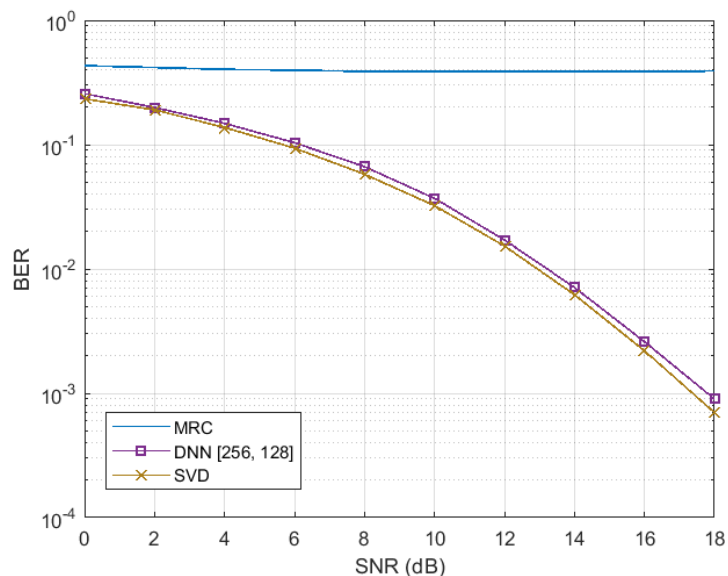


**Figure 7.** BER performance comparison for  $R=6$  bits/second/Hz.

Figure 7 shows the BER performance curves of SM receivers for a data rate of  $R=6$  bits/second/Hz. MIMO system structure is determined as  $N_t = 2$ ,  $N_r = 4$  and 32-QAM. Here, it shows almost the same BER performance as the SVD algorithm, even though the same DNN structure is used and the data rate and signal set size are increased compared to the MIMO configuration in Figure 6. It should be noted that although the computational load of the MRC and SVD algorithms grows with the constellation size,  $M$ , there isn't any increase for the DNN.

## 5. CONCLUSION

SM is a new and interesting transmission technique for MIMO systems that will be a candidate for 5G and beyond communications with its features such as high data rate, using a single RF chain in the transmitter, and completely eliminating ICI. Simultaneously, DNN-based solution methods have begun to be used in today's technologies due to the many advantages it offers. In this paper, the use of DNN-based detector in the receiver structure

## *A New Receiver Design for Spatial Modulation Systems*

of SM is examined. As can be seen from the computer simulations, DNN-based SM receiver offers high performance without the need for many hidden (FC) layers and number of neurons. At the same time, even when the data rate is increased, the same DNN structure (without increasing the processing load) shows better/same performance than the detectors in the literature.



*Gökhan ALTIN*

**CONFLICT OF INTEREST STATEMENT**

The author declares no conflict of interest.

## REFERENCES

- Albinsaid, H., Singh, K., Biswas, S., Li, C.-P., & Alouini M.-S. (2020). "Block deep neural network-based signal detector for generalized spatial modulation". *IEEE Communications Letters*. Vol. 24, No. 12, pp. 2775-2779. doi:10.1109/LCOMM.2020.3015810.
- Al-Nahhal, I., Basar, E., Dobre, O.-A., & Ikki, S. (2019). "Optimum Low-Complexity Decoder for Spatial Modulation". *IEEE Journal on Selected Areas in Communications*. Vol. 37, No. 9, pp. 2001-2013. doi:10.1109/JSAC.2019.2929454.
- Altın, G. (2022). "Deep neural network-based detection of index modulated MIMO-OFDM". *Physical Communication*. Vol. 52, 101669. doi:10.1016/j.phycom.2022.101669.
- Bishop, C.-M. (2006). *Pattern Recognition and Machine Learning*. Springer-Verlag, New York, NY, USA.
- Dai, L., Jiao, R., Adachi, F., Poor, V.-H., & Hanzo, L. (2020). "Deep learning for wireless communications: An emerging interdisciplinary paradigm". *IEEE Wireless Communications*. Vol. 27, No. 4, pp. 133-139. doi:10.1109/MWC.001.1900491.
- Hassoun, M. (2003). *Fundamentals of Artificial Neural Networks*. A Bradford Book, Cambridge, MA, USA, MIT Press.
- IEEE Std. 802.16. (2017). *IEEE 802.16 Standard: Fixed broadband wireless access systems*. IEEE SA. Retrieved from <https://standards.ieee.org/ieee/802.16/4184/>
- IEEE Std. 802.11. (2020), *IEEE 802.11 Standard: Wireless Local Area Networks*. IEEE SA. Retrieved from <https://standards.ieee.org/ieee/802.11/7028/>
- Jeganathan, J., Ghayeb, A., & Szczecinski, L. (2008). "Spatial modulation: optimal detection and performance analysis". *IEEE Communications Letters*. Vol. 12, No. 8, pp. 545-547. doi:10.1109/LCOMM.2008.080739.

- Jeganathan, J., Ghrayeb, A., Szczecinski, L., & Ceron, A. (2009). "Space shift keying modulation for MIMO channels". *IEEE Transactions on Wireless Communications*. Vol. 8, No. 7, pp. 3692-3703. doi:10.1109/TWC.2009.080910.
- Jiang, Y., Wang, Y., Wen, J., Shao, M., & Li Y. (2015). "Spatial Modulation Scheme With Low-Complexity Detection Algorithms". *IEEE Communications Letters*. Vol. 19, No. 8, pp. 1422-1425. doi:10.1109/LCOMM.2015.2435741.
- Kim, J., Ro, H., & Park H. (2021). "Deep learning-based detector for dual mode OFDM with index modulation". *IEEE Wireless Communications Letters*. Vol. 10, No. 7, pp. 1562-1566. doi:10.1109/LWC.2021.3074433.
- Liu, T.-H., Ye, Y.-Z., Huang, C.-K., Chen, C.-E., Hwang, Y.-T., & Chu, Y. S. (2019). "A Low-Complexity Maximum Likelihood Detector for the Spatially Modulated Signals: Algorithm and Hardware Implementation". *IEEE Transactions on Circuits and Systems-II: Express Briefs*. Vol. 66, No. 11, pp. 1820-1824. doi:10.1109/TCSII.2019.2896350.
- Luong, T.-V., Ko, Y., Vien, N.-A., Nguyen, D.-H.-N., & Matthaiou, M. (2019). "Deep learning-based detector for OFDM-IM". *IEEE Wireless Communications Letters*. Vol. 8, No. 4, pp. 1159-1162. doi:10.1109/LWC.2019.2909893.
- Men, H., & Jin, M. (2014). "A Low-Complexity ML Detection Algorithm for Spatial Modulation Systems With M-PSK Constellation". *IEEE Communications Letters*. Vol. 18, No. 8, pp. 1375-1378. doi:10.1109/LCOMM.2014.2331283.
- Mesleh, R., Haas, H., Ahn, C.-W., & Yun S. (2006). "Spatial modulation—a new low complexity spectral efficiency enhancing technique". *2006 First International Conference on Communications and Networking in China*, Beijing, China, pp. 1-5. doi:10.1109/CHINACOM.2006.344658.
- Mesleh, R., Haas, H., Sinanovic, S., Ahn, C.-W., & Yun, S. (2008). "Spatial modulation". *IEEE Transactions on Vehicular Technology*. Vol. 57, No. 4, pp. 2228-2241. doi:10.1109/TVT.2007.912136.

Mesleh, R., Ikki, S.-S., & Aggoune H.-M. (2015). "Quadrature spatial modulation," *IEEE Transactions on Vehicular Technology*. Vol. 64, No. 6, pp. 2738-2742. doi:10.1109/TVT.2014.2344036.

Pillay, N., & Xu, H. (2013). "Comments on 'Signal Vector Based Detection Scheme for Spatial Modulation'," *IEEE Communications Letters*. Vol. 17, No. 1, pp. 2-3. doi:10.1109/LCOMM.2012.120312.122165.

Rajashekar, R., Hari, K.-V.-S., & Hanzo L. (2014). "Reduced-Complexity ML Detection and Capacity-Optimized Training for Spatial Modulation Systems". *IEEE Transactions on Communications*. Vol. 62, No. 1, pp. 112-125. doi:10.1109/TCOMM.2013.120213.120850.

Shamasundar, B., & Chockalingam, A. (2020). "A DNN architecture for the detection of generalized spatial modulation signals". *IEEE Communications Letters*. Vol. 24, No. 12, pp. 2770-2774. doi:10.1109/LCOMM.2020.3018260.

Tang, Q., Xiao, Y., Yang, P., Yu, Q., & Li, S. (2013). "A New Low-Complexity Near-ML Detection Algorithm for Spatial Modulation". *IEEE Wireless Communications Letters*. Vol. 2, No. 1, pp. 90-93. doi:10.1109/WCL.2012.120312.120601.

Tarokh, V., Jafarkhani, H., & Calderbank, A. (1999). "Space-time block codes from orthogonal designs". *IEEE Transactions on Information Theory*. Vol. 45, No. 5, pp. 1456-1467. doi:10.1109/18.771146.

Telatar, E. (1999). "Capacity of Multi-antenna Gaussian Channels," *European Transactions on Telecommunications*. Vol. 10, No. 6, pp. 585-595. doi:10.1002/ett.4460100604.

Tse, D., & Viswanath, P. (2005). *Fundamentals of Wireless Communication*. Cambridge, Cambridge University Press.

Wang, J., Jia, S., & Song, J. (2012). "Signal Vector Based Detection Scheme for Spatial Modulation". *IEEE Communications Letters*. Vol. 16, No. 1, pp. 19-21. doi:10.1109/LCOMM.2011.111611.112127.

- Wen, W., Zheng, B., Kim, K.-J., Di Renzo, M., & Tiftsis, T.-A. (2019). "A survey on spatial modulation in emerging wireless systems: Research progresses and applications". *IEEE Journal on Selected Areas in Communications*. Vol. 37, No. 9, pp. 1949-1972. doi:10.1109/JSAC.2019.2929453.
- Wolniansky, P.-W., Foschini, G.-J., Golden, G.-D., & Valenzuela R.-A. (1998). "V-BLAST: an architecture for realizing very high data rates over the rich-scattering wireless channel". *1998 URSI International Symposium on Signals, Systems, and Electronics*. Pisa, Italy, pp. 295-300. doi:10.1109/ISSSE.1998.738086.
- Yang, L. (2011). "Transmitter preprocessing aided spatial modulation for multiple-input multiple-output systems". *IEEE 73rd Vehicular Technology Conference (VTC Spring)*, Budapest, Hungary, pp. 1-5. doi:10.1109/VETECS.2011.5956573.
- Yang, P., Xiao, Y., Xiao, M., Guan, Y.-L., Li, S., & Xiang, W. (2019). "Adaptive spatial modulation MIMO based on machine learning". *IEEE Journal on Selected Areas in Communications*. Vol. 37, No. 9, pp. 2117-2131. doi:10.1109/JSAC.2019.2929404.
- Younis, A., Seramovski, N., Mesleh, R., & Haas, H. (2010). "Generalised spatial modulation". *2010 Conference Record of the Forty Fourth Asilomar Conference on Signals, Systems and Computers*. pp. 1498-1502. doi:10.1109/ACSSC.2010.5757786.
- Zhang, W., & Yin Q. (2014). "Adaptive Signal Vector Based Detection for Spatial Modulation". *IEEE Communications Letters*, Vol. 18, No. 11, pp. 2059-2062. doi:10.1109/LCOMM.2014.2361859.

*\*An ethical committee approval and/or legal/special permission has not been required within the scope of this study.*

**MECHANICAL GYROSCOPE-BASED ROLL MOTION  
REDUCTION OF MARINE VEHICLES: AN EDUCATIONAL  
SETUP\***

**Şefik CİNAL<sup>1</sup>**   
**İlyas EMİNOĞLU<sup>2</sup>** 

<sup>1</sup>*Ondokuz Mayıs University, Department of Electrical and Electronics  
Engineering, Samsun, Turkey,  
sefikcinal@gmail.com*

<sup>2</sup>*Ondokuz Mayıs University, Department of Electrical and Electronics  
Engineering, Samsun, Turkey,  
ilyaseminoglu@hotmail.com*

**Received: 03.02.2022**

**Accepted: 24.05.2022**

### ABSTRACT

*In this study, simple hardware (model boat and mechanical gyroscope) setup is presented to teach the fundamentals of angular momentum and gyroscopic stabilizing concepts. The tool consists of a model boat, hobby-type servo motor for generating roll motion, dc motor-powered mechanical gyroscope, a mini water pool, measuring, and control subsystems. A graphical user interface (GUI) with MATLAB was designed for adjusting and controlling the tool, observing and recording the roll motion of the model boat. Hence, the construction of the stabilizing torque is visually explained and presented within the setup as a product of angular momentum (due to spin of the flywheel) and external torque (due to external mechanical disturbance or waves). The tools help undergraduate students to understand what the gyroscopic effect is and how gyroscopic stabilizers dampen the roll motion of the model boat practically.*

**Keywords:** Gyrostabilizer, Roll Stabilization, Experimental Setup.

**MEKANİK JİROSKOP İLE DENİZ ARAÇLARINDA YALPA  
HAREKETİNİN SÖNÜMLENDİRİLMESİ: BİR EĞİTİM SETİ  
TASARIMI**

**ÖZ**

*Bu çalışmada, açısız momentum ve jiroskopik dengeleme kavramlarının öğretilmesi için tasarlanan basit bir deney düzeneđi (model bot ve mekanik jiroskop) sunulmuştur. Deney düzeneđi, model bir tekne, dalga benzetimi için bir servo sistemi, dc motor ile çalışan mekanik bir jiroskop, küçük bir su havuzu ile ölçme ve kontrol sisteminden oluşmaktadır. Deney setinin kontrolü, izlenmesi ve yalpa hareketinin kaydedilmesi için MATLAB tabanlı bir grafik ara yüzü tasarımı yapılmıştır. Bu sayede, açısız momentum (jiroskobun dönmesi) ve harici tork (dalga etkisi) ile oluşan dengeleme torku görsel olarak anlatılmıştır. Deney seti, lisans öğrencilerinin jiroskopik etkinin ne olduğunu ve jiroskopik dengeleyicilerin model teknenin yalpa hareketini pratik bir şekilde nasıl sönümlediđini anlamalarına yardımcı olur.*

**Anahtar Kelimeler:** *Jiroskopik Dengeleyiciler, Yalpa Sönümleme, Deney Düzeneđi.*



## 1. INTRODUCTION

Wave-induced roll motion is a major problem for marine vessels. This undesirable oscillating movement can reduce crew performance and passenger comfort, or can damage the cargo (Perez & Blanke, 2012). It is necessary to reduce the roll motion for safety and comfort. Various stabilizing systems are used in marine vehicles such as fin roll, rudder roll, magnus effect, moving mass, active tank, and gyroscopic stabilizers (Townsend & Sheno, 2014). Rudder roll, fin roll, and magnus stabilizers are external systems that create the stabilizing torques outside the hull of the marine vessel. Active tanks, moving mass, and gyroscopic stabilizers are internal systems that create the stabilizing torques throughout the body (Townsend et al., 2007). Three types of ship stabilizer systems that are commonly used are the active fin stabilizers, the magnus effect stabilizers, and the gyroscopic stabilizers.

Two fins are placed on the port and starboard side of the ship in the active fin stabilizers. A gyroscopic sensor measures the roll angle of the ship and the fin controller adjusts the angle of the fins to reduce the roll motion. Magnus effect stabilizers use rotating cylinders instead of active fins as shown in Figure 1. The direction and speed of the cylinders are controlled with an electronic gyroscopic sensor and controller. Rotating cylinders use the magnus effect principle and generate up or down pressure according to their direction and rotation. Active fin and Magnus Effect stabilizer systems are closed-loop systems and designing a controller is necessary.

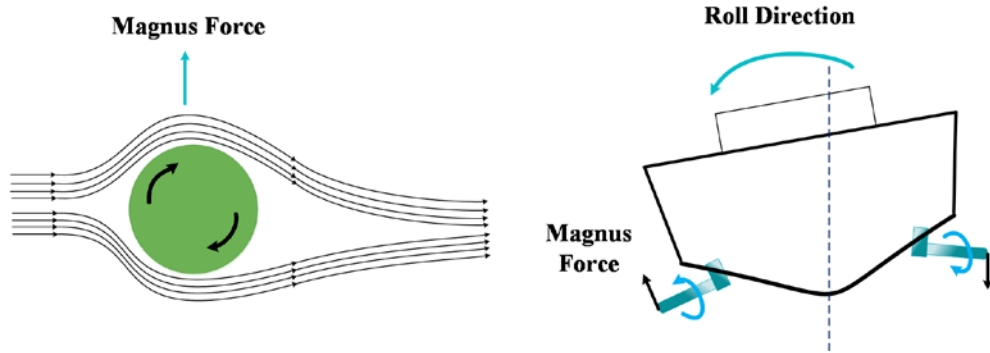


**Figure 1.** Magnus effect and rotor stabilizer.

*Mechanical Gyroscope-based Roll Motion Reduction of Marine Vehicles:  
An Educational Setup*

Gyro stabilizers can be mounted to the inside of the ship. They use gyroscopic moments to reduce the roll motion of the ship. Gyro stabilizing is a passive and open-loop method, and it does not require a controller and a device for measuring roll motion.

The earliest suggestion of using gyroscopic stabilizers was made by Schlick (1904). Brennan (1903) and Forbes (1904) also proposed gyroscopic stabilizers for marine vessels. One of the first applications of gyroscopic stabilizers was made by Sperry (1910). Gyroscopic stabilizers have also been used in nonmarine applications such as two-wheeled vehicles (Karnopp, 2002), satellite systems, and autonomous underwater vehicles (Woolsey & Leonard, 2002). Yamada et al. (1997) used gyrostabilizers to control the wind-induced oscillations of tall buildings and high towers

Oleg et al. (2016) designed a robotic boat setup for control research and educational purposes. They aimed to develop the practical experience of the students with this setup. Lavieri et al. (2012) used an experimental boat set up to develop a sliding mode controller for reducing the roll motion. Gyro stable platform (Quanser, n.d.) and Control Moment Gyroscope (ECP, n.d.) are commercial training sets designed for educational purposes. These training sets are used to investigate the rotational dynamics of gyroscopes. In principle, these educational sets are related to the concept of reorientation of space satellite problems. Several satellites now provide commercial earth imagery for customers (such as Google Earth etc.). The earth imagery requires an agile satellite, meaning that the satellite achieves comparatively high angular rates and accelerations to reorient itself and slew payloads quickly from one attitude to another. A technology known as the control moment gyroscope makes satellites sufficiently agile (Leve et al., 2015). Up to 3 axes can be controlled and reoriented this way. One other example of the gyroscopic effect is missile stability. Most likely, in close range, the most widely used air to air missile is the Sidewinder in the West, with roughly over 100,000 missiles produced for more than two dozen nations. It has four fins at the back of the missile that provides stability and four movable control surfaces are located in the front part, just behind the infrared seeker. This configuration has a natural tendency of roll motion that makes guidance and control difficult. To prevent roll motion (spinning

around its longitudinal axes) and to simplify the aerodynamic structure, a clever solution has been proposed and used. Four metal discs (rollerons or a kind of rotor) are attached at the end of the four tail wings. Once the missile is fired, due to high speed, all four rollerons spin at very high rpm and prevent any undesired roll motion. This gyroscopic effect in the tail wing prevents the missile from spinning in flight (Taur & Chern, 1999). It is effective and is still in use. Recently, in a similar principle of stabilizing effect of the fast-spinning rotor, several companies have produced marine stabilizers commercially. Commercial products of well-known companies are shown in Figure 2 (Seakeeper, n.d.) (DMS, n.d.), (Wesmar, n.d.).

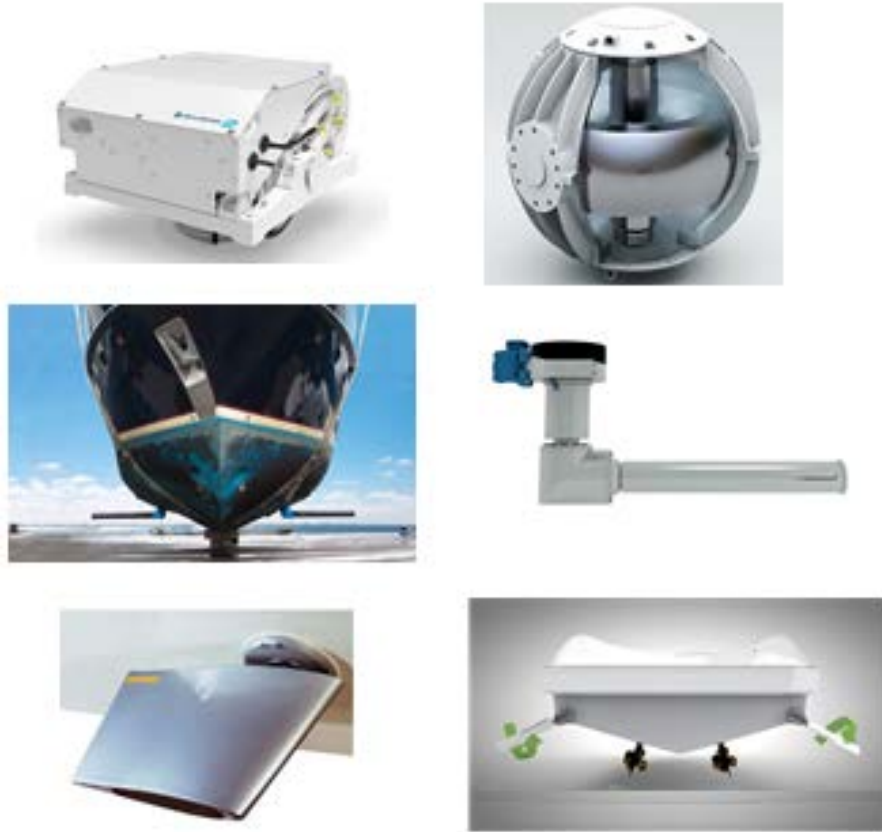


**Figure 2.** Various boat stabilizers: Gyrostabilizer, rotor stabilizers, fin roll stabilizers (Seakeeper, n.d.), (DMS, n.d.), (Wesmar, n.d.).

*Mechanical Gyroscope-based Roll Motion Reduction of Marine Vehicles:  
An Educational Setup*

This paper presents a demo setup for understanding the concept of the gyroscopic effects for the wide sense gyroscopic stabilizing process, which was not explicitly discussed in Electrical Engineering majors at OMÜ, Samsun, Türkiye. The tool was designed for the undergraduate level Automatic Control Laboratory and Autonomous Vehicle Applications courses given for the same department. As it is known, applied teaching plays a key role in engineering education (Bernstein, 1999) and this setup serves this purpose.

The rest of the paper is organized as follows. Section 2 gives the working principle of gyroscopic stabilizers. Section 3 provides the details of the educational tool design. Experimental results obtained from the setup are provided in Section 4. Finally, conclusions obtained from the practical construction of the setup and experimentation are provided in Section 5.

## **2. PRINCIPLE OF GYROSCOPIC STABILIZERS**

A rotating flywheel produces an angular momentum that is perpendicular to the plane of rotation. Angular momentum is a vector quantity and its direction can be determined by the right-hand rule as seen in Figure 3.

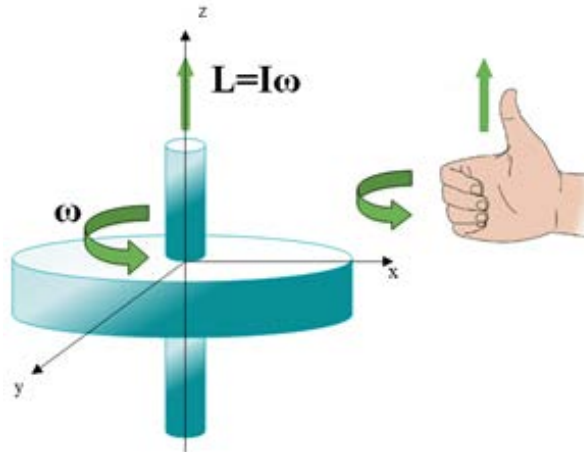


**Figure 3.** Angular momentum of rotating flywheel.

Angular momentum is the product of moment of inertia,  $I$  and Angular Velocity,  $\omega$

$$\vec{L} = I\vec{\omega} \quad (1)$$

To investigate the principles of gyroscopic stabilizers we can consider a gyroscope that is symmetrical about the z-axis and free to rotate about its three axes as shown in Figure 4. The gyroscope has a spin rate,  $\phi$ , and angular momentum,  $L$ . Acting moments of each axis ( $M_x$ ,  $M_y$  and  $M_z$ ) can be derived from general equations of motion (Housner & Hudson, 1959).  $\omega_x$ ,  $\omega_y$ , and  $\omega_z$  are the angular velocities for each axis and  $\dot{\phi}$  is the spin rate of the gyroscope.

$$M_x = I(\dot{\omega}_x - \omega_y\omega_z) + I_z\omega_y(\omega_z + \dot{\phi}) \quad (2)$$

$$M_y = I(\dot{\omega}_y - \omega_x\omega_z) - I_z\omega_x(\omega_z + \dot{\phi}) \quad (3)$$

$$M_z = I_z(\dot{\omega}_z + \dot{\phi}) \quad (4)$$

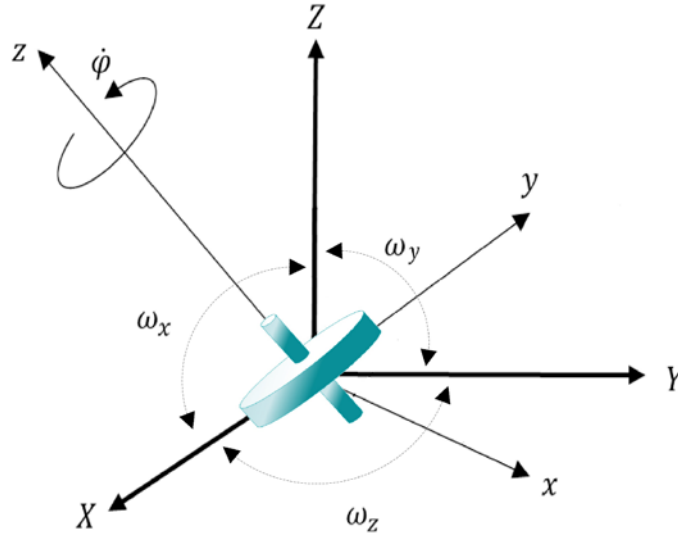


**Figure 4.** Axes of a gyroscope.

*Mechanical Gyroscope-based Roll Motion Reduction of Marine Vehicles:  
An Educational Setup*

If we examine (2), (3), and (4) we can see the additional moments that are related to the spin rate of the flywheel ( $\dot{\phi}$ ).

$$M_x = I_z \omega_y \dot{\phi} \quad (5)$$

$$M_y = -I_z \omega_x \dot{\phi} \quad (6)$$

$M_x$  and  $M_y$  are called gyroscopic moments. According to (5) and (6), the gyroscopic moment acting on the x-axis is related to the angular velocity of the y-axis, and the moment acting on the y-axis is related to the angular velocity of the x-axis. Therefore, if a force is applied to any axis of the gyroscope, it produces a moment perpendicular to the applied force.

When the gyroscope is used as a marine stabilizer, one of its axes is fixed to the ship's rolling axis. The gyroscope is free to rotate about the pitch axis. Stabilizing torque is created in three steps and these steps occur at the same time.

1) Sea waves make the boat roll. This can be represented with a force ( $F_x$ ) pair along the x-axis. At that time the gyroscope is rotating counterclockwise direction and produces an angular momentum on the z-axis.

2) The gyroscope rolls with the boat because it is fixed to the roll axis. The gyroscope has an  $\omega_x$  angular velocity because of the roll motion. According to (6) this angular velocity produces a moment ( $M_y$ ) in the y-axis as seen in Figure 5.  $M_y$  results as a direction change ( $\Delta L$ ) in angular momentum (Lewin, 2015) and gyroscope sweeps along the y-axis. This motion is called the precession of the gyroscope.  $L_1$  is the resultant angular momentum.

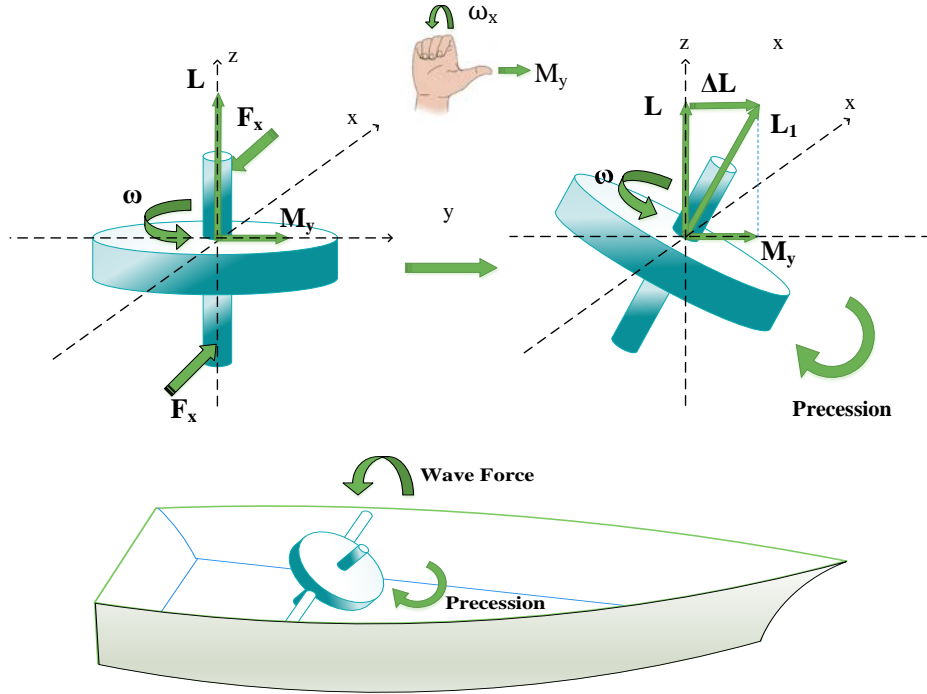


**Figure 5.** Change of angular momentum of the gyroscope.

3) Gyroscope has an angular  $\omega_y$  velocity because of the precession motion. This angular velocity produces a momentum ( $M_x$ ) perpendicular to its direction according to (5) as seen in Figure 6. Angular velocity ( $\omega_y$ ) has the maximum value at the beginning of the precession motion and consequently  $M_x$  is maximum at that time.  $M_x$  and  $L_1$  result as  $M_s$  stabilizing moment. This moment is in the same plane but opposite direction of the roll motion and is called stabilizing moment. The stabilizing moment occurs at the same time as the precession motion and resists the forces caused by the sea waves.

*Mechanical Gyroscope-based Roll Motion Reduction of Marine Vehicles:  
An Educational Setup*

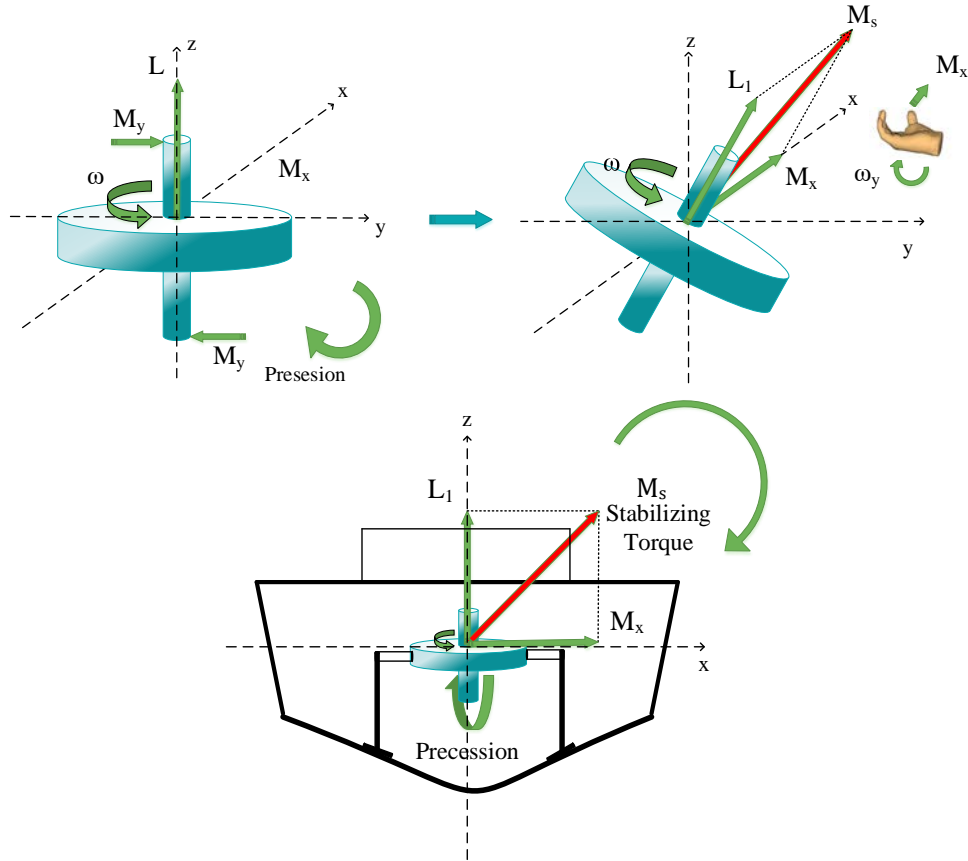


**Figure 6.** Creation of stabilizing moment.

### 3. DESIGN OF THE EDUCATIONAL TOOL

Two experimental setups were designed: dry and wet. The dry setup is designed for use in the laboratory without the need for water and the wet setup is for use with water. The dry setup consists of a mechanical gyroscope, a model boat, a servo system for roll motion generation, and a control circuit to measure the angle of roll motion and drive the servo motor with the intended speed. The model boat that weighs 3 kg is placed on a wooden base and can freely move on the roll axis. A servo motor is attached



to the body of the boat with a stretchy rope. The stretchy rope stimulates the boat in the forward and backward directions as well as allows the gyroscope to get over the wave forces that are generated by the servo system. The servo system swings the boat on the roll axis. These pull and release motions simulate the boat roll due to water waves. The speed of the servo motor can be adjusted to change the stimulated wave effect (amplitude and frequency). The general view of the dry setup is shown in Figure 7.

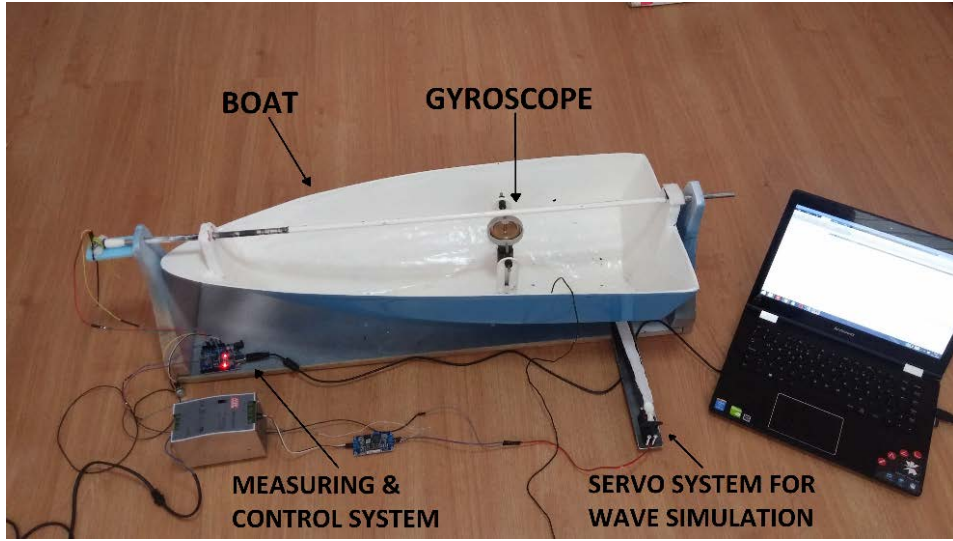


**Figure 7.** General view of the dry setup.

The general view of the wet setup is shown in Figure 8. It consists of a model boat, a mini water pool, a servo motor for roll motion generation, a mechanical gyroscope, and an electronic control system. The model boat weighs 1 kg and it can freely move on the water. A geared dc motor and a metal plate are assembled to generate waves. The metal plate is moved forward and backward periodically in the water to generate waves. The amplitude and frequency of waves can be adjusted by motor speed and angle of the metal plate.

*Mechanical Gyroscope-based Roll Motion Reduction of Marine Vehicles:  
An Educational Setup*

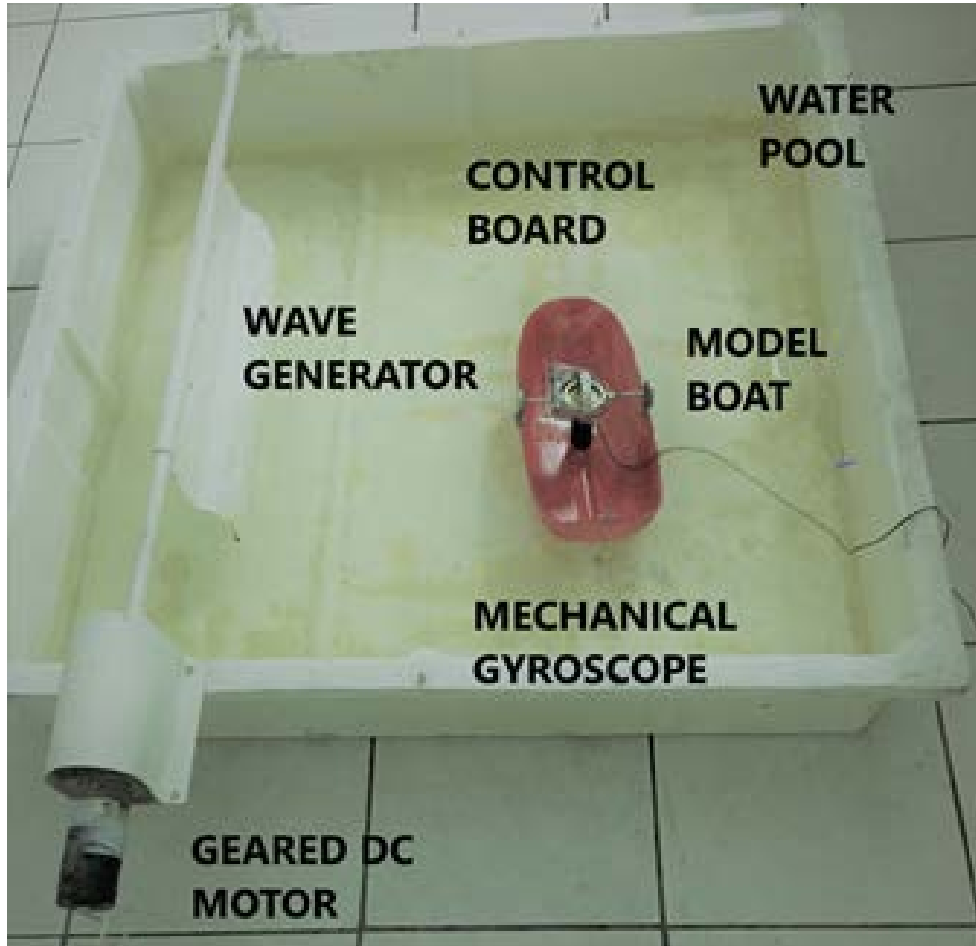


**Figure 8.** General view of the wet setup.

A mechanical gyroscope that is made of brass material is used as a stabilizer. The used gyroscope can be seen on the website at (Gyroscope, n.d.). It has an aluminum frame for bushing and fixing. It is driven by a dc motor that runs up to 12000 rpm. The total weight of the gyroscope is 145 g without the motor and its outer diameter is 62.5 mm. The mechanical gyroscope with dc motor is shown in Figure 9.



**Figure 9.** Mechanical gyroscope.

Three-axis gyro and accelerometer sensor MPU6050 is used to measure the angle of roll motion. It is widely used in acceleration and angle measurements because of its accuracy and low cost. The general diagram of the system is shown in Figure 10.

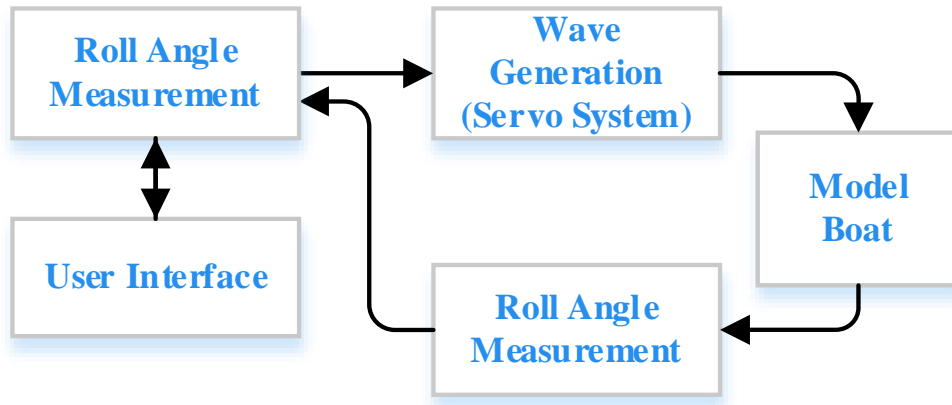


**Figure 10.** General block diagram of the system.

A MATLAB-based graphical user panel is designed to monitor and control the experimental setup. Control of the gyroscope and servo system can be set via the user panel. The angle of the boat's roll motion can be monitored and recorded with the panel. The user panel can be seen in Figure 11.

*Mechanical Gyroscope-based Roll Motion Reduction of Marine Vehicles:  
An Educational Setup*

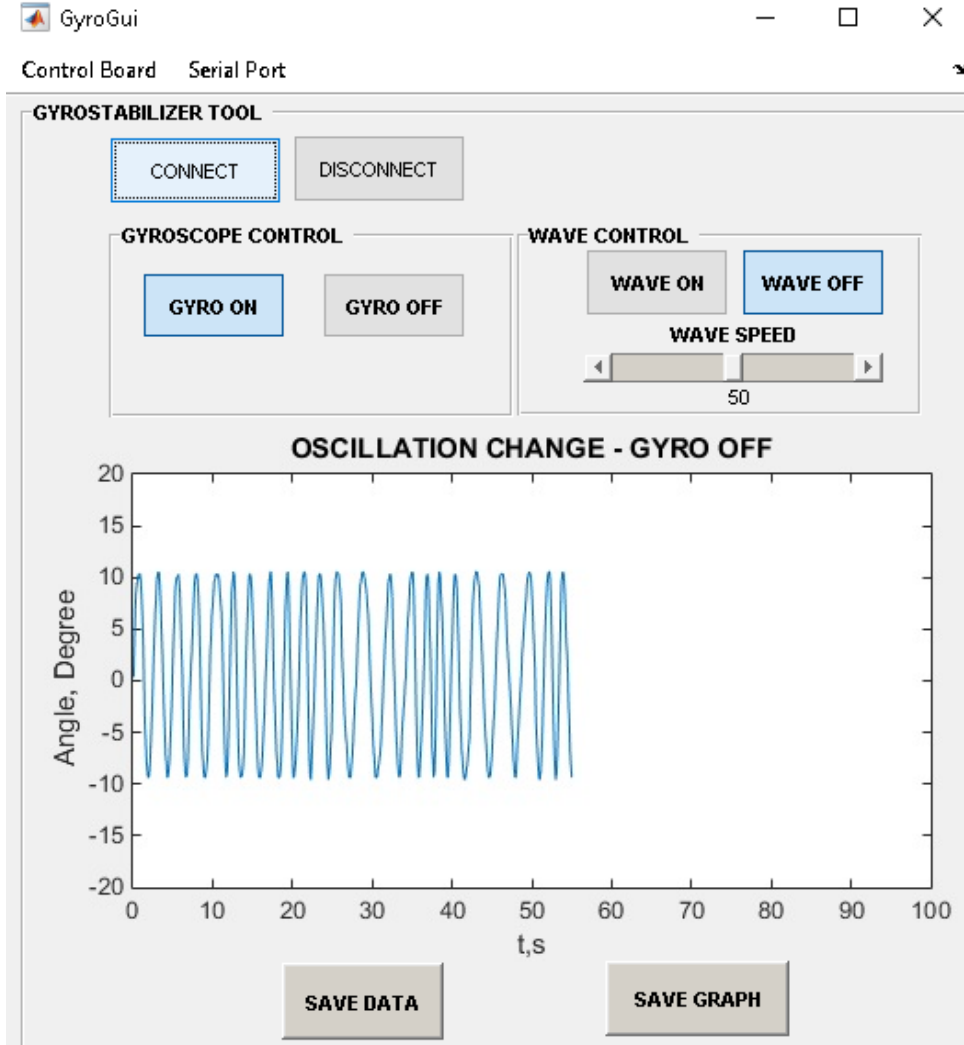


**Figure 11.** Graphical user interface panel.

#### **4. EXPERIMENTAL RESULTS**

The roll angle of the model boat was measured right after releasing the boat from a roll angle position of 20 Degree. The change in the natural rolling

motion is shown in Figure 12. This data can be useful for modeling and finding the damping characteristics of the system (Ertogan et al., 2018).

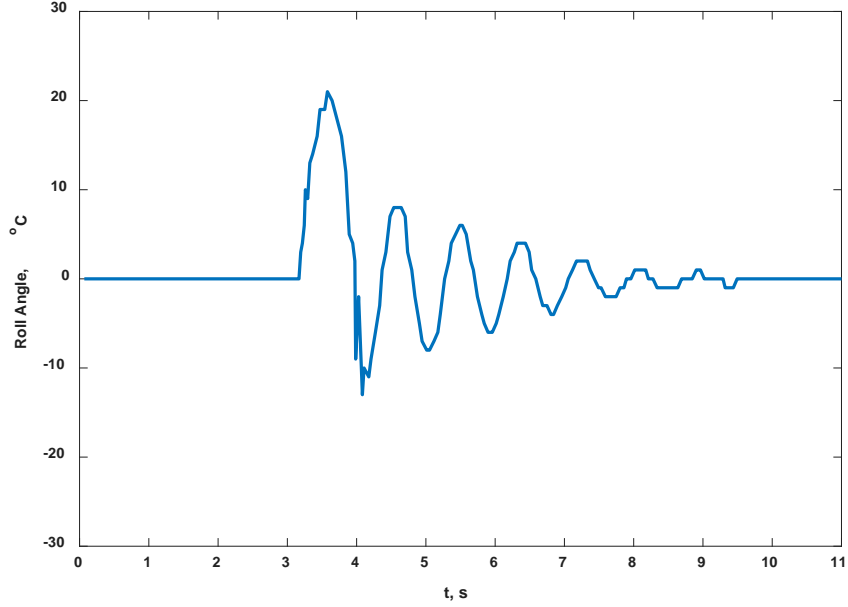


**Figure 12.** Natural roll motion of the model boat.

The gyroscopic effect and creation of the stabilizing moment can be explained step by step with the dry setup. Before running the setup automatically, the vectorial quantity of angular momentum and external torque acting on the boat and the precession of the gyroscope were investigated. When the gyroscope runs at full speed and rotates clockwise direction the angular momentum occurs towards the bottom of the boat. The direction of the angular momentum is shown in Figure 13.

*Mechanical Gyroscope-based Roll Motion Reduction of Marine Vehicles:  
An Educational Setup*

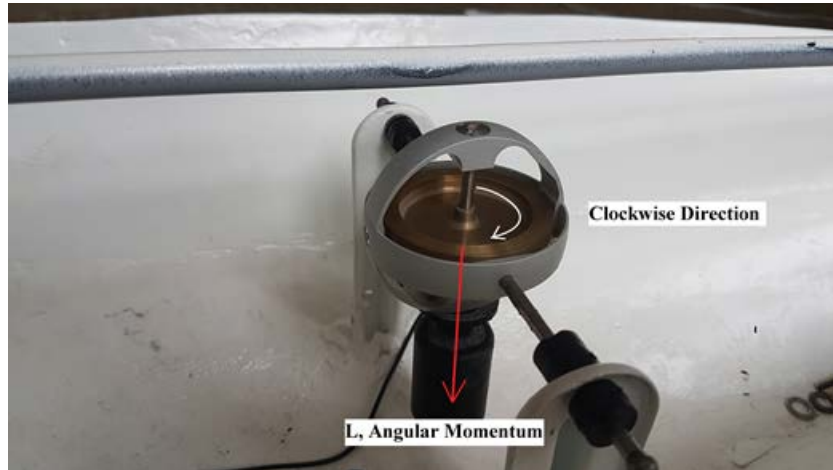


**Figure 13.** Angular momentum of a mechanical gyroscope.

Manual forces applied to the boat can explain the precession of the gyroscope. A force was manually applied to the starboard of the boat by hand while the mechanical gyroscope was rotating clockwise direction. According to the right-hand rule precession motion of the gyroscope is to the foreship direction (or bow part) as seen in Figure 14. It can be confidently stated that Angular momentum ( $L$ ) always follows external torque ( $M_y$ ) and  $L_1$  (stabilizing torque) comes into existence by product of  $L$  and  $M_y$ .



**Figure 14.** Precession motion of the gyroscope while a force is applied to the starboard of the boat.

When the force is applied to the port side of the boat by hand while the mechanical gyroscope is rotating clockwise, the precession motion of the gyroscope is towards the aft part of the boat (or stern part) as seen in Figure 15.

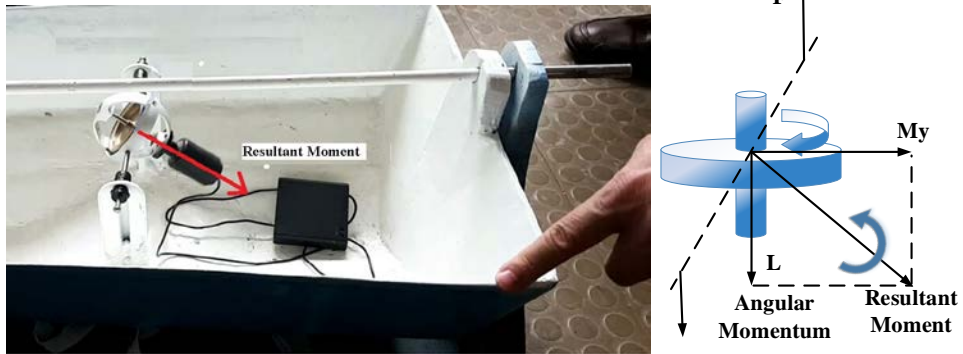


**Figure 15.** Precession motion of the gyroscope while a force is applied to the larboard of the boat.

A pair of forces ( $F$ ) that mimics hand force applied to the port side of the boat is in the  $y$  plane as seen in Figure 16. The gyroscope has an angular velocity  $\omega_y$  because of the precession. This angular velocity and gyroscope spin rate result in a moment in the  $x$ -axis, according to equation (5). This  $M_s$  torque (moment) is in the opposite direction of the applied force and is called stabilizing torque.

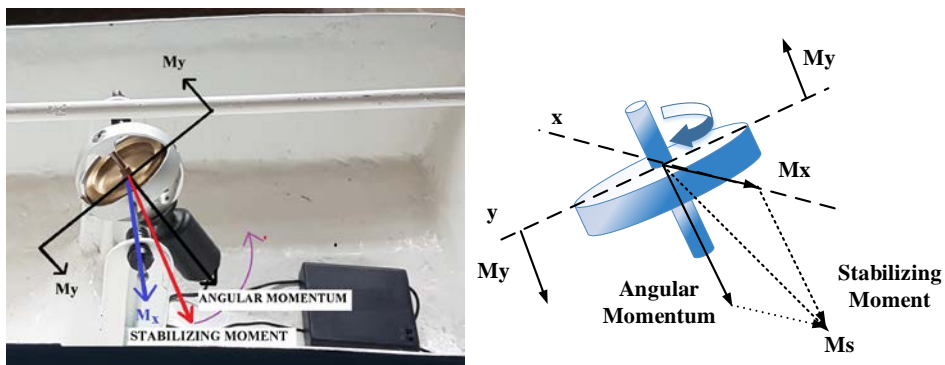


**Figure 16.** Creation of the stabilizing moment.

*Mechanical Gyroscope-based Roll Motion Reduction of Marine Vehicles:  
An Educational Setup*

The boat of dry setup was made to roll at an average wave speed with the servo system. Figure 17 shows the roll angle while the gyroscope is on and off. The roll angle was  $\pm 10$  degrees while the gyroscope was not operating. Two minutes after the gyroscope was powered on, the roll angle was measured as  $\pm 2$  degrees. The transition of the roll angle, while the gyroscope is initially powered on and later on powered off, is shown in Figure 18.

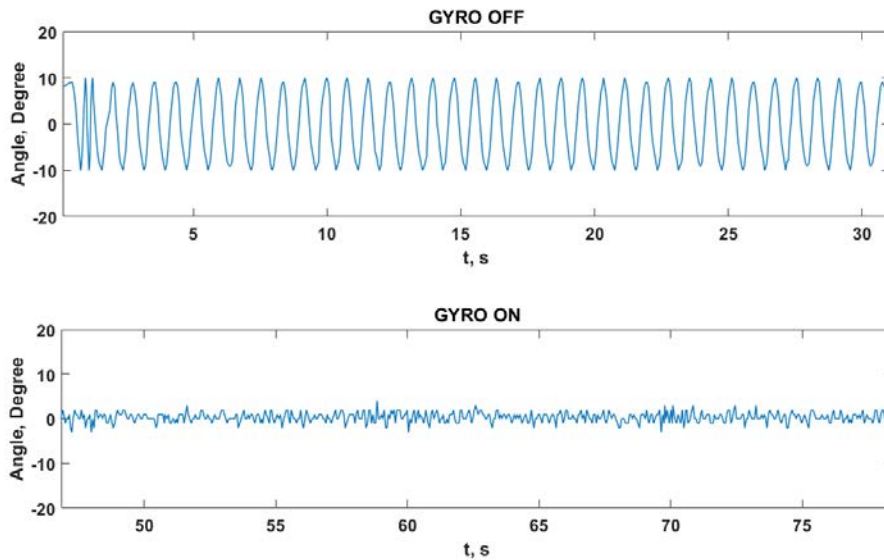


**Figure 17.** The angle of roll motion of the model boat when the gyroscope is on and off for the dry setup.



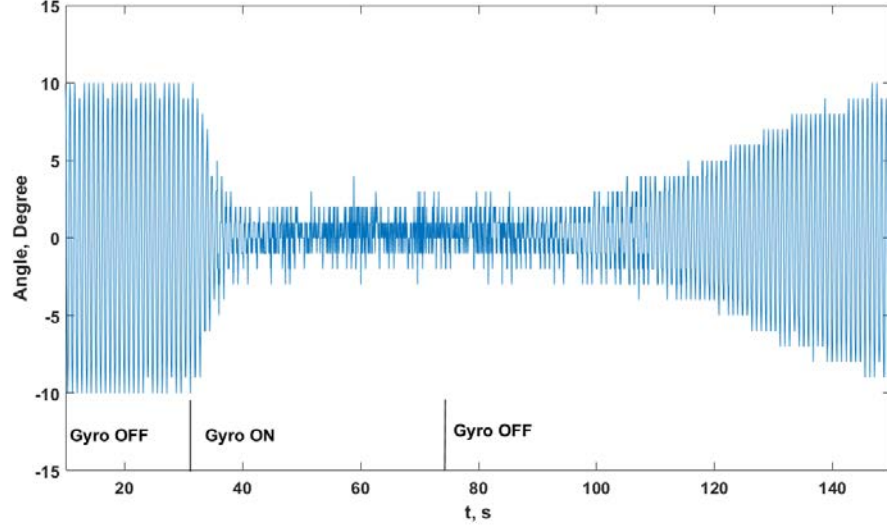


**Figure 18.** The angle of roll motion of the model boat while on and off transitions of the gyroscope for the dry setup.

The second experiment was conducted in the mini water pool with the wet setup. The wave generator was run, and the roll angle was measured and recorded. The roll angle change is shown in Figure 19 and Figure 20 while the gyroscope is powered on and off, respectively. While the gyroscope is off, the angle of the roll motion is approximately  $\pm 30$  degrees. After the gyroscope is turned on, the angle decreases to a range of  $\pm 6$  to  $\pm 8$  degrees.

*Mechanical Gyroscope-based Roll Motion Reduction of Marine Vehicles:  
An Educational Setup*

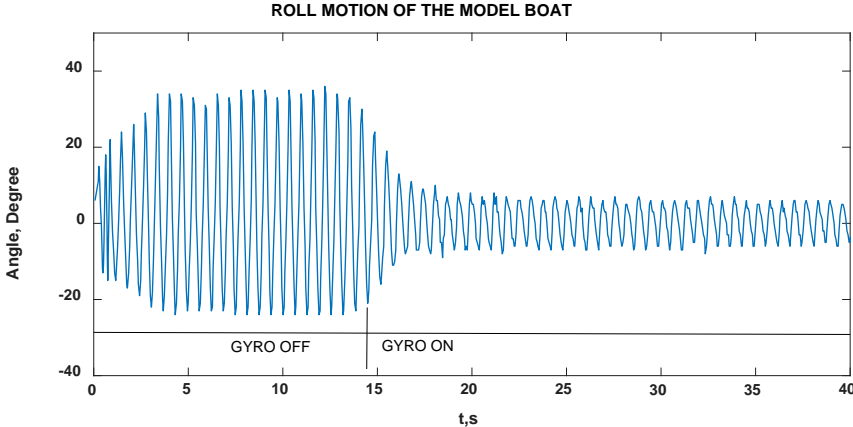


**Figure 19.** The angle of roll motion of the model boat when the gyroscope is on and off for the wet setup.

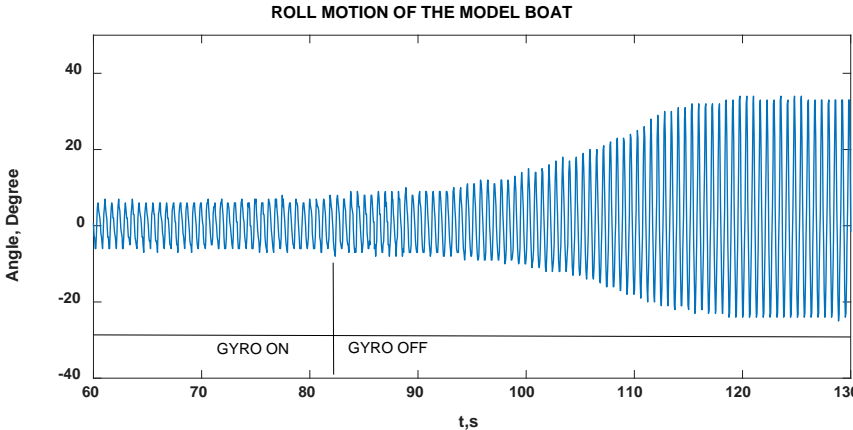


**Figure 20.** The angle of roll motion of the model boat when the gyroscope is on and off for the wet setup.

## **5. CONCLUSION**

Design of educational setups of gyro stabilizers for model marine boats is presented. Electrical and mechanical parts (model boat, dc powered gyroscope, wave generation, measurement of the angle of roll via GUI) of the setups were explained in detail. The performance of the gyro stabilizers was investigated in dry and wet setups and the results were presented. Damping of roll motion of model boats is presented experimentally and the obtained results are discussed. The mechanism of counterforce to balance the wave-generated roll motion is explained and discussed in terms of momentums given in (5) and (6), which include the spin rate and precession motion of the flywheel. The construction of stabilizing torque is alternatively explained and visually depicted with the combination (product) of two vectors (angular momentum vector -due to spin of the flywheel- and external torque -resulting from roll motion of the model due to waves-) in pictures. The second explanation (or combination of two vectors) is easy to trace for students.

Generally speaking, the developed tools will be useful for mechanic, physic, and control laboratories at undergraduate and graduate levels. They will also assist students and researchers in their research on angular momentum and gyroscopic effects.

The current setup provides a basic understanding of the stabilization of the marine vehicle systems and highlights the practical issues in the construction of such a system. Future extensions of the study are to add fin stabilizers and rotor stabilizers to the existing setup to investigate and compare the stabilizing methods. Another future work is to construct a larger wet setup to simulate more realistic ocean waves is being considered, which will be used to develop a control system applying artificial intelligence for marine vehicle stabilization.

*Mechanical Gyroscope-based Roll Motion Reduction of Marine Vehicles:  
An Educational Setup*

**CONFLICT OF INTEREST STATEMENT**

The authors declare no conflict of interest.

## REFERENCES

Bernstein, D. S. (1999). "Enhancing undergraduate control education". *IEEE Control System Magazin*, 19(5), 40-43.

Brennan, L. (1903). *Improvements in and relating to the imparting of stability to otherwise unstable bodies, structures or vehicles* (UK Patent No. 27,212).

DMS (n.d.). "DMS Magnus Master". Retrieved from <https://www.dmsolland.com/en/stabilizers/magnusmaster-2/>

ECP (n.d.). "Model 750: Control Moment Gyroscope". Retrieved from [http://www.ecpsystems.com/controls\\_ctrlgyro.htm](http://www.ecpsystems.com/controls_ctrlgyro.htm)

Ertogan, M., Ertuğrul, S., Wilson, P. A., & Tayyar, G. T. (2018). "Marine measurement and real-time control systems with case studies". *Ocean Engineering*, 159(1), 457-469.

Forbes, T. C. (1904). *Device for steadying ships* (USA Patent No. 769693).

Gyroscope (n.d.). "Super Precision Gyroscope (without gimbals)". Retrieved from <https://www.gyroscope.com/d.asp?product=SUPER2>

Housner, G. W., & Hudson, D. E. (1959). *Applied Mechanics Dynamic*. Van Nostrand Company, Inc.

Karnopp, D. (2002). "Tilt control for gyro-stabilized two-wheeled vehicles". *Vehicle System Dynamics*, 37(2), 145-156.

Lavieri, R. S., Getschko, N., & Tannuri, E. A. (2012). "Roll Stabilization Control System by Sliding Mode". In *9th IFAC Conference on Manoeuvring and Control of Marine Craft*, 45(27), 448-452.

Leve, F. A., Hamilton, B. J., & Peck, M. A. (2015). *Spacecraft Momentum Control Systems*. Springer, Cham.

*Mechanical Gyroscope-based Roll Motion Reduction of Marine Vehicles:  
An Educational Setup*

Lewin, W. (2015, February 08). *Lect 24 - Rolling Motion, Gyroscopes* [Video]. Youtube. Retrieved from [https://www.youtube.com/watch?v=XPUuF\\_dECVI](https://www.youtube.com/watch?v=XPUuF_dECVI)

Oleg, I. B., Vladislav, S. G., Anton, A. P., Alexey, A. B., & Nikolay, A. N. (2016). "Robotic Boat Setup for Control Research and Education". *IFAC-PapersOnLine*, 49(6), 256-251.

Perez, T., & Blanke, M. (2012). "Ship roll damping control". *Annual Reviews in Control*, 36(1), 129-147.

Quanser (n.d.). "Gyro/Stable Platform". Retrieved from <https://www.quanser.com/products/gyrostable-platform/>

Schlick, E. O. (1904). "The gyroscopic effect of flywheels on board ship". *Transactions of the Institute of Naval Architects*, 23(1), 117-134.

Seakeeper (n.d.). "Seakeeper Gyrostabilizers". Retrieved from <https://www.seakeeper.com/>

Sperry, E. A. (1910). "The gyroscope for marine purposes". *Transactions of the Society of Naval Architects and Marine Engineers*, 18(1), 143.

Taur, D. R., & Chern, J. S. (1999). "Rolleron dynamics in missile applications". In *24th Atmospheric Flight Mechanics Conference*, 718-733.

Townsend, N. C., Murphy, A. J., & Sheno, R. A. (2007). "A new active gyrostabilizer system for ride control of marine vehicles". *Ocean Engineering*, 34(1), 1607-1617.

Townsend, N. C., & Sheno, R. A. (2014). "Control Strategies for Marine Gyrostabilizers". *IEEE Journal of Oceanic Engineering*, 39(2), 243-255.

Wesmar (n.d.). “Roll Fin Stabilizing Systems”. Retrieved from <https://www.wesmar.com/commercial-fin-stabilizer-systems>

Woolsey, C. A., & Leonard, N. E. (2002). “Stabilizing underwater vehicle motion using internal rotors”. *Automatica*, 38(12), 2053-2062.

Yamada, M., Higashiyama, H., Namiki, M., & Kazao, Y. (1997). “Active vibration control system using a gyro-stabilizer”. *Control Engineering Practice*, 5(9), 1217-1222.

*Journal of Naval Sciences and Engineering*  
2022, Vol. 18, No. 2, pp. 205-230  
*Electrical-Electronics Engineering/Elektrik-Elektronik Mühendisliđi*

*RESEARCH ARTICLE*

*\*An ethical committee approval and/or legal/special permission has not been required within the scope of this study.*

**THE EFFECT OF FOV ANGLE ON A RSSI-BASED VISIBLE  
LIGHT POSITIONING SYSTEM\***

**Özlem AKGÜN** 

*Barbaros Naval Sciences and Engineering Institute, National Defence  
University, Istanbul, Turkey,  
oakgun@dho.edu.tr*

**Received: 24.06.2022**

**Accepted: 04.08.2022**



Özlem AKGÜN

### ABSTRACT

*The effect of field of view (FOV) angle on the positioning performance in a visible light positioning (VLP) system utilizing light-emitting diodes (LEDs) is examined. Due to its simplicity and low cost, the received signal strength indication (RSSI) technique with trilateration is used for distance measurement. Since being robust to noise sources, the optical code division multiple access (CDMA) is preferred for broadcasting the unique identification and location information of each LED at the same time. LEDs are deployed on the ceiling of a highly reflective room with the aim of providing homogenous and suitable lighting. The varying angle of FOV - 30° up to 88° with 2° increments - is considered in the photodetector (PD) to obtain the effect of FOV on six different VLP scenarios with respect to the number of LEDs. All scenarios have the non-line of sight (NLOS) channel models up to three reflections. Simulation results show that increasing the number of transmitters (Tx) decreases the distance error sensitivity to the changes in the FOV angle. Consequently, indoor scenarios with increased Tx allow the use of low FOV angles. Acceptable distance errors are obtained even in harsh conditions, i.e., near the corner of the room.*

**Keywords:** *Visible Light Positioning, Field of View Angle, Received Signal Strength Indication, Non-Line of Sight Channel Model.*

## **BİR RSSI TABANLI GÖRÜNÜR IŞIK KONUM BELİRLEME SİSTEMİ ÜZERİNE FOV AÇISININ ETKİSİ**

### **ÖZ**

*Bu çalışmada, ışık yayan diyot (LED) kullanan bir görünür ışık konum belirleme (VLP) sisteminde fotodedektör görüş alanı (FOV) açısının konumlandırma performansı üzerindeki etkisi incelenmiştir. Kolay uygulanabilir ve düşük maliyetli oluşu sebebiyle mesafe ölçümü için trilaterasyon ile birlikte, alınan sinyal şiddeti göstergesi tekniği kullanılmıştır. Her bir LED'in kimlik ve konum bilgisini eş zamanlı yaymak için optik kod bölmeli çoklu erişim tekniği, gürültü kaynaklarına dayanıklı olduğundan tercih edilmiştir. Homojen ve yeterli aydınlatma sağlamak amacıyla LED'ler yüksek yansıtıcılığa sahip bir odanın tavanına yerleştirilmiştir. Görüş açısının etkisini elde etmek üzere altı farklı VLP senaryosunda 30°'den 88°'ye kadar 2°'lik artışlarla fotodedektörün FOV açısındaki değişim dikkate alınmıştır. Her bir senaryo üç yansımaya kadar açık görüş gerektirmeyen kanal modeline sahiptir. Simülasyon sonuçları göstermektedir ki verici sayısını artırmak, FOV açısındaki değişikliklere karşı mesafe hatası duyarlılığını azaltır. Sonuç olarak, artırılmış vericilere sahip iç mekân senaryoları, düşük FOV açılarının kullanılmasına izin verir. Oda köşesi gibi zorlu koşullarda dahi kabul edilebilir mesafe hataları elde edilebilir.*

**Anahtar Kelimeler:** *Görünür Işık Konum Belirleme, Görüş Alanı Açısı, Alınan Sinyal Gücü Göstergesi, Açık Görüş Gerektirmeyen Kanal Modeli.*

## **1. INTRODUCTION**

Accurate estimation of a user location is crucial for navigation-based services. In challenging contexts such as indoors, the Global Positioning System (GPS) is inaccurate due to satellites' attenuated and discontinued signals (Zhuang et al., 2018). To overcome this drawback, positioning systems, particularly for indoor environments, utilize indoor wireless signals such as wireless fidelity (Wi-Fi) (Zhuang, Syed et al., 2016), Bluetooth (Hossain & Soh, 2007; Zhuang, Yang et al., 2016), and radio frequency identification (RFID) (Ruiz et al., 2012). These systems, however, have lower positioning accuracy and higher costs (Do & Yoo, 2016; Hassan et al., 2015). Besides, radio frequency (RF) solutions have harmful effects on specific equipment with lower electromagnetic immunity, such as Magnetic Resonance Imaging scanners in health care facilities (Do & Yoo, 2016; Khan, 2017).

The ever-increasing energy demands of the world enable the transition to solid-state lighting (SSL). Energy-efficient LEDs are critical components of this transition. In addition to energy efficiency, LEDs have many key features such as high bandwidth, a long lifetime with reliable lighting, and cost-efficiency. These advantages make LEDs simultaneously used for illumination and indoor positioning (Hann et al., 2010; Lou et al., 2012). Consequently, VLP systems based on LEDs have become extremely popular. Moreover, the VLP system with LEDs obtained more accurate results (0.1-0.35 m positioning error) compared to Wi-Fi (1-7 m), Bluetooth (2-5 m), and RFID ( $\leq 2$  m) (Hassan et al., 2015).

Major positioning algorithms with trilateration rely on time or signal strength measurement. Such measurements are obtained via the so-called time of arrival (TOA), time difference of arrival (TDOA), and RSSI techniques. TOA, the absolute arrival time of a wireless signal from the Tx to the receiver (Rx), is a powerful technique. However, it requires precisely synchronized Tx and Rx. An additional timestamp, causing an increase in the complexity, must be added to the transmitting signal (Hui et al., 2007; Zekavat & Buehrer, 2019). TDOA addresses TOA by overcoming the necessity of synchronization between the Tx and the Rx. But, in TDOA, synchronization is still needed among the Tx to ensure minimum

positioning error (Zhuang et al., 2018). Compared to the techniques mentioned above, the RSSI-based distance measurement using the trilateration algorithm is a promising candidate because of being simple and cost-efficient. Received signal values are easily obtained through a single PD so that there is no need for additional devices. Unlike TOA and TDOA, the performance of RSSI measurements does not strongly depend on the availability of line-of-sight (LOS) channels (Zekavat & Buehrer, 2019). Besides, the trilateration algorithm does not require prior information of an indoor environment as fingerprinting, which is also a positioning algorithm based on the RSSI technique (Guowei et al., 2013; Yiu et al., 2016). Though using the RSSI with trilateration algorithm has attracted much attention, it is generally applied with LOS channels (Kim et al., 2013; Yang et al., 2013; Li et al., 2014; Zhang, Chowdhury et al., 2014). Consequently, research using different channel models, such as those involving NLOS components, is still needed. This study aims to relate the significant advantages of the RSSI-based trilateration positioning algorithm for an NLOS channel model.

The luminous flux emitted from LEDs diffuses in certain directions and reflects from walls, the ceiling, and objects in a room. Though the specular-type light reflections may occur from a shiny object such as a mirror, most reflections are generally diffuse type, which can be modeled well with a Lambertian radiation pattern (Gfeller & Bapst, 1979; Barry, 1994; Kahn et al., 1995). These reflected components of light, briefly NLOS components, significantly contribute to the received signal strength at the PD. In (Mohammed & Elkarim, 2015), the contribution of NLOS components up to three reflections is explored. The localization error distribution for the PD positions in the whole room is obtained for LOS and NLOS cases. In the study (Gu et al., 2016), the effect of multipath reflections on the positioning accuracy is investigated for particularly selected locations. In addition, calibration approaches for selecting LED signals and decreasing the distance between the LEDs are discussed to increase the positioning accuracy. Based on the calibration approach of (Gu et al., 2016), in the work (Tang et al., 2017), the selection of the four strongest LED signals, including multipath reflections, is made by a hybrid algorithm. Then, a weighted centroid algorithm is proposed to detect improved positions. An RSSI-based VLP system with NLOS contributions is studied in (Mousa et al., 2018), where

the system's performance is tested for the case of noisy and noiseless channels. The authors of (Mousa et al., 2018) reported a positioning accuracy of less than 10 cm at a signal-to-noise ratio (SNR) value of more than 12 dB. In the study (Çelik, 2019), with the motivation to increase the overall system performance of RSSI-based VLP, homogeneous illumination is aimed to maximize the individual SNR of each LED. Consequently, the effect of LED deployment is studied to fulfill the aim. Increasing the number of LEDs resulted implicitly in a decreased mean square error (MSE) of distance (Çelik, 2019). Nevertheless, *most* of these studies were conducted under the assumption of a fixed FOV angle of the PD though it is one of the essential features of a VLP system. A switching estimated receiver position scheme is proposed by (Sertthin et al., 2009), where the experiments were performed for three different types of FOV receivers. Each receiver has a constant FOV angle: 25°, 17.5°, and 10°. In the study, however, the distance error performance is analyzed with respect to the tilt angle of a 6-axis geomagnetic and gravity acceleration sensor that increases the complexity of the system. Besides, a two-dimensional positioning error of 29.8 cm was reported for the FOV angle of 10° as the best case. A two-phase hybrid algorithm additional to the conventional triangulation is proposed by (Prince & Little, 2012), where the FOV angle as a function of the receiver's azimuth and elevation orientation is discussed. Course-phase algorithm is tested for FOV angles to detect poor or numerically ill-defined locations. Observations showed that a course estimation could not be made for some orientation configurations when  $FOV \notin [70^\circ, 110^\circ]$ . The most accurate position estimation is provided for the FOV angle of 90° since the receiver could not detect enough light for a smaller FOV angle to make a positioning estimation. Distributions of received power, SNR, and BER are given by (Sendani & Ghahramani, 2017) for three different FOV angles: 30°, 60°, and 90°. Although the authors did not precisely mention the number of transmitters in the system, according to Figure 1 of the study, only four Tx's in a single indoor scenario were considered. Besides, the authors did not discuss the positioning accuracy of the system, which was examined only in the framework of visible light communication (VLC). In the study of (Seguel et al., 2019), FOV analysis is given for imaging receivers to test the proposed algorithm according to the parameter changes of the detector. The authors reported that FOV angles have low impact on

the proposed algorithm, which is an expectable fact since four PDs are used to form an imaging receiver. Additionally, the effect of multipath reflections is not considered in the studies of (Sertthin et al., 2009; Sendani & Ghahramani, 2017; Seguel et al., 2019).

To accurately estimate a position on the PD plane using the trilateration algorithm, at least three LEDs with known locations are required from the LOS model of the channel in the VLP system (Xu et al., 2017). Therefore, NLOS contributions in the RSSIs degrade the localization performance of the VLP. Choosing a small FOV angle in the PD seems to be an easy solution to minimize these contributions. However, it is not too realistic for an indoor environment. Since the vertical distance between the PD plane and the ceiling is constant, the minimum FOV angle of the PD depends on the distances between the Tx points. These distances vary according to the number of Txs used in the indoor scenario, so does FOV. This fact is the primary motivation of our study as we investigate the effect of FOV angle via considering various numbers of indoor scenarios on the performance of RSSI-based VLP system.

## **2. SYSTEM OVERVIEW**

We consider a generalized indoor environment of cubic space, which we will refer to as a room for the rest of the study. Figure 1 illustrates a typical prototype of the system model, where several Txs are deployed on the ceiling for illumination. We assume that the Txs are 0.5 m below the ceiling plane, and a PD is placed anywhere in the room at 0.85 m in height above the ground plane. These assumptions are the same as in the studies (Mohammed & Elkarim, 2015; Çelik, 2019). Each Tx in Figure 1 transmits a unique global identification (ID) code in addition to its local coordinates with respect to the room's origin. The major challenge in the VLP system is to determine the PD's local position from Txs' location coordinates. Once the PD's position is determined, the PD may send its local position to a server. The origin of the room in the local coordinate has a known latitude, longitude, and altitude in the global coordinate. Thus, the server transforms the PD position into a global coordinate.

Each Tx in the room needs a processor for encoding global IDs and local coordinates into bit sequences. Then, a driver circuit switches the LEDs in a

Tx into an on-off state based on a particular modulation scheme. A frequently used method for modulation is the On-Off Keying (OOK). Bit sequences modulate the intensity of the light emitted from each LED. That is why the technique is called intensity modulation (IM). Since there are multiple Txs in the room, a multiplexing protocol is required to distinguish the different signals of each Tx. In this study, as the multiplexing technique, we use the optical CDMA (Lausnay et al., 2015; Lausnay et al., 2014), which can easily be implemented by the OOK modulation and the Walsh codes. Unlike RF communication systems employing complex-valued bipolar signals, VLC (Celik & Çolak, 2020) systems require unipolar real-valued signals when modulating light. A DC bias signal and a turn-off-voltage are added to the bipolar CDMA signal to obtain a unipolar one at the Tx side. The resulting electrical signal is used by the driver circuit switching the LEDs. At the Rx side, we consider the direct detection of the optical carrier belonging to the incoherent light source simply the LEDs. Thus, the baseband VLC channel model, used in this study, is given by (Kahn et al., 1995; Komine et al., 2009; Zhou et al., 2012)

$$y(t) = x(t) \otimes h(t) + n(t), \quad (1)$$

where  $y(t)$  is the output photocurrent,  $x(t)$  is the non-negative optical input power,  $h(t)$  is the channel's impulse response, and the symbol “ $\otimes$ ” stands for the convolution. In Eq.(1),  $n(t)$  corresponds to the signal-independent additive Gaussian noise. There are two types of noise mainly affecting the PD current. One is the shot noise caused by the incident optical power, which includes the desired signal and the background light already present in the VLP environment. Although the background light components in the Rx can be reduced by optical filtering, it still causes shot noise. The second is the thermal noise due to the increasing temperature of the PD during its working process. Thus, in this study, we model the noise,  $n(t)$ , as a signal-independent, zero-mean Gaussian random variable whose variance is  $\sigma^2 = N_0/2$  per dimension. The time-average transmitted optical power which is emitted from each LED in the  $i^{th}$  Tx can be written as

$$P_{t,i}^o = \frac{1}{T_c} \int_0^{T_c} x_i(t) dt, \quad (2)$$

where  $T_c$  is the chip period of the optical CDMA signal. When the optical CDMA signal reaches Rx, the DC component of the photocurrent is first filtered out so that the orthogonality between the CDMA codes is preserved. Next, correlation with known code sequences is performed. After decoding the CDMA signal, the received signal strength is measured and sent as input to the positioning estimator.

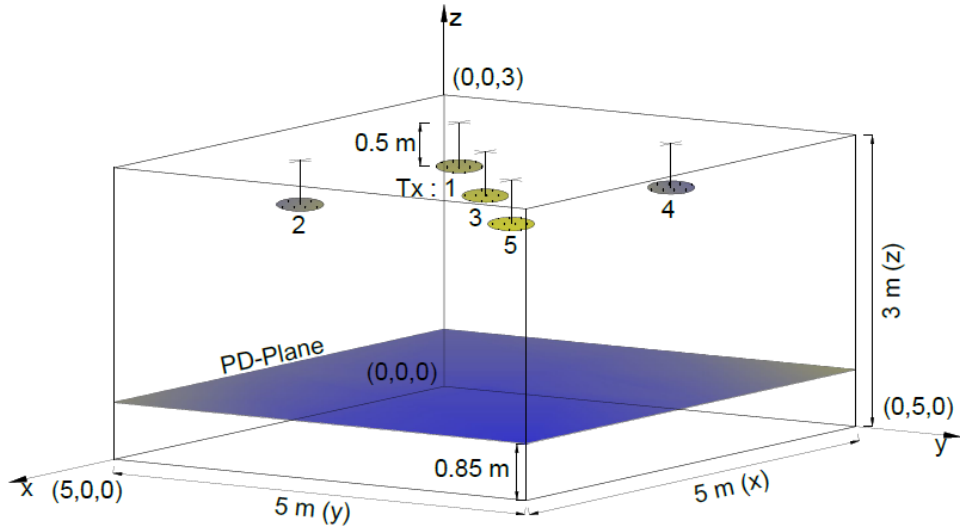


**Figure 1.** Indoor geometry for  $N_t = 5$ .

In this study, we have adopted six different VLP scenarios from (Çelik, 2019) with respect to the number of Tx's,  $N_t$ , to examine the FOV effect which is not discussed in (Çelik, 2019). In each scenario, it is assumed that transmitters are deployed on the ceiling, thereby obtaining the maximum individual SNR from each Tx. The deployment of  $N_t$  transmitters also ensures illumination with a non-flicking effect. These are strong reasons to adopt the indoor scenarios of the study (Çelik, 2019). The coordinates for varying number of Tx's are given in Table 1. According to (Qiu et al., 2018), the VLC-CDMA system using OOK has an SNR value of 20 dB when the bit error ratio (BER) almost reaches  $10^{-3}$  for bipolar-to-unipolar codes with 16 users. As stated by (Qiu et al., 2018), these results are sufficient enough to acquire reliable VLC with CDMA based OOK modulation. Since the study (Çelik, 2019) reported a minimum SNR value of 45 dB for its VLP



scenarios, and this value is much better than the one in (Qiu et al., 2018), we conclude that the multiple access interference (MAI) is prevented thoroughly in our study.

**Table 1.** x-y positions of Tx's.

$N_t$	x-y positions (m)
4	{1.25-1.25; 1.25-3.75; 3.75-1.25; 3.75-3.75}
5	{1.03-1.03; 3.96-1.03; 2.50-2.50; 1.03-3.96; 3.96-3.96}
8	{0.85-0.85; 4.14-0.85; 2.50-1.29; 1.29-2.50; 3.70-2.50; 2.50-3.70; 0.85-4.14; 4.14-4.14}
9	{0.83-0.83; 2.50-0.83; 4.16-0.83; 0.83-2.50; 2.50-2.50; 4.16-2.50; 0.83-4.16; 2.50-4.16; 4.16-4.16}
12	{0.70-0.70; 3.10-0.70; 1.90-1.46; 4.29-1.46; 0.70-2.12; 3.10-2.12; 1.90-2.87; 4.29-2.87; 0.70-3.54; 3.10-3.54; 1.90-4.29; 4.29-4.29}
16	{0.62-0.62; 1.87-0.62; 3.12-0.62; 4.37-0.62; 0.62-1.87; 1.87-1.87; 3.12-1.87; 4.37-1.87; 0.62-3.12; 1.87-3.12; 3.12-3.12; 4.37-3.12; 0.62-4.37; 1.87-4.37; 3.12-4.37; 4.37-4.37}

### 3. METHODOLOGY

#### 3.1. Optical Received Power

In the channel model, we consider the LOS and the NLOS link with three reflections for varying numbers of Tx's, particularly,  $N_t = 4, 5, 8, 9, 12,$  and  $16$ . The relating channel gain coefficient for the VLC link between the  $i^{th}$  Tx and the single Rx is given by  $h_i$ , having two components as follows

$$h_i = h_i^{LOS} + \sum_{n=1}^k h_i^{NLOS(n)}, \quad (3)$$

where  $n$  counts the number of reflections;  $n = \{1, 2, \dots, k\}$ , particularly,  $k = 3$  as we consider three reflections. Since a Lambertian pattern of radiation models the diffuse-type reflections well,  $h_i^{LOS}$  is written by (Barry, 1994)

$$h_i^{LOS} = \frac{(m+1)A}{2\pi d_i^2} \cos^m(\alpha_i) \cos(\beta_i) \text{rect}\left(\frac{\beta_i}{FOV}\right), \quad (4)$$

where  $m$  represents the order of the Lambertian radiation pattern and is related to the semi-angle at half illuminance of the LED.  $A$  is the PD's effective area. The link distance between the  $i^{th}$  Tx and the PD is given by  $d_i$ . While the argument  $\alpha_i$  measures the angle of emergence from the Tx's plane normal to the link between the  $i^{th}$  Tx and the PD,  $\beta_i$  measures the angle of incidence from the PD's plane normal. Since the ceiling and the PD planes are parallel,  $\alpha_i$  is equal to  $\beta_i$  for the LOS link. The  $FOV$  denotes the PD's field of view angle. Finally, the rectangular function,  $\text{rect}\left(\frac{\beta_i}{FOV}\right)$ , equals 1 when the absolute value of its argument is lesser or equal to 1, otherwise it is 0.

As noted in the previous section, most reflections of the visible light rays are generally of the diffuse type as room surfaces are rough compared to the wavelength of visible light. Therefore, it is assumed that the room surfaces consist of numerous differential areas, each of which acts as a transmitter that emits light rays independent of the angle of incidence. Each differential transmitter has a Lambertian radiation pattern then, the NLOS channel gain coefficient from the  $i^{th}$  Tx with  $k$  reflections is as follows (Lee et al., 2011)

$$h_i^{NLOS(k)} = L_i^{(1)} L_i^{(2)} \dots L_i^{(k+1)} \text{rect}\left(\frac{\beta_i^{(k+1)}}{FOV}\right), \quad (5)$$

where

$$\begin{aligned} L_i^{(1)} &= \frac{(m+1)dA}{2\pi d_{i(1)}^2} \cos^m(\alpha_i^{(1)}) \cos(\beta_i^{(1)}), \\ L_i^{(2)} &= \frac{dA}{\pi d_{i(2)}^2} \cos^m(\alpha_i^{(2)}) \cos(\beta_i^{(2)}) \rho_i^{(2)}, \\ L_i^{(k+1)} &= \frac{dA}{\pi d_{i(k+1)}^2} \cos^m(\alpha_i^{(k+1)}) \cos(\beta_i^{(k+1)}) \rho_i^{(k+1)}. \end{aligned} \quad (6)$$

In Eq.(6),  $dA$  is the differential area of the reflecting surface. The parameter  $d_{i(1)}$  represents the link distance between the  $i^{th}$  Tx and the first differential surface, whereas  $d_{i(k+1)}$  denotes the distance after the  $k^{th}$  reflection to the PD. The argument  $\alpha_i^{(1)}$  measures the angle of emergence from the  $i^{th}$  Tx plane normal to the link up to the first differential surface. Similarly,  $\beta_i^{(1)}$  measures the angle of incidence to the first differential reflecting surface. The arguments  $\alpha_i^{(k+1)}$  and  $\beta_i^{(k+1)}$  represent the emergence and the incidence angles after the  $k^{th}$  reflections from the  $i^{th}$  Tx, respectively. The parameter  $\rho_i^{(k+1)}$  is the reflection coefficient indicating the proportion of diffusive reflection of the  $k^{th}$  reflecting surface (Gfeller & Bapst, 1979).

In a multipath channel, the power delay profile (PDP) represents the intensity of the received signal as a function of time delay. According to the PDP analysis, if the correlation bandwidth of the channel is much larger than the bandwidth of the signal, inter-symbol interference (ISI) is not an issue through the channel. In (Çelik, 2019), the PDP analysis of the channel is examined for some of the indoor scenarios adopted in our study. The analysis showed that the ISI effect could be completely ignored for the indoor scenarios under study. In other words, the intensity of light emitted from Tx's in a symbol period is received within the same period. Hence, the optical channel consists of the light intensity collected in a symbol period regardless of time. This fact is another strong reason for adopting the channel models in the study (Çelik, 2019). Therefore, without loss of significance, we may assume that the optical filter gain,  $T_s(\beta)$ , and the optical concentrator gain,  $G(\beta)$ , are equal to 1. Finally, the optical received power can be written as follows (Komine et al., 2009)

$$P_r^o = \sum_{i=1}^{N_t} P_i^o h_i, \quad (7)$$

where  $P_i^o$  is the optical power emitted from each LED in the  $i^{th}$  Tx and equals  $0.45 \sqrt{W}$ . To ensure a fair comparison between the indoor scenarios with respect to the number of Tx's,  $N_t$ , we keep the total optical power constant, which is  $P_{tot}^o = 324 \sqrt{W}$ , by arranging different numbers of LEDs

in each indoor scenario. Table 2 shows the number of LEDs,  $N_{LED}$ , contained in the Tx, and the optical power of each Tx,  $P_{Tx}^o$ .

**Table 2.** Tx Parameters.

$N_t$	$N_{LED}$	$P_i^o (\sqrt{W})$	$P_{Tx}^o (\sqrt{W})$	$P_{tot}^o (\sqrt{W})$
4	180	0.45	81	324
5	144		64.8	
8	90		40.5	
9	80		36	
12	60		27	
16	45		20.25	

### 3.2. RSSI-Based Trilateration Algorithm

This subsection examines the trilateration positioning algorithm based on the RSSI technique. Once the PD has received the transmitted data, the signals from different Tx are separated through the CDMA decoder thanks to the orthogonality of the codes. The PD determines the locations of the Tx, and also measures the electrical power of the received signal from each Tx. The trilateration algorithm (Gu et al., 2014) generally uses at least four link distances between the Tx and the PD to determine the exact location of the PD in three-dimensional (3D) space. Since the link and the vertical distances are not available for an unknown PD location, an iteration algorithm is applied to provide the 3D coordinates of the PD. By estimating the height of the PD to the final estimation, the link distance is calculated, from which the horizontal distance between the Tx and the PD is determined. If the PD is mobile in a known plane, see Figure 1, then, three Tx with known location data are sufficient for the algorithm to adequately determine the PD's position.

A PD which is a direct-detection (DD) receiver has the square-law nature (Barry, 1994). This means that its output electric power is proportional to the square of the input optical power. Hence, the electrical power received from the  $i^{th}$  Tx is written as follows

$$P_{r(i)}^e = (P_i^o h_i R)^2, \quad (8)$$

where  $R$  is the responsivity of the PD. For the LOS link, the angles  $\alpha_i$  and  $\beta_i$  in Eq.(4) are equal to each other so we can write the following relation

$$\cos^{(m+1)}(\alpha_i) = \left(\frac{d_v}{d_i}\right)^{(m+1)} \quad (9)$$

in terms of the link distance,  $d_i$ , and the vertical distance between the Tx and the PD planes, where  $d_v = 1.65 \text{ m}$ . After substituting Eq.(9) and Eq.(4) into Eq.(8), we get the link distance between the  $i^{\text{th}}$  Tx and the PD as follows

$$d_i = \sqrt{(2m+6) \frac{\left(RP_i^o(m+1)A d_v^{(m+1)}\right)^2}{4\pi^2 P_{r(i)}^e}}. \quad (10)$$

Once the link distance is calculated via Eq.(10), at least three horizontal distances between the  $i^{\text{th}}$  Tx and the PD can easily be determined. These horizontal distances can be expressed as (Gu et al., 2014)

$$\begin{aligned} d_1^2 &= (x_{Rx} - x_1)^2 + (y_{Rx} - y_1)^2 + (z_{Rx} - z_1)^2, \\ d_2^2 &= (x_{Rx} - x_2)^2 + (y_{Rx} - y_2)^2 + (z_{Rx} - z_2)^2, \\ d_3^2 &= (x_{Rx} - x_3)^2 + (y_{Rx} - y_3)^2 + (z_{Rx} - z_3)^2. \end{aligned} \quad (11)$$

Here,  $(x_{Rx}, y_{Rx}, z_{Rx})$  is the coordinates of the PD in 3D space, whereas the other coordinates at the right-hand sides of Eq.(11) belong to the three Txs. The last terms for the  $z$ -coordinates of Eq. (11) are all the same since the PD is mobile in the plane with a known altitude. Therefore, subtracting the second and the third equations from the first of Eq.(11) yields the following matrix (Kim et al., 2013)

$$\mathbf{B} = \mathbf{A}\mathbf{x}, \quad (12)$$

where

$$\begin{aligned} \mathbf{B} &= \frac{1}{2} \begin{bmatrix} d_1^2 - d_2^2 + x_2^2 + y_2^2 - x_1^2 - y_1^2 \\ d_1^2 - d_3^2 + x_3^2 + y_3^2 - x_1^2 - y_1^2 \end{bmatrix}, \\ \mathbf{A} &= \begin{bmatrix} x_2 - x_1 & y_2 - y_1 \\ x_3 - x_1 & y_3 - y_1 \end{bmatrix}, \quad \mathbf{x} = \begin{bmatrix} x_{Rx} \\ y_{Rx} \end{bmatrix}. \end{aligned} \quad (13)$$

Eq.(12) can be solved using the linear least square method that is  $\mathbf{x} = (\mathbf{A}^T \mathbf{A})^{-1} \mathbf{A}^T \mathbf{B}$  (Reichenbach et al., 2006).

The received signal strength is sensitive to the indoor environment; therefore, neglecting noise in a VLP system has unrealistic consequences that should be avoided. As stated in the previous section, we model the noise parameter as the signal-independent additive Gaussian noise with a variance of  $\sigma^2$ . The variance is equal to the noise power as its mean value is zero. In (Çelik, 2019), the noise power of the system model is calculated as  $2.5 \times 10^{-12} W$  by using the noise parameters of (Zhang, Duan et al., 2014). Another essential parameter for determining the performance of a VLP system is the signal-to-noise ratio (SNR). The electrical SNR for the  $i^{th}$  Tx in terms of  $\sigma^2$  is given as follows

$$SNR_i = \frac{P_{r(i)}^e}{\sigma^2}. \quad (14)$$

According to (Mohammed & Elkarim, 2015), in the case of the LOS link, the highest received signal power is obtained just under the TxS, where *only*  $N_t = 4$  is studied whose locations are the same as ours, see Table 1. The main factor controlling the localization accuracy is the SNR since the minimum localization error,  $0.18 mm$ , is obtained where the best SNR value is recorded. As the Rx moves to the room corners, the received power gradually decreases. The minimum SNR value is obtained at the corner; consequently, the worst localization error is recorded as  $14.06 cm$ . For the overall link, which consists of LOS and NLOS components, a dramatic increase in the received power near the walls is observed due to their high reflectivity. The reflections have a minor effect at the room center; hence, the SNR is at its maximum value, whereas the localization error is minimal,  $6 cm$ . However, the latter localization error is far worse than that of the LOS link. From this fact, we can conclude that although we have to consider the NLOS contribution for a realistic model of a VLP system, the contribution must be reduced. In this study, the following section with *novel* results discusses the role of *FOV* in reducing the negative effect of NLOS contribution on the positioning accuracy.

#### 4. SIMULATIONS

This section presents the simulation results for the distance error performance with respect to the  $FOV$  angle. Table 3 summarizes the simulation parameters for the considered VLP system.

**Table 3.** Simulation parameters.

Elevation of the LEDs	$-90^\circ$
Azimuth of the LEDs	$0^\circ$
Semi-angle at half power ( $\Phi_{1/2}$ )	$60^\circ$
Lambertian order ( $m$ )	1
Elevation of the PD	$90^\circ$
Azimuth of the PD	$0^\circ$
Responsivity ( $R$ )	$0.4 A/\sqrt{W}$
Area of the PD ( $A$ )	$0.0001 m^2$
Wall reflectivity coefficient ( $\rho_w$ )	0.8
Ceiling reflectivity coefficient ( $\rho_c$ )	0.5
Floor reflectivity coefficient ( $\rho_f$ )	0.3
Area of differential elements ( $dA$ )	$0.04 m^2$

In the simulations, we select three typical PD positions to analyze the effect of the  $FOV$  angle on the distance error performance of the VLP system. The first location is near the center of the room, the other is near the wall edge, and the third location is near the corner of the room, which is the severest case considering the multipath reflections. Figure 2 shows the distance error versus the  $FOV$  angle when the PD is located near the center of the room. It can be seen from Figure 2 that for the indoor scenario with  $N_t = 12$ , the best performance is obtained for the  $FOV$  angles from  $32^\circ$  up to  $88^\circ$ . If a generalization is made from the figure, we can say that the distance error performance improves with the increasing number of TxS, so that the sensitivity of the distance error to the  $FOV$  angle decreases. The exceptions to this generalization are the indoor scenarios for  $N_t = 5$ , and 9 due to the LED deployment that takes into account the illumination issues, see (Çelik,

2019). For those cases, the distance error increases significantly due to the increase in the FOV angle. Another important extraction from Figure 2 is that an increase in the number of Tx's allows lower FOV angles since at least three Tx's must be in the range of the PD due to the trilateration algorithm. This fact also results in reduced reflected signals and improved distance error performance.

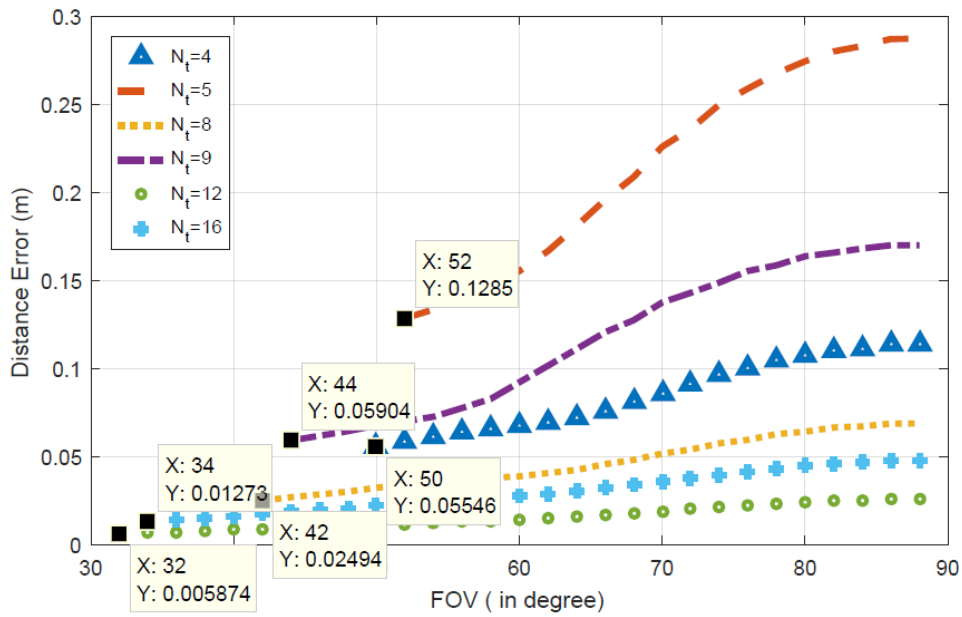


**Figure 2.** Distance error with respect to the FOV angle for the PD position near the center of the room.

Figure 3 demonstrates the distance error performance when the PD is near the left wall edge, chosen intentionally to take severe reflections from one wall. For the left wall, we refer to a typical room geometry in which the left wall is between the wall with an entrance to the room and the wall having windows. The indoor scenarios for  $N_t = 5, 12,$  and  $16$  achieve the minimum distance error with low sensitivity to the changes in the FOV angle. The general idea that the distance error performance increases with the increasing number of Tx's, extracted from Figure 2, is also valid for Figure 3 except for  $N_t = 5$ . For this case, with the aim of uniform illumination, Tx: 3, located at the center of the ceiling plane, pushes the



illuminance of the other four toward the corners, see Figure 1. Thus, the reflections going through the PD weaken for this indoor scenario. Another remarkable situation is that the distance error sensitivity to the  $FOV$  angle is very high for  $N_t = 8$ . When we compare the ordinates of Figure 2 and Figure 3, the distance error gets worse for Figure 3 due to the PD location near the wall edge, which causes severe reflections.

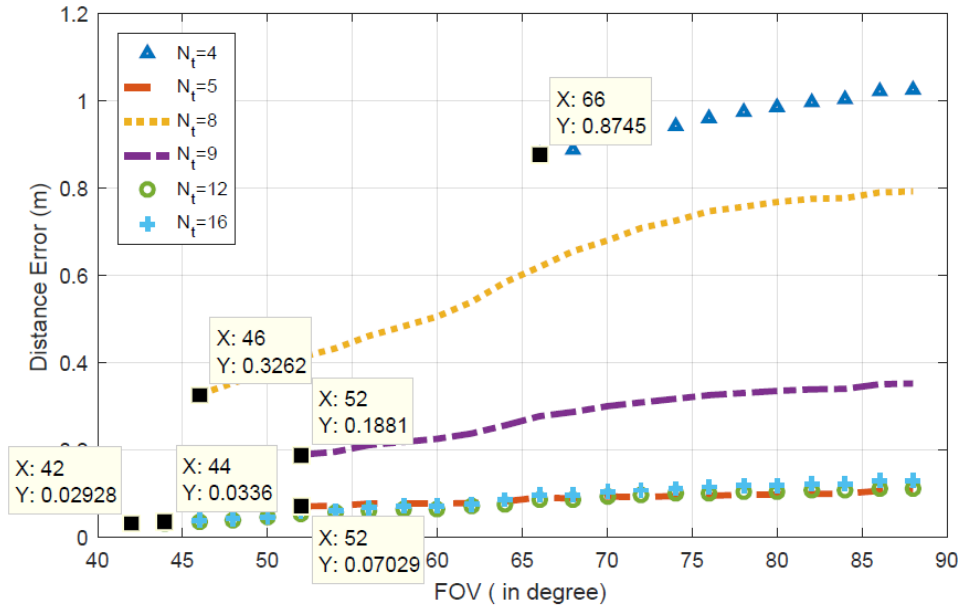


**Figure 3.** Distance error with respect to the  $FOV$  angle for the PD position near the left wall of the room.

In Figure 4, we show the distance error versus the  $FOV$  angle for the PD location near the corner of the room, chosen as the severest case due to intense reflections from the four walls. Compared to others, the scenarios with  $N_t = 12$  and 16 achieve minimum distance errors for all *available*  $FOV$  angles. Besides, the distance error sensitivity to the  $FOV$  angle increases noticeably for these cases. As expected, when we compare the ordinates of Figures 2, 3, and 4, the distance error is the worst for Figure 4. However, it is still possible to achieve satisfactory error performances, i.e., 0.049 m, using an increased number of Tx's and low  $FOV$  angles, i.e.,  $40^\circ$ .

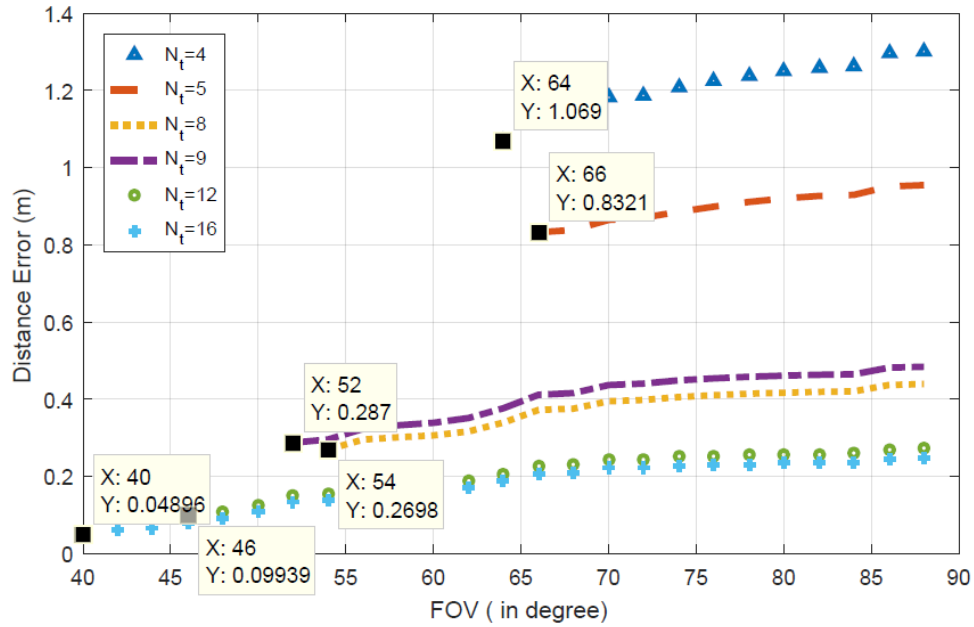


**Figure 4.** Distance error with respect to FOV in the position close to the corner of the room for different indoor scenarios.

## 5. CONCLUSION

In this study, we have investigated the effect of the *FOV* angle of a planar PD for an RSSI-based VLP system. We have also considered illumination constraints in the system model. Positioning errors are evaluated according to the number of TxS, particularly  $N_t = 4, 5, 8, 9, 12,$  and  $16$  at varying *FOV* angles from  $30^\circ$  to  $88^\circ$  with  $2^\circ$  increments. Simulation results have demonstrated that increasing the number of TxS decreases the distance error sensitivity to the changes in the *FOV* angle. Consequently, indoor scenarios with increased transmitters allow the use of low *FOV* angles. Besides, acceptable distance errors are obtained even in harsh conditions, i.e., near the corner of the room.

*Özlem AKGÜN*

**CONFLICT OF INTEREST STATEMENT**

The author declares no conflict of interest.

## REFERENCES

- Barry, J. R. (1994). *Wireless Infrared Communications*. New York: Springer.
- Celik, Y., & Çolak, S. A. (2020). “Quadrature spatial modulation sub-carrier intensity modulation (QSM-SIM) for VLC”. *Physical Communication*, 38, 1-10.
- Çelik, Y. (2019). “The effect of LED deployment on RSSI-based VLP systems”. *European Journal of Science and Technology*, 17, 823-832.
- Do, T. H., & Yoo, M. (2016). “An in-depth survey of visible light communication based positioning systems”. *Sensors*, 16(5), 1–40.
- Gfeller, F. R., & Bapst, U. (1979). “Wireless in-house data communication via diffuse infrared radiation”. *Proceedings of the IEEE*, 67(11), 1474–1486.
- Gu, W., Aminikashani, M., Deng, P., & Kavehrad, M. (2016). “Impact of multipath reflections on the performance of indoor visible light positioning systems”. *Journal of Lightwave Technology*, 34(10), 2578–2587.
- Gu W., Zhang, W., Kavehrad, M., & Feng, L. (2014). “Three-dimensional light positioning algorithm with filtering techniques for indoor environments”. *Optical Engineering*, 53(10), 107107-1–107107-11.
- Guowei, Z., Zhan, X., & Dan, L. (2013). “Research and improvement on indoor localization based on RSSI fingerprint database and K-nearest neighbor points”. *International Conference on Communications, Circuits and Systems* (pp. 68-71). Chengdu, China.
- Hann, S., Kim, J. H., Jung, S. Y., & Park, C. S. (2010). “White LED ceiling lights positioning systems for optical wireless indoor applications”. *36<sup>th</sup> European Conference and Exhibition on Optical Communication* (pp. 1–3). Torino, Italy.

Hassan, N. U., Naeem, A., Pasha, M. A., Jadoon, T., & Yuen, C. (2015). "Indoor positioning using visible LED lights: A survey". *ACM Computing Surveys*, 48(2), 1–32.

Hossain, A. K. M. M. & Soh, W. S. (2007). "A comprehensive study of Bluetooth signal parameters for localization". *18<sup>th</sup> IEEE Annual International Symposium on Personal, Indoor and Mobile Radio Communications* (pp. 1–5). Athens, Greece.

Hui, L., Darabi, H., Banerjee, P., & Liu, J. (2007). "Survey of wireless indoor positioning techniques and systems". *IEEE Transactions on Systems, Man and Cybernetics-Part C: Applications and Reviews*, 37(1), 1067–1080.

Kahn, J. M., Krause, W. J., & Carruthers, J. B. (1995). "Experimental characterization of non-directed indoor infrared channels". *IEEE Transactions on Communications*, 43(2/3/4), 1613–1623.

Khan, L. U. (2017). "Visible light communication: Applications, architecture, standardization and research challenges". *Digital Communications and Networks*, 3(2), 78–88.

Kim, H. S., Kim, D. R., Yang, S. H., Son, Y. H., & Han, S. K. (2013). "An indoor visible light communication positioning system using a RF carrier allocation technique". *Journal of Lightwave Technology*, 31(1), 134–144.

Komine, T., Lee, J. H., Shinichiro, H., & Nakagawa, M. (2009). "Adaptive equalization system for visible light wireless communication utilizing multiple white LED lighting equipment". *IEEE Transactions on Wireless Communications*, 8(6), 2892-2900.

Lausnay, S. D. Strycker, L. D., Goemaere, J. P., Stevens, N., & Nauwelaers, B. (2014). "Optical CDMA codes for an indoor localization system using VLC". *3<sup>rd</sup> International Workshop in Optical Wireless Communications* (pp. 1-5). Funchal, Madeira, Portugal.

*The Effect of FOV Angle on a RSSI-Based Visible Light Positioning System*

- Lausnay, S. D., Strycker, L. D., Goemaere, J. P., Stevens, N., & Nauwelaers, B. (2015). "Influence of MAI in a CDMA VLP system". *International Conference on Indoor Positioning and Indoor Navigation* (pp. 1–9). Banff, AB, Canada.
- Lee, K., Park, H., & Barry, J. R. (2011). "Indoor channel characteristics for visible light communications". *IEEE Communications Letters*, 15(2), 217–219.
- Li, L., Hu, P., Peng, C., Shen, G., & Zhao, F. (2014). "Epsilon: A visible light based positioning system". *11<sup>th</sup> USENIX Symposium Networked Systems Design and Implementation* (pp. 331–343). Seattle, WA, USA.
- Lou, P., Zhang, H., Zhang, X., Yao, M., & Xu, Z. (2012). "Fundamental analysis for indoor visible light positioning system", *1<sup>st</sup> International Workshop on Optical Wireless Communications* (pp. 59–63). Beijing, China.
- Mohammed, N. A., & Elkarim, M. A. (2015). "Exploring the effect of diffuse reflection on indoor localization systems based on RSSI-VLC". *Optics Express*, 23(16), 20297–20313.
- Mousa, F. I. K., Almaadeed, N., Busawon, K., Bouridane, A., Binns, R., Elliot, I. (2018). "Indoor visible light communication localization system utilizing received signal strength indication technique and trilateration method". *Optical Engineering*, 57(1), 1–10.
- Prince, G. B., & Little, T. D. C. (2012). "A two phase hybrid RSS/AoA algorithm for indoor device localization using visible light". *IEEE Global Communications Conference* (pp. 3347-3352). Anaheim, CA, USA.
- Qiu, Y., Chen, S., Chen, H. H., & Meng, W. (2018). "Visible light communications based on CDMA technology". *IEEE Wireless Communications*, 25(2), 178–185.

Reichenbach F., Born, A., Timmermann, D., & Bill, R. (2006). “A distributed linear least squares method for precise localization with low complexity in wireless sensor networks”. *2<sup>nd</sup> IEEE International Conference on Distributed Computing in Sensor Systems* (pp. 514-528). San Francisco, CA, USA.

Ruiz, A. R. J., Granja, F. S., Honorato, J. C. P., & Rosas, J. I. G. (2012). “Accurate pedestrian indoor navigation by tightly coupling foot-mounted IMU and RFID measurements”. *IEEE Transactions on Instrumentation and Measurement*, 61(1), 178–189.

Seguel, F., Krommenacker, N., Charpentier, P., & Soto, I. (2019). “A novel range free visible light positioning algorithm for imaging receivers”. *Optik*, 195, 163028-1–163028-21.

Sendani, N., & Ghahramani, R. (2017). “Study the effect of FOV in Visible Light Communication”. *International Research Journal of Engineering and Technology*, 4(10), 759-763.

Sertthin, C., Tsuji, E., Nakagawa, M., Kuwano, S., & Watanabe, K. (2009). “A switching estimated receiver position scheme for visible light based indoor positioning system,” *4th International Symposium on Wireless Pervasive Computing* (pp. 1–5). Melbourne, Australia.

Tang, W., Zhang, J., Chen, B., Liu, Y., Zuo, Y., Liu, S., Dai, Y. (2017). “Analysis of indoor VLC positioning system with multiple reflections”. *16th International Conference on Optical Communications and Networks* (pp. 1–3). Wuzhen, China.

Xu, Y., Wang, Z., Liu, P., Chen, J., Han, S., ... Yu, J., (2017). “Accuracy analysis and improvement of visible light positioning based on VLC system using orthogonal frequency division multiple access”. *Optics Express*, 25(26), 32618–32630.

Yang, S. H., Jeong, E. M., Kim, D. R., Kim, H. S., Son, Y. H., Han, S. K. (2013). "Indoor three-dimensional location estimation based on LED visible light communication". *Electronics Letters*, 49(1), 1–2.

Yiu, S., Dashti, M., Claussen, H., & Perez-Cruz, F. (2016). "Locating user equipments and access points using RSSI fingerprints: A Gaussian process approach". *IEEE International Conference on Communications*. (pp. 1-6). Kuala Lumpur, Malaysia.

Zekavat, S. A. R., & Buehrer, R. M. (2019). *Handbook of Position Location: Theory, Practice, and Advances*. Hoboken, NJ: John Wiley & Sons.

Zhang, W., Chowdhury, M. I. S., & Kavehrad, M. (2014). "Asynchronous indoor positioning system based on visible light communications". *Optical Engineering*, 53(4), 045105-1–045105-10.

Zhang X., Duan, J., Fu, Y., & Shi, A. (2014). "Theoretical accuracy analysis of indoor visible light communication positioning system based on received signal strength indicator". *Journal of Light Wave Technology*, 32(21), 4180–4186.

Zhou, Z., Kavehrad, M., & Deng, P. (2012). "Indoor positioning algorithm using light-emitting diode visible light communications". *Optical Engineering*, 51(8), 085009-1–085009-6.

Zhuang, Y., Hua, L., Qi, L., Yang, J., Cao P., Cao Y., ... Haas, H. (2018). "A survey of positioning systems using visible LED lights". *IEEE Communications Surveys & Tutorials*, 20(3), 1963–1988.

Zhuang, Y., Syed, Z., Li, Y., & El-Sheimy, N. (2016). "Evaluation of two WiFi positioning systems based on autonomous crowdsourcing of handheld devices for indoor navigation". *IEEE Transactions on Mobile Computing*, 15(8), 1982–1995.



*Özlem AKGÜN*

Zhuang, Y., Yang, J., Li, Y., Qi, L., & El-Sheimy, N. (2016). "Smartphone-based indoor localization with Bluetooth low energy beacons". *Sensors*, 16(5), 1-20.

RESEARCH & REVIEW ARTICLE

*\*An ethical committee approval and/or legal/special permission has not been required within the scope of this study.*

**AN EXTENSION OF THE LAST WORK OF OLEG A. TRETYAKOV:  
A NOVEL FORMAT OF THE WAVE EQUATION IN SI UNITS\***

**Fatih ERDEN<sup>1</sup>\***   
**Ahmet Arda ÇOŞAN<sup>1,2</sup>** 

<sup>1</sup>*National Defence University, Turkish Naval Academy,  
Department of Electrical and Electronics Engineering, Istanbul, Turkey,  
ferden@dho.edu.tr*

<sup>2</sup>*Gebze Technical University,  
Department of Electronics Engineering, Kocaeli, Turkey,  
acosan@dho.edu.tr*

**Received: 25.09.2022**

**Accepted: 26.10.2022**

**ABSTRACT**

*Professor Oleg Alexandrovich Tretyakov is recognized in the field of radiophysics as founder of Evolutionary Approach to Electromagnetics (EAE). His analytical time domain approach which was acknowledged as an alternative to the method of complex amplitudes successfully applied to cavity and waveguide problems. In his final years, he proposed a novel format of Maxwell's equations in SI units where electric and magnetic field strength vectors have a common physical dimension of inverse meter. In this article, we pay special tribute to his exceptional career and contributions to science and extend his last work to derive a novel format of the wave equation in SI units.*

**Keywords:** *Maxwell's Equations, Time-domain Electrodynamics, Electromagnetics, Evolutionary Approach, Wave Equation.*

**OLEG A. TRETYAKOV'UN SON ALIŐMASININ BİR UZANTISI:  
SI BİRİM SİSTEMİNDE YENİ BİR DALGA DENKLEMİ FORMATI**

**ÖZ**

*Profesör Oleg Alexandrovich Tretyakov, radyofizik alanında Elektromanyetik Teoriye Evrimsel Yaklaşım'ın (ETEY) kurucusu olarak tanınmaktadır. Frekans domeni metodlarına bir alternatif olarak kabul edilen Tretyakov'un analitik zaman domeni metodu, kavite ve dalga kılavuzu problemlerine başarıyla uygulanmıştır. Son yıllarında, elektrik ve manyetik alan şiddet vektörlerinin bir bölü metre'lik ortak bir fiziksel boyuta sahip olduğu, SI birimler sisteminde yeni bir Maxwell denklemler formu önermiştir. Bu makalede, istisna kariyerine ve bilime yaptığı katkılara özel bir saygı sunarak önerdiği yeni formdaki Maxwell denklemler sisteminden faydalanarak SI birimler sisteminde yeni bir dalga denklemi formu önerilmiştir.*

**Anahtar Kelimeler:** Maxwell Denklemleri, Zaman Uzayı Elektrodinamiği, Elektromanyetik, Evrimsel Yaklaşım, Dalga Denklemi.

## 1. INTRODUCTION

Professor Oleg Alexandrovich Tretyakov passed away on Tuesday, January 25, 2022, after a short battle with lung cancer. His contributions to the growth of electromagnetics research in Ukraine and Turkey are remarkable. He will be greatly missed by his friends and colleagues around the world.

As the Chairman of Commission B of the International Union of Radio Science (URSI) Committee of Ukraine since 1993, and a member of the Institute of Electrical and Electronics Engineers (IEEE), he was a distinguished reviewer of the November 2021 issue of the Journal of Naval Sciences and Engineering. Both URSI Radio Science Bulletin and IEEE Antennas and Propagation Magazine announced the sad news to the radiophysics and electromagnetic communities by publishing the *In Memoriam* letters reflecting his scientific career and main contributions (Erden, 2022a; Erden, 2022b).

In this article, we pay special tribute to his exceptional career and contributions to science and extend his final work to derive a novel format of the wave equation in SI units.

## 2. EVOLUTIONARY APPROACH

Professor Tretyakov is best known for the *Evolutionary Approach to Electromagnetics (EAE)* which was proposed by him for the analytical solution of cavity and waveguide problems directly in the time domain (Tretyakov, 1986; Tretyakov, 1993).

His approach was acknowledged as an alternative to *the classical time-harmonic field method*, namely *the method of complex amplitudes* (Tretyakov & Erden, 2012; Tretyakov, 2018). It was proved that the set of natural cavity modes originates a complete set of vector functions of coordinates in an appropriate class of quadratically integrable functions (i.e., it is a *modal basis*). Following the pioneering work by Kisunko (1949), Tretyakov (1989; 1994) pushed his approach into the waveguide problems.

Hence, by making use of this approach, the electromagnetic fields in cavities and waveguides were presented as *series in terms of their natural modes with their amplitudes sought for* where the cavity modal amplitudes depend on

time  $t$ , and the waveguide modal amplitudes are functions of  $t$  and axial coordinate  $z$ . In the cavity case, *evolutionary ordinary* differential equations were derived for the modal amplitudes via projecting Maxwell's equations onto the modal basis. As for the waveguide modal amplitudes, *evolutionary partial* differential equations were obtained.

For the cavity problem, the time-dependent modal amplitudes were obtained explicitly when an impressed force is given as an arbitrary *integrable* function of time. For the waveguide problem, the evolutionary equations for the waveguide modes were obtained. Longitudinal components of the waveguide modes satisfy some partial differential equations, which are generalizations of the well-known Klein-Gordon equation. Modal amplitudes for transverse fields were found as  $z$ - and  $t$ - *derivatives* of the longitudinal components. Using his approach, exact explicit solutions for the cavity oscillations, and for waveforms propagating in waveguides are successfully studied over decades.

### 3. IMPLEMENTATION OF THE APPROACH

The method, first, was applied to free space, considered a regular structure, in a cylindrical coordinate system. Modes for this case had already been found in the frequency domain. Tretyakov and Dumin (2000) shifted this approach to the time domain for analysis of transient beam radiation and propagation using an expansion over Bessel modes with mode amplitudes being governed by the Klein-Gordon equation (KGE) formulated earlier. The main peculiarity, in this case, is that since the transverse domain is now unbounded, the mode spectrum is continuous which leads to integrals instead of sums in the mode expansion.

Butrym and Tretyakov (2002) introduced the next main improvement of the method for waveguides where in an inhomogeneous waveguide the permittivity and permeability functions of the filling are some functions of transverse coordinates (which goes into the boundary value problem for the modes) and a function of the longitudinal coordinate and time. The latter goes into the evolutionary waveguide equations as coefficients that govern the modes' amplitude transformation with propagation. In this case, the mode coupling was unavoidable.

## A Novel Format of the Wave Equation in SI Units

A detailed implementation of the EAE for studying a time-variant hollow cavity system was published by Aksoy and Tretyakov (2002). Later, Aksoy and Tretyakov (2003a, 2003b) obtained explicit solutions for the cavity oscillations excited by a set of digital signals.

Within EAE, Butrym et al. (2004) solved the problems of short pulse propagation and diffraction from a permittivity step in a waveguide with a detailed time-domain energy flow analysis. Later, Butrym and Legenkiy (2009) considered the same problem for a conductive boundary with emphasis on the effect of transient charge displacement by a pulsed E-wave.

Aksoy et al. (2005) compared the calculation results of EAE with the Finite Difference Time Domain (FDTD) for the cavity filled with a dispersive medium. Antyufeyeva et al. (2009) considered a cavity with a double negative medium as an example. It was shown that due to the interaction of a spatial resonance in the cavity (due to waves bouncing between the walls) with local medium resonances (due to molecular oscillations), there are several possible frequency resonances for a single spatial mode distribution. Antyufeyeva and Tretyakov (2010) considered the problem of the transient (nonstationary) homogeneous medium in a cavity.

Erden and Tretyakov (2008) studied excitation of the electromagnetic fields by a wide-band current surge in a hollow cavity, and later, in a cavity filled with Debye and Lorentz kind dispersive medium (Tretyakov and Erden, 2008). The results were presented in several international conferences (Tretyakov & Erden, 2006; Erden & Tretyakov, 2011; Erden & Tretyakov, 2014; Erden, Tretyakov, & Bicer, 2016; Erden & Tretyakov, 2019). Therein, the Debye and Lorentz equations play the role of the dynamic constitutive relation between the polarization vector and the electric field. Tretyakov and Erden (2007) also presented the instantaneous and dynamic parts of polarization separately for the Debye medium.

Later, the interaction of the cavity fields with plasma is studied within EAE, making use of the motion equation for plasma (Erden, 2017a; Erden, 2017b; Erden, 2018; Erden, 2015; Erden & Bicer, 2016).

Regarding the waveguide problem, Aksoy and Tretyakov (2004) considered the excitation and propagation problem of digital signals in a hollow waveguide by making use of the method. Solving the KGE explicitly, a

special case has been considered by Tretyakov and Akgun (2010) where the modal amplitudes of the waveguide fields are expressible explicitly via the Airy functions from mathematical physics. The complete set of TE- and TM-time-domain modal waves is established and studied in detail by Tretyakov and Kaya (2012; 2013). As a result of dealing with real-valued functions in the time domain, Eroglu, Aksoy, & Tretyakov (2012), Akgun and Tretyakov (2015) and Erden (2017) obtained explicit solutions for the energetic properties of the modal waveforms.

The velocity of transportation of the modal field energy, defined by the power flow and energy densities, is derived, and presented as a function of time and axial coordinate (Erden, Cosan, & Tretyakov, 2016; Tretyakov & Erden, 2016; Erden & Tretyakov, 2017; Cosan, Erden, & Tretyakov, 2019). Recently, analytical solutions for the causal oscillations in a cavity with lossy walls presented through the upgraded version of the EAE (Erden, 2021a; Erden, 2021b; Erden et al, 2021; Tretyakov et al., 2021).

Lately, the electromagnetic inertia and the mechanical momentum of the electromagnetic fields for any closed cylindrical waveguide are obtained and presented to the radiophysics community (Tretyakov, 2017; Erden & Tretyakov, 2017; Erden, Tretyakov, & Cosan, 2018; Erden, Cosan, & Tretyakov, 2017; Erden & Tretyakov, 2018; Erden, Cosan, & Tretyakov, 2018; Tretyakov & Erden, 2020; Tretyakov & Erden, 2021).

Ongoing research within the framework of the evolutionary approach by Professor Tretyakov's former students and colleagues is listed in detail in the recent book chapter (Tretyakov, Butrym, & Erden, 2021).

#### **4. A NOVEL FORMAT OF MAXWELL'S EQUATIONS**

In his final years, Professor Tretyakov presented a novel format of Maxwell's equations in SI units (Tretyakov & Erden, 2020; Tretyakov & Erden, 2021, Tretyakov, Butrym, & Erden, 2021). Quantities occurring in Maxwell's equations are rescaled so that the various relationships appear in a dimensionally simpler format.

This perspective is implemented in the evolutionary approach to develop an adequate time-domain theory of cavities and waveguides. As the new format

## A Novel Format of the Wave Equation in SI Units

of Maxwell's equations is rather simpler than the standard one, the upgraded version of the EAE was found more convenient for practical applications (Kobayashi & Smith, 2021, p. 16).

Utilizing the novel format of Maxwell's equations proposed by Professor Tretyakov, energetic and mechanical field characteristics are obtained as functions of time, and the concept of modes in the time-harmonic setting for oscillations in cavities and waves in waveguides has its counterpart in time-dependent modal amplitudes.

The central point in rearranging Maxwell's equations to a new format in SI units is based on the *novel definition* of the free-space constants and charge density as

$$\varepsilon_0^V = \sqrt{\frac{1N}{\varepsilon_0}} \left[ V = \frac{Nm}{As} \right], \quad \mu_0^A = \sqrt{\frac{1N}{\mu_0}} [A], \quad \varrho = \frac{\rho}{\sqrt{N\varepsilon_0}} [m^{-2}] \quad (1)$$

where  $N$  is a force of one *newton*.  $\varepsilon_0^V$ , with its numerical value of  $3.361 \times 10^5$ , and  $\mu_0^A$ , with its numerical value of  $8.921 \times 10^2$ , are used as the *scaling coefficients* for the standard electric,  $\mathcal{E}$ , and magnetic,  $\mathcal{H}$ , fields to divide the physical dimensions of  $[V/m]$  and  $[A/m]$  as

$$\left. \begin{aligned} \underbrace{\mathcal{E}(\mathbf{r}, t)}_{[V/m]} &= \underbrace{\varepsilon_0^V}_{[V]} \underbrace{\mathbb{E}(\mathbf{r}, t)}_{[1/m]} = \frac{3.361 \times 10^5}{[V]} \times \underbrace{\mathbb{E}(\mathbf{r}, t)}_{[1/m]} \\ \underbrace{\mathcal{H}(\mathbf{r}, t)}_{[A/m]} &= \underbrace{\mu_0^A}_{[A]} \underbrace{\mathbb{H}(\mathbf{r}, t)}_{[1/m]} = \frac{8.921 \times 10^2}{[A]} \times \underbrace{\mathbb{H}(\mathbf{r}, t)}_{[1/m]} \\ \underbrace{\mathcal{J}(\mathbf{r}, t)}_{[A/m^2]} &= \underbrace{\mu_0^A}_{[A]} \underbrace{\mathbb{J}(\mathbf{r}, t)}_{[1/m^2]} = \frac{8.921 \times 10^2}{[A]} \times \underbrace{\mathbb{J}(\mathbf{r}, t)}_{[1/m^2]} \end{aligned} \right\} \quad (2)$$



The SI dimensions of volt  $[V]$  and of ampere  $[A]$  are assigned to the factors  $\varepsilon_0^V$  and  $\mu_0^A$ , in the new definition. So, instead of the standard format of Maxwell's equations in SI units presented as

$$\begin{aligned}
 \nabla \times \mathcal{H}(\mathbf{r}, t) &= \varepsilon_0 \frac{\partial}{\partial t} \mathcal{E}(\mathbf{r}, t) + \mathcal{J}(\mathbf{r}, t) \\
 \nabla \times \mathcal{E}(\mathbf{r}, t) &= -\mu_0 \frac{\partial}{\partial t} \mathcal{H}(\mathbf{r}, t) \\
 \nabla \cdot \mathcal{H}(\mathbf{r}, t) &= 0 \\
 \nabla \cdot \mathcal{E}(\mathbf{r}, t) &= \frac{1}{\varepsilon_0} \rho(\mathbf{r}, t)
 \end{aligned} \tag{3}$$

the *new SI format* of the set of Maxwell's equations was proposed as

$$\begin{aligned}
 \nabla \times \mathbb{H}(\mathbf{r}, t) &= \frac{1}{c} \frac{\partial}{\partial t} \mathbb{E}(\mathbf{r}, t) + \mathbb{J}(\mathbf{r}, t) \\
 \nabla \times \mathbb{E}(\mathbf{r}, t) &= -\frac{1}{c} \frac{\partial}{\partial t} \mathbb{H}(\mathbf{r}, t) \\
 \nabla \cdot \mathbb{H}(\mathbf{r}, t) &= 0 \\
 \nabla \cdot \mathbb{E}(\mathbf{r}, t) &= \varrho(\mathbf{r}, t)
 \end{aligned} \tag{4}$$

where  $c$  is the speed of light. The convenience of the *new format* of Maxwell's equations (4) to upgrade the EAE for solving some practical problems was exhibited in late studies (Erden, Tretyakov, & Cosan, 2018; Erden & Tretyakov, 2017; Tretyakov, 2018; Tretyakov, Butrym, & Erden, 2021; Tretyakov & Erden, 2021). One can easily obtain the standard format (3) by making use of the novel format of Maxwell's equations (4) together with equation (2). The novel field vectors in (4),  $\mathbb{E}$  and  $\mathbb{H}$ , have the inverse meter  $[1/m]$  physical dimension, whereas the standard field vectors in (3),  $\mathcal{E}(\mathbf{r}, t)$  and  $\mathcal{H}(\mathbf{r}, t)$ , have physical dimension of  $[V/m]$  and  $[A/m]$ , respectively.

## 5. DERIVATION OF A NOVEL FORMAT OF WAVE EQUATION

Tretyakov and Erden (2021) exhibited Maxwell's equations in the novel format for the fields in free space, plasma and dielectrics. The mathematical format of (4) one-to-one coincides with the Heaviside-Lorentz form of Maxwell's equations (Carron, 2015; Rothwell & Cloud, 2001) albeit the latter have been derived within the framework of the CGS metric system. There is one more coincidence between (4) and Heaviside-Lorentz form, namely: the electric and magnetic field vectors have their common dimensions. In Heaviside-Lorentz form, this dimension is in centimeter-gram-second as  $\left[ g^{\frac{1}{2}} cm^{\frac{1}{2}} s^{-1} \right]$ . But in (4);  $\mathbb{E}$  and  $\mathbb{H}$ , have the common SI dimension meter of  $\left[ 1/m \right]$  (Tretyakov & Erden, 2021).

Derivation of the Lorentz force law with new field vectors was presented in (Tretyakov & Erden, 2021, p. 88275). Energetic characteristics (i.e., field energy, Poynting vector, the velocity of transportation of energy), and mechanical equivalents of the energetic field characteristics were also derived with the novel field vectors  $\mathbb{E}$  and  $\mathbb{H}$  in (Tretyakov, Butrym, & Erden, 2021; Tretyakov & Erden, 2021).

Herein, we aim to derive an *uncoupled second-order partial differential equation*, that is wave equation, from the novel format of Maxwell's equations, which is a set of *coupled first-order partial differential equations*.

The first two equations of the novel format of Maxwell's equations in differential form, as given by (4), are first-order coupled differential equations; that is, both unknown fields ( $\mathbb{E}$  and  $\mathbb{H}$ ) appear in each equation. Usually, it is very desirable to uncouple these equations. This can be accomplished at the expense of increasing the order of the differential equations to the second order (Balanis, 2012).

Taking the curl of both sides of the first two equations of (4) and assuming a homogeneous medium, we can write that

$$\begin{aligned}\nabla \times \nabla \times \mathbb{H}(\mathbf{r}, t) &= \frac{1}{c} \frac{\partial}{\partial t} \nabla \times \mathbb{E}(\mathbf{r}, t) + \nabla \times \mathbb{J}(\mathbf{r}, t) \\ \nabla \times \nabla \times \mathbb{E}(\mathbf{r}, t) &= -\frac{1}{c} \frac{\partial}{\partial t} \nabla \times \mathbb{H}(\mathbf{r}, t)\end{aligned}\tag{5}$$

Using the vector identity

$$\nabla \times \nabla \times \mathbb{F} = \nabla(\nabla \cdot \mathbb{F}) - \nabla^2 \mathbb{F}\tag{6}$$

into the left side of (5), we can rewrite it as

$$\begin{aligned}\nabla(\nabla \cdot \mathbb{H}(\mathbf{r}, t)) - \nabla^2 \mathbb{H}(\mathbf{r}, t) &= \frac{1}{c} \frac{\partial}{\partial t} \nabla \times \mathbb{E}(\mathbf{r}, t) + \nabla \times \mathbb{J}(\mathbf{r}, t) \\ \nabla(\nabla \cdot \mathbb{E}(\mathbf{r}, t)) - \nabla^2 \mathbb{E}(\mathbf{r}, t) &= -\frac{1}{c} \frac{\partial}{\partial t} \nabla \times \mathbb{H}(\mathbf{r}, t).\end{aligned}\tag{7}$$

Substituting; (i) the first equation of (4) into the right side of the second equation of (7), (ii) the second equation of (4) into the right side of the first equation of (7), (iii) the third equation of (4) into the left side of the first equation of (7), (iv) the fourth equation of (4) into the left side of the second equation of (7) as

$$\begin{aligned}\nabla(0) - \nabla^2 \mathbb{H}(\mathbf{r}, t) &= \frac{1}{c} \frac{\partial}{\partial t} \left( -\frac{1}{c} \frac{\partial}{\partial t} \mathbb{H}(\mathbf{r}, t) \right) + \nabla \times \mathbb{J}(\mathbf{r}, t) \\ \nabla(\varrho(\mathbf{r}, t)) - \nabla^2 \mathbb{E}(\mathbf{r}, t) &= -\frac{1}{c} \frac{\partial}{\partial t} \left( \mathbb{J}(\mathbf{r}, t) + \frac{1}{c} \frac{\partial}{\partial t} \mathbb{E}(\mathbf{r}, t) \right)\end{aligned}\tag{8}$$

and rearranging its terms, we have that

$$\begin{aligned}\nabla^2 \mathbb{H}(\mathbf{r}, t) - \frac{1}{c^2} \frac{\partial^2 \mathbb{H}(\mathbf{r}, t)}{\partial t^2} &= -\nabla \times \mathbb{J}(\mathbf{r}, t) \\ \nabla^2 \mathbb{E}(\mathbf{r}, t) - \frac{1}{c^2} \frac{\partial^2 \mathbb{E}(\mathbf{r}, t)}{\partial t^2} &= \frac{1}{c} \frac{\partial \mathbb{J}(\mathbf{r}, t)}{\partial t} + \nabla \varrho(\mathbf{r}, t)\end{aligned}\tag{9}$$

uncoupled second-order differential equations for the new field vectors  $\mathbb{E}$  and  $\mathbb{H}$ . Equations in (9) can be referred to as the *vector wave equation for the novel field vectors  $\mathbb{E}$  and  $\mathbb{H}$* .

## A Novel Format of the Wave Equation in SI Units

For source-free ( $\mathbb{J}=0$ ,  $\varrho=0$ ) and lossless ( $\sigma=0$ ) media, equations in (9) reduce to the simplest form of the vector wave equation for the novel field vectors

$$\begin{aligned}\nabla^2\mathbb{H}(\mathbf{r},t)-\frac{1}{c^2}\frac{\partial^2\mathbb{H}(\mathbf{r},t)}{\partial t^2}&=0 \\ \nabla^2\mathbb{E}(\mathbf{r},t)-\frac{1}{c^2}\frac{\partial^2\mathbb{E}(\mathbf{r},t)}{\partial t^2}&=0.\end{aligned}\tag{10}$$

For time-harmonic fields (time variations of the form  $e^{j\omega t}$ ), replacing  $\partial/\partial t \equiv j\omega$ ,  $\partial^2/\partial t^2 \equiv (j\omega)^2 = -\omega^2$ , and the instantaneous new field vectors  $\mathbb{E}$  and  $\mathbb{H}$ , respectively, with the complex field vectors  $\mathbf{E}$  and  $\mathbf{H}$ , in (9) results in

$$\begin{aligned}\nabla^2\mathbf{H}(\mathbf{r})+\frac{\omega^2}{c^2}\mathbf{H}(\mathbf{r})&=-\nabla\times\mathbf{J}(\mathbf{r}) \\ \nabla^2\mathbf{E}(\mathbf{r})+\frac{\omega^2}{c^2}\mathbf{E}(\mathbf{r})&=\frac{j\omega}{c}\mathbf{J}(\mathbf{r})+\nabla\varrho(\mathbf{r})\end{aligned}\tag{11}$$

where  $\frac{\omega^2}{c^2} = \omega^2 \mu_0 \varepsilon_0 = k^2$ , and  $k$  represents the wave number.

For source-free ( $\mathbb{J}=0$ ,  $\varrho=0$ ) and lossless ( $\sigma=0$ ) media, equations in (11) reduce to

$$\begin{aligned}\nabla^2\mathbf{H}(\mathbf{r})+k^2\mathbf{H}(\mathbf{r})&=0 \\ \nabla^2\mathbf{E}(\mathbf{r})+k^2\mathbf{E}(\mathbf{r})&=0\end{aligned}\tag{12}$$

which are homogeneous vector Helmholtz's equations. Analogously, it is possible to derive the wave equation for the novel vector potential  $\mathbb{A}$ , and the wave equation for the novel scalar potential  $V$ .

## **7. CONCLUSION**

The analytical time domain approach presented to the literature by Professor Oleg A. Tretyakov, i.e., Evolutionary Approach to Electromagnetics, allows including the well-developed mathematical theory of evolutionary differential equations to powerful tools of electromagnetics. In the general case of *EAE*, the evolutionary equations may be obtained as linear or nonlinear: as the constitutive relations for a medium under consideration dictate it. A series of young scientists are attracted by his idea and pursue their research to advance the method.

The upgraded version of the EAE with the novel format of Maxwell's equations, proposed lately by Tretyakov, will be more convenient for practical applications since the solutions can be found in the class of the real-valued functions. Obtaining the energetic and mechanical field characteristics as the functions of time opens a way to study the energetic wave processes that should inevitably accompany the oscillations in cavities and waves in waveguides.

Nowadays, multiscale and multiphysics disciplines are appealing for the development of modern techniques and technologies, i.e., Quantum Electromagnetics. Possibly, applying a factorization of the physical dimensions, as Tretyakov presented in the novel format of Maxwell's equations, may be useful also for further development of these modern topics.

Professor Tretyakov showed a commitment to radiophysics and electrodynamics throughout his career. The breadth and depth of his technical knowledge made him an outstanding professor, respected and sought out by both students and the radiophysics community. As students, colleagues, and friends, we not only lost a prominent scientist and mentor, but also a remarkable person. He will be sorely missed.

## A Novel Format of the Wave Equation in SI Units

### **ACKNOWLEDGMENT**

The authors would like to express their gratitude to the two anonymous reviewers for their useful comments and editorial suggestions. This work was supported in part by the Scientific and Technological Research Council of Turkey (TÜBİTAK) under Project 120E390.

## REFERENCES

Akgun, O., & Tretyakov, O. A. (2015). "Solution to the Klein–Gordon equation for the study of time-domain waveguide fields and accompanying energetic processes". *IET Microwaves, Antennas & Propagation*, 9, 1337–1344. doi: 10.1049/iet-map.2014.0512

Aksoy, S., & Tretyakov, O. A. (2002). "Study of a time variant cavity system". *Journal of Electromagnetic Waves and Applications*, 16, 1535–1553. doi: 10.1163/156939302X00985

Aksoy, S., & Tretyakov, O. A. (2003a). "Walsh waves propagation along hollow rectangular waveguides". *IEEE International Conference on EMC*. doi: 10.1109/ICSMC2.2003.1429020

Aksoy, S., & Tretyakov, O. A. (2003b). "Evolution equations for analytical study of digital signals in waveguides". *Journal of Electromagnetic Waves and Applications*, 17(12), 1665–1682. doi:10.1163/156939303322760209

Aksoy, S., & Tretyakov, O. A. (2004). "The evolution equations in study of the cavity oscillations excited by a digital signal". *IEEE Transactions on Antennas and Propagation*, 52(1), 263–270. doi:10.1109/TAP.2003.822399

Aksoy, S., Antyufeyeva, M., Basaran, E., Ergin, A.A., & Tretyakov, O. A. (2005). "Time-domain cavity oscillations supported by a temporally dispersive dielectric". *IEEE Transactions on Microwave Theory and Techniques*, 53(8), 2465–2471. doi: 10.1109/TMTT.2005.852784

Antyufeyeva, M. S., Butrym, A. Y., & Tretyakov, O. A., (2009). "Transient electromagnetic fields in a cavity with dispersive double negative medium". *Progress in Electromagnetics Research M*, 8, 51–65. doi: 10.2528/PIERM09062307

Antyufeyeva, M. S., & Tretyakov, O. A., (2010). "Electromagnetic fields in a cavity filled with some nonstationary media". *Progress in Electromagnetics Research B*, 19, 177–203. doi: 10.2528/PIERB09112402

## A Novel Format of the Wave Equation in SI Units

Balanis, C. A. (2012), *Advanced Engineering Electromagnetics*. Wiley & Sons. ISBN 978-0-470-58948-9

Butrym, A. Y., Zheng, Y., & Tretyakov, O. A., (2004). "Transient diffraction on a permittivity step in a waveguide: Closed-form solution in time domain". *Journal of Electromagnetic Waves and Applications*, 18(7), 861–876. doi: 10.1163/156939304323105709

Butrym, A. Y., & Legenkiy, M. N., (2009). "Charge transport by a pulse E-wave in a waveguide with conductive medium". *Progress In Electromagnetics Research B*, 15, 325–346. doi: 10.2528/PIERB09050703

Butrym, A. Y., & Tretyakov, O. A. (2002). " Electromagnetic signals in a waveguide filled with an inhomogeneous time-variant medium". *International Conference on Mathematical Methods in Electromagnetic Theory (MMET)*. doi: 10.1109/MMET.2002.1106865

Carron, N. (2015). "Babel of units. The evolution of units systems in classical electromagnetism". doi: 10.48550/arXiv.1506.01951

Cosan, A. A., Erden, F., & Tretyakov, O. A. (2019). "Derivation of energetic properties of the waveguide fields in time-domain". *Journal of the Faculty of Engineering and Architecture of Gazi University (in Turkish)*, 34(1), 327–338. doi: 10.17341/gazimmfd.416495

Erden, F., & Tretyakov, O. A. (2008). "Excitation by a transient signal of the real-valued electromagnetic fields in a cavity". *Physical Review E*, 77(5), 056605. doi:10.1103/PhysRevE.77.056605

Erden, F., & Tretyakov, O. A. (2011). "Temporal evolution of the irrotational and solenoidal cavity modes". *XXXth URSI General Assembly and Scientific Symposium*. doi: 10.1109/URSIGASS.2011.6050488

Erden, F., & Tretyakov, O. A. (2014). "Analytical approach for studying a time-domain cavity problem". *IEEE Antennas and Propagation Society International Symposium (AP-S/URSI)*. doi: 10.1109/APS.2014.6904397



Erden, F., & Tretyakov, O. A. (2014). "Studying oscillations caused by a current surge via Evolutionary Approach to Electromagnetics". *International Conference on Software, Telecommunications and Computer Networks*. doi: 10.13140/2.1.3548.6722

Erden, F. (2015). "Evolution of a double-exponential pulse signal in a rectangular cavity filled with a plasma". *International Conference on Software, Telecommunications and Computer Networks (SoftCOM)*. doi: 10.1109/SOFTCOM.2015.7314092

Erden, F., & Bicer, U. (2016). "Evolution of the fields excited by a pulse signal in a cavity filled with a plasma" (in Turkish). *Dokuz Eylul University Engineering Faculty Science and Engineering Journal*, 18(2:53), 164–177. doi: 10.21205/deufmd.20165318378

Erden, F., Cosan, A. A., & Tretyakov, O. A. (2016). "Properties of the time-domain waveguide modes". *IEEE International Symposium on Antennas and Propagation & USNC/URSI National Radio Science Meeting*. doi: 10.1109/APS.2016.7696513

Erden, F., Tretyakov, O. A., & Bicer, U. (2016). "Evolution of the solenoidal and irrotational modal fields in a cavity excited by a signal" (in Turkish). *Signal Processing and Communication Application Conference (SIU)*. doi: 10.1109/SIU.2016.7495707

Erden, F. (2017a). "Evolutionary approach to solve a novel time-domain cavity problem". *IEEE Transactions on Antennas and Propagation*, 65(11), 5918–5931. doi:10.1109/TAP.2017.2752240

Erden, F. (2017b). "Study of the energetic field characteristics of the TE-modal waves in waveguides". *Turkish Journal of Physics*, 41, 47–54, 2017. doi: 10.3906/fiz-1605-1

Erden, F., Cosan, A. A., & Tretyakov, O. A. (2017). "Time-domain energetic properties of the TM-modes in a lossy waveguide" in Turkish. *IEEE Signal Processing and Communications Applications Conference*. doi: 10.1109/SIU.2017.7960209

## A Novel Format of the Wave Equation in SI Units

Erden, F., & Tretyakov, O. A. (2017). "Analytical study of the TE–waveguide modes in time domain". *IEEE International Symposium on Antennas and Propagation & USNC/URSI National Radio Science Meeting*. doi: 10.1109/APUSNCURSINRSM.2017.8072065

Erden, F., & Tretyakov, O. A. (2017). "Mechanical properties of the waveguide modal fields in the time domain". *Progress In Electromagnetics Research Symposium (PIERS) 2017*. doi: 10.13140/RG.2.2.20636.18569

Erden, F., Tretyakov, O. A., & Cosan, A. A. (2018). "Inertial properties of the TE waveguide fields". *Progress In Electromagnetics Research M*, 68, 11-19. doi:10.2528/PIERM18020609

Erden, F. (2018). "Study of the surge signals in a plasma-filled rectangular cavity". *Physics of Wave Phenomena*, 26(2), 139–149. doi: 10.3103/S1541308X18020085

Erden, F., Cosan, A. A., & Tretyakov, O. A. (2018). "Massic properties of the TE-modes in a lossless waveguide" in Turkish. *IEEE Signal Processing and Communications Applications Conference*. doi: 10.1109/SIU.2018.8404278

Erden, F., & Tretyakov, O. A. (2018). "Electromagnetic inertia of the waveguide modes". *2nd URSI Atlantic Radio Science Meeting (AT-RASC 2018)*, 2(1). doi:10.13140/RG.2.2.30508.31367

Erden, F., & Tretyakov, O. A. (2019). "Causal dynamic constitutive relations for lossy dispersive dielectrics". *2019 URSI International Symposium on Electromagnetic Theory (EMTS)*. doi: 10.23919/URSI-EMTS.2019.8931444

Erden, F. (2021a). "Free oscillations in cavities with metallic surfaces". *The International Conference on Electromagnetics in Advanced Application (ICEAA)*. doi: 10.1109/ICEAA52647.2021.9539671

Erden, F. (2021b). "Causal Oscillations in Cavities with Metallic Surfaces". *URSI Radio Science Letters*, 3. doi: 10.46620/21-0007

Erden, F., Yavuz Erkan, A., Cosan, A. A., Aksoy, A. (2021). "An analytical solution for the electromagnetic oscillations caused by a rectangular pulse in a cavity with lossy walls". *Journal of Naval Sciences and Engineering*, 17(2), 413 – 428.

Erden F. (2022a). "In Memoriam: Oleg Alexandrovich Tretyakov". *The Radio Science Bulletin*, 377, 60–61.

Erden F. (2022b). "Reflections on the Life of Oleg A. Tretyakov". *IEEE Antennas and Propagation Magazine*, 64(5). doi:10.1109/MAP.2022.3197347

Eroglu, E., Aksoy, S., & Tretyakov, O. A. (2012). "Surplus of energy for time-domain waveguide modes". *Energy Education Science and Technology Part A: Energy Science and Research*, (29)1, 495-506.

Kisunko, G. V. (1949). *Electrodynamics of Hollow Systems* (in Russian), VKAS: Leningrad.

Kobayashi, K., & Smith, P. D. (2021). *Advances in Mathematical Methods for Electromagnetics*. Institution of Engineering and Technology. doi:10.1049/sbew528e

Rothwell, E. J., & Cloud, M. J. (2001). *Electromagnetics*. CRC Press. doi: 10.1201/9781420058260

Tretyakov, O. A. (1986). "The method of modal basis", *Radiotekhnika i Elektronika*, (in Russian), 31, 1071-1082.

Tretyakov, O. A. (1989). "Waveguide evolutionary equations". *Radiotekhnika i Elektronika*, (in Russian), 34(5), 917–926.

Tretyakov, O. A. (1993). Essentials of Nonstationary and Nonlinear Electromagnetic Field Theory. In M. Hashimoto, M. Idemen, & O. A. Tretyakov, *Analytical and Numerical Methods in Electromagnetic Wave Theory*. Science House Co. Ltd.

## A Novel Format of the Wave Equation in SI Units

Tretyakov, O. A. (1994). "Evolutionary equations for the theory of waveguides". *Proceedings of IEEE Antennas and Propagation Society International Symp. and URSI National Radio Science Meeting*, 2465–2471.

Tretyakov, O. A., & Dumin, A. N. (2000). "Emission of nonstationary electromagnetic fields by a plane radiator", *Telecommunications and Radio Engineering*, 54(1). doi: 10.1615/TelecomRadEng.v54.i1.10

Tretyakov, O. A., & Erden, F. (2006). "Temporal cavity oscillations caused by a wide-band double-exponential waveform". *4th International Workshop on Electromagnetic Wave Scattering (EWS 2006)*. doi: 10.13140/2.1.4591.6165

Tretyakov, O. A., & Erden, F. (2007). "Separation of the instantaneous and dynamic polarizations in studies of dispersive dielectrics". *The Sixth International Kharkov Symposium on Physics and Engineering of Microwaves, Millimeter and Submillimeter Waves (MSMW)*, 42–48. doi: 10.1109/MSMW.2007.4294572

Tretyakov, O. A., & Erden, F. (2008). "Temporal cavity oscillations caused by a wide-band waveform". *Progress in Electromagnetics Research B*, 6, 183–204. doi: 10.2528/PIERB08031222

Tretyakov, O. A., & Akgun, O. (2010). "Derivation of Klein-Gordon equation from Maxwell's equations and study of relativistic time-domain waveguide modes". *Progress In Electromagnetics Research*, 105, 171–191. doi: 10.2528/PIER10042702

Tretyakov, O. A., & Erden, F. (2012). "Evolutionary approach to electromagnetics as an alternative to the time-harmonic field method". *2012 IEEE International Symposium on Antennas and Propagation and USNC-URSI National Radio Science Meeting*. doi: 10.13140/2.1.2283.4242

Tretyakov, O. A., & Erden, F. (2016). "Evolution of the quadratic functions of the time-domain waveguide fields". *URSI International Symposium on Electromagnetic Theory*. doi: 10.1109/URSI-EMTS.2016.7571420

Tretyakov, O. A., & Kaya, M. (2012). "The real-valued time-domain TE-modes in lossy waveguides". *Progress in Electromagnetics Research*, 127, 405–426. doi: 10.2528/PIER12031402

Tretyakov, O. A., & Kaya, M. (2013). "Time-domain real-valued TM-modal waves in lossy waveguides". *Progress in Electromagnetics Research*, 138, 675–696. doi: 10.2528/PIER13030206

Tretyakov, O. A. (2017). "Factorizing physical dimensions of the quantities ingressed in Maxwell's equations in SI units". *Progress In Electromagnetics Research Symposium (PIERS) 2017*. doi:10.13140/RG.2.2.30148.73604

Tretyakov, O. A. (2018). "Innovating SI Units in Maxwell's Equations. Evolutionary Approach to Electrodynamics as an Alternative to the Time-Harmonic Field Concept". *2018 2nd URSI Atlantic Radio Science Meeting, AT-RASC 2018*. doi:10.23919/URSI-AT-RASC.2018.8471496

Tretyakov, O. A., & Erden, F. (2020). "A new simple format of Maxwell's equations in SI units". *IEEE International Kharkov Symposium on Physics and Engineering of Microwaves, Millimeter and Submillimeter Waves (MSMW)*. doi: 10.13140/RG.2.2.27799.80806

Tretyakov, O. A., Butrym, O., & Erden, F. (2021). Innovative tools for SI units in solving various problems of electrodynamics. In K. Kobayashi, & P. D. Smith, *Advances in Mathematical Methods for Electromagnetics* (673–707). Institution of Engineering and Technology. doi:10.1049/sbew528e\_ch27

Tretyakov, O. A., & Erden, F. (2021). "A Novel Simple Format of Maxwell's Equations in SI Units". *IEEE Access*, 9, 88272 - 88278. doi: 10.1109/ACCESS.2021.3089673

Tretyakov, O. A., Erden, F., Cosan, A. A., & Aksoy, S. (2021). "Kayıplı yüzeylere sahip kavite alanları için analitik çözüm". *URSI Turkey General Assembly and Scientific Meeting (in Turkish)*.

*\*An ethical committee approval and/or legal/special permission has not been required within the scope of this study.*

**INVESTIGATION OF THE EFFECT OF THE FLOW  
REGULATORS ON THE FLOW AROUND A GENERIC  
SUBMARINE SAIL\***

**Gökay SEVGİ<sup>1,2</sup>** 

**Barış BARLAS<sup>3</sup>** 

**Uğur Oral ÜNAL<sup>4</sup>** 

<sup>1</sup>*Istanbul Technical University, Department of Naval Architecture and  
Marine Engineering, Istanbul, Turkey,  
sevgig@itu.edu.tr*

<sup>2</sup>*STM Inc., Naval Projects Directorate, Istanbul, Turkey,  
gokay.sevgi@stm.com.tr*

<sup>3</sup>*Istanbul Technical University, Department of Naval Architecture and  
Marine Engineering, Istanbul, Turkey,  
barlas@itu.edu.tr*

<sup>4</sup>*Istanbul Technical University, Department of Naval Architecture and  
Marine Engineering, Istanbul, Turkey,  
ounal@itu.edu.tr*

**Received: 28.02.2022**

**Accepted: 17.05.2022**

## ABSTRACT

*In this study, the viscous flow field around the mainsail of the DARPA Suboff AFF8 generic submarine fitted with two flow regulators in tandem configuration was investigated by means of computational fluid dynamics. An effective solution for the improvement of the mainsails of some of the current submarine classes of the Turkish Navy was aimed by covering the prepositioned periscopes by the flow regulators to avoid drag and vorticity increases due to the complex flow structure generated by these appendages and to provide a smoother flow topology. Three different NACA profiles with the same chord and span lengths were specified for regulating the flow. The effect of the NACA profile geometries on the hydrodynamic resistance and the flow field characteristics around the sail was demonstrated. It was shown that different profiles selected for the flow regulators considerably affect the computed resistance, velocity, pressure and vorticity characteristics of the flow field around the flow regulators. However, the flow structure at the side zones of the mainsail was not affected by the flow regulators. The profiles selected from NACA 6-digit and NACA 16-digit series give better hydrodynamic performance than their classical NACA 4-digit equivalent.*

**Keywords:** *Submarine, Tandem Hydrofoils, Computational Fluid Dynamics, RANS.*

**AKIŞ DÜZENLEYİCİLERİN BİR JENERİK DENİZALTI YELKENİ  
ETRAFINDAKİ AKIŞA ETKİSİNİN İNCELENMESİ**

**ÖZ**

*Bu çalışmada, üzerine tandem konfigürasyonda iki akış düzenleyicinin konumlandırıldığı jenerik DARPA Suboff AFF8 denizaltısının yelkeni etrafında gelişen viskoz akım alanı hesaplamalı akışkanlar dinamiği ile incelenmiştir. Türk Donanması'nın mevcut denizaltı sınıflarından bazılarının ana yelkenlerinin iyileştirilmesi için periskopların oluşturduğu karmaşık akış yapısından kaynaklanan direnç ve girdaplılık artışlarını önlemek ve daha düzgün bir akış topolojisi sağlamak amacıyla, önceden konumlandırılmış bu takıntılar akış düzenleyiciler ile çevrelenerek efektif bir çözüm hedeflenmiştir. Akışı düzenlemek için aynı giriş ve açıklık boyuna sahip üç farklı NACA profili belirlenmiş ve bu NACA profili geometrilerinin hidrodinamik dirence ve yelken etrafındaki akım alanı karakteristiğine etkisi gösterilmiştir. Akış düzenleyiciler için seçilen farklı profillerin, akış düzenleyicilerin etrafındaki akım alanı için hesaplanan direnç, hız, basınç ve girdaplılık karakteristiklerini önemli ölçüde etkilediği görülürken ana yelkenin yan bölgelerindeki akım yapısını etkilemediği gözlemlenmiştir. NACA 6 ve NACA 16 serilerinden seçilen profiller, klasik NACA 4 serisi eşdeğerlerinden daha iyi bir hidrodinamik performans vermektedir.*

**Anahtar Kelimeler:** *Denizaltı, Tandem Hidrofoiller, Hesaplamalı Akışkanlar Dinamiği, RANS.*



## **1. INTRODUCTION**

The design of a submarine and its appendages with respect to hydrodynamics point of view is one of the most critical stages in overall submarine design since providing a minimized hydrodynamic resistance force exerted on it and a minimized acoustic signature are vital for its operability and secrecy. However, during the modernization activities carried out for a submarine, longer periscopes than the existing ones may need to be integrated into the submarine and this situation may result in the upper parts of the new periscopes to be outside of the submarine sail and thus may disrupt the hydrodynamic design of the submarine form. In such situations, it is required that these periscopes must be covered by some hydrofoil appendages which are also called flow regulators to avoid from the negative hydrodynamic effects of the periscopes being directly opened to the seawater. The forms of these flow regulators which are usually in tandem configuration must be optimized as an appendage design by taking into consideration of the restrictions such as the fixed positions of the periscope outlets and the hydrodynamic interaction between them.

Various researchers have investigated the flow around the submarines and their appendages to optimize their form by reducing their hydrodynamic resistance. In this context, Kale (2020) investigated the hydrodynamic resistance of a bare and an appended generic DARPA Suboff form by using a commercial code as well as an open-source code. Takahashi and Sahoo (2019) studied the resistance forces and moments exerted onto a DARPA Suboff submarine for straight translation and turning conditions. Lungu (2019) solved the flow problem around a DARPA Suboff form unsteadily by both detached eddy simulation and explicit algebraic stress model and analysed the computed wake behind the hull. Kukner et al. (2016) focused on the pressure distribution on a submarine for different forward speeds and examined the effect of the sail and the stern appendages on the computed hydrodynamic pressures on the hull. Budak and Beji (2016) executed a numerical investigation for nine different variants of a bare DARPA Suboff generic submarine model by keeping its body as the basis and varying the bow and stern sections in order to obtain an improved geometrical form. On the other hand, Chase (2012) executed a detailed investigation to compute

*Investigation of the Effect of the Flow Regulators on the Flow Around a  
Generic Submarine Sail*

and visualize the hydrodynamic drag characteristics of a DARPA Suboff generic submarine model with appendages by using an in-house code. Wilson-Haffenden et al. (2010) conducted both numerical simulations and towing tank experiments for a bare DARPA Suboff submarine model which operates near the free surface in different submergence depths and Froude numbers to show the effect of the wave-making resistance on the total resistance. Baker (2004) also presented a methodology on how to model the boundary layer flow developed around a bare submarine form used for the studies of DRDC - Atlantic by means of computational fluid dynamics methods and validated his results with the experimental data from the wind tunnel tests.

The researches to investigate the hydrodynamic interaction between tandem hydrofoils with respect to varying distances, angles of attack and profiles have also been carried out by some researchers. Shang and Horrillo (2021) studied two two-dimensional NACA 0012 profiles aligned in tandem configuration for 788 combinations of different parameters such as spacing between the profiles and angles of attack of upstream and downstream profiles by a commercial code and artificial neural network method. Moreover, Maraam et al. (2021) examined two NACA 4412 profiles in two-dimension numerically in single-phase and multi-phase flows and showed the free surface effect on the results for varying submergence depths, distances between the profiles and angles of attack by using a commercial code. They also considered the cavitation occurrence on tandem profiles in their study. In the study of Chao et al. (2017), different combinations in sizes and kinematics of two hydrofoils in tandem configuration were investigated for the purpose of the reduction in drag forces. Furthermore, Kinaci (2015) approached to the problem of the hydrodynamic interaction between tandem hydrofoils in a different way. He used an iterative boundary element method and a Reynolds-averaged Navier-Stokes method to investigate the results for six different parameters in potential flow and viscous flow, respectively.

In the literature survey, although it was identified that several researches were conducted on the flow around submarines, their appendages and isolated tandem hydrofoils, there exist no study that deals with the

hydrodynamic interaction between tandem hydrofoils located on a submarine sail. In light of this, the present study focuses on merging these two subjects by considering a tandem hydrofoil system fitted on a generic submarine sail. This configuration is a widely encountered problem in engineering of the submarines, which aims to cover the prepositioned periscopes to avoid drag and vorticity increases due to the complex flow structure generated by these appendages and to provide a smoother flow topology.

In the context of the present study, the effect of the NACA profile geometry of the two flow regulators in the tandem configuration on the viscous flow around a generic submarine sail was investigated. The geometrical parameters such as the chord and span lengths of these flow regulators were kept constant in all cases investigated to solely evaluate the effect of the NACA profile geometry on the flow structure and hydrodynamic characteristics by means of computational methods. Accordingly, an effective solution for the improvement of the mainsails of some of the current submarine classes of the Turkish Navy was aimed.

## **2. GEOMETRIES**

The submarine sail geometry used in the case studies was derived from the sail of the DARPA Suboff AFF8 submarine model which is a widely used geometry in the associated literature whose geometrical data is available in (Groves et al., 1989). The sail of this generic submarine model was scaled to give the sail length of 10.55 m, which approximately corresponds to the mainsail length of some of the submarine classes in the Turkish Navy. Hence the full-scale geometry of the sail was considered in the computations. The scaled mainsail used in the study has a height of 6.32 m and maximum breadth of 1.9 m. A view of the derived mainsail from the DARPA Suboff AFF8 submarine model is shown in Figure 1.

*Investigation of the Effect of the Flow Regulators on the Flow Around a Generic Submarine Sail*



**Figure 1.** DARPA Suboff AFF8 submarine sail used in the case studies.

In this study, the following three cases were investigated.

- The case that the flow regulators on the submarine sail are NACA 66-021 profile shaped from NACA 6-digit series.
- The case that the flow regulators on the submarine sail are NACA 0021 profile shaped from NACA 4-digit series.
- The case that the flow regulators on the submarine sail are NACA 16-021 profile shaped from NACA 16-digit series.

From a hydrodynamic point of view, a slender form of the flow regulators is desirable to obtain lower resistance values, whilst the regulators should be thick enough to be able to cover the appendages of the sail such as the search and attack periscopes, etc. By taking these limitations into consideration, in all computational cases, the maximum thicknesses in percent of the chord lengths of the profiles from different NACA series were retained as 21%. All the profiles of the flow regulators were also

selected to be symmetrical with respect to their chord lines which means that these profiles have no camber. The representative section views of the selected profiles for the cases are shown in Figure 2.

The coordinates required to create the curves of the profiles were extracted from the data provided by Abbott and von Doenhoff (1959) in the stage of three-dimensional modelling of the geometries for the specified cases. In all the cases investigated, the chord and the span lengths of these flow regulators were kept constant while their positions are fixed on the submarine sail. The prepared three-dimensional geometries for the cases are shown in Figure 3.

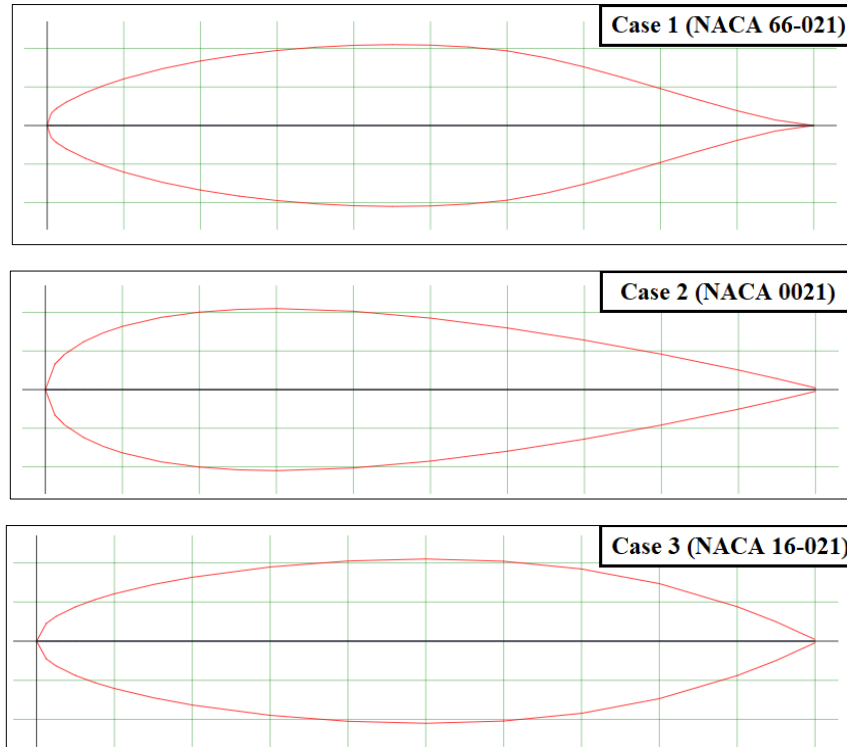


**Figure 2.** Representative section views of the selected profiles for the cases.

*Investigation of the Effect of the Flow Regulators on the Flow Around a  
Generic Submarine Sail*

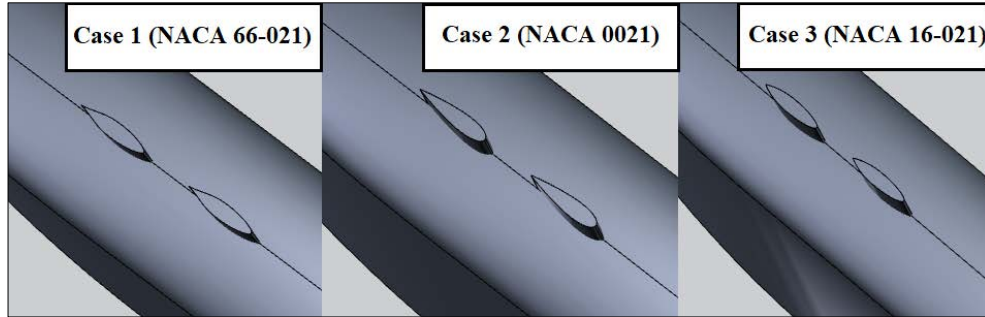


**Figure 3.** Prepared geometries for the cases.

### 3. COMPUTATIONAL DETAILS

#### 3.1. Governing Equations and Numerical Technique

Incompressible steady Reynolds-averaged Navier-Stokes (RANS) equations (Wilcox, 2006) were solved by means of finite volume discretisation to compute the viscous flow around the mainsail and flow regulators. An unsteady approach will perhaps increase the accuracy; however, it will also significantly affect the computational time and resource demand. Since the work presented is mainly a comparative study, the steady approach would provide reliable hydrodynamic assessments. In Cartesian tensor notation, the above equations can be expressed as follows:

$$\frac{\partial U_i}{\partial x_i} = 0 \quad (1)$$

$$\rho \frac{\partial U_j U_i}{\partial x_j} = -\frac{\partial P}{\partial x_i} + \frac{\partial}{\partial x_j} (\mu S_{ij} - \overline{\rho U'_i U'_j}) \quad (2)$$

In these equations;  $\rho$ ,  $\mu$ ,  $P$ ,  $U$  and  $U'$  denote fluid density, dynamic viscosity, average static pressure, average velocity and fluctuating velocity, respectively.  $S_{ij}$  represents the average strain rate tensor and the term  $\overline{\rho U'_i U'_j}$  indicates the Reynolds stresses which imply the turbulent fluctuations. The line over this term means the term is averaged. In order to solve the turbulence field, Shear Stress Transport k- $\omega$  turbulence model of Menter (1994) which computes the Reynolds stress tensor by Boussinesq

hypothesis (Tennekes and Lumley, 1972) was employed. Pseudo transient computation was utilized in all the computational analyses and the hybrid initialization technique was used before starting the computations. The details for pseudo transient computation and the hybrid initialization technique are available in the documentation by ANSYS Inc. (2013).

The pressure and velocity coupling problem was solved by standard coupled scheme which solves the aforementioned momentum and pressure-based continuity equations simultaneously and distance-based Rhie-Chow interpolation method was chosen for the flux type (Rhie and Chow, 1983). Furthermore, second order approach was employed for the spatial discretization of the convective variables while the gradient was discretized by least squares cell-based method. The theory of these numerical methods can be found in Pletcher et al. (2011). On the other hand, the iterations were run until the scaled residuals of continuity, momentum and turbulence equations decreased to  $10^{-4}$  in all computations. The convergences of the resistance forces of the front flow regulators, the back flow regulators and the total resistances were also monitored according to the number of iterations in all the cases.

### **3.2. Computational Domain, Boundary Conditions and Mesh Structure**

The computational domain was created to be a rectangular prism-shaped domain. Since the computations involve slender bodies, extremely large domain dimensions were not considered. The inflow and outflow boundaries were placed at  $L$  and  $2L$ , respectively, from the submarine sail, where  $L$  denotes the length of the submarine sail. The sail was also located in the centreline of the specified  $2L$  width in the base plane of the computational domain. Moreover, the computational domain was given a height of  $1.5L$  starting from the baseline of the submarine sail. The additional simulations performed with larger domain sizes led to no appreciable changes in the results. A smaller rectangular prism was also created in order to generate more refined grids in the wake region of the flow regulators. A general view of the computational domain can be seen in Figure 4.

*Investigation of the Effect of the Flow Regulators on the Flow Around a Generic Submarine Sail*

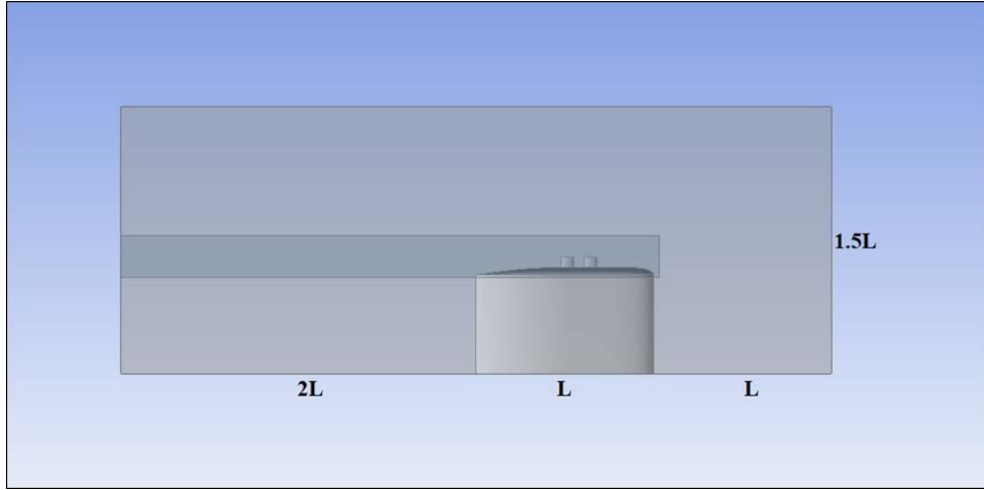


**Figure 4.** Profile view of the computational domain.

Liquid water was defined as the working fluid of the computational domain and  $1025 \text{ kg/m}^3$  of density was assumed for liquid water. The entrance of the fluid to the computational domain was defined as velocity-inlet whose velocity is 20 knots in magnitude as normal to boundary which corresponds to a Reynolds number of approximately  $10^7$  for the mainsail geometry. It is of note that the flow velocity selected also corresponds to the submerged maximum speed of some of the submarine classes of the Turkish Navy. Furthermore, the exit of the fluid from the computational domain was defined as pressure-outlet where 0 Pa gauge pressure was assigned. For both velocity-inlet and pressure-outlet boundary conditions, turbulent intensity and turbulent viscosity ratio were defined as 5% and 10, respectively. On the other hand, the lateral surfaces of the computational domain were selected as symmetry boundary condition. Moreover, the geometric components such as the mainsail and the flow regulators were defined as wall boundary condition to solve the near wall regions by wall function to avoid the long solution times of viscous layer. Also, no slip condition and smooth surface condition were assumed at walls. The depiction of the specified boundary conditions can be seen in Figure 5.



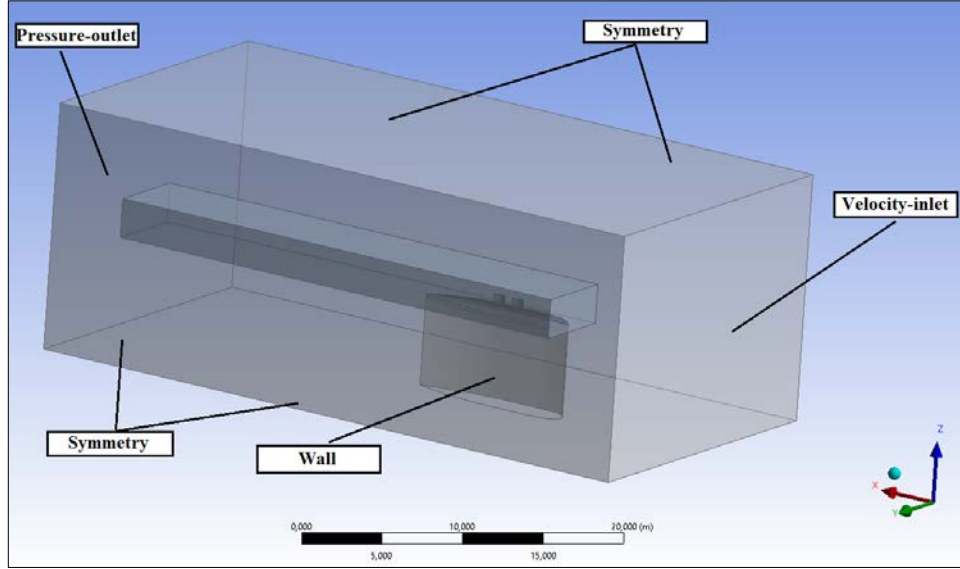


**Figure 5.** Boundary conditions.

An unstructured grid system with tetrahedral elements was used to discretize the computational domain for all the cases. In order to better model the boundary layer on the near wall regions of the sail and the flow regulators, the sizes of the elements were systemically kept low in these regions. In order to achieve this, advanced face sizing functions of the mesh generation software used with high smoothing and slow transition were employed. It was also benefited from the local mesh controls options for further improvement of the quality of the mesh structure. Since the Reynolds number considered is rather high, the boundary layer could not be fully resolved up to the viscous sublayer. The non-dimensional distance from the walls of the mainsail and the flow regulators was kept around  $y^+=50$ . However, the enhanced wall functions approach of the flow solver was employed which uses a blending function for a single wall law for the entire wall region. This approach made the use of the turbulence model selected possible. Also, the numbers of the elements were intentionally increased in the wake region of the flow regulators in order to predict the vorticities and velocities due to the flow regulators more accurately. Moreover, the same resolution parameters were employed for all the cases and thus similar grid sizes were obtained for all considered cases. However,

*Investigation of the Effect of the Flow Regulators on the Flow Around a  
Generic Submarine Sail*

the final grid resolution to be used in computational analyses was specified after the verification study to be explained in detail in Section 4.

#### **4. VERIFICATION STUDY**

In order to make sure whether the computational results were independent from the grid resolution, a verification study was carried out. Grid Convergence Index (GCI) calculation which was introduced by Celik et al. (2008) was executed to verify the results. For the verification study, Case 1 was selected and three grids in different resolutions were generated for this case by considering that the grid spacing ratio between the successive two grids to be greater than 1.3 as recommended by Celik et al. (2008). In the end of the verification study, the grids of element numbers of approximately 1.04 M, 2.38 M and 5.51 M were generated for the coarse, medium and fine grids, respectively. The grid dependency results for the total resistance for Case 1 are given in Table 1. In the table,  $e$  and GCI represent the relative error between the results and the numerical discretization uncertainty for the total resistance value in percent, respectively.

**Table 1.** Grid dependency for the total resistance values of Case 1.

<b>Grid Resolution</b>	<b>Total Resistance (kN)</b>	<b><math>e</math> (%)</b>	<b>GCI (%)</b>
Coarse	34.0	-	-
Medium	33.2	2.4	3.6
Fine	32.7	1.5	2.0

A monotonic convergence can be identified from the numerical results presented in the table. The relative errors and the discretization uncertainties gradually decrease when the grid resolution is increased. The final GCI value of the fine grid structure was calculated as 2% for the total resistance value. Further refinement of the discretization of the computational domain was, hence, not needed and the structure of the fine grid was decided to be used for the other cases. The general view of the fine grid structure is depicted in Figure 6.

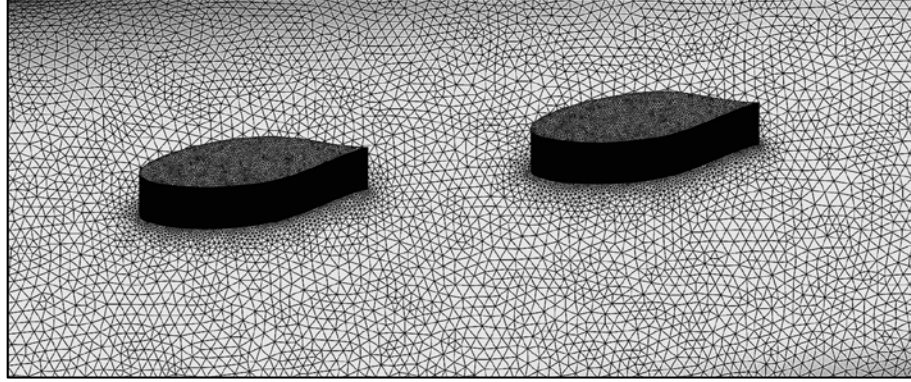


**Figure 6.** The general view of the fine grid structure.

## 5. RESULTS AND DISCUSSION

### 5.1. Resistance Computations

The obtained resistance values from the computational analyses by using the verified fine grid structure for the three cases explained previously are shown in Table 2. In this table, the approximate element numbers created when this verified fine grid structure is employed for these cases are also presented.

**Table 2.** General computation results obtained from the investigated cases.

Case	Element Number (x10 <sup>6</sup> )	Total Resistance (kN)	Resistance of Front Flow Regulator (N)	Resistance of Back Flow Regulator (N)
Case 1	5.51	32.7	285.5	594.0
Case 2	5.49	32.9	331.9	643.2
Case 3	5.50	32.8	293.0	654.1

The numerical data obtained from the computational analyses show that Case 1 with a flow regulator profile NACA 66-021 gives the best resistance results. It can also be seen from Table 2 that Case 2, where NACA 0021 profile was selected for the flow regulators, gives the highest resistance.

*Investigation of the Effect of the Flow Regulators on the Flow Around a  
Generic Submarine Sail*

However, it was seen that there are not so many differences between the results with respect to the total resistance values. Moreover, the resistance of back flow regulator was computed 94% to 123% higher than the resistance of front flow regulator in all the cases. It is assessed that this situation occurs due to the impact of the vortices formed while the fluid is passing through the front flow regulator.

## **5.2. Flow Fields**

The contours of the velocity magnitudes around the mainsail at the plane  $z = 2.4$  m, which is 2.4 m above the centre of gravity of the sail is depicted in Figure 7. The flow direction is from left to right. The location of the plane is very close to the top surface of the mainsail. It can be seen that the flow is nearly identical for all cases considered. This indicates that a large portion of the flow around the mainsail is essentially unaffected from the flow field generated by the flow regulators.

Shown in Figure 8 are the velocity magnitude distributions around the flow regulators at  $z=3.25$  m, which is a plane slightly above the top surface of the mainsail. For all cases the fluid velocity is higher around the front flow regulator as expected. Due to its thicker leading-edge, highest velocity levels of above 13 m/s may be observed around the NACA 0021 profile. While higher flow speeds occur towards the second portion of the profiles for Case 1 and 3, Case 2 exhibits large velocities near the leading-edge. The interaction zone between the two regulators can be clearly seen in all cases. The lowest velocity levels are displayed by Case 3.

The velocity magnitude distributions at  $z=3.7$  m, which corresponds to a horizontal level close to the top surface of the regulators, can be seen in Figure 9. It may be observed that the levels are much lower than those encountered at the plane close to the mainsail due to the effect of the tip vortices arising from the open end of the regulators. Large differences detected between the flow structures around the front and back flow regulators are also due to the helical motion created by the tip vortices. The zones that are strongly affected by the helical motion are apparent towards to trailing edge of the profiles for Case 1 and 3. For Case 2, the beginning of same zone is close to the midsection of the regulator. The velocity

distributions around the back flow regulator of Case 2 and 3 exhibit significantly lower levels than those of Case 1.

The non-dimensional pressure distributions on the surfaces of the flow regulators and the mainsail can be examined in Figure 10. Due to its thicker leading edge form, the pressure levels at the leading edge region of Case 2 are higher than those of the leading edge regions of Case 1 and Case 3. For the same reason, the suction zone following the leading edge is larger and the level of the suction is stronger in Case 2. A smoother pressure distribution can be observed in Case 3. The pressure recovery of Case 1 appears to be rather high compared to the other two cases which can be identified by examining the high pressure zone around the trailing edge. Figure 11 presents the non-dimensional pressure contours at  $z=3.7$  m. It can be seen that the effect of the adverse pressure gradient is more pronounced in Case 1 and 3. The weaker pressure recovery of the back flow regulators and the effect of the tip vortices on the pressure field in the wake of the front regulators are more clearly seen in the figure.

The iso surfaces of  $Q$  criterion may be examined in Figure 12.  $Q=50 \text{ s}^{-2}$  were selected for a clearer presentation. The iso surfaces were coloured by the turbulent kinetic energy. For all cases, the organized vortex structures can be identified around the edges of the top surfaces of the flow regulators. For Case 2 and 3 the coherent structures around the front flow regulators nearly reach to the back flow regulator displaying an elongated form. Case 3 also presents large vortex structures on top of the mainsail in the zone between the two regulators and around the bottom edge of the back flow regulator. The turbulent intensity appears to be higher in Case 2 particularly around the top edges of the regulators whilst the other two cases exhibit a similar turbulence character. The plots indicate that Case 1 displays a better performance in terms of the vorticity characteristics.

The vorticity characteristics of the flow regulators are also presented in Figure 13 where the streamwise vorticity levels at the planes following the trailing edges of the regulators as well as the plane immediately before the leading edge of the back flow regulator. The traces of the two pairs of counter-rotating vortex structures are primarily apparent close the tip of the

*Investigation of the Effect of the Flow Regulators on the Flow Around a Generic Submarine Sail*

regulators for all cases. Eventually the vortices emerging from the front flow regulator merges and a pair of counter-rotating vortices arrive to the back flow regulator. Smaller vortices are also notable along the trailing edges of the regulators for Case 2 and 3. The plots point out that the streamwise vorticity levels and the area of the affected zone are smaller in Case 1.

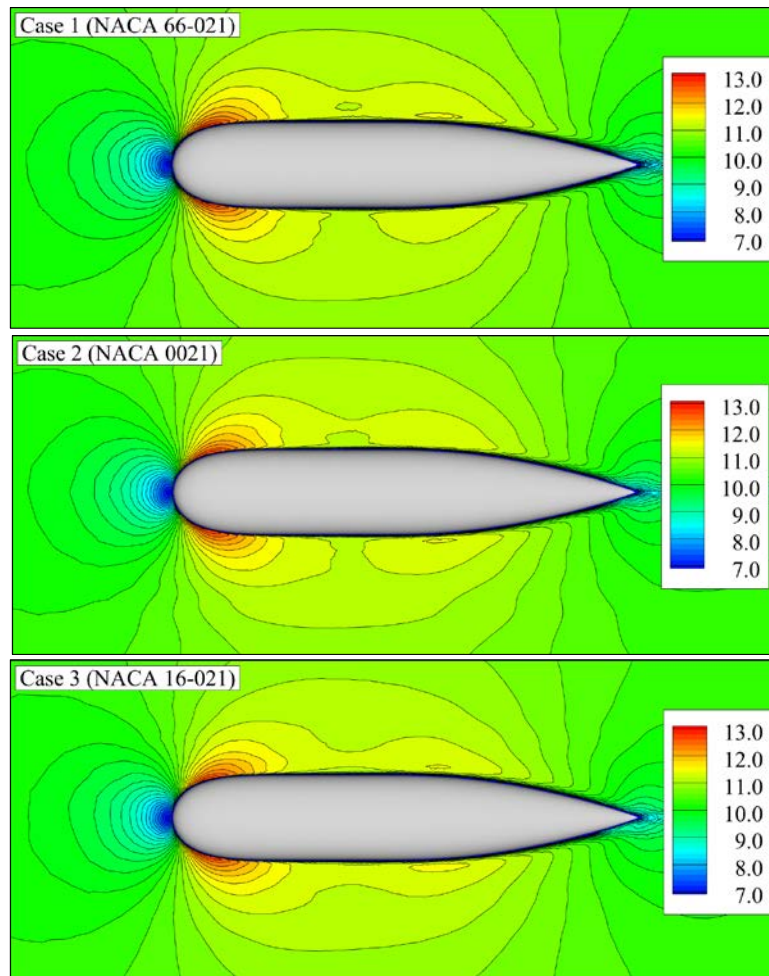


**Figure 7.** Contours of velocity magnitudes (m/s) around the mainsail at  $z = 2.4$  m.

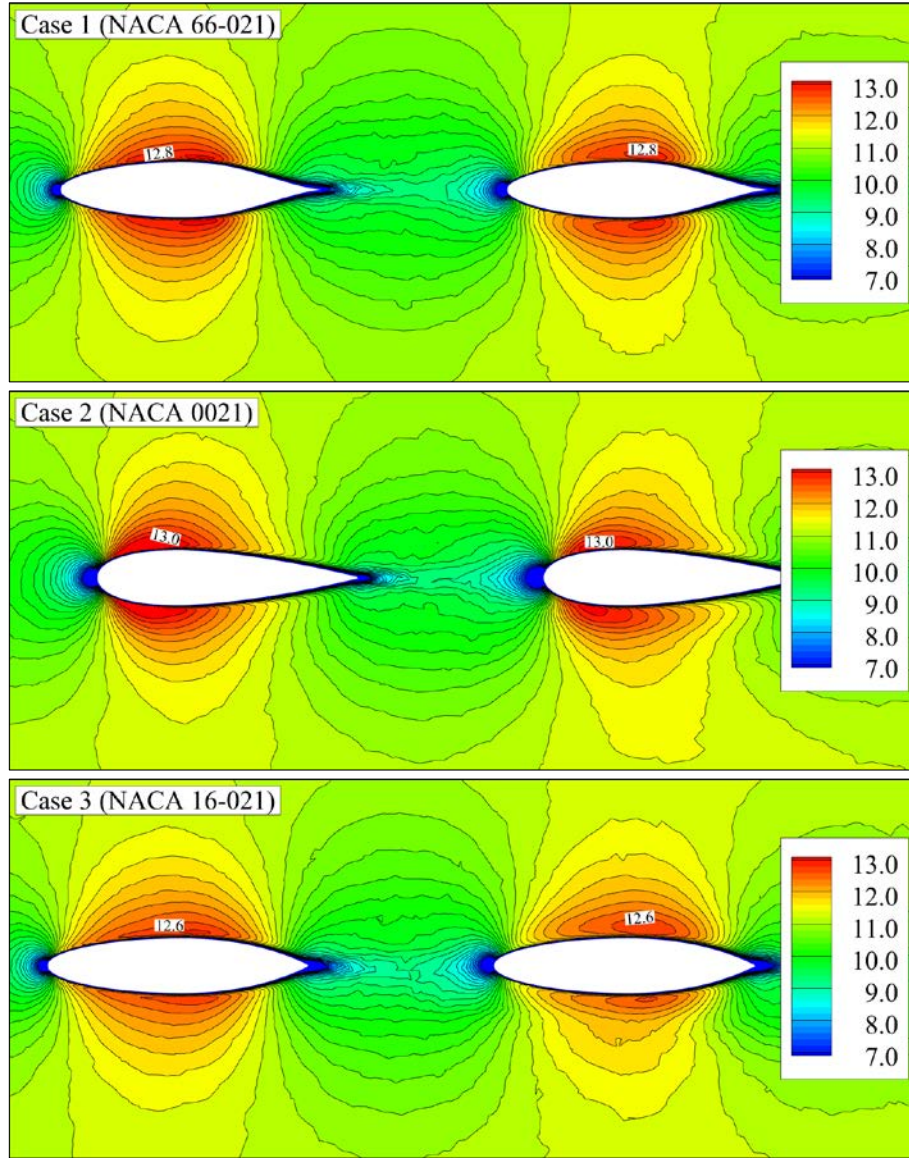


**Figure 8.** Contours of velocity magnitudes (m/s) around the flow regulators at  $z = 3.25$  m.



*Investigation of the Effect of the Flow Regulators on the Flow Around a Generic Submarine Sail*

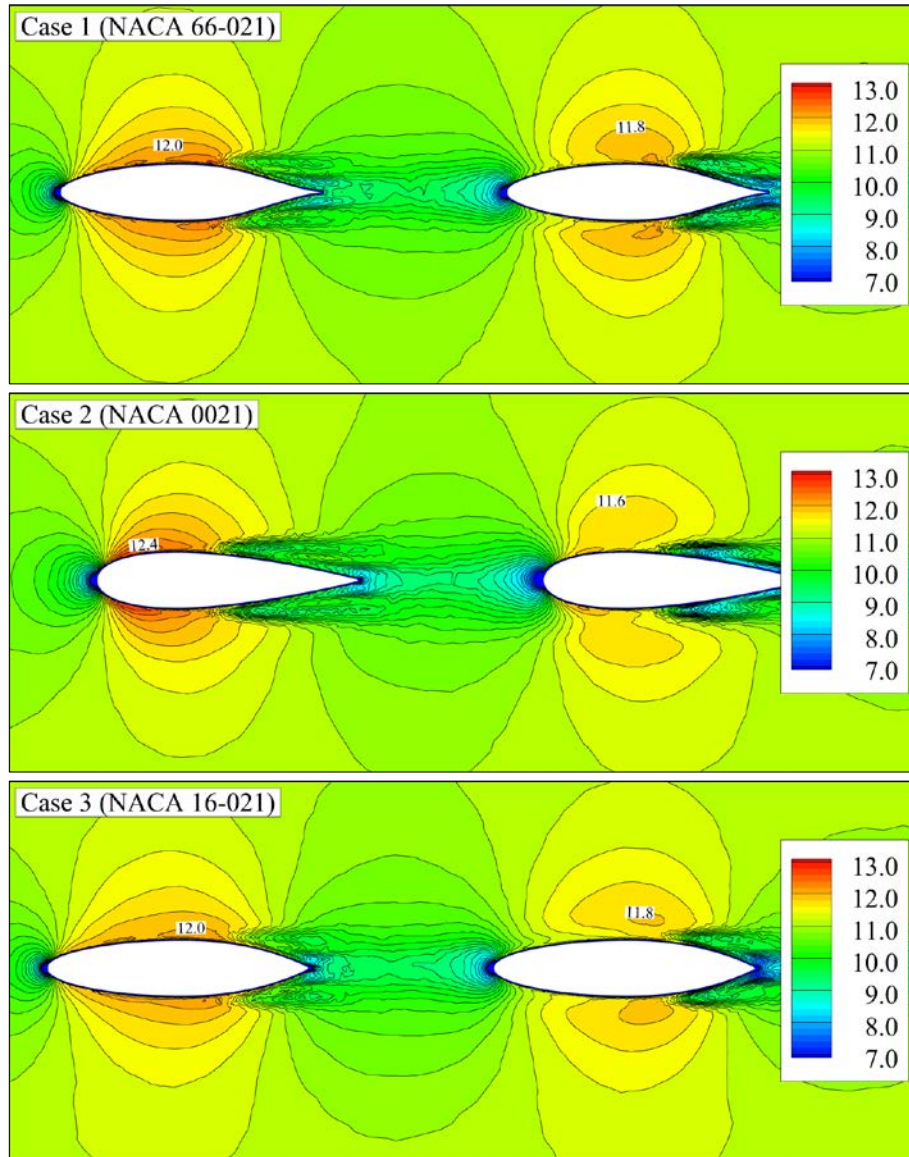


**Figure 9.** Contours of velocity magnitudes (m/s) around the flow regulators at  $z = 3.7$  m.



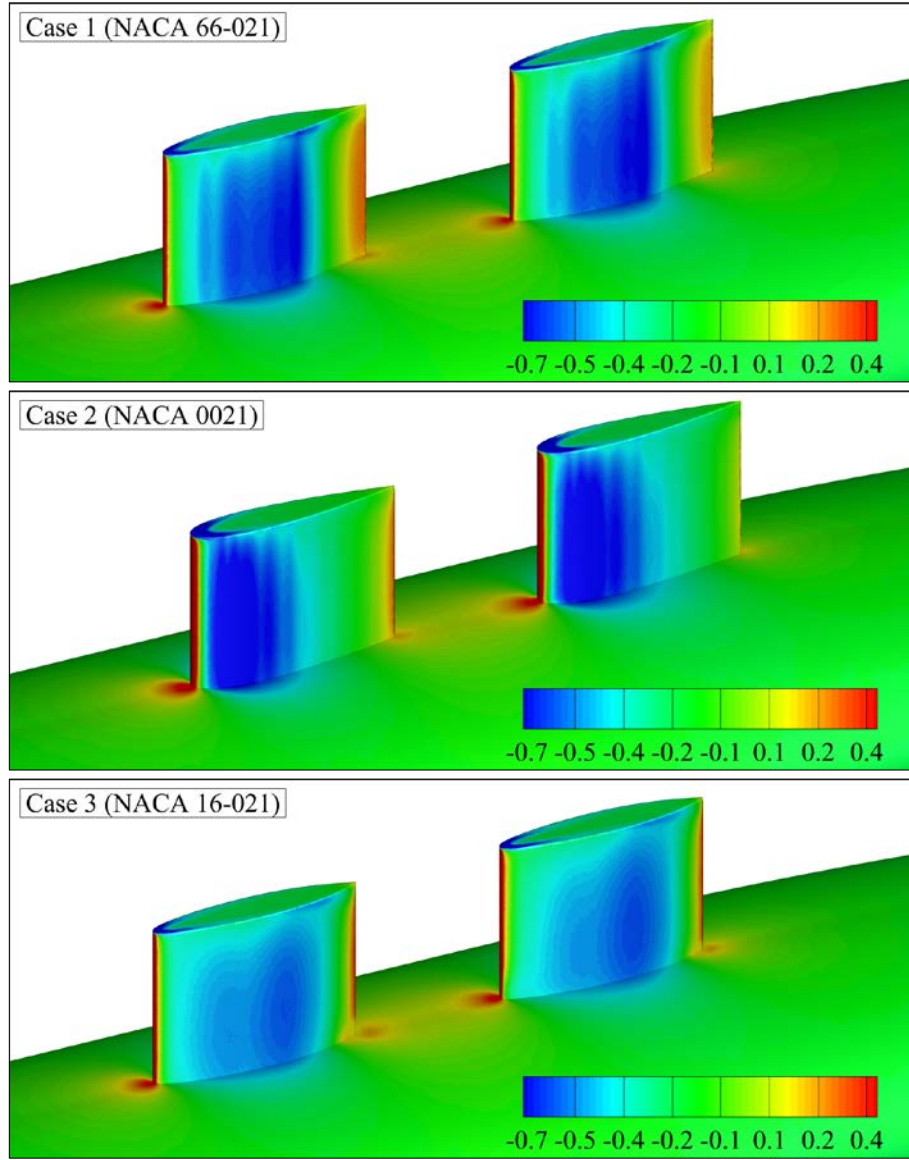


**Figure 10.** Non-dimensional pressure distributions on the surfaces of the flow regulators and the mainsail.

*Investigation of the Effect of the Flow Regulators on the Flow Around a Generic Submarine Sail*

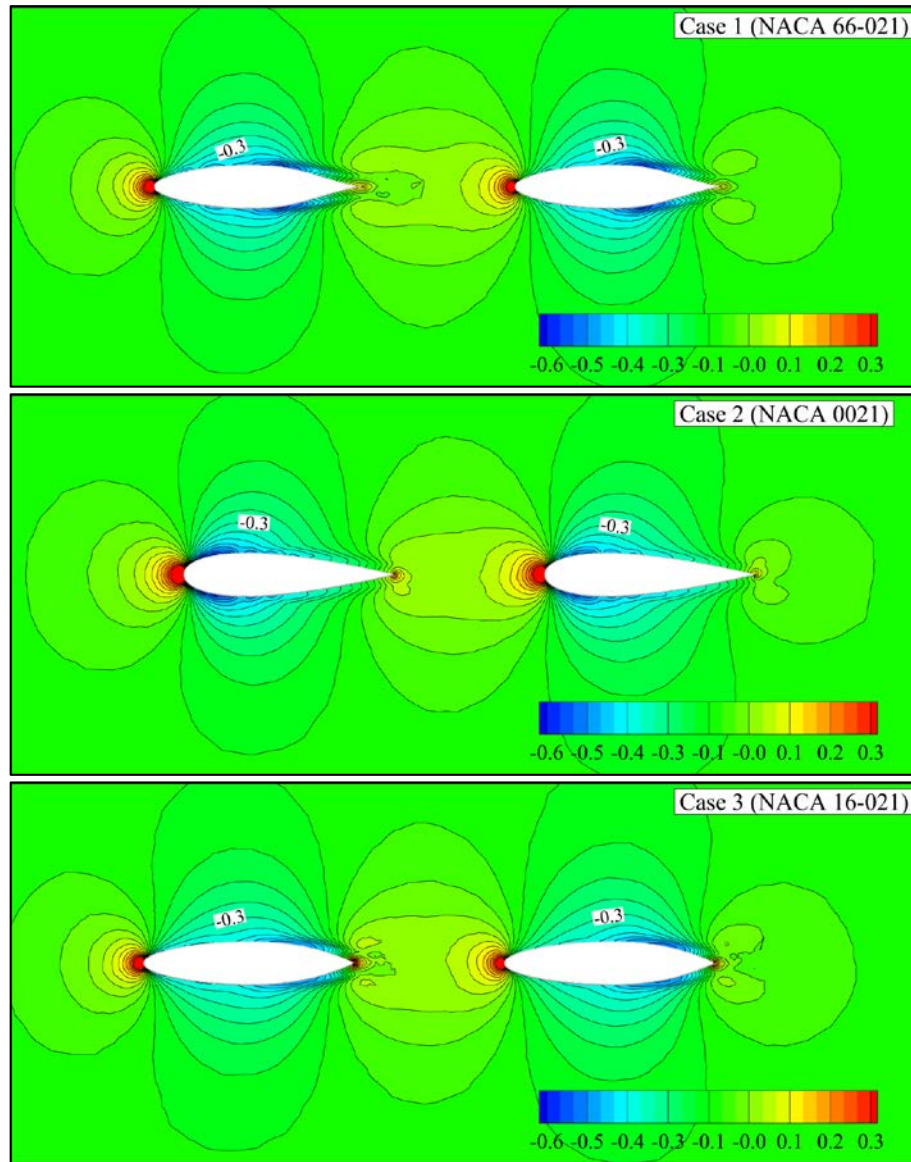


**Figure 11.** Non-dimensional pressure distributions around the flow regulators at  $z = 3.7$  m.

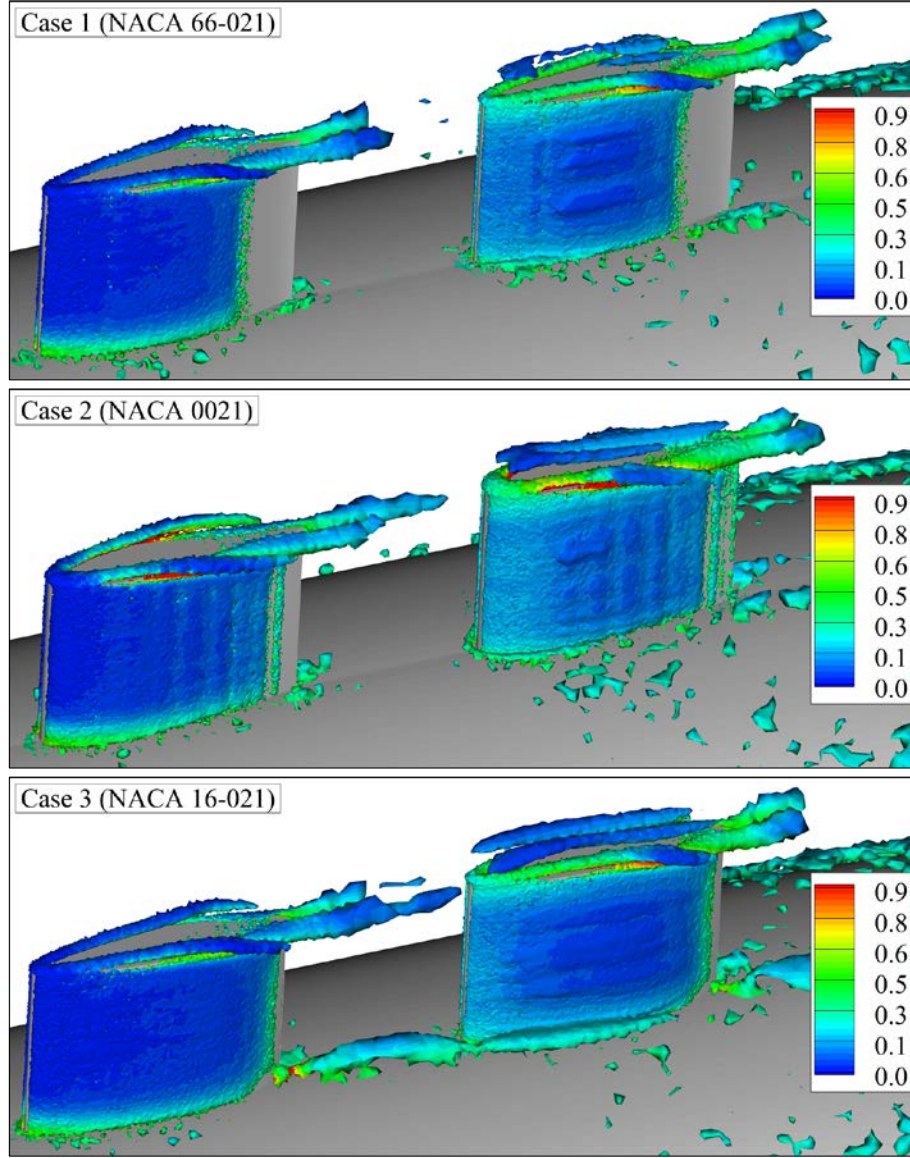


**Figure 12.** Q criterion iso surfaces around the flow regulators ( $Q=50 \text{ s}^{-2}$ , coloured by turbulent kinetic energy,  $\text{m}^2\text{s}^{-2}$ ).

*Investigation of the Effect of the Flow Regulators on the Flow Around a Generic Submarine Sail*

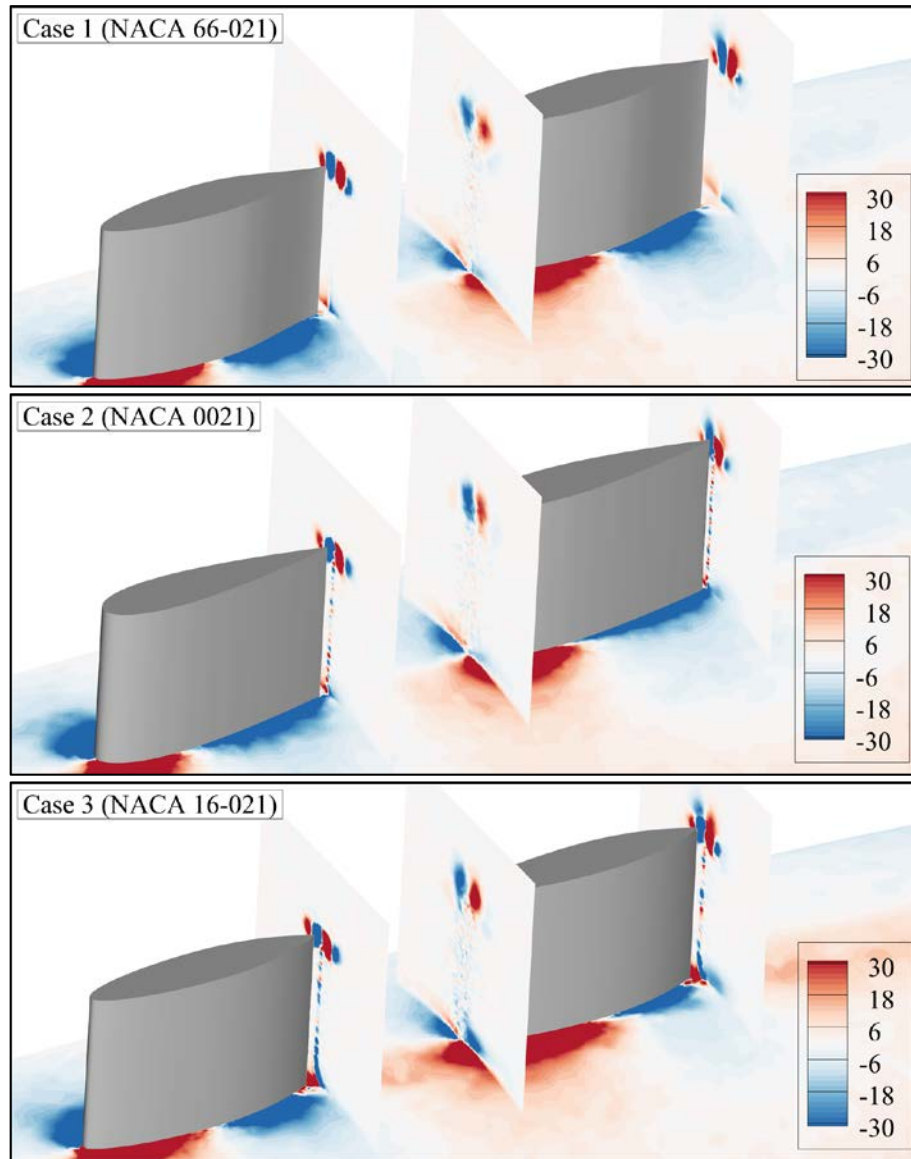


**Figure 13.** Streamwise vorticity levels ( $s^{-1}$ ) at the vertical planes near the leading and trailing edges of the flow regulators.

## **6. CONCLUSION**

In this study, the flow around a generic submarine sail with two flow regulators in tandem configuration assembled on it was investigated for three different cases. A scaled geometry derived from the mainsail of the DARPA Suboff AFF8 generic submarine model was used as the main platform. NACA 66-021, NACA 0021 and NACA 16-021 sectioned flow regulators with the same chord and span lengths at the fixed positions on the submarine sail were selected for the computational study in order to demonstrate the effect of the different profiles of the flow regulators on the flow characteristics. RANS computations were conducted by using the SST  $k-\omega$  turbulence model at a Reynolds number of approximately  $10^7$ .

It was shown that different profiles selected for the flow regulators considerably affect the computed resistance, velocity, pressure and vorticity characteristics of the flow field around the flow regulators. However, it was clearly identified that the flow structure at the sides of the mainsail was not affected by the flow regulators fitted as expected. Hence, most of the attention was paid to the region where the flow regulators exist. One of the most important outcomes was that a NACA 6-digit and a NACA 16-digit profile give better hydrodynamic performance than their classical NACA 4-digit equivalent in the same exact flow conditions for the flow around this submarine sail with respect to the total resistance values. Moreover, it was observed that Case 1 which gave the least computed resistance values in the study also displayed the least vorticity levels indicating that flow regulators with NACA 66-021 profile will also have an advantageous hydro-acoustic characteristic. It was also seen that the condition of the back flow regulator is highly critical as it is exposed to the vortices by the front flow regulator.

It is assessed that this study may be extended to include the hydro-acoustic analyses of noise generated by these flow regulators to examine the silent operability of this submarine sail. Moreover, a single larger flow regulator geometry that covers both periscope outlets can also be designed and analysed in the same flow conditions considered and its numerical results can be compared with the three cases investigated in the present study. The computational analyses for speeds slower than 20 knots can also be

*Investigation of the Effect of the Flow Regulators on the Flow Around a  
Generic Submarine Sail*

conducted to more reliably obtain generalised results. Additionally, the cases discussed in this study may be analysed by a time-dependent RANS simulation which may provide more reliable results.

It is believed that this research article provides practical and encouraging information about the improvement of the hydrodynamic/hydro-acoustic characteristics of the current submarine classes of the Turkish Navy.

*Gökay SEVGİ, Barış BARLAS, Uğur Oral ÜNAL*

#### **ACKNOWLEDGEMENT**

The authors would like to thank STM Inc. for the valuable discussions related to the topic.

#### **CONFLICT OF INTEREST STATEMENT**

All authors declare that they have no conflicts of interest and no financial support was received for this study.

*Investigation of the Effect of the Flow Regulators on the Flow Around a  
Generic Submarine Sail*

**REFERENCES**

Abbott, I. H., and von Doenhoff, A. E. (1959). *Theory of Wing Sections: Including a Summary of Airfoil Data*, Dover Publications Inc., New York, USA.

ANSYS Inc. (2013). *ANSYS Fluent User's Guide*, Canonsburg, USA.

Baker, C. (2004). "Estimating Drag Forces on Submarine Hulls". *Contract Report*, Defence Research and Development Canada - Atlantic, Canada.

Budak, B., and Beji, S. (2016). "Computational Resistance Analyses of a Generic Submarine Hull Form and Its Geometric Variants". *Journal of Ocean Technology*, Vol. 11, No. 2, 76-86.

Celik, I. B., Ghia, U., Roache, P. J., Freitas, C. J., Coleman, H., and Raad, P. E. (2008). "Procedure for Estimation and Reporting of Uncertainty due to Discretization in CFD Applications". *Journal of Fluids Engineering*, Vol. 130, Issue 7. doi:10.1115/1.2960953.

Chao, L. M., Zhang, D., and Pan, G. (2017). "Roles of Size and Kinematics in Drag Reduction for Two Tandem Flexible Foils". *Modern Physics Letters B*, Vol. 31, No. 33. doi:10.1142/S0217984917503110.

Chase, N. (2012). *Simulations of DARPA Suboff Submarine Including Self-propulsion with the E1619 Propeller*. [Master's Thesis]. The University of Iowa Graduate College, Iowa, USA.

Groves, N. C., Huang, T. T., and Chang, M. S. (1989). "Geometric Characteristics of DARPA Suboff Models". David Taylor Research Center, Bethesda, USA.

Kale, F. M. (2020). *Numerical Investigation of Flow around a Submarine by Openfoam and ANSYS Fluent*. [Master's Thesis]. Istanbul Technical University Institute of Science, Istanbul, Turkey.



Kinaci, O. K. (2015). “A Numerical Parametric Study on Hydrofoil Interaction in Tandem”. *International Journal of Naval Architecture and Ocean Engineering*, Vol. 7, Issue 1, 25-40. doi:10.1515/ijnaoe-2015-0003.

Kukner, A., Duran, A., and Cinar, T. (2016). “Investigation of Flow Distribution around a Submarine”. *Journal of Naval Science and Engineering*, Vol. 12, Issue 2, 1-26.

Lungu, A. (2019). “DES-based Computation of the Flow around the DARPA Suboff”. *IOP Conference Series: Materials Science and Engineering*, 591. doi:10.1088/1757-899X/591/1/012053.

Maraam, M. A., Ghafari, H. R., Ghassemi, H., and Ghiasi, M. (2021). “Numerical Study on the Tandem Submerged Hydrofoils Using RANS Solver.” *Mathematical Problems in Engineering*, Vol. 2021. doi:10.1155/2021/8364980.

Menter, F. R. (1994). “Two-equation Eddy-viscosity Turbulence Models for Engineering Applications”. *AIAA Journal*, Vol. 32, No. 8, 1598-1605. doi:10.2514/3.12149.

Pletcher, R. H., Tannehill, J. C., and Anderson, D. A. (2011). *Computational Fluid Mechanics and Heat Transfer*, 3<sup>rd</sup> Edition. CRC Press, Florida, USA.

Rhie, C. M., and Chow, W. L. (1983). “Numerical Study of the Turbulent Flow Past an Airfoil with Trailing Edge Separation”. *AIAA Journal*, Vol. 21, No. 11, 1525-1532. doi:10.2514/3.8284.

Shang, Y., and Horrillo, J. J. (2021). “Numerical Simulation and Hydrodynamic Performance Predicting of 2 Two-dimensional Hydrofoils in Tandem Configuration”. *Journal of Marine Science and Engineering*, Vol. 9, Issue 5, 462-477. doi:10.3390/jmse9050462.

*Investigation of the Effect of the Flow Regulators on the Flow Around a Generic Submarine Sail*

Takahashi, K., and Sahoo, P. K. (2019). “Fundamental CFD Study on the Hydrodynamic Performance of the DARPA Suboff Submarine”. *Proceedings of the 38<sup>th</sup> International Conference on Ocean, Offshore & Arctic Engineering*, Volume 2: CFD and FSI, Glasgow, UK.  
doi: 10.1115/OMAE2019-96190.





Tennekes, H., and Lumley, J. L. (1972). *A First Course in Turbulence*, MIT Press, Cambridge, UK.

Wilcox, D. C. (2006). *Turbulence Modeling for CFD*, 3<sup>rd</sup> Edition, DCW Industries, California, USA.

Wilson-Haffenden, S., Renilson, M., Ranmuthugala, D., and Dawson, E. (2010). “An Investigation into the Wave Making Resistance of a Submarine Travelling below the Free Surface”. *International Maritime Conference 2010: Maritime Industry - Challenges, Opportunities and Imperatives*, Sydney, Australia.

*\*An ethical committee approval and/or legal/special permission has not been required within the scope of this study.*

**BATHYMETRIC ANALYSIS OF LYSTAD BAY, HORSESHOE  
ISLAND BY USING HIGH RESOLUTION MULTIBEAM  
ECHOSOUNDER DATA\***

**Emre TÜKENMEZ<sup>1</sup>**   
**Emre GÜLHER<sup>2</sup>**   
**Özgür KAYA<sup>3</sup>**   
**H. Fatih POLAT<sup>4</sup>** 

<sup>1</sup>*Office of Navigation, Hydrography and Oceanography, Istanbul, Turkey,  
etukenmez@shodb.gov.tr*

<sup>2</sup>*Office of Navigation, Hydrography and Oceanography, Istanbul, Turkey,  
egulher@shodb.gov.tr*

<sup>3</sup>*Office of Navigation, Hydrography and Oceanography, Istanbul, Turkey,  
okaya@shodb.gov.tr*

<sup>4</sup>*Office of Navigation, Hydrography and Oceanography, Istanbul, Turkey,  
hfpolat@shodb.gov.tr*

**Received: 05.12.2021**

**Accepted: 21.04.2022**

*Emre TÜKENMEZ, Emre GÜLHER, Özgür KAYA, H. Fatih POLAT*

### **ABSTRACT**

*In this study the compatibility between high resolution multibeam echosounder data of Lystad Bay, Horseshoe Island obtained during Turkish Antarctic Expedition-III and the soundings of British Admiralty (BA) 2974&3213 nautical charts produced by United Kingdom Hydrographic Office (UKHO) was investigated. The bay was charted in 1960, first, by Lieut.C.J.C. Wynne-Edwards (Royal Navy)'s survey data and no chart has been produced with any new measurements since then. BA charts were created by means of single beam echosounder data. The comparison of the newly gathered data in the surveyed area (6.9km<sup>2</sup>) which covers half of the Lystad Bay indicate that soundings on the nautical charts of BA2974 & BA3213 are shallower and coastlines are not compatible. Additionally, the data from February 2019 depicts depths as varying between 2.8-94.6 meters. Dense multibeam echosounder data made 3D analyzes achievable, which shows that the sea bottom topography has not only trenches but also shoals that should be considered in order to navigate safely in the bay. Moreover, modern satellite-based positioning systems provide more accuracy than terrestrial positioning systems. The sound velocity is measured as 1446.5 and 1447.5 m/s at the surface and decreasing with increasing depth.*

**Keywords:** *Horseshoe Island, Lystad Bay, Multibeam Echosounder Data, Bathymetry.*

**YÜKSEK ÇÖZÜNÜRLÜKLÜ ÇOK BİMLİ İSKANDİL VERİLERİ İLE HORSESHOE ADASI, LYSTAD KÖRFEZİ'NİN BATİMETRİK ANALİZİ**

**ÖZ**

*Bu çalışmada Üçüncü Ulusal Antarktika Bilim Seferi'nde Horseshoe Adası, Lystad Körfezi'nde toplanan çok bimli iskandil verileri ile Birleşik Krallık Hidrografi Ofisi tarafından üretilen BA2974 & BA3213 numaralı seyir haritalarındaki derinlik değerleri arasındaki uyumluluk araştırılmıştır. Söz konusu körfez ilk kez 1957 yılında Yüzbaşı Wynne-Edwards (Kraliyet Donanması) tarafından toplanan verilerle 1960 yılında haritalandırılmıştır ve bu zamandan beri yeni ölçümlerle hiçbir harita üretilmemiştir. Söz konusu İngiliz haritaları tek bimli iskandil verisi kullanılarak oluşturulmuştur. Lystad Körfezi'nde mesahası yapılan ve yaklaşık yarısını kapsayan sahada (6.9km<sup>2</sup>) toplanan batimetrik verilerden elde edilen sonuçlar BA2974 & BA3213 numaralı seyir haritalarındaki iskandil değerlerinin Şubat 2019'daki ölçümlerden daha sığ değerlere sahip olduğunu ve sahil hatlarının uyumlu olmadığını göstermektedir. İlaveten Şubat 2019 verileri 2.8-94.6m arasında değişken derinlikler göstermektedir. Yoğun çok bimli iskandil verileri körfezde güvenli seyir icra etmek için dikkate alınması gereken hem çukurları hemde sığılıkları olan deniz tabanı topografyasını gösteren 3 boyutlu analizlerin yapılmasını mümkün kılmıştır. Ayrıca modern uydu tabanlı konumlandırma sistemleri kara tabanlı konumlandırma sistemlerinden daha fazla doğruluk sağlamaktadır. Ses hızı yüzeyde 1446.5 ve 1447.5m/s olarak ölçülmüştür ve artan derinlikle birlikte azalmaktadır.*

**Anahtar Kelimeler:** *Horseshoe Adası, Lystad Körfezi, Çok Bimli İskandil Verisi, Batimetri.*

## **1. INTRODUCTION**

A bathymetric measurement is a complex process since sailors/mariners always demand reliable value on nautical charts. An accurate map of the sea floor is not only vital to the safety of navigation in nautical chart production but also critical for other purposes such as ocean circulation models (i.e. HYCOM, MOHID, ROMS, NEMO, POM) used in physical, chemical, biological oceanography. Seafloor topography has a crucial role in understanding climate change effects since they can deliver significant information about sea-level rise, potential changes in shoreline, sediment transport, benthic habitat mapping and distribution of clay minerals on the surface sediments (Kenny et al., 2003; Bart et al., 2016; Jung et al., 2021). Also, depth information is of great importance for understanding ocean circulation dynamics, patterns and Earth's structure. The previously made studies in the Antarctic region validate the above-mentioned cases.

The understanding of the Antarctic ecosystem and ocean circulation could be improved with more accurate and high-resolution bathymetric data. Especially the western part of the Antarctic Peninsula, which is ice-free, gets people's attention from all around the world since many bases in Antarctica (%30) are situated in this specific region. Due to its advantages (being close to mainland, being ice-free etc.) scientists focus more on the South Shetlands Islands for their research. However, studies in the southern part of the Antarctic Peninsula are rare as opposed to the South Shetlands Islands and especially bathymetric data are still sparse.

Accurate, reliable and up-to-date depth information is imperative to navigate in the bay, especially along shipping routes for carrying camping and scientific equipments in Antarctica where limited depth information is available. Strong winds prevail outside the bay and there is no pier/port for vessels to take shelter. High resolution bathymetric data are needed to navigate safely and as closely as possible to the Turkish Scientific Research Camp so that wind effect can be minimized. Another necessity is to ensure the right place for anchoring.

Hydrographers and oceanographers have used different methods and tools to collect and process data during survey. In the past, depth was measured by placing weight on the rope. After that echo sounding systems have been

*Bathymetric Analysis of Lystad Bay, Horseshoe Island by Using High Resolution Multibeam Echosounder Data*

used for measuring depths by transmitting acoustics pulses in seafloor mapping since the beginning of 20<sup>th</sup> century. A variety of techniques including visual, mechanical, acoustic methods can be used to obtain bathymetric data however most common tools and methods known today are quantitative ones such as single beam and multi beam echosounders.

In general, single beam echosounder which makes a single depth measurement has been used until 1960s (L-3 Communications SeaBeam Instruments, 2000). It is most basic echo sounding device and has some limitations that make it not appropriate. It falls short of producing depth measurements for well-defined locations and conducting a survey in a reasonable time (not a time-sufficient tool). That device cannot provide detailed sea bottom mapping and may miss valuable depth information such as seamounts, wrecks and covers a limited area with low spatial resolution data. A single beam measures the range at a point below the ship and could give better results for flat bottom however for irregular sea floor it cannot produce an accurate detailed depth measurement. On the other hand a new technique uses multiple depth sounding beams allow surveyors to produce higher spatial resolution with less endeavors (Parnum et al., 2009). Multibeam echo sounders that have their transducers mounted to the hull of the ship has become available to scientific community for about four decades and can map larger areas with multiple beams and swath width (Clarke, 2018). Multibeam echosounders send many beams and have the ability to measure different locations simultaneously. The received signal is a complicated pulse since it is strongly influenced by shape of bottom and sediment type. For bathymetry, unique characteristics and superior capabilities of multibeam echosounder make it more common to use for depicting ocean bottom mapping (Brissette and Clarke, 2015; Zhao, 2015).

South Shetland Islands located in Antarctic Peninsula (northwestern part of Antarctica) is the region where a large percentage of bases are located due to its ideal conditions like mentioned before. Horseshoe Island in which Turkish Scientific Research Camp established is close to South Shetland Islands as displayed in Figure 1. The closest base to Turkish Scientific Research Camp is located 46km western side of the Rothera Base (belongs to UK) on the Adelaide Island (Figure 2) in the Marguerite Bay. The

detailed information regarding the boundaries and co-ordinates of Lystad Bay are presented in Table 1.

The existing British Admiralty (BA) charts, BA2974 and BA3213, were produced by means of single-beam echosounder data gathered in 1957, and are pretty old. They house low resolution data with the scales of 1:150000 and 1:50000, respectively. BA3213 was produced in 1960 by using 1957's survey data. In 2012, BA2974 covering the area of Marguerite Bay was published and updated however survey data of 1957 was used for the region of Lystad Bay. Despite the high attention towards the region, only those charts shown in Figure 3 are at sailors's service. Apart from the surveys made for the production of the before said charts, unfortunately, no studies or surveys have been carried out for hydrographic purposes, until 2019.

The Horseshoe Island where Turkish Scientific Research Camp is established covers an area of 60km<sup>2</sup>, has one bay and two coves, most part of its coastline is ice-free, just 23 km (36%) of it being ice-covered (Yıldırım, 2019). The archipelago of Marguerite Bay, where the Lystad Bay is located was covered by sheet of ice at ca. 20ka ago (Bentley et al., 2011). However, the ice-sheet was removed with the effects of climatic events by ca. 9.5ka (Çiner et al., 2019). The geomorphology of the Horseshoe Island shows that it is still under the influence of glaciers (Yıldırım, 2019). That indicates coastlines and surroundings of the island continue interacting with ice, so topography of it will continue changing over a long-term time scale. Glaciers can transport material beneath them and carry rocks far away from their original locations (Spellman, 2021). Moreover they can reshape the seafloor with respect to their weight over hundreds or thousands of years (Spellman, 2021). So it could be stated that ice reshapes the bathymetry of the region in the long term and gives the idea to the geologists about the historical change of geological formation.

The aim of the study is not only to obtain bathymetry of the area but also to compare with BA charts. The scope of the area is the Turkish Scientific Research Camp in Antarctica. That's why this study is crucial for the reach of achievement of future scientific research in Antarctica.



*Bathymetric Analysis of Lystad Bay, Horseshoe Island by Using High Resolution Multibeam Echosounder Data*

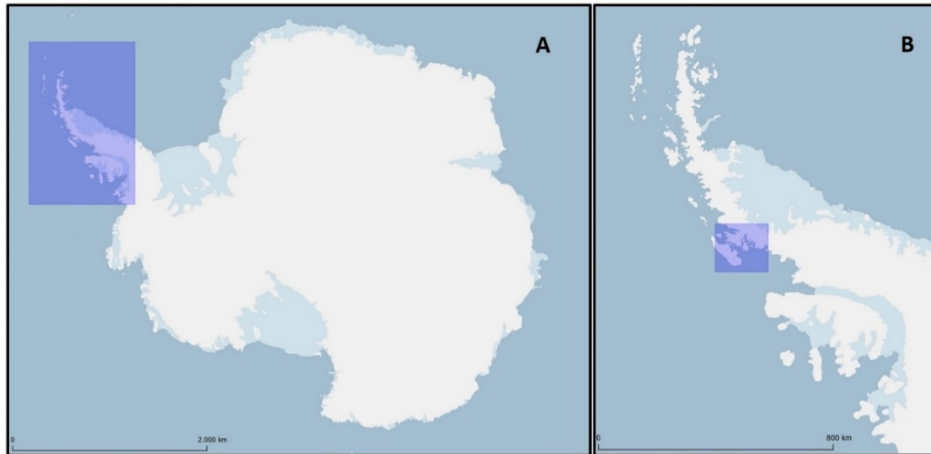


**Figure 1.** Location map of Antarctica (A) and Antarctic Peninsula (B).

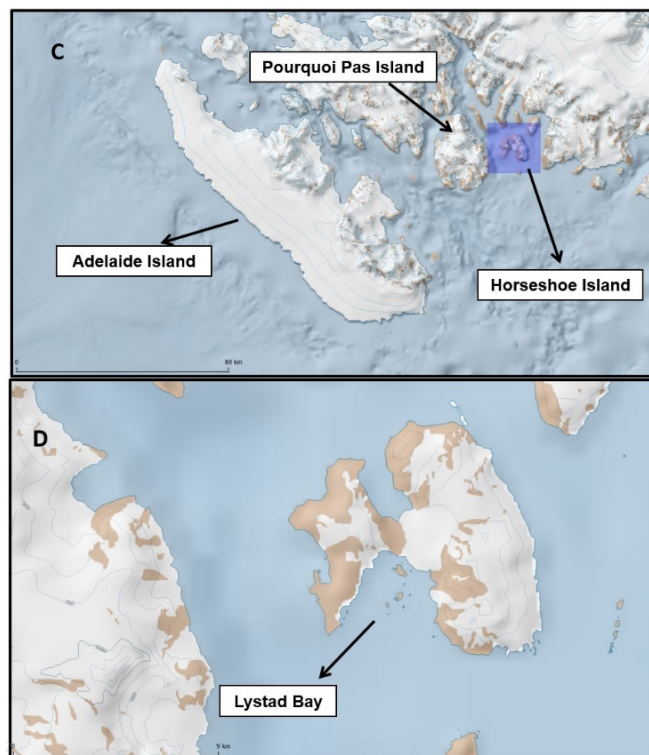


**Figure 2.** Surroundings of Horseshoe Island (C) and Lystad Bay (D).

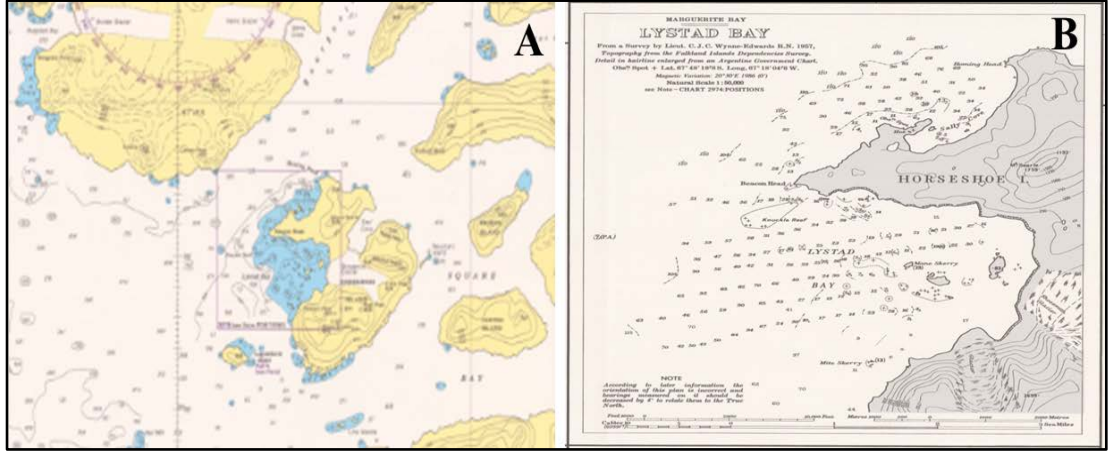


**Figure 3.** The charts of BA2974 (A) with scale of 1:150000 & BA3213 (B) with scale of 1:50000.

**Table 1.** Boundaries of Lystad Bay.

Corners	Latitude	Longitude
Northwestern	67°49'22.40'' S	067°20'47.63'' W
Northeastern	67°49'33.33'' S	067°14'25.24'' W
Southeastern	67°50'52.22'' S	067°14'04.21'' W
Southwestern	67°52'05.59'' S	067°18'21.76'' W

The remainder of this paper is organized as follows: Section 2 describes the data, equipments and methods, Section 3 presents the results and Section 4 concludes the study with a summary.

*Bathymetric Analysis of Lystad Bay, Horseshoe Island by Using High Resolution Multibeam Echosounder Data*

## **2. MATERIAL AND METHODS**

Sound velocity in the environment during data collection period is of great importance for accurate hydrographic surveying and calculations (Alkan et al., 2006). Sound can travel in water more easily than air and has the ability to move great distances in water environment (L-3 Communications SeaBeam Instruments, 2000). Sound speed is a function of the parameters of salinity, temperature and pressure. In general, typical sound velocity of seawater under the nominal condition (0 °C, 35 psu) is 1500 m/s and calculated as shown below;

$$\text{Sound Speed} = \text{Frequency} \times \text{Wavelength}$$

Low frequency sound is attenuated slowly while high frequency can travel impeded throughout the sea since attenuation of sound is based on the frequency (L-3 Communications SeaBeam Instruments, 2000). During depth measurement, the amount of energy reflected or scattered depends on the characteristics of the material and the angle of incidence. The name of the returning signal is “echo”.

Passive sonars that just listen and active sonars that both listen and produce sound waves are two basic types of sonars. With respect to definitions it is clear that active sonar principle is used for bathymetric measurements. The idea depends on the time delay between transmitted and received signals, where depth information is obtained by using time delay and velocity of echo. In other words echo time is the time of round trip. Speed of sound in water column is obtained from portable CTD equipment in this survey. After getting all those parameters range (depth) could be calculated as shown below;

$$\text{Depth} = 1/2 * \text{Velocity} * \text{Echo Time}$$

Tide is another parameter that should be taken into account. Soundings are reduced to chart datum which refers to lowest astronomical tide or mean sea level in order to include tide on the measurements. If there is not a tide gauge in the survey area, tide measurements should be specifically done or tide gauge can be installed. Fortunately, in the study region there is a permanently installed tide gauge in Rothera which used to obtain the depth

values to be reduced to chart datum. Using the tide data of previously established tide stations is also advised by IHO M-13 document.

All those parameters are processed and used to create reliable bathymetric datasets. For data quality control and processing of bathymetric data CARIS HIPS & SIPS software is used. Interpolation technique (angle cube etc.) is not applied to data since interpolated points do not reveal realistic values.

Total vertical uncertainty is calculated with the formula shown below. In this formula, the parameter of “a” represents the rate of the uncertainty that does not change with depth, “b” is the rate of the uncertainty that varies with depth and “d” means the depth value (IHO S44). In accordance with these calculations, maximum errors of the depth measurements with increasing depth are displayed in Figure 4.

$$error = \pm\sqrt{a^2 + (b + d)^2}$$

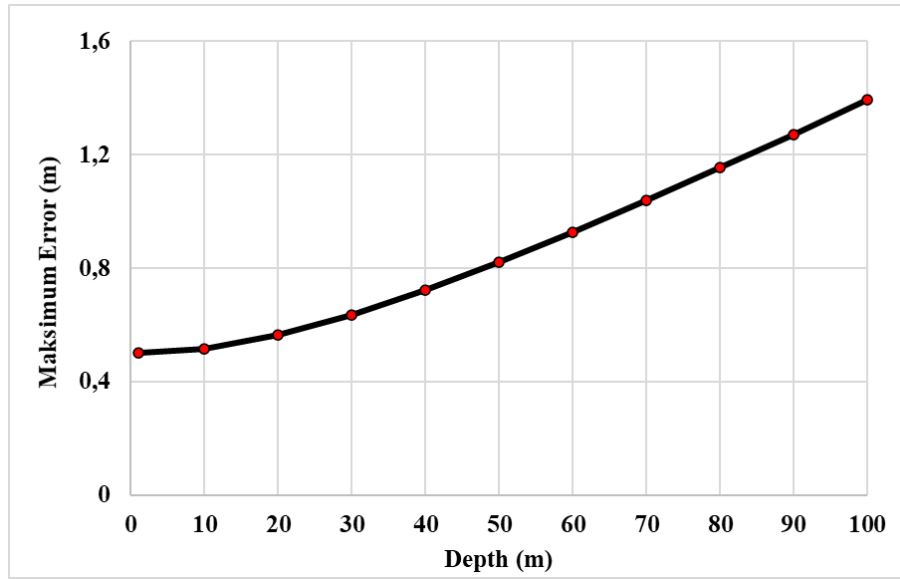


**Figure 4.** Graph of maximum errors for Order 1a.

High resolution bathymetric data gathered during the Turkish Antarctic Expedition-III in February 2019 and the survey area is located in the south-

*Bathymetric Analysis of Lystad Bay, Horseshoe Island by Using High Resolution Multibeam Echosounder Data*

central part of the Antarctic Peninsula and focuses on Lystad Bay. During data process and collection period, International Hydrographic Organization (IHO) Standards-44 are applied to bathymetric data. Accuracy of data is “Order 1a” in accordance with minimum bathymetry standards for safety of navigation hydrographic surveys of IHO S-44 at 95% confidence. WGS 84 Datum and UTM 19S Projection are used for all co-ordinates and the resolution of the surveyed data is 1m.

Accurately mapping is the paramount for getting accurate solutions and analyses in evaluations. In this study bathymetric data that consist of three parameters named as \*.xyz (latitude, longitude, sounding) are obtained by the R2SONIC 2022 multibeam echosounder (Figure 5) that uses acoustic waves. Details about the equipments and softwares utilized in this study are shown in Table 2. All those materials and data belong to Turkish Navy Office of Navigation, Hydrography and Oceanography. The instrument of R2SONIC 2022 has 256 beams and 400kHz (1\*1 degree beam width). Main components of an echo sounder are transducer, transmitter, receiver and recorder. Survey speed was around 5kts. Coastline measured with TOPCON GR-3 GNSS (Global Navigation Satellite System) refers to the line where coast and water meet (IHO S32). Additionally, a free GIS package for research, education and operation in Antarctica which is called Quantarctica V3 is used too.

**Table 2.** Information about the equipments and softwares.

<b>Purpose</b>	<b>Equipment</b>
Hydrographic Surveying	R2SONIC 2022 400 Khz
Temperature, Salinity, Sound Speed	Valeport CTD
Coastline	TOPCON GR-3 GNSS
Data process / analysis	CARIS HIPS and SIPS
Tide	Rothera Station Tide Gauge (UK)



**Figure 5.** Equipment of R2SONIC 2022 400 Khz Multibeam Echosounder (A) and Valeport CTD (B).

### **3. RESULTS**

Horseshoe Island, the third largest island in the Marguerite Bay, has the dimensions of approximately 9km by 10 km, covers an area of 64.29km<sup>2</sup> and its coastline is 53.75km long. The survey area is located in the Lystad Bay which is in the southern part of the Horseshoe Island and covers an area of 13.62 km<sup>2</sup> with some small islands. The numbers found in the study of Yıldırım (2019) are compatible with our calculations.

Lystad Bay of Horseshoe Island is first charted in 1960 by using Lieut. C.J.C. Wynne-Edwards's survey data and neither a new chart has been produced with new measurements nor a new survey has been carried out since 1957. For the updated version of BA2974, Lieut. C.J.C. Wynne-Edwards's data were used again in 2012. Since this survey conducted six decades ago when terrestrial methods were used, the data of it needs to be corrected and revised with respect to new satellite-based positioning systems. Terrestrial methods used in the past to minimize positioning errors with mechanical, optical, electronic means are sextant, triangulation/intersection, visual, range-azimuth (IHO M-13). Sextant

*Bathymetric Analysis of Lystad Bay, Horseshoe Island by Using High Resolution Multibeam Echosounder Data*

positioning that performed by simultaneous measurement of two horizontal angles between three position-known objects is not considered accurate today. Recently the other technique called visual position method that used for structures of navigation aids is very little used (IHO M-13). Range-Azimuth Positioning, based on the generation of a position through the perpendicular intersection between lines of locations, once was a very common and most used method (IHO M-13).

Availability of Global Positioning System (GPS) positioning methods make it become the worldwide and take place of the all-previous techniques after 1990s (IHO M-13). GPS positioning devices used in this new study can provide better accuracy for positioning than terrestrial positioning methods with the advantages of satellites (IHO M-13).

CTD is used before gathering hydrographic data since sound speed is needed to apply the instrument of R2SONIC 2022. Sound speed is the final and crucial product which depends on salinity, temperature and pressure and calculated by those parameters. The locations of portable CTD measurements and sound velocity profile are presented in Figure 6. With respect to Figure 6, it could be said that sound velocity ranges from 1446.5 to 1447.5 m/s at the surface and decreases from surface to deeper parts. When sound speed values of this study are compared with Mediterranean Sea, annual horizontal distribution sound speed at 50m in Mediterranean Sea is clearly greater than Southern Ocean with values between 1506 and 1527 (Salon et al., 2003) due to its warmer waters. During the data process session, critical sound speed data are strictly applied to surveyed data since those regions have unique characteristics with low temperature and hence low sound velocity data. Sound travels faster with higher temperature which strongly influences the sound speed. In other words, sound propagates slower in cold water than warm water (Fofonoff and Millard, 1983).

As mentioned in material and methods, sea level measurements of Rothera Station are used since it was the closest station to the bay. According to Figure 7, mean sea level values of the dates of 20-24 February 2019 vary from about 0.48m to 1.97m. Tide values during the survey time subtracted from measured data in order to reduce soundings to chart datum.

In the Turkish Antarctic Expedition of 2019, the proportion of surveyed area (6.9 km<sup>2</sup>) to the total area of the bay is approximately %50. For the surveyed area, Bathymetry of the bay has sharp changes and the depth from the coastline to Marguerite Bay increases from 2.8 m to 94.6m as depicted in Figure 8.

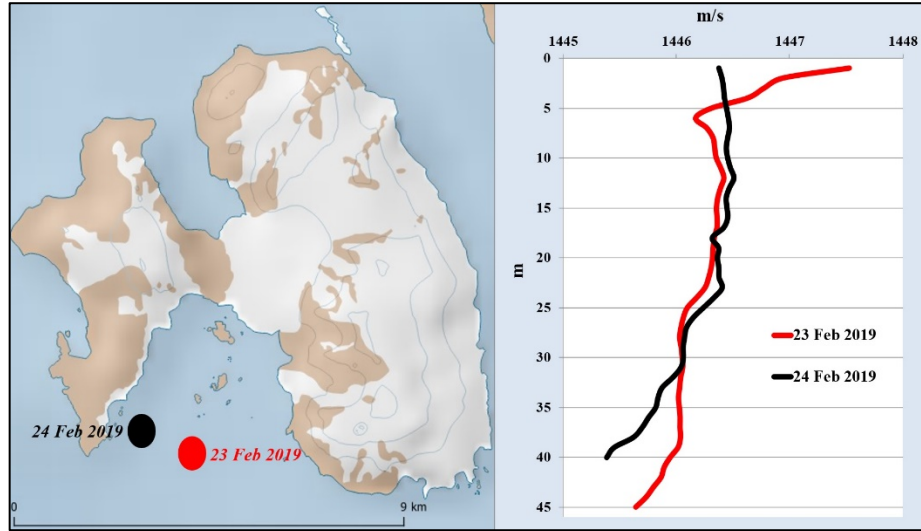


**Figure 6.** Location of CTD measurements and sound velocity profile of Lystad Bay.

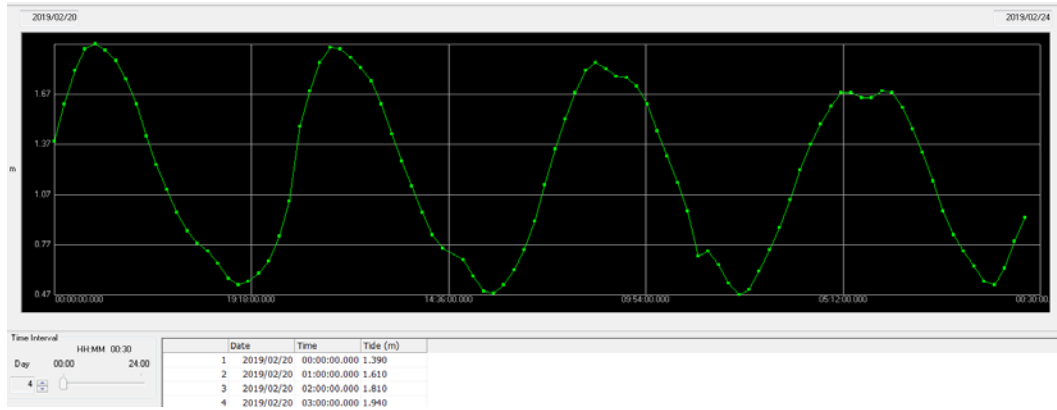


**Figure 7.** Sea level measurements of Rothera Station (20-24 February 2019).



*Bathymetric Analysis of Lystad Bay, Horseshoe Island by Using High Resolution Multibeam Echosounder Data*

Modern multi-beam echo sounders provide very detailed full seafloor coverage. By the help of that high resolution bathymetric data, 3D picture of the sea floor can be visualized with all features such as seamounts, trenches. That is why 3D Picture of the surveyed area is created. Depth is changeable with trenches and shallow areas in the bay. The deepest point is 94.6m ( $67^{\circ} 49' 45.22''S$ ,  $067^{\circ} 19' 38.15''W$ ) and the shallowest point is 2.8m ( $67^{\circ} 49' 53.77''S$ ,  $67^{\circ} 15' 26.92''W$ ) as shown in Figure 8. The unnamed trench/deep in the bay is dedicated to prominent Turkish cartographer Piri Reis. On the other hand the resolution and accuracy of old data were not good enough to draw a 3D picture of seafloor.

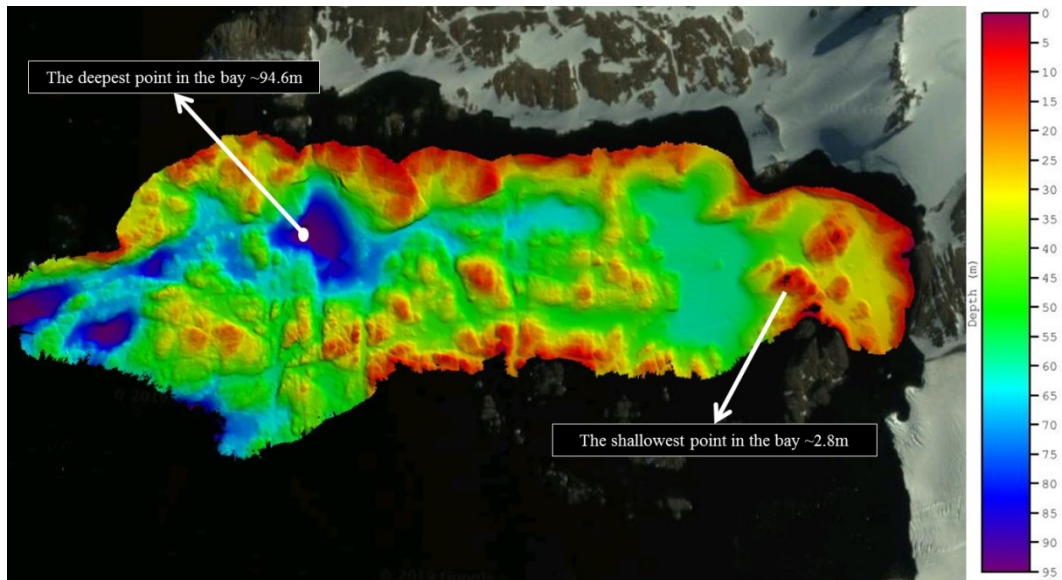


**Figure 8.** 2D Picture of the surveyed area.

The new survey data gives the advantage to see all features of bottom topography and provides detailed examination. For instance, two selected shallow areas examined whether those locations are obstacle to navigational safety. These analyses represent that the point located in the central part does not need to be considered as a problem for ships that have draft lower than 8m however the point closes to the camp is shallow (2.8m) and has risks for safety of mariners (Figure 10).

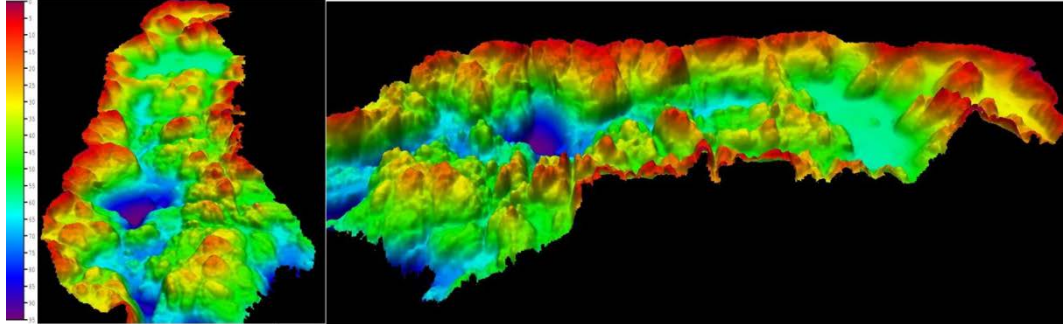


**Figure 9.** 3D Picture of the surveyed area.

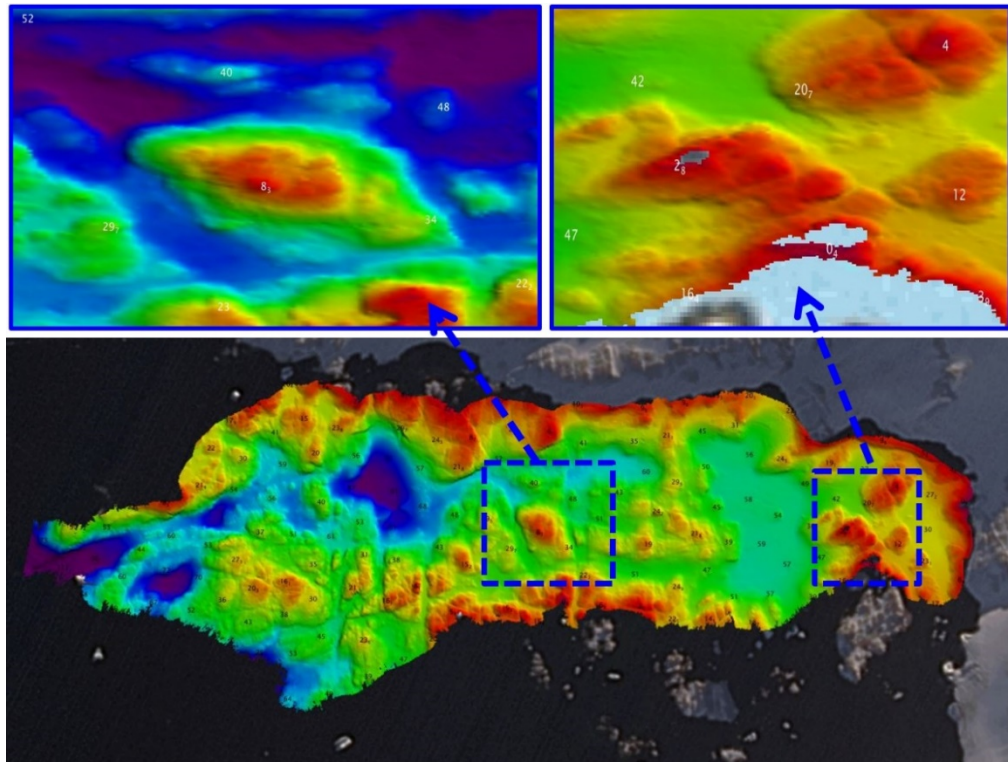


**Figure 10.** Detailed analyses of critical positions.

In general, the analyses of the comparisons discussed herein indicated highly differences of coastline and depth for new and old survey. The point-to-point comparisons with visual inspection confirm that there is a clear

*Bathymetric Analysis of Lystad Bay, Horseshoe Island by Using High Resolution Multibeam Echosounder Data*

difference between depth information (Figure 11-12). Figure 11-12 present that soundings in BA2974 and BA3213 are shallower than the new survey data and the positions of the coastline data are shifted 70m in east and west direction due to differences in sensitivity of past & recent technologies.

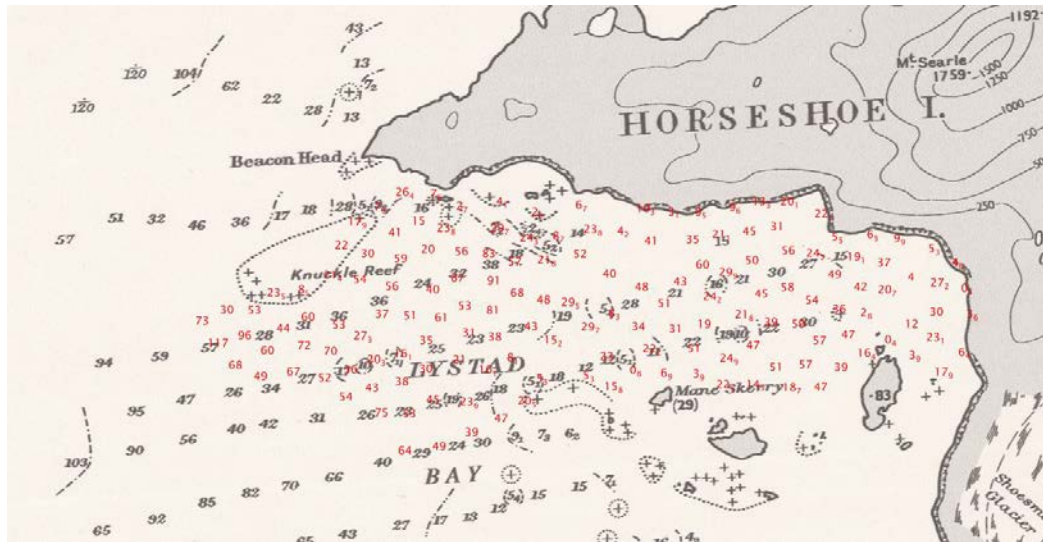


**Figure 11.** Comparison of BA3213 (black coloured) and survey data of February 2019 (red coloured).

Coastline of new data is not following the same pattern with BA charts. The differences between soundings and coastline of BA charts with new survey are due to modern techniques and technology used in 2019 not the glaciers since influences of glaciers over sea floor topography take more than hundreds or thousands of years. Additionally, to see the variations and glaciers effect not only long time period but also high-resolution data are needed. In the light of that information old data do not meet the requirements to understand the glaciers impact on sea floor.

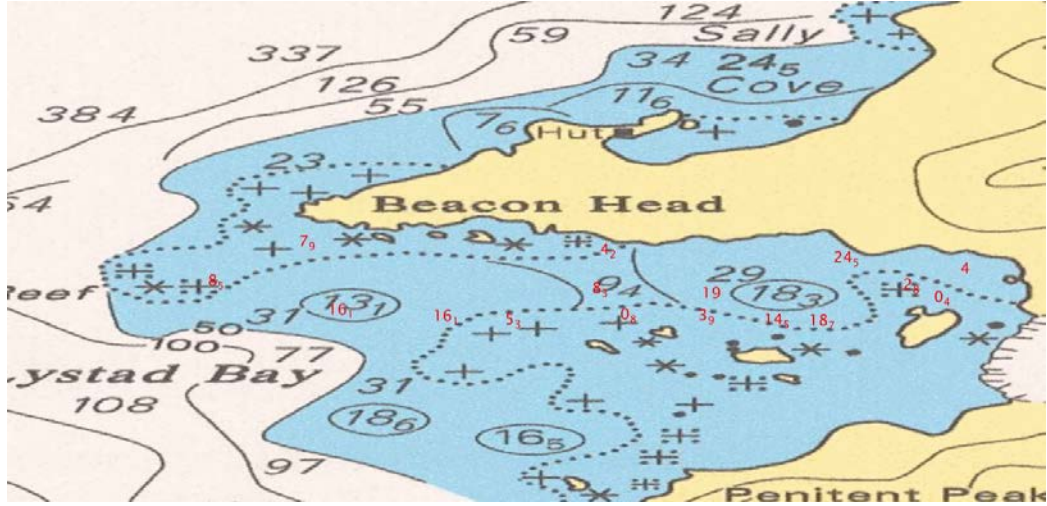


**Figure 12.** Comparison of BA2974 (black coloured) and survey data of February 2019 (red coloured).

#### 4. CONCLUSION AND DISCUSSION

The focus of this study lies on Lystad Bay where data is most needed for following Turkish Antarctic Expeditions. In this study the values obtained with new survey conducted in 2019 and comparisons of BA charts with high resolution data were presented. The results give useful preliminary information on bathymetric characteristics in Lystad Bay. The collected data shows variation of depth information between 2.8m to 94.6m and the overall bathymetric data of Lystad Bay reveals differences between new & old survey data. It is discovered that multibeam echosounder data are significantly deeper than single beam data of BA charts. The differences observed for the region are due to techniques and technology not the glaciers since it takes more than hundreds or thousands of years to mention about the impact of glaciers.

Single-beam echo sounders just provides one line of depth information along the survey vessel route so missed features (trench, wreck etc.) could be found in port and starboard sides of the track. However multi-beam echo sounders can compute both port/starboard and fore/aft at the same time and provides seafloor coverage with more soundings than single-beam echo



*Bathymetric Analysis of Lystad Bay, Horseshoe Island by Using High Resolution Multibeam Echosounder Data*

sounders. In this survey portable multibeam echosounder (R2SONIC 2022, 400 Khz) is used to gather depth information. Another advantage of this new study is that GNSS services are being used to derive positions. Satellite-based positioning equipments provide higher accuracy than land-based positioning systems. All new technology tools increase the accuracy of the data and give confidence to hydrographers during producing nautical charts.

Our data comparison shows that multibeam echosounder data have a great potential for Antarctica for following years. In order to support safety of navigation BA2974 and BA3213 charts should be updated with respect to new data gathered by Turkish Navy-Office of Navigation, Hydrography and Oceanography since no points in the charts are matching with new data.

Lastly the remaining unsurveyed part (%50) of the bay should be surveyed in the near future. The data gathered in old techniques should be replaced with new high-resolution data since low resolution data may miss all features. Sidescan sonar is another way for getting detailed data from the sea floor and it can display a mosaic map of topography.

*Emre TÜKENMEZ, Emre GÜLHER, Özgür KAYA, H. Fatih POLAT*

#### **ACKNOWLEDGEMENT**

This study was presented in the 5th National Polar Science Workshop on 30 November 2021.

This study was carried under the auspices of Presidency of the Republic of Türkiye, was supported by the Ministry of Industry and Technology, and was coordinated by Istanbul Technical University (ITU) Polar Research Center (PolReC).

The authors would like to express their gratitude to Ministry of National Defence, Turkish Naval Forces Command, Office of Navigation, Hydrography and Oceanography that guided and led to make this survey and study happen. Also, the authors wish to say “thank you” to scientists, who joined Turkish Antarctic Expedition-III and R/V BETANZOS personnel for their help and support during survey.

#### **CONFLICT OF INTEREST STATEMENT**

The authors declare no conflict of interest.

*Bathymetric Analysis of Lystad Bay, Horseshoe Island by Using High Resolution Multibeam Echosounder Data*

**REFERENCES**

Alkan, R. M., Kalkan, Y., Aykut, N. O. (2006). "Sound velocity determination with empirical formulas and bar check". *Proceedings of 23rd FIG Congress*, Oct. 8-13, Munich, Germany, pp. 1-14.

Bart, P. J., Mullally, D., Golledge, N. R. (2016). "The influence of continental shelf bathymetry on Antarctic Ice Sheet response to climate forcing". *Global and Planetary Change*, Vol. 142, pp. 87-95.

Bentley, M. J., Johnson, J. S., Hodgson, D. A., Dunai, T., Freeman, S.P.H.T., Cofaigh, O. C. (2019). "Rapid Deglaciation of Marguerite Bay, Western Antarctic Peninsula in the Early Holocene". *Quaternary Science Reviews*, Vol. 30, Issues 23-24, pp. 3338-3349.

Brissette, M. B., Clarke, J. E. (2015). "Side Scan versus Multibeam Echosounder Object Detection: A Comparative Analysis". *The International Hydrographic Review*, Vol. 76, No. 2.

British Admiralty Nautical Chart of BA2974. (2012). Adelaide Island to Neny Fjord[map]. 1:150000. British Government Surveys.

British Admiralty Nautical Chart of BA3213. (1960). Lystad Bay[map]. 1:50000. British Government Surveys.

Çiner, A., Yıldırım, C., Sarıkaya, M. A., Seong, Y. B., Byung, Y. Y. (2019). "Cosmogenic <sup>10</sup>Be exposure dating of glacial erratics on Horseshoe Island in western Antarctic Peninsula confirms rapid deglaciation in the Early Holocene". *Antarctic Science*, Vol. 31, Issue 6, pp. 319-331.

Fofonoff, N. P., Millard, R. C. (1983). "Algorithms for computation of fundamental properties of seawater". *UNESCO Technical Papers in Marine Science*, No. 44.

Clarke, J.E.H. (2018). “Multibeam Echosounders”. In Micallef, A., Krastel, S., and Savini, A. (Eds.), *Submarine Geomorphology* (Chapter 3, pp. 25–42), New York, Springer International Publishing.

International Hydrographic Organization (IHO) (2020). “IHO Standards for Hydrographic Surveys”. Publication No. 44. 6<sup>th</sup> Edition. Monaco. Published by the IHO.

International Hydrographic Organization (IHO) (2019). “Hydrographic Dictionary / Multilingual Reference for IHO Publications”. Publication No. 32.

International Hydrographic Organization (IHO) (2005). “Manual on Hydrography”. Publication No. M-13. 1<sup>st</sup> Edition. Monaco. Published by the IHO.

Jung, J., Ko, Y., Lee, J., Yang, K., Park, Y. K., Kim, S., Moon, H., Kim, H. J., Yoo, K. C. (2021). “Multibeam Bathymetry and Distribution of Clay Minerals on Surface Sediments of a Small Bay in Terra Nova Bay, Antarctica”. *Minerals*, Vol. 11, Issue 72, pp. 1-12.

Kenny, A. J., Cato, I., Desprez, M., Fader, G., Schüttenhelm, R.T.E., Side, J. (2003). “An overview of seabed-mapping technologies in the context of marine habitat classification”. *ICES Journal of Marine Science*, Vol. 60, Issue 2, pp. 411-418.

L-3 Communications SeaBeam Instruments. (2000). “Multibeam sonar theory of operation”. Retrieved from <https://www3.mbari.org/data/mbsystem/sonarfunction/SeaBeamMultibeamTheoryOperation.pdf>

Norwegian Polar Institute (2021). A free GIS for Antarctica. Quantarctica 3.2 GIS Software. Retrieved from <https://www.npolar.no/quantarctica/>



*Bathymetric Analysis of Lystad Bay, Horseshoe Island by Using High Resolution Multibeam Echosounder Data*

Parnum, I., Siwabessy, J., Gavrilov, A., Parsas, M. (2009). "A comparison of Single Beam and Multibeam Sonar Systems in Seafloor Habitat Mapping". *3<sup>rd</sup> International Conference & Exhibition on Underwater Acoustics Measurements: Technologies & Results*. pp. 155-162.

Salon, S., Crise, A., Picco, P., Marinis, E., Gasparini, O. (2003). "Sound speed in the Mediterranean Sea: An analysis from a climatological data set". *Annales Geophysicae*, Vol. 21, pp. 833-846.

Spellman, F. R. (2021). *Understanding Climate Change: A Practical Guide*. Maryland, Bernan Press.

Yıldırım, C. (2019). "Geomorphology of Horseshoe Island, Marguerite Bay, Antarctica". *Journal of Maps*, Vol. 16, Issue 2, pp. 56-67.

Zhao, D. N., Wu, Z. Y., Zhou, J. Q. (2015). "A new method of automatic SVP optimization based on MOV algorithm". *Marine Geodesy*, Vol. 38 Issue 3, pp. 225-240.

*Journal of Naval Sciences and Engineering*  
2022, Vol. 18, No. 2, pp. 305-332  
*Computer Engineering/Bilgisayar Mühendisliği*

RESEARCH ARTICLE

*\*An ethical committee approval and/or legal/special permission has not been required within the scope of this study.*

**AN EVALUATION ON WEAPON TARGET ASSIGNMENT  
PROBLEM\***

**Tolga ÖNEL<sup>1</sup>**   
**Elif BOZKAYA<sup>2</sup>** 

<sup>1</sup>*HAVELSAN A.Ş., Istanbul, Turkey,  
tonel@havelsan.com.tr*

<sup>2</sup>*National Defence University, Turkish Naval Academy, Department of  
Computer Engineering, Istanbul, Turkey,  
ebozkaya@dho.edu.tr*

**Received: 13.09.2021**

**Accepted: 04.04.2022**

Tolga ÖNEL, Elif BOZKAYA

### ABSTRACT

*Network-Centric Warfare (NCW) envisions taking the advantage of information technology developments by replacing traditional war management strategies. It affects both the fast and accurate decision-making process by providing organization and information exchange between military forces in geographically different locations. Combat management systems help to manage and maintain components such as sensors, weapons, platforms to create the tactical picture. As a result of the threat evaluation with a network-centric approach, effective defense strategies can be developed through the problem of weapon assignment and sensor allocation among military forces. In this paper, threat evaluation concept and parameters are firstly explained, and the static and dynamic target-based weapon assignment and sensor allocation problem are defined. We also simulate a scenario for weapon target assignment (WTA) problem and compare different approaches. Then, the concept of NCW and the problems that may be encountered are detailed.*

**Keywords:** *Network Centric Warfare (NCW), Threat Evaluation (TE), Weapon Assignment and Sensor Allocation (WASA) Problem, Combat Management Systems.*

## **SİLAH HEDEF ATAMA PROBLEMİ ÜZERİNE BİR DEĞERLENDİRME**

### **ÖZ**

*Ağ merkezli savaş, geleneksel savaş yönetim stratejilerini değiştirerek bilgi teknolojisi gelişmelerinden faydalanmayı öngörür. Coğrafi olarak farklı konumlardaki askeri birimler arasında organize olmayı ve aralarında bilgi alışverişi sağlayarak hem hızlı hem de doğru karar verme sürecine etki eder. Savaş yönetim sistemleri, taktik resmin oluşturulması için sensör, silah, platform gibi bileşenlerin yönetilmesi ve idamesine yardımcı olur. Ağ merkezli bir yaklaşım ile tehdit değerlendirmesinin gerçekleştirilmesi neticesinde askeri birimler arasında silah atama ve sensör tahsisi problemi üzerinden etkin savunma stratejileri geliştirilebilir. Bu makalede, öncelikle, tehdit değerlendirme kavram ve parametreleri açıklanarak, durağan ve dinamik hedefe dayalı silah atama ve sensör tahsisi problemi tanımlanmıştır. Sonrasında, silah-hedef atama problemi için bir senaryo verilerek, simülasyon ortamında farklı yaklaşımlar karşılaştırılmıştır. Son olarak ağ merkezli savaş kavramı ve karşılaşılabilecek problemler detaylandırılmıştır.*

**Anahtar Kelimeler:** *Ağ Merkezli Savaş, Tehdit Değerlendirme, Silah Atama ve Sensör Tahsisi Problemi, Savaş Yönetim Sistemleri.*

## 1. THREAT EVALUATION

Combat management consists of consecutive stages including threat detection, tracking, discrimination of real threats and decoys, identification, planning, weapon target assignment (WTA), engagement, kill/damage assessment (Athans, 1987) as in Fig. 1. Threat detection is based upon the data from several sensors. Tracking is the process of estimating the future target parameters like speed and position. Tracking process makes use of the target observations history. Identification involves the classification of the detected target. WTA process assigns the appropriate weapons to the identified threat, WTA is deemed as the resource allocation. The engagement phase is the execution of the planning and assignment phases in real time. Outcomes of the engagement are assessed in the assessment phase. Recent advancements in computer, network and communication make the Network Centric Warfare (NCW) possible. In NCW, the diverse warfighting platforms share their knowledge about the scene with each other through the communication links.

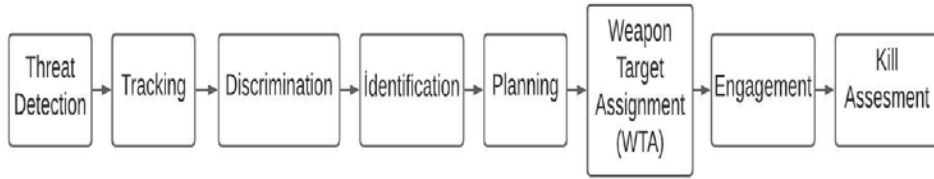


**Figure 1.** Combat management stages.

Command Control Communications Computer Intelligence Surveillance Reconnaissance (C4ISR) systems help the formation of the tactical picture in which the warfare scene including the warfighting components, their sensory information and weapons are managed. Combat Management Systems control and coordinate all these components, manage the operation, and build a decision support system.

Threat Evaluation (TE) is the use of multi-disciplinary actions to classify the threat levels. Threat levels allow the determination of minimum security reactions by military units, taking into account the prevailing conditions.

## *An Evaluation on Weapon Target Assignment Problem*

According to threat level, reaction is either independently or jointly applied in specific areas. TE and reaction are based on the type of the threat, scope of the mission or the size of the operational area.

In the case of multiple attacks on a combat ship, the operators or decision makers have to evaluate the situation and threat levels in real time to protect the force. More importantly, due to the limited time to give a decision against to the attack, all possible factors have to be considered. TE process requires data from radar and associated sensors. With the collected attributes and on-board computation, the threat value is determined. The attributes are classified in the research of (2014) M.L. Truter and J.H. van Vuuren as follows:

- **Proximity:** The parameters are evaluated based on the distance between a threat and the defended assets. If the threat is far away the defended assets, it cannot be classified as a possible threat.
- **Capability:** The parameters are evaluated based on the threat's capability so that the damage can be determined in the event of an attack.
- **Intent:** The parameters are evaluated based on threat's attitude. For example, a threat can follow its attack maneuvers.

Thus, for a combat scenario, there are various parameters that affect the decision-making process. They can be listed as follows:

- The properties and capabilities of sensors such as range, type, time;
- The properties and capabilities of weapons such as range, type, time;
- The capabilities and types of targets, their fuel capacity;
- Operational area.

All these parameters make the Weapon Assignment Sensor Allocation (WASA) problem more complex. The military units jointly select the best-suited subsets of the weapons and sensors that minimize the total expected value of the surviving targets. However, it brings multiple challenges, which we itemize as follows:

- Distributed resource allocation requires perfect coordination and synchronization among units. In a real problem where every millisecond is very important, there is no compensation for the consequences of an error in the calculation.
- The subgroup of sensors and weapons cannot be chosen arbitrary. The decision-making mechanism to be applied for each target not only depends on the characteristics of the target, but also differs in every time according to the possibilities and capabilities of the friendly units.
- A long-term scheduling is needed to prevent the rapid depletion of resources. Otherwise, an error in planning will have irreversible consequences.

In addition to a wide range of weapons and sensors that support warfare, threat features and damage properties are also varied. Effective defense eliminates all the threats with minimum damage received. Effective defense is that our own forces receive the least damage while eliminating all possible threats. For this purpose, the right weapons and sensors must be engaged at the right time with the right targets. This process is called Threat Evaluation Weapon Assignment and Sensor Allocation (TEWASA). Modern combat management systems should solve the TEWASA problem fast and autonomously.

This paper provides general guidance for using the existing algorithmic solutions in executing the Weapon Assignment and Sensor Allocation (WASA) problem. There are two types of weapon target assignment problem: static WTA and dynamic WTA. In static WTA, all weapons engage the targets at a single stage. All parameters are known by the decision makers. Thus, the aim is to find optimal assignment solution for a defined task. On the other hand, dynamic WTA is a multistage problem, thus decision makers assess each engagement for the next decisions till all threats are destroyed or all weapons are used. Dynamic WTA is more complex than static WTA (Xin et al., 2016). The problem described above relates to a scheduling and resource allocation problem, where the number of accomplished tasks needs to be maximized and resources should be available for possible use in the near future. The thread level or executing a

specific mission is out of the scope. Our main goal is to provide a comparison to maintain an efficient use of limited resources while maximizing the number of accomplished tasks. We explain the distributed sensor allocation and weapon assignment relation with a simulation environment.

The rest of the paper is structured as follows. WASA problem is described in Section II. Network Centric Warfare is detailed in Section III. In Section IV, we simulate a scenario and compare different approaches for weapon target assignment problem. In Section V, we review the existing literature on the WASA problem and solutions. Finally, we conclude the paper in Section VI.

## **2. WEAPON ASSIGNMENT SENSOR ALLOCATION**

Efficient resource management requires coordination of sensors and weapons in the combat systems. Different from the traditional resource allocation problems, WASA creates a resource pool via sharing its own resources. These are leveraged collectively or independently to address WASA problem. The defenders can provide a fixed number of sensors and weapons to tract the threat. Therefore, evaluating the threat and dynamically allocating sensor and assigning weapon are fundamental challenges to enable survivability of the force. WASA is a decision-making problem that actively manages sensors and weapons to maximize the resource utilization. The underlying challenge in WASA is to manage weapons and sensors for long-term benefits in the face of unpredictability.

As shown in Fig. 2, consider a combat scenario where military units equipped with sensors and weapons coordinate together. This is a distributed management of the resource allocation that requires perfect coordination and synchronization among sensors and weapons. The target sensors and weapons cannot be arbitrarily chosen. The sensors and weapons allocated for each possible threat (surface, underwater and aerial target) will differ. This turns the problem from a simple scheduling problem into a more complex one that minimizes the total expected value of the surviving targets.



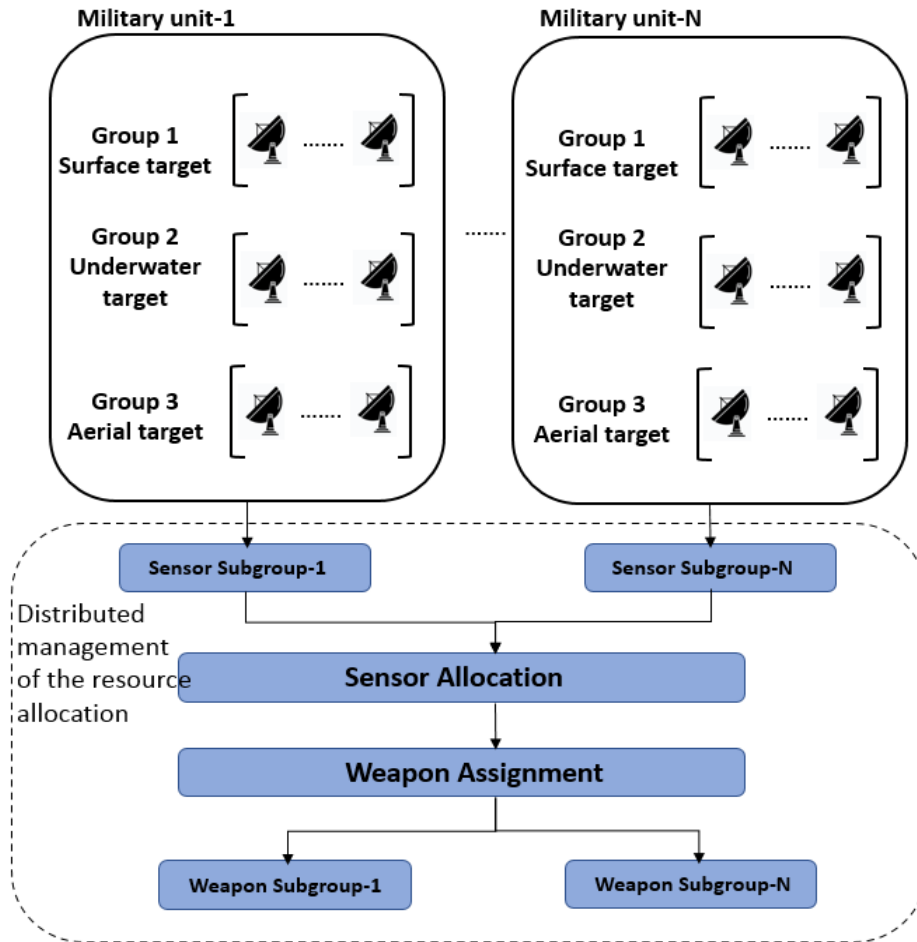


**Figure 2.** The considered combat scenario.

The research of (2010) F. Johansson and G. Falkman emphasize that the evaluations for sensor-weapon allocation problems are problematic since there are no standard scenarios to test the solutions. Therefore, they presented a testbed SWARD (System for Weapon Allocation Research and Development) for the static weapon allocation algorithms. The research of (2019) B. Xin, Y. Wang, and J. Chen propose a marginal-return-based constructive heuristic algorithm to solve sensor weapon target assignment

## *An Evaluation on Weapon Target Assignment Problem*

problems. They use a mathematical model with the collaboration of sensors and weapons.

While evaluating the WASA problem, besides defining the problem, performance evaluation also comes to the fore. Two of these parameters, survivability and engagement effectiveness are defined below.

Survivability is the ability to remain mission capable and to continue their operations of the defended assets in a hostile environment. Survivability is a vital feature for military forces which aims to retain the functionalities in the face of threats.

In the research of (2010) F. Johansson, survivability is defined as follows:

$$s = \frac{\sum_{j=1}^D w_j u_j}{\sum_{j=1}^D w_j} \quad (1)$$

where  $D$  is the number of defended assets,  $w_j$  is the importance of the  $j^{\text{th}}$  defended asset and  $u_j$  is a binary variable.  $u_j$  is equal to 1 if  $j^{\text{th}}$  defended asset survives, otherwise it will be 0. This represents the value of the importance of surviving assets against threats.

Another important parameter is engagement effectiveness. It depends on the platform reaction time, command and control, fire control systems, weapon performance characteristics, threat capabilities and importance.

In the research of (2014) M.L. Truter and J.H. van Vuuren, engagement effectiveness metric is defined as follows:

$$E = \frac{\sum_{j=1}^T v_j e_j}{\sum_{j=1}^T v_j} \quad (2)$$

where  $T$  is the number of threats,  $v_j$  is the importance value of the  $j^{\text{th}}$  destroyed threat and  $e_j$  is a binary variable.  $e_j$  is equal to 1 if  $j^{\text{th}}$  threat destroys, otherwise it will be 0.

WASA problem is addressed to allocate the sensors and assign the weapons to the enemy targets. The problem is also referred as Weapon Target Assignment (WTA) problem and can be classified as static and dynamic target-based. The difference between static WTA and dynamic WTA is whether the time is considered as a dimension (Zhang, Zhou, Yang, Pan & Kong, 2019). In the static WTA problem, there are defensive weapons deployed at certain points and threats directed at this defense. Each weapon has a different possibility of neutralizing a particular threat. Threats are also prioritized based on their distance, arrival time and impact. The aim is to destroy threats with appropriate weapons according to their priorities so that the defense receives the least damage. There can be different numbers of weapons and threats. Moreover, a threat can be engaged with more than one weapons. The reason for the problem being called static is that all weapon target assignment decisions are made in advance and that they remain unchanged during the engagement. Static WTA problem is proven to be NP-complete (Lloyd & Witsenhouse, 1986). On the other hand, in the dynamic WTA problem, decisions are spread over a period of time and carried out gradually. The result of the previous stages is reflected in the subsequent stages. This gives dynamic engagement flexibility to dynamic threats. Another distinction for the WTA problem is whether it is target-based or asset-based. The goal in the target-based method is to destroy as many dangerous targets as possible. The asset-based method aims to protect the most valuable assets from threats. Although the target-based problem can be considered as an example of the asset-based problem, it is examined separately. This is due to the need for additional information on which asset the targets are directed to in the asset-based problem (Hosein, 1990). In the next subsections, we formulate these two different approaches.

### 2.1. Static Target-based Problem

Each weapon has a different kill probability to destroy the targets. The objective is to assign weapons to the targets and minimize the total expected value of the surviving targets. Please note that in the assignment problem; each weapon can be only assigned one target at a time and more than one weapon can be assigned to the same target because of the high value. The problem is illustrated in Fig. 3. In the figure, green circles represent the weapons with the kill probability ( $P$ ). Orange and blue circles represent the value of assigned and unassigned target, respectively. Similarly, the orange lines give the assignments. For example, weapon 2 and  $w$  are assigned to  $v_T$ .

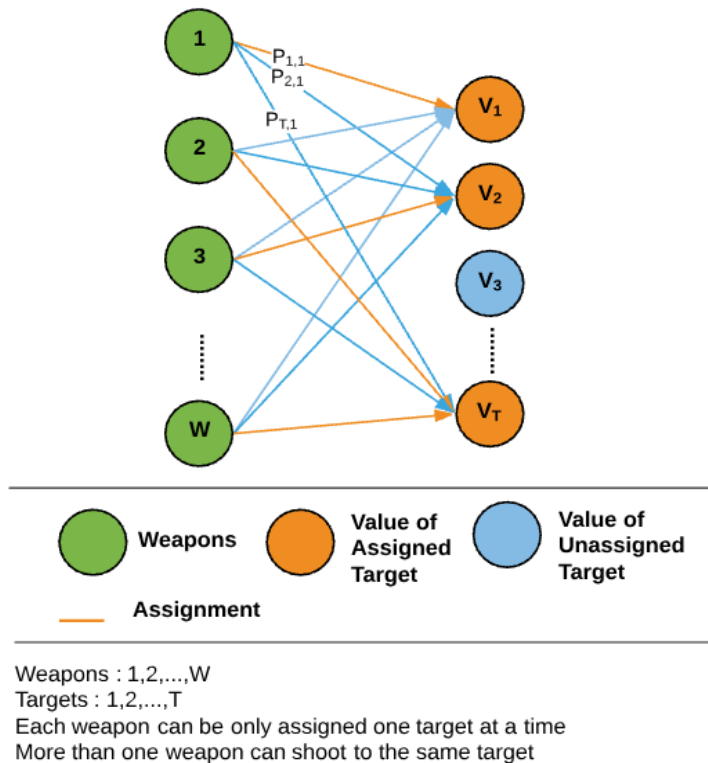


**Figure 3.** Static weapon-target assignment problem.

The problem optimally assigns a set of weapons to a number of targets such that it is aimed that total expected survival value of the targets is minimal after the engagements. The problem can be defined for single class of weapons in static target-based problem as follows (Hosein, 1990):

$$\min \sum_{i=1}^T V_i (1 - P_{ij})^{x_{ij}} \quad (3)$$

subject to

$$\sum_{i=1}^T x_{ij} = 1, \quad j = 1, 2, \dots, W \quad (4)$$

where  $x_{ij}$  is a decision variable and equals to 1 if a weapon  $j$  is assigned to the target  $j$ . Otherwise,  $x_{ij} = 0$ .  $T$  is the number of targets,  $V_i$  is the value of the target  $i$  and  $W$  is the number of weapons assigned to target  $i$  and  $P_i$  represents the kill probability of the weapon on target  $i$ .

## 2.2. Dynamic Target-based Problem

Dynamic decision-making process is divided into several time segments (Hosein, 1990). In the initial stage, a subset of weapons is chosen and assigned to the targets. Then, based on this observation, second stage is constructed with the remaining weapons. Therefore, the objective is to assign weapons to the targets, and minimize the total expected value of the surviving targets and maximize the combat benefits at the final stage (Hu et al., 2020). Please note that in the assignment problem; more than one weapon can be assigned to the same target because of the high value. The problem is illustrated in Fig. 4. At each stage, remaining weapons are assigned to the surviving targets. The process is continued until all weapons are used or all targets are destroyed. In the figure, green and grey circles represent the remaining weapons with the kill probability ( $P$ ) and used weapons, respectively. Orange and blue circles represent the value of destroyed and surviving target, respectively. The orange lines give the assignments.

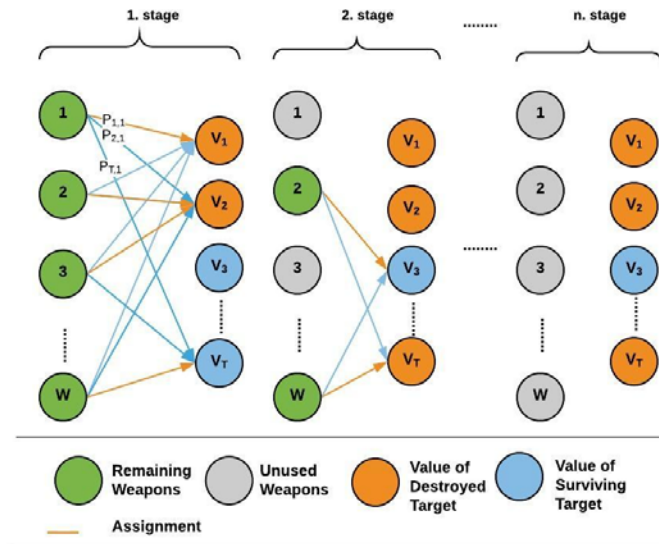


**Figure 4.** Dynamic weapon-target assignment problem.

### 3. WHAT IS NETWORK CENTRIC WARFARE (NCW)?

The advancements in information technology (such as sensor networks, mobile computing, data transmission etc.) have enabled to development of battlefield weapons and increased both speed and accuracy in decision making in the fields of Intelligence, Surveillance and Reconnaissance (ISR). Advances in technology have not only transformed weapons, warships, or aircraft, but also accelerated communication and information sharing among forces over the network. In this way, military assets in different locations are connected to decision makers and to each other over computer, radio and data networks link. NCW concept has been identified as one of the key warfare concepts in the future (Roux & van Vuuren, 2007). All the information collected from the sensors is shared with the weapons in the network environment (Xin, Wang & Chen, 2019).

NCW is defined in the research of (2000) D. S. Alberts, J. J. Garstka & F.P. Stein as “an information superiority-enabled concept of operations that generates increased combat power by networking sensors, decision makers,

and shooters to achieve shared awareness, increased speed of command, higher tempo of operations, greater lethality, increased survivability, and a degree of self-synchronization.”

With the NCW concept, the ability of sharing and accessing the information increase the combat power by networking sensors, decision makers, and shooters. NCW focuses on a robust flow of information between platforms and military personnel using high-speed data links. While information sharing increases the quality of information, situational awareness and mission effectiveness also increase (Anand, Raja & Rajan, 2011).

More specifically, information technology has allowed the development of new policies and procedures that ensure the timely collection, management and analysis of accurate information. However, in this process, we also encounter problems arising from the network-centric approach. The first of these is the requirement for robust and seamless network connectivity. Different types of networks (for example: satellite networks, heterogeneous sensor networks, radio nets) cause problems in terms of communication difficulties and information sharing. There will be many entities in the network environment, from sensors to platforms, from servers to users. Considering that many participants are autonomous, the management and coordination of assets is another issue to consider. In addition, bandwidth limits are even more constrained for satellite and tactical radio communications. It may not be possible to increase capacity due to increasing demand (Renner, 2003). In the network-centric approach, privacy and security will also be essential parameters.

The time it takes for the Commanding Officer to evaluate to make a decision and then convey it in combat is critical and vital. Speed is one of the most important parameters in terms of sustainability and efficiency of the operation. When military forces are geographically different locations from each other, their ability to act together, organize and exchange information are related to the speed factor in the network environment. Therefore, NCW is a network-centric approach for a new way of thinking. Thus, we simulate a network-centric scenario for WTA problem and compare different approaches.

#### **4. COMPARISON OF WTA STRATEGIES THROUGH SIMULATION**

In this subsection, we conduct a simulation environment with the following parameters from (Xie et al., 2018). Three targets and five fire units are considered in the simulations. Damage probability threshold of each target is set to 0.8. Damage probabilities for the solutions below that threshold value are deemed as unsuccessful solutions and they are ignored. Damage probabilities of each firing unit to each target in the scenarios are used as in Table 1.

**Table 1.** Damage probabilities of each firing unit to each target in the scenarios.

	<b>Target 1</b>	<b>Target 2</b>	<b>Target 3</b>
<b>Fire Unit 1</b>	0.824	0.851	0.752
<b>Fire Unit 2</b>	0.782	0.692	0.822
<b>Fire Unit 3</b>	0.683	0.863	0.834
<b>Fire Unit 4</b>	0.810	0.831	0.721
<b>Fire Unit 5</b>	0.843	0.790	0.795

Threat degree of each target in the scenarios are used as in Table 2.

**Table 2.** Threat degree of each target in the scenarios.

	<b>Target 1</b>	<b>Target 2</b>	<b>Target 3</b>
<b>Target Threat Degree</b>	0.17	0.51	0.32

Remaining times in seconds for each target to enter the fire unit's firing zones are used as in Table 3. Using these parameters, we compare five WTA strategies of which the first is from (Xia et al., 2016) and the second is from (Xie et al., 2018).



**Table 3.** Remaining time in seconds for each target to enter the fire unit's firing range in the scenarios.

	<b>Target 1</b>	<b>Target 2</b>	<b>Target 3</b>
<b>Fire Unit 1</b>	10	15	19
<b>Fire Unit 2</b>	16	12	9
<b>Fire Unit 3</b>	11	8	17
<b>Fire Unit 4</b>	9	12	15
<b>Fire Unit 5</b>	13	11	12

**Scenario 1:** Assignment of fire units to targets with the aim of maximizing the damage probability, while minimizing the ammunition cost (Xia et.al., 2016).

**Scenario 2:** Assignment of fire units to targets with the aim of maximizing the ratio of (Xie et al., 2018).

$$\frac{\text{Target Threat Degree}}{\text{Remaining Time to Enter the Fire Unit's Range}} \quad (5)$$

**Scenario 3:** Assignment of fire units to targets with the aim of maximizing the damage probability.

**Scenario 4:** Assignment of fire units to targets with the aim of minimizing the target's remaining time to enter the fire unit's range. Scenario 4 tries to give priority to the closer targets in fire unit assignment.

**Scenario 5:** Assignment of fire units to targets with the aim of maximizing the ratio of.

$$\frac{\text{Target Threat Degree} * \text{Damage Probability}}{\text{Remaining Time to Enter the Fire Unit's Range}} \quad (6)$$

*An Evaluation on Weapon Target Assignment Problem*

WTA solutions for each scenario are as in Tables 4 through 8 for scenarios 1 through 5 respectively. In Table 4, Fire Unit 5 is assigned to Target 1, Fire Unit 1 is assigned to Target 2, and Fire Unit 3 is assigned to Target 3. Assignment solutions in the Tables 5 through 8 should be interpreted similarly.

**Table 4.** Firing unit to target assignment solutions for the scenario 1.

<b>Scenario 1</b>	<b>Target 1</b>	<b>Target 2</b>	<b>Target 3</b>
<b>Fire Unit 1</b>	0	1	0
<b>Fire Unit 2</b>	0	0	0
<b>Fire Unit 3</b>	0	0	1
<b>Fire Unit 4</b>	0	0	0
<b>Fire Unit 5</b>	1	0	0

**Table 5.** Firing unit to target assignment solutions for the scenario 2.

<b>Scenario 2</b>	<b>Target 1</b>	<b>Target 2</b>	<b>Target 3</b>
<b>Fire Unit 1</b>	0	0	0
<b>Fire Unit 2</b>	0	0	1
<b>Fire Unit 3</b>	0	1	0
<b>Fire Unit 4</b>	1	0	0
<b>Fire Unit 5</b>	0	0	0

**Table 6.** Firing unit to target assignment solutions for the scenario 3.

<b>Scenario 3</b>	<b>Target 1</b>	<b>Target 2</b>	<b>Target 3</b>
<b>Fire Unit 1</b>	1	0	0
<b>Fire Unit 2</b>	0	0	1
<b>Fire Unit 3</b>	0	1	0
<b>Fire Unit 4</b>	1	0	0
<b>Fire Unit 5</b>	0	0	1

**Table 7.** Firing unit to target assignment solutions for the scenario 4.

<b>Scenario 4</b>	<b>Target 1</b>	<b>Target 2</b>	<b>Target 3</b>
<b>Fire Unit 1</b>	0	0	0
<b>Fire Unit 2</b>	0	0	1
<b>Fire Unit 3</b>	0	1	0
<b>Fire Unit 4</b>	1	0	0
<b>Fire Unit 5</b>	0	0	0

**Table 8.** Firing unit to target assignment solutions for the scenario 5.

<b>Scenario 5</b>	<b>Target 1</b>	<b>Target 2</b>	<b>Target 3</b>
<b>Fire Unit 1</b>	1	0	0
<b>Fire Unit 2</b>	0	0	1
<b>Fire Unit 3</b>	0	1	0
<b>Fire Unit 4</b>	1	0	0
<b>Fire Unit 5</b>	0	0	1

The damage probabilities and target remaining times to enter the firing units firing zones for the WTA solutions of scenarios 1 through 5 are as in Table 9. As the scenario 3 only tries to maximize the firing unit's damage probability to the target, it achieves the maximum damage probability. However, scenario 3, does not give priority to the nearer targets which should be attacked earlier than the far away targets. Scenario 4 aims to attack nearer targets first. Hence, scenario 4 achieves the minimum remaining time for the targets to enter the firing zone of the firing units. When the damage probability of the scenario 4 is considered, it is least among the other scenarios. In addition to the targets remaining time to enter the firing unit's firing zone, taking the target's threat degree into account as in scenario 2, does not make any significant difference with respect to the scenario 4. Scenario 1 also tries to maximize the damage probability while maintaining the minimum ammunition cost, it seems that the scenario 1 achieves this aim by engaging the far away targets first.

**Table 9.** Damage probabilities and targets remaining times to enter the firing units firing zones.

	Damage Probability to All Targets	Damage Probability to Individual Targets			Average Remaining Time for All Targets to Enter Fire Unit's Firing Zone	Average Remaining Time for Individual Targets to Enter Fire Unit's Firing Zone		
		Target 1	Target 2	Target 3		Target 1	Target 2	Target 3
<b>Scenario 1</b>	0.598	0.843	0.851	0.834	15.0	13.0	15.0	17.0
<b>Scenario 2</b>	0.575	0.81	0.863	0.822	8.667	9.0	8.0	9.0
<b>Scenario 3</b>	0.804	0.967	0.863	0.964	9.333	9.5	8.0	10.5
<b>Scenario 4</b>	0.575	0.81	0.863	0.822	8.667	9.0	8.0	9.0
<b>Scenario 5</b>	0.804	0.967	0.863	0.964	9.333	9.5	8.0	10.5

Hence the maximum time to enter the firing units firing zone for the targets is encountered with the scenario 1. Besides that, scenario 1 achieves slightly more damage probability than the scenarios 2 and 4, and less damage probability than the scenarios 3 and 5. Scenario 5, tries to consider the target threat degree, target remaining time to enter the firing units firing zone, and the firing unit's damage probability to the target all at once. Hence, scenario 5 seems like a balance between the firing unit's damage probability and the target's remaining time to enter the firing unit's firing zone.

## 5. RELATED WORK

TE and WASA are two important components in Command and Control (C2) system (Ghanbari et al., 2021). Performing these processes and finding optimal results are possible with good decision making and planning. Dynamic and time-critical decision making, multiple criteria decision making, uncertain situations come among the problems that need to be addressed. The problems become more complicated when the human factor, stress and time constraint are added to the semi-autonomous or non-autonomous mode of TEWA (Naseem et al., 2017). Therefore, in this study, it is argued that the inclusion of a decision support system in the problem will reduce the risks arising from human errors. Decision support system takes the inputs of information of threats and weapons, operating tactics, Geographical Information System (GIS) mapping for vulnerable areas and produces the scheduling of weapons and weapon supply and inventory management strategy.

In this subsection, we discuss the proposed solutions in the combat scenarios as seen in Fig. 5.

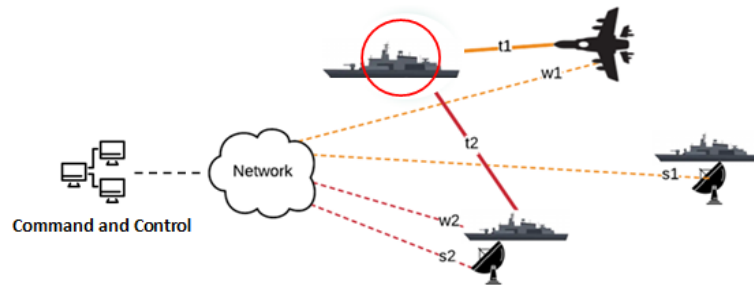


**Figure 5.** Network-centric combat scenario.

Many studies use Genetic Algorithm (GA), Tabu Search (TS), Simulated Annealing (SA) and Ant Colony Optimization (ACO) techniques to weapon target assignment problem and compare the results with each other. The optimization problem is to maximize the total value of surviving defense assets. Among these, GA is based on the survival of the fittest through natural evolution (Hillier & Lieberman, 2010). GA algorithm creates an initial population and uses genetic operators to alter composition of

## *An Evaluation on Weapon Target Assignment Problem*

offspring, thus potential solutions are represented until it reaches better solutions. The research of (2018) H. Sun, X. Xie and T. Sun model anti-aircraft WTA problem and GA algorithm is used including damage probability, flying time from target to weapon and the target threat degree. The research of (2016) Y. Yan, Y. Zha, L. Qin and K. Xu also use GA algorithm to analyze the damage to target and losses on defense assets.

In the research of Lu et al. (2006), the fire-allocation of naval fleet air defense is studied, and an improved GA model is proposed for optimal weapon-target assignment problem. It is assumed that there are 7 batches targets and 11 weapons. The importance weight of targets and kill probability of weapon to the targets are created. Accordingly, average kill expectation and achieved global optimal assignment are calculated for improved GA and simple GA.

The research of (2019) Wang et al. studies a specific type of WTA problem and proposes a ground target attacking WTA since the ground targets are diverse and suitable for many types of weapons,. The authors design a GA based variable value control method for solving large-scale problems. Weapon consumption value and time consumption are calculated. The parameters are the mean of the weapon value required to meet the specified damage requirement and the mean of the run times of 20 simulations, respectively.

In the research of (2020) K. Zhang, D. Zhou, Z. Yang, W. Kong and L. Zeng, threat evaluation model is defined according to altitude, velocity, short course, remaining intercept time. Then, sensor detection probability and weapon killing probability are formulated. The authors formulate dynamic sensor heterogeneous weapon assignment problem including threat evaluation model, sensor detection and weapon killing probabilities, decision timing and propose an evolutionary algorithm for ground-to-air defense scenarios.

ACO models the observations. Each one of the ants handles a candidate solution from source to destination. They coordinate their activities through indirect communication mediated by the modification of the environment in

which they move. At each step, a decision policy is used, and the decisions are given based on the local information. The probability of using a trail increases as more ants choose it. The research of (2008) G. Shang aims to minimize the loss of defense assets by modelling static WTA problem. The authors first consider GA with local search to solve the optimization problem. The local search starts with a feasible solution found and iteratively searches an improvement for the current assignment. When a better solution is found, it replaces the existing solution, and the process continues until a criterion is satisfied. Then, SA is used for the optimization problem, which tries to avoid local optima by accepting probabilistically moves to solutions. Better solutions are always accepted, while worse solutions are accepted with a probability. SA uses the analogy of a physical annealing process, and it is conducted until no improved solution found for a few iterations. Then, the authors implement ACO algorithm. In the modified ACO algorithm, a heuristic is executed between colonies for only the best solution through a greedy reformation.

In the research of (2017) Li et al., a modified Pareto ACO algorithm is proposed to maximize the total effectiveness of attack and minimize the cost of missiles for static WTA problem. Different strategies are embedded into the traditional Pareto ACO to improve the optimization performance, including dynamic heuristic information calculation approach, improved movement probability rule, dynamic evaporation rate strategy, global updating rule of pheromone, and boundary symmetric mutation strategy. It is observed that Pareto ACO is more suitable for solving large-scale problems.

The research of (2018) Chang et al. addresses the dynamic weapon target assignment problem. An improved artificial bee colony algorithm is proposed for solving the battlefield firepower optimization in multiple stages and multiple rounds. 4 kinds of rule-based heuristic factors are considered to improve the quality of the initial solution. These are weapon-choice-priority, target-choice-priority, target-choice-priority with a random sequence, and target-choice-priority with a random sequence and Cannikin Law. The authors use “shoot-look-shoot” strategy. In the shoot strategy, weapon allocation decision to the targets is calculated and the attack is

executed. In the look strategy, decision makers observe the battle field to identify the targets and available weapons.

The research of (2019) K. Zhang, D. Zhou, Z. Yang, Q. Pan & W. Kong propose a multi-objective evolutionary algorithm for WTA model and aim to minimize the expected survival probability of targets and weapon consumption by including unit type, damage effect, lethal radius etc. The authors focus on two main challenges: (i) handling the multi-constraints and (ii) finding the complete Pareto-optimal set. The constraints are based on the actual operational requirements of security avoidance, survival threshold, and preference assignment.

In the research of Li et al. (2018), multi-objective evolutionary algorithm is proposed based on decomposition for asset-based static WTA problem. The asset-based problem aims to maximize the expected total value of assets which are defended by the defensive weapons. If the higher number of weapons is used, there is greater probability of destroying the target. However, if less weapons are used, then the targets have a higher probability of surviving in the engagement. Therefore, the consumption of weapons and the destruction of targets are conflicting objectives. In this study, the authors convert the asset-based problem into a multi-objective optimization problem.

## **6. CONCLUSION**

Information technology enables the development of new policies and procedures that allow the timely collection, management, and analysis of accurate information. With the network-centric warfare concept, the ability of sharing and accessing the information increase the combat power by networking sensors, decision makers, and shooters. In this paper, we explain the threat evaluation concept with a network-centric approach and define weapon assignment and sensor allocation problem. More specifically, we give static and dynamic target-based problem, and also simulate a scenario for WTA problem and compare different approaches. Then, we explain the concept of NCW and the problems that may be encountered are detailed.



*Tolga ÖNEL, Elif BOZKAYA*

**CONFLICT OF INTEREST STATEMENT**

The authors declare no conflict of interest.

**REFERENCES**

Athans, M. (1987). "Command and Control (C2) Theory: A Challenge to Control Science". *IEEE Transactions on Automatic Control*, 32(4), pp. 286-293.

Truter, M. L., & van Vuuren, J.H. (2014). "Prerequisites for the Design of a Threat Evaluation and Weapon Assignment System Evaluator". *In Proceedings of the 2014 ORSSA Annual Conference*, pp. 54-61.

Johansson, F., & Falkman, G. (2010). "SWARD: System for Weapon Allocation Research & Development". *In 13th IEEE International Conference on Information Fusion*, Edinburgh, UK, pp. 1-7.

Xin, B., Wang, Y., & Chen, J. (2019). "An Efficient Marginal-Return-Based Constructive Heuristic to Solve the Sensor-Weapon-Target Assignment Problem". *IEEE Transactions on Systems, Man, and Cybernetics: Systems*, 49(12), pp. 2536-2547.

Johansson, F. (2010). "Evaluating the Performance of TEWA Systems". [Doctoral Dissertation]. Örebro University, Sweden. Retrieved from <https://www.diva-portal.org/smash/get/diva2:354687/FULLTEXT02>

Lloyd, S. P., & Witsenhouse, H. S. (1986). "Weapon Allocation is NP-complete". *In Proceedings of IEEE Summer Simulation Conference*, Reno, Nevada, pp. 1054-1058.

Hosein, P. A. (1990). "A Class of Dynamic Nonlinear Resource Allocation Problems". [Doctoral Dissertation]. Massachusetts Institute of Technology, USA. Retrieved from <https://dspace.mit.edu/handle/1721.1/14258>

Zhang, K., Zhou, D., Yang, Z., Pan Q., & Kong, W. (2019). "Constrained Multi-Objective Weapon Target Assignment for Area Targets by Efficient Evolutionary Algorithm". *IEEE Access*, 7, pp. 176339-176360.

Alberts, D. S., Garstka, J. J., & Stein, F. P. (2000). *Network Centric Warfare: Developing and Leveraging Information Superiority*. 2nd Edition (Revised), pp. 1-293. Retrieved from [https://www.researchgate.net/publication/46988836\\_Network\\_Centric\\_Warfare\\_Developing\\_and\\_Leveraging\\_Information\\_Superiority](https://www.researchgate.net/publication/46988836_Network_Centric_Warfare_Developing_and_Leveraging_Information_Superiority)

Roux, J. N., & van Vuuren, J. H. (2007). "Threat Evaluation and Weapon Assignment Decision Support: A Review of the State of the Art". *The Operations Research Society of South Africa*, 23(2), pp. 151-187.

Anand, D., Raja, C., & Rajan, E. G. (2011). "Network Centric Warfare-Concepts and Challenges". *International Journal of Networking and Communication Engineering*, 3(14), pp. 898-902.

Renner, S. (2003). "Building Information Systems for Network-Centric Warfare". In *8th International C2 Research and Technology Symposium*, pp. 1-8, Washington, DC.

Hillier, F. S., & Lieberman, G. J. (2010). *Introduction to Operations Research*. 9th Edition. McGraw-Hill.

Sun, H., Xie, X., & Sun, T. (2018). "Improved Assignment Model and Genetic Algorithm for Solving Antiaircraft Weapon-Target Assignment". In *10th International Conference on Intelligent Human-Machine Systems and Cybernetics (IHMSC)*, pp. 89-92.

Yan, Y., Zha, Y., Qin L., & Xu, K. (2016). "A research on weapon-target assignment based on combat capabilities". In *IEEE International Conference on Mechatronics and Automation*, pp. 2403-2407.

Zhang, K., Zhou, D., Yang, Z., Kong, W., & Zeng, L. (2020). "A Novel Heterogeneous Sensor-Weapon-Target Cooperative Assignment for Ground-to-Air Defense by Efficient Evolutionary Approaches". *IEEE Access*, 8, pp. 227373-227398.

*An Evaluation on Weapon Target Assignment Problem*

Shang, G. (2008). "Solving Weapon-Target Assignment Problems by a New Ant Colony Algorithm". In *International Symposium on Computational Intelligence and Design*, pp. 221-224.

Ghanbari, A. A., Mohammadnia, M., Sadatinejad, S. A., & Alaei, H. (2021). "A Survey on Weapon Target Allocation Models and Applications", In *Computational Optimization Techniques and Applications*. London, United Kingdom: IntechOpen.

Naseem, A., Shah, S. T. H. Shoab, Khan, A., & Malik, A. W. (2017). "Decision support system for optimum decision making process in threat evaluation and weapon assignment: Current status, challenges and future directions". *Annual Reviews in Control*, Vol. 43, pp. 169-187.

Lu, H., Zhang, h., Zhang, X., & Han, R. (2006). "An Improved Genetic Algorithm for Target Assignment, Optimization of Naval Fleet Air Defense". *6th World Congress on Intelligent Control and Automation*, pp. 3401-3405.

Chang, T., Kong, D., Hao, N., Xu, K., & Yang, G. (2018). "Solving the dynamic weapon target assignment problem by an improved artificial bee colony algorithm with heuristic factor initialization". *Applied Soft Computing*, Vol. 70, pp. 845-863.

Li, Y., Kou, Y., Li, Z., Xu, A., and Chang, Y. (2017). "A Modified Pareto Ant Colony Optimization Approach to Solve Biobjective Weapon-Target Assignment Problem". *Hindawi, International Journal of Aerospace Engineering*, Vol. 2017, pp. 1-14.

Wang, C., Fu, G., Zhang, D., Wang, H., & Zhao, J. (2019) "Genetic Algorithm-Based Variable Value Control Method for Solving the Ground Target Attacking Weapon-Target Allocation Problem". *Hindawi, Mathematical Problems in Engineering*, Vol. 2019, pp. 1-9.

Li, X., Zhou, D., Pan, Q., Tang, Y., & Huang, J. (2018). “Weapon-Target Assignment Problem by Multiobjective Evolutionary Algorithm Based on Decomposition”. *Hindawi, Complexity*, Vol. 2018, pp. 1-19.

Xin, B., Chen, J., Peng, Z., Dou, L., & Zhang, J. (2011) “An Efficient Rule-Based Constructive Heuristic to Solve Dynamic Weapon-Target Assignment Problem”. In *IEEE Transactions on Systems, Man, and Cybernetics - Part A: Systems and Humans*, Vol. 41, No. 3, pp. 598-606.

Hu, L., Yi, G., Huang, C., Nan, Y., & Xu, Z. (2020). “Research on Dynamic Weapon Target Assignment Based on Cross-Entropy”, *Hindawi, Mathematical Problems in Engineering*, Vol. 2020, pp. 1-13.

Xia, W., Liu, X. X., Fan, Y. T., & Yuan, F. G. (2016). “Weapon-Target Assignment with an Improved Multi-Objective Particle Swarm Optimization Algorithm”. *Acta Armamentarii*, 37(11), pp. 2085-2093.

*\*An ethical committee approval and/or legal/special permission has not been required within the scope of this study.*

**MACHINE AND DEEP LEARNING-BASED INTRUSION  
DETECTION AND COMPARISON IN INTERNET OF THINGS\***

**Siham AMARUCHE<sup>1</sup>**   
**Kerem KÜÇÜK<sup>2</sup>** 

<sup>1</sup>*Kocaeli University, Department of Computer Engineering, Kocaeli,  
Turkey,  
siham.m.amarouche@gmail.com*

<sup>2</sup>*Kocaeli University, Department of Software Engineering, Kocaeli, Turkey,  
kkucuk@kocaeli.edu.tr*

**Received: 17.02.2022**

**Accepted: 23.04.2022**

**ABSTRACT**

*In today's technology world, intrusion detection is an important topic for the Internet of Things (IoT) systems. With the growth of using tiny devices connected to wireless networks in IoT, the amount of data is growing rapidly. This data may be vulnerable to attacks so IoT systems need to secure it for increasing the system's confidentiality, availability, and reliability. The progress of detecting attacks using artificial intelligence (AI) autonomously has become a more convenient method in network intrusion detection systems (NIDS). In this article, we propose a new detecting technique to improve performance and increase accuracy in NIDS. We present different machine learning (ML) and deep learning (DL) methods to detect the different types of attacks on IoT systems. We also provide the experiments to find out the best way to identify the anomaly in the IoT system environment, make comparisons between different AI models. The experiment was evaluated with the open database UNSW-NB15.*

**Keywords:** *Deep Learning, IoT Security, Machine Learning, Intrusion Detection, Cyber Security.*

**MAKİNE VE DERİN ÖĞRENME YÖNTEMLERİ İLE  
NESNELERİN İNTERNETİ İÇİN SALDIRI TESPİTİNİN  
KARŞILAŞTIRILMASI**

**ÖZ**

*Günümüz teknoloji dünyasında, Nesnelerin İnterneti (IoT) sistemleri için izinsiz giriş tespiti önemli bir konudur. IoT'de kablosuz ağlara bağlı küçük cihazların kullanımının artmasıyla birlikte veri miktarı ihtiyacı da hızla artmaktadır. Bu veriler saldırılara karşı savunmasız olabilmektedir. Bu nedenle IoT sistem çözümlerinin gizliliğini, kullanılabilirliğini ve güvenilirliğini sağlamak için bu verilerin güvenceye alınması gereklidir. Yapay zekânın (AI) otonom biçimde kullanarak saldırıların tespit edilmesi, ağ saldırı tespit sistemlerinde (NIDS) daha uygun bir yöntem haline gelmiştir. Bu çalışmada, bu tespit sistemlerinin performansını iyileştirmek ve doğruluğu artırmak için yeni tespit tekniği önerilmektedir. IoT sistemleri için farklı saldırı türlerini tespit etmek için farklı makine öğrenimi (ML) ve derin öğrenme (DL) yöntemleri birlikte sunulmaktadır. Ayrıca, IoT sistem ortamındaki anomaliyi tanımlamanın en iyi yolunu bulmak için deneyler sunulmaktadır. Bununla birlikte farklı AI modelleri arasında karşılaştırmalar yapılmaktadır. Deneyler için, UNSW-NB15 veri seti kullanılmıştır.*

**Anahtar Kelimeler:** *Derin Öğrenme, IoT Güvenliği, Makine Öğrenmesi, Saldırı Tespiti, Siber Güvenlik.*

## **1. INTRODUCTION**

The Internet of Things (IoT) is a technology in which a network connects anything with the Internet, based on embedded systems, specific protocols, and sensors to conduct information exchange and communications in order to obtain smart recognitions, monitoring, localization, tracking, and control systems (Patel & Patel, 2016). The sensitivity and importance of the information carried out by IoT devices and networks signifies the importance of its security. To overhead challenges and problems on the server end we used different models as a decision engine to decide about traffic data type, whether it is normal or malicious. Cyber threats have become more widespread and several new types of attacks have been generated targeting organizations, companies, and governments. Furthermore, the number of devices and objects that are connected to wireless networks increased since the IoT has emerged. The proposed research here is found on the intersection between intrusion detection and mitigation, and Artificial Intelligence (AI) technologies. To mitigate cyber-attack, cyber security analysts heavily depend on Intrusion Detection System (IDS). IDS can detect malicious activities by matching patterns of known attacks using the signature-based detection method or observing anomaly activities using anomaly-based intrusion detection systems this method is introduced to detect unknown attacks (Khraisat, Gondal, & Vamplew, 2019).

Obviously, we can see that all governments and security intelligence try to protect their information and not allow spies to eavesdrop on it and its decisions. For the importance of cyber security topics, we research in this work the effectiveness of using ML and DL models in cyber security as well as current challenges that face security analysts and we aim to use different methodologies to prevent, mitigate attacks and drop the malicious packets and threats.

In the literature, there are many studies utilizing various machine learning and deep learning techniques on different datasets to enhance the IDS performance. In this section, we will handle anomaly-based IDS techniques which are dependent on heuristics, statistics, or rules, rather than signatures or patterns. As in the study (Alsamiri & Alsubhi, 2019), new features were extracted from the Bot-IoT and compared with existing studies from the



literature. Alsamiri et al. extracted features using CICFlowMeter. In the evaluation phase, seven different machine learning (KNN, QDA, ID3, RF, AdaBoost, MLP, and NB) were used. They observed that Adaboost was the best performing algorithm, followed by KNN and ID3. Also, in (Kasongo & Sun, 2020), the authors tried to analyze the performance of intrusion detection system using a feature selection method on the UNSW-NB15 dataset, then implemented the following machine learning approaches using the reduced feature space: Support Vector Machine, k-Nearest-Neighbour, Logistic Regression, Artificial Neural Network, and Decision Tree. The feature selection method that is applied was a filter-based feature reduction technique using the XGBoost algorithm. The results showed that the XGBoost-based feature selection method allows models such as the Decision tree model to enhance their test accuracy rate from 88.13% to 90.85% for the binary classification scheme. Vinayakumar, Soman, and Poornachandran (2017) inferred from their work that experiments of families of RNN architecture achieved a low false positive rate in comparison to the traditional machine learning classifiers. The reason for that is that RNN architecture is able to memorize information over time. This work applied to publically available ID datasets, KDDCup '99' and UNSW-NB15.

Our article is comprehensive with different experiences and concepts. We considered two schemes binary and multiclass classification configurations. We made a comparison between different Machine Learning (ML) and Deep Learning (DL) methods. We evaluated the applied models with different performance parameters. We applied Random Forest algorithm over the selected dataset to calculate the feature importance measure for each feature, select more important features and generate reduced optimal feature vectors, this process may increase the accuracy of intrusion detection and increase the speed of models to get performance results. We selected this algorithm because it belongs to the category of embedded methods where these methods combine the qualities of filter and wrapper methods, are more accurate, and generalize better. We applied the feature selection method only for machine learning models because in neural networks the important features are chosen automatically. We tried to make a comparison between performance results for ML models with a full feature space and

ML models with a reduced optimal vector that was generated using the feature selection method. Also for deep learning methods to exceed the overfitting problem, we used different techniques like cross-validation, and early stopping techniques. In some DL models, we designed different architectures where one architecture is more complicated than the other. In addition, we implemented different hyperparameters such as epoch numbers and batch size values over the best-performing multiclass classification based deep learning model, to find the best hyperparameters that could be applied to improve our model's performance. We noticed the effect of parameters on the model's accuracy.

## **2. MATERIALS AND METHODS**

In the literature, there are a lot of relevant intrusion detection datasets. An example, KDD99, NSL-KDD, DS2OS, UNSW-NB15, CIC-IDS 2017, MQTT-IOT-IDS2020, and Bot-IoT Datasets. However, in this section, we describe the dataset we used in our work.

### **2.1. UNSW-NB15 Dataset**

In our study, we used the UNSW-NB15 dataset which is created by the Cyber Range Lab of the Australian Centre for Cyber Security (Moustafa & Slay, 2015). We selected this dataset because it is a public dataset not private, diversity of attack types included in this dataset, the difficulty of evaluating and analyzing the UNSWNB15 on existing classification systems demonstrated that this data set contains complex patterns, the training and testing sets have a similar probability distribution, and regular updates that can be applied to this dataset. The Bro-IDS, Argus tools are employed and twelve algorithms are developed to extract 49 features with the class label (Moustafa & Slay, 2015). The number of instances in the training set is 175,341 (68.05%) records and the testing set is 82,332 (31.95%) records from the different types of attack and normal. The UNSW-NB15 dataset includes nine types of attack classifications to describe malicious behaviors. Attack types included in the UNSW-NB15 dataset are Fuzzers, Analysis, Backdoors, DoS, Exploits, Generic, Reconnaissance, Shellcode, and Worms.

## **2.2. Technologies Overview**

In our work, we used Python programming language, Python is interpreted, high-level, and object-oriented. Today, machine learning has become more popular and attracted the attention of students, scientists, and researchers. Python with its useful packages and libraries enables to make complex computational tasks easily. Python has a lot of libraries such as Keras, Scikit-learn, Tensorflow, pandas, Numpy, and Matplotlib, etc. We used these libraries in our study to help us implementing feature engineering process over the dataset, classical machine learning, and deep learning methods. The proposed models in our work are implemented in Jupyter Notebook by using the Python language and its libraries.

## **2.3. Pre-processing Data**

### ***2.3.1. Feature Transformation and Standardization***

Before feeding the data to classical machine learning and deep learning models, feature transformation has been applied and this step is important because models accept only numerical data as input for that, all non-numerical values of the dataset are converted into numerical data. In this work, we used one hot encoding (ohe) technique to encode categorical features as a one-hot numeric array. The encoder derives the unique values for each feature and represents it as a one-hot array. On the other side, for the standardization process, we used the StandardScaler technique over the numerical data because the values of the dataset are in different ranges and we tried to standardize data in the same range. Standardization is a scaling technique where input values are centered on the mean with a unit standard deviation.

### ***2.3.2. Feature Selection and Dimensionality Reduction***

In this step, we select the most important features and delete unnecessary features or reduce the dimensions of features in the dataset. For the task of feature extraction and dimension reduction processes, we can use different models like Principal component analysis (PCA), Linear discriminant analysis (LDA), Autoencoder, and t-SNE models. On the other hand, feature selection is used to reduce irrelevant and redundant variables and it measures the relevance of each feature with the output labels/classes based

on feature importance metric. Feature selection technologies are divided into embedded, wrapper, and filter methods (Chandrashekar & Sahin, 2014). Our goal in applying the feature selection method and reducing the number of input variables is to improve the performance of the model in some cases and reduce the computing cost and time of the training model.

In this study, we applied only feature selection methods using Random Forest that depends on tree-based strategies and belongs to the category of embedded methods. Embedded methods combine the qualities of filter and wrapper methods, are more accurate, and generalize better. Features importance and its scores that calculated using Random Forest method as shown in Figure 1:

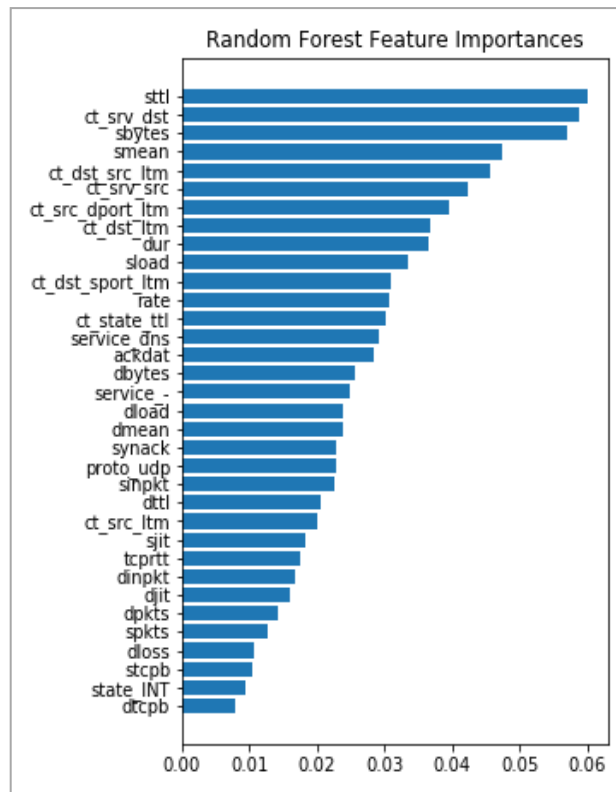


**Figure 1.** Feature selection using random forest.

### **3. METHODS FOR INTRUSION DETECTION SYSTEM**

#### **3.1. Classical Machine Learning Methods**

##### **3.1.1. Naïve Bayes**

Naive Bayes (NB) is a subset of Bayesian decision theory and it is a simple probabilistic machine learning model based on the Bayes theorem where assumptions between features are considered independent. This method is used for classification tasks. There are different types of Naive Bayes as Multi-nominal, Bernoulli, and Gaussian Naive Bayes algorithms (Kaviani & Dhotre, 2017). In our work, we used Bernoulli Naive Bayes model. Bayes theorem mathematically can be described as follows:

$$P(A|B) = \frac{P(B|A)P(A)}{P(B)} \quad (1)$$

##### **3.1.2. K-nearest Neighbors**

K-nearest neighbors (KNN) is an ML algorithm that is capable of both supervised and unsupervised approaches and it is used for both classification and regression problems. In this research, we used it for supervised binary and multiclass classification tasks. KNN algorithm assumes that similar instances exist in the same area and proximity. Different distance metrics are used in this model. Distance metrics find the distance between two instances between a new data point and an existing point in the training dataset (Chomboon, Chujai, Teerarassamee, Kerdprasop, & Kerdprasop, 2015). One of the commonly used distance metrics is Euclidean distance, the formula of it as follows:

$$d(x, y) = \sqrt{\sum_{i=1}^n (x_i - y_i)^2} \quad (2)$$

This formula is based on Pythagorean Theorem; and it can be used to calculate the distance between two data points x and y in Euclidean space.

### **3.1.3. Logistic Regression**

Logistic regression (LR) is a statistical method used for binary classification tasks. Although its name regression, it is a classification algorithm. Logistic regression tries to make a logarithmic line that distinguishes between classes and its estimation is done through maximum likelihood. LR model depends on the Sigmoid function where its logistic curve is limited between 0 and 1 values (Boateng & Abaye, 2019). The expression of Sigmoid function is as follows:

$$\sigma(x) = \frac{1}{1 + e^{(-x)}} \quad (3)$$

### **3.1.4. Decision Tree**

Decision Tree (DT) is a decision support tool that uses a tree-like method. DT is a supervised model consisting of internal nodes that represent attributes, branches that represent the outcome of the tests, and leaf nodes that represent classes/labels and decisions after the computing process. The paths between root and leaf represent decision rules for classification tasks (Safavian & Landgrebe, 1991).

### **3.1.5. Random Forest Classification**

Random Forest (RF) is an ensemble method for classification and regression. RF model is a combination of different decision trees. The ensemble method is a machine learning technique that combines several base models or decision trees to produce one optimal model and predict with better performance than utilizing a single model (Breiman, 2001).

## **3.2. Deep Learning Methods**

Deep learning (DL) is a subfield of machine learning inspired by the structure of the human brain and biological neural networks. DL is known with its high performance and efficiency across many types of data.

### **3.2.1. Deep Neural Network**

Deep neural network (DNN) is an artificial neural network (ANN) model with high complexity, usually with at least two hidden layers. This model

has become a popular model for classification, regression, clustering, controlling models, and prediction in many applications (Abiodun et al., 2018). Deep net process data by employing sophisticated math methods (Sze, Chen, Yang, & Emer, 2017). The feed-forward neural network was the first of neural networks (NN) that found and simplest type. In this network, the data move forwardly from the input layer through any hidden layer to the output without loops. The model can give different performance results depends on the number of hidden layers, the number of nodes in each layer, and the type of activation layer (Abiodun et al., 2018).

This model is applied in a supervised manner with the class labels and the input attributes. In this model, we have forwarding propagation which aims to predict results as an attack or normal by using a perceptron classifier. The main Equation of the perceptron in the artificial neural network is mentioned in Equation (4):

$$y = \sum_{i=1}^n X_i W_i + b \quad (4)$$

Where  $n$  denotes the number of nodes in the layer,  $X$  denotes the values of these nodes which are the samples values,  $W$  refers to weights (connection strength), and  $b$  to the biases of these nodes. These results will be inserted into different activation functions which return the probabilities for each class and then choose the largest value from the vector of probability values to give a more accurate value. Sigmoid, ReLU, Softmax, and Tanh are among the most frequently used activation functions; this model employed ReLU activation functions in the hidden layers stated in Equation (5).

$$R(z) = \begin{cases} z, & z > 0 \\ 0, & z \leq 0 \end{cases} \quad (5)$$

Also, we used Softmax activation function in the output layer stated in Equation (6).

$$\sigma(\vec{z})_i = \frac{e^{z_i}}{\sum_{j=1}^K e^{z_j}} \quad (6)$$

Here Softmax function transforms a vector of numbers into a vector of probabilities between 0 and 1. After the forwarding propagation stage, the backpropagation step comes and is a technique to train deep neural networks by modifying the weights and biases. It includes loss function and optimizer (Manaswi, 2018). In this step, the loss between predicted and true values will be calculated, then adjust the weights in the neural network according to the loss. Categorical cross entropy loss function has been applied in this work. The loss function needs to reach the optimal values of parameters (weight and bias) for that we used Adam optimizer to get the best parameter values. The optimizer is a way of tuning parameters (Manaswi, 2018). In our work for DNN models, we used two different architectures: DNN-2 and DNN-1. DNN-2 structure is more complicated than DNN-1 where we added one more hidden layer.

### ***3.2.2. Convolutional Neural Network***

Convolutional neural network (CNN) is one of the most powerful models in deep learning. CNN has excellent performance with different applications like image classification, video recognition, action recognition, and natural language processing (NLP). It handles input data as matrices for that we reshaped our input data before feeding it to be more convenient for the CNN module. CNN models have multiple layers, including convolutional layer, pooling layer, non-linearity layer, and fully connected layer (Albawi, Mohammed, & Al-Zawi, 2017).

In our work, we used 1D-CNN architecture for intrusion detection tasks while 2D-CNN architecture is mainly used for image processing tasks. Similarly, to DNN model, ReLU activation function was used for hidden layers, Softmax activation function was applied in the output layer, categorical cross entropy was used as a loss function, and Adam was used as an optimizer. We designed two different CNN models, where the structure of CNN-2 is more complicated than CNN-1 and we added one more hidden layer in the CNN-2 model.

### ***3.2.3. Recurrent Neural Network***

A recurrent neural network is a type of artificial neural network in which nodes' connections form a directed graph through a temporal sequence.



RNNs can process variable-length sequences of inputs by utilizing their internal state (memory) (Medsker & Jain, 2001). RNN model is used to memorize and remember previous computations. This model allows the use of previous outputs as inputs while maintaining hidden states (Sherstinsky, 2020) where for each timestep  $t$ , the activation function and the output are stated as follows;

$$a^{<t>} = g_1 (W_{aa}a^{<t-1>} + W_{ax}x^{<t>} + b_a) \quad (7.a)$$

$$\text{and } y^{<t>} = g_2 (W_{ya}a^{<t>} + b_y) \quad (7.b) \quad (7)$$

Where  $W_{ax}$ ,  $W_{aa}$ ,  $W_{ya}$ ,  $b_a$ ,  $b_y$  are temporally shared coefficients and  $g_1$ ,  $g_2$  activation functions.

RNN model in some cases can face the long-term dependency problem, the vanishing gradient, and exploding gradient problems. In order to solve these problems, LSTM and gated recurrent unit (GRU) networks have been proposed.

#### **3.2.4. Long Short-Term Memory**

Long short-term memory is an artificial recurrent neural network architecture. In contrast to standard feed forward neural networks, LSTMs include feedback connections and process the data as sequences (Hochreiter & Schmidhuber, 1997). LSTM can be used to perform tasks such as connected handwriting recognition, speech recognition, and anomaly detection in network systems or intrusion detection systems (IDS) (Graves, 2012). The main difference from a simple RNN is that memory blocks are used in place of nonlinear units in the hidden layers and this model offers three units called gates which are input gate, forget gate, and output gate. The following Equations (8) represent the gates in LSTM (Van Houdt, Mosquera, & Nápoles, 2020);

$$i_t = \sigma (w_i[h_{t-1}, x_t] + b_i) \quad (8.a)$$

$$f_t = \sigma (w_f[h_{t-1}, x_t] + b_f) \quad (8.b) \quad (8)$$

$$o_t = \sigma (w_o[h_{t-1}, x_t] + b_o) \quad (8.c)$$

Where “i” for the input gate, “f” for the forget gate, “o” for the output gate, “ $\sigma$ ” is the Sigmoid function, “ $b_i$ ” is the biases for the gate(x), “ $h_{t-1}$ ” is the output of the previous LSTM block, and “ $x_t$ ” is the current input.

### **3.2.5. Gated Recurrent Unit**

The GRU is similar to a long short-term memory (LSTM) with a forget gate, but requires fewer parameters due to the absence of an output gate (Hochreiter & Schmidhuber, 1997). GRU is a simplified version of LSTM and it merges the forget and the input gates into a single “update gate”, as well as merges cell and hidden state (Jozefowicz, Zaremba, & Sutskever, 2015).

In RNN, LSTM, and GRU models, we employed Tanh activation function in the hidden layers; also we used Softmax activation function in the output layer. Sparse categorical cross entropy loss function and Adam optimizer have been applied for these models.

### **3.2.6. CNN-LSTM Model**

CNN-LSTM model is a hybrid model that combines convolutional neural networks (CNN) and LSTM networks. This architecture involves using CNN layers for feature extraction from input dataset, followed by an LSTM model to detect intrusions sequentially. In our work, we constructed our own CNN-LSTM model using Python’s Keras library, the activation function that is used is ReLU for CNN model, Tanh for LSTM model and Softmax for the output layer, loss function is sparse categorical cross entropy and the optimizer is Adam; shown as below in Figure 2:

```
1 def cnn_lstm_model():
2
3     cnn_lstm = Sequential()
4     cnn_lstm.add(Conv1D(16, 3, padding='same', activation="relu", input_shape=(nb_features, 1)))
5
6     cnn_lstm.add(MaxPooling1D())
7
8     cnn_lstm.add(LSTM(16, return_sequences=True))
9     cnn_lstm.add(Dropout(0.01))
10    cnn_lstm.add(LSTM(16, return_sequences=False))
11    cnn_lstm.add(Dropout(0.01))
12
13    cnn_lstm.add(Dense(n_classes, activation="softmax"))
14
15    cnn_lstm.compile(loss="sparse_categorical_crossentropy", optimizer="adam", metrics=['accuracy'])
16    return cnn_lstm
```

**Figure 2.** Keras library usage for CNN-LSTM model.

### **3.3. Evaluation Metrics**

The applied models are evaluated by defining five performance parameters: accuracy, false alarm rate, precision, recall, and f1 score.

$$\text{Accuracy} = \frac{\text{TN} + \text{TP}}{\text{FP} + \text{FN} + \text{TP} + \text{TN}} \quad (9)$$

$$\text{FAR} = \frac{\text{FP} + \text{FN}}{\text{FP} + \text{FN} + \text{TP} + \text{TN}} \quad (10)$$

$$\text{Precision} = \frac{\text{TP}}{\text{TP} + \text{FP}} \quad (11)$$

$$\text{Recall} = \frac{\text{TP}}{\text{TP} + \text{FN}} \quad (12)$$

$$\text{F1}_{\text{score}} = 2 * \frac{\text{Precision} * \text{Recall}}{\text{Precision} + \text{Recall}} \quad (13)$$

In addition to the accuracy, we used different evaluation metrics such as precision, recall, and F1 since our dataset is imbalanced. In this case, the accuracy may cause to mislead evaluation of performance in some situations. As we can see from Equation (13) F1 score is the harmonic mean value of recall and precision.

### **3.4. Flow Diagram and Architecture**

Flow diagram of this study shown as in flow chart Figure 3, we applied different Artificial Intelligence (AI) models: Deep Learning (DL) and Machine Learning (ML) models. Besides that, we handled our data with two different perspectives: binary and multiclass classification. We implemented Random Forest feature selection method only for machine learning models. In deep learning models we excluded the need to the feature selection method because these models are inherently black boxes and generate the non-linear combinations where the features have less effect get lesser weights automatically.

*Machine and Deep Learning-based Intrusion Detection and Comparison in Internet of Things*

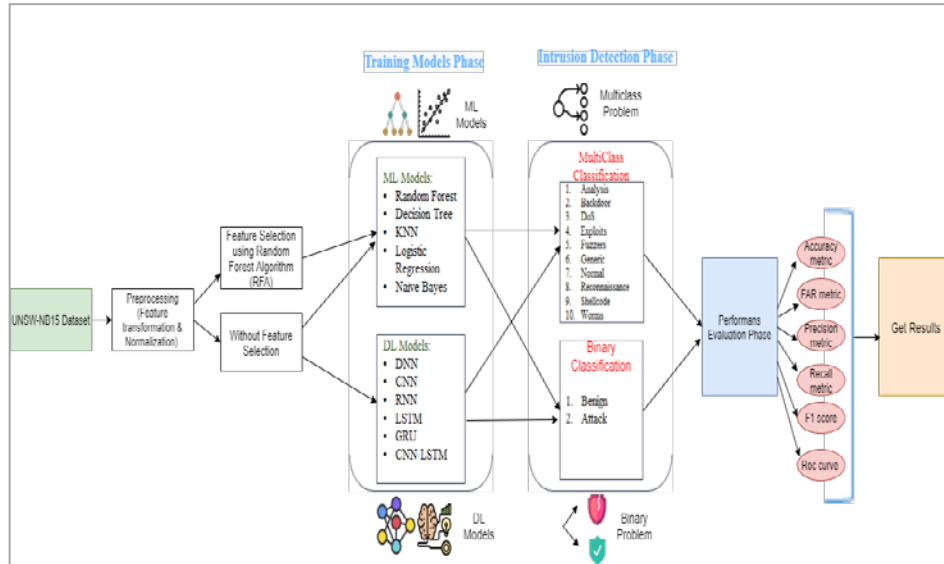


**Figure 3.** Architecture and flow diagram of proposed work.

**4. ANALYSIS AND RESULTS**

As we can see in Table 1 and 2, we employed all feature space of UNSW-NB15 dataset for multiclass classification and binary configuration. In Table 2 and 4 we used reduced feature vectors for multiclass classification and binary setting. In the experimental process, we applied different AI models that contain ML models and DL models. Here in the analysis section, we have 4 stages. In the first step, we tried to compare performance results for ML (binary and multiclass approaches) with full feature space that contains 42 attributes and with a reduced optimal vector (34 features) that generated using the Random Forest method. In the second stage, we tried to compare multiclass classification with binary configurations. In the third phase, we compare performance results between different DL models. In the fourth phase, we tried to compare DL performance results with ML results. In each table, Test Accuracy is the accuracy that obtained on testing data.

From Table 1 and 2, the performance results demonstrated that the feature selection methodology allows improving accuracies for such models as Random Forest accuracy increased from 75.38% to 75.90% and Decision

Tree accuracy increased from 73.43% to 73.86%. These results represented for multiclass classification scheme.

For Table 3 machine learning (ML) models for binary classification were applied without feature selection by using all our 42 features and for Table 4 our ML models were applied with a random forest feature selection method and we selected the most important 34 features. As we can see from Table 3 and 4 there is no performance improvement for binary classification tasks with the feature selection technique.

If we tried to compare multiclass classification results with binary classification results either with using the feature selection technique or without it, obviously we can see that accuracies improved for models in binary classification approach. As we can see from Table 1 and 3 with all 42 features, Random Forest accuracy increased from 75.38% to 87.09%, Decision Tree accuracy increased from 73.43% to 86.36%, KNN from 70.93% to 84.48%, Logistic Regression from 68.51% to 80.93%, and Naive Bayes from 53.45% to 74.78%. Also, from Table 2 and 4 with applying the feature selection method, Random Forest accuracy increased from 75.90% to 86.97%, Decision Tree accuracy increased from 73.86% to 86.18%, KNN from 70.59% to 82.10%, Logistic Regression from 67.92% to 80.33%, and Naive Bayes from 54.44% to 73.06%. This is a normal case because when classes number decreased, possible probabilities decrease, and the success rate will be increases and improves.

**Table 1.** Results using ML models with 42 features – multiclass classification.

ML Model	Cross Validation Results				Evaluation Results on Testing Data				
	CV Accuracy mean	CV Precision mean	CV Recall mean	CV F1 mean	Test Accuracy	Test FAR rate	Test Precision	Test Recall	Test F1
Random Forest	82.43	82.30	82.43	81.54	75.38	24.62	83.80	75.38	77.51
Decision Tree	80.94	80.98	80.94	80.55	73.43	26.57	80.75	73.43	76.26
KNN	76.52	76.86	76.52	76.51	70.93	29.07	79.04	70.93	73.85
Logistic Regression	77.07	76.88	77.07	75.25	68.51	31.49	76.94	68.51	69.96
Naive Bayes	63.90	72.83	63.90	64.84	53.45	46.55	74.91	53.45	58.35

*Machine and Deep Learning-based Intrusion Detection and Comparison in Internet of Things*

**Table 2.** Results using ML models with 34 features (features selection) – multiclass classification.

ML Model	Cross Validation Results				Evaluation Results on Testing Data				
	<i>CV Accuracy mean</i>	<i>CV Precision mean</i>	<i>CV Recall mean</i>	<i>CV F1 mean</i>	<i>Test Accuracy</i>	<i>Test FAR rate</i>	<i>Test Precision</i>	<i>Test Recall</i>	<i>Test F1</i>
Random Forest	82.90	82.75	82.90	81.93	75.90	24.10	83.54	75.90	77.87
Decision Tree	81.08	80.93	81.08	80.53	73.86	26.14	80.52	73.86	76.35
KNN	76.31	76.80	76.31	76.37	70.59	29.41	78.72	70.59	73.53
Logistic Regression	76.34	75.88	76.34	74.39	67.92	32.08	76.04	67.92	69.52
Naive Bayes	65.13	73.69	65.13	65.61	54.44	45.56	72.95	54.44	58.22

**Table 3.** Results using ML models with 42 features – binary classification.

ML Model	Cross Validation Results				Evaluation Results on Testing Data				
	<i>CV Accuracy mean</i>	<i>CV Precision mean</i>	<i>CV Recall mean</i>	<i>CV F1 mean</i>	<i>Test Accuracy</i>	<i>Test FAR rate</i>	<i>Test Precision</i>	<i>Test Recall</i>	<i>Test F1</i>
Random Forest	95.95	95.93	95.95	95.93	87.09	12.91	88.84	87.09	86.77
Decision Tree	94.87	94.88	94.87	94.87	86.36	13.64	87.29	86.36	86.13
KNN	93.79	93.76	93.79	93.76	84.48	15.52	86.17	84.48	84.07
Logistic Regression	93.52	93.75	93.52	93.37	80.93	19.07	84.03	80.93	80.07
Naive Bayes	74.63	82.26	74.63	75.47	74.78	25.22	76.68	74.78	74.74

**Table 4.** Results using ML models with 34 features (features selection) – binary classification.

ML Model	Cross Validation Results				Evaluation Results on Testing Data				
	<i>CV Accuracy mean</i>	<i>CV Precision mean</i>	<i>CV Recall mean</i>	<i>CV F1 mean</i>	<i>Test Accuracy</i>	<i>Test FAR rate</i>	<i>Test Precision</i>	<i>Test Recall</i>	<i>Test F1</i>
Random Forest	95.87	95.86	95.87	95.85	86.97	13.03	88.82	86.97	86.64
Decision Tree	94.79	94.79	94.79	94.79	86.18	13.82	87.20	86.18	85.94
KNN	93.74	93.71	93.74	93.70	82.10	17.90	83.13	82.10	81.72
Logistic Regression	93.37	93.74	93.37	93.18	80.33	19.67	83.71	80.33	79.38
Naive Bayes	77.65	82.16	77.65	78.38	73.06	26.94	73.32	73.06	73.12

Table 5 and 6 obtained DL performance results by using full feature space with 42 features for multiclass classification and binary classification, respectively. In deep learning methods, we eliminate the need for features selection since these methods act as black boxes and generate non-linear combinations while the features that have less effect get lesser weight automatically. As introduced in Table 5, the best performing models for multiclass classification tasks are the more complicated models and more convenient models for the used dataset, such as DNN-2 with 77.36% accuracy, RNN with 76.69% accuracy, and CNN-LSTM with 76.50% accuracy. Besides that, in Table 6 for binary classification tasks, CNN-LSTM with 87.34% accuracy, LSTM with 86.64% accuracy, and RNN with 86.24% achieved better results for intrusion detection in our dataset. Also, as we explained, we know that DNN-2 is more complicated than DNN-1 and the structure of CNN-2 is more convoluted than CNN-1. In Table 5, DNN-2 (77.36%) model achieved better accuracy than DNN-1 (74.61%). The same for CNN models in Table 6 the results demonstrated that the accuracy increased from 86.98% for CNN-1 to 85.80% for CNN-2.

For the multiclass classification problem, Table 5 shows that DNN-1 has 74.61% accuracy and GRU has 72.96% accuracy these models get lower performance results. While for the binary classification task, CNN-2 with 84.91% accuracy and CNN-1 with 84.50% accuracy perform lower

*Machine and Deep Learning-based Intrusion Detection and Comparison in Internet of Things*

accuracies than other DL models and we think this happened with convolutional neural networks because our dataset in the binary classification problem has smaller dimensions, which leads to overfitting problem. In Table 5, we can observe that the best performing models run a lower number of epochs with early stopping based on 5-fold cross-validation and this method prevents overfitting problems in the dataset.

To comparison between ML and DL, we can say that DL models achieved higher accuracies than ML models. From Table 1 and 5, we observed that while accuracies in DL models for multiclass classification between 77.36% and 72.96%; the accuracy results in ML models decreased until 53.45%, and in general accuracies values are between 75.38% and 53.45%.

From Table 3 and 6, we can see that while accuracies in DL models for binary classification between 87.34% and 84.50%; the accuracy results in ML models decreased until 74.78%, and in general accuracies values are between 87.09% and 74.78%. We observed that random forest and decision tree perform well this is because it is ensemble methods. Ensemble methods are techniques that use multiple classifiers, and then combine them to provide enhanced performance. The predictions of ensemble methods are collected to determine the most often occurring outcome and usually produce more accurate results than a single model. Also, we observed that families of RNN architecture achieved a high accuracy rate in comparison to the traditional machine learning classifiers and the reason for that is the RNN architectures are capable of retraining information over time and maintaining connection sequence data. As a result, from the experiments, we notice that are more complex models get higher accuracies in some cases. We applied 5-fold cross-validation for both the DL and ML models to get more accurate results about the performance and compared intrusion detection accuracies between different models.



**Table 5.** Results using DL models with 42 features – multiclass classification.

DL Model	Cross Validation Results					Evaluation Results on Testing Data				
	<i>Epochs for early stopping based on 5-fold CV</i>	<i>CV Accuracy mean</i>	<i>CV Precision mean</i>	<i>CV Recall mean</i>	<i>CV F1 mean</i>	<i>Test Accuracy</i>	<i>Test FAR rate</i>	<i>Test Precision</i>	<i>Test Recall</i>	<i>Test F1</i>
DNN-2	23, 2, 2, 7, 1	81.55	81.53	81.55	79.36	77.36	22.64	81.26	77.36	77.07
RNN	24, 22, 1, 5, 1	80.89	80.84	80.89	78.11	76.69	23.31	79.64	76.69	76.22
CNN-LSTM	31, 6, 1, 7, 9	81.41	81.26	81.41	78.66	76.50	23.50	81.25	76.50	76.76
CNN-1	20, 9, 1, 11, 3	79.84	80.36	79.84	76.78	75.93	24.07	79.21	75.93	75.44
LSTM	44, 5, 1, 3, 1	81.76	81.49	81.76	79.64	75.83	24.17	79.94	75.83	76.19
CNN-2	24, 2, 3, 3, 5	80.54	79.94	80.54	77.52	74.80	25.20	82.29	74.80	74.92
DNN-1	24, 5, 1, 2, 1	81.10	80.92	81.10	79.37	74.61	25.39	81.41	74.61	75.08
GRU	45, 2, 1, 2, 3	81.65	81.66	81.65	79.61	72.96	27.04	80.57	72.96	74.51

**Table 6.** Results using DL models with 42 features – binary classification.

DL Model	Cross Validation Results					Evaluation Results on Testing Data				
	<i>Epochs for early stopping based on 5-fold CV</i>	<i>CV Accuracy mean</i>	<i>CV Precision mean</i>	<i>CV Recall mean</i>	<i>CV F1 mean</i>	<i>Test Accuracy</i>	<i>Test FAR rate</i>	<i>Test Precision</i>	<i>Test Recall</i>	<i>Test F1</i>
CNN-LSTM	41, 3, 6, 2, 4	94.96	94.95	94.96	94.93	87.34	12.66	89.01	87.34	87.03
LSTM	18, 12, 2, 6, 4	94.89	94.87	94.89	94.85	86.64	13.36	88.14	86.64	86.33
RNN	28, 5, 5, 12, 2	94.82	94.81	94.82	94.78	86.24	13.76	88.04	86.24	85.88
DNN-1	21, 1, 2, 3, 7	94.71	94.71	94.71	94.66	86.13	13.87	88.13	86.13	85.74
GRU	24, 21, 1, 4, 2	94.87	94.85	94.87	94.84	86.05	13.95	87.90	86.05	85.67

*Machine and Deep Learning-based Intrusion Detection and Comparison in Internet of Things*

**Table 6. (Cont.)** Results using DL models with 42 features – binary classification.

DL Model	Cross Validation Results					Evaluation Results on Testing Data				
	Epochs for early stopping based on 5-fold CV	CV Accuracy mean	CV Precision mean	CV Recall mean	CV F1 mean	Test Accuracy	Test FAR rate	Test Precision	Test Recall	Test F1
DNN-2	25, 1, 2, 1, 3	94.92	94.91	94.92	94.88	86.03	13.97	87.89	86.03	85.66
CNN-2	17, 5, 1, 5, 1	94.70	94.73	94.70	94.63	84.91	15.09	87.73	84.91	84.35
CNN-1	23, 1, 6, 2, 1	94.49	94.56	94.49	94.41	84.50	15.50	87.42	84.50	83.91

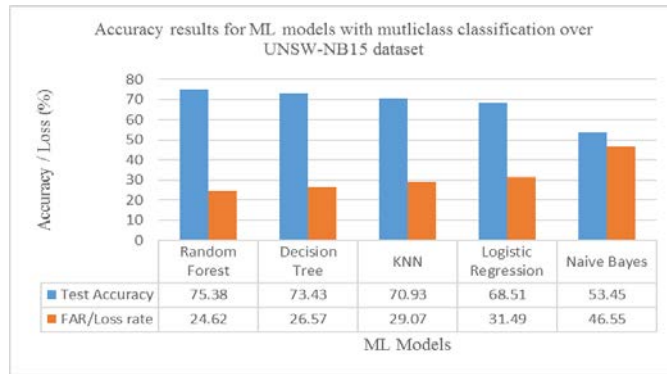


**Figure 4.** ML models performance over multiclass classification with 42 features.

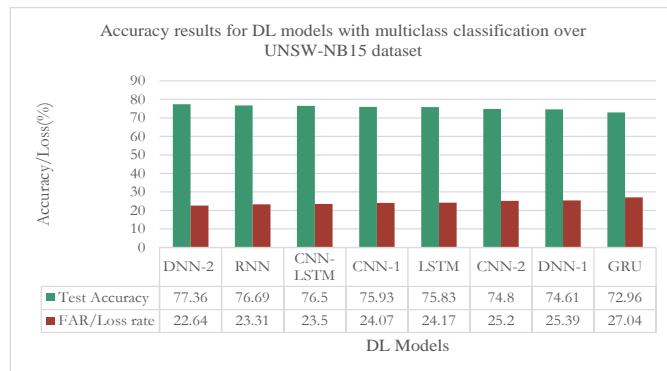


**Figure 5.** DL models performance over multiclass classification.

As we can observe from above Figure 4 and 5, the traditional machine learning model's performance decreased to 53.45% against the case in the deep learning model the accuracy results decreased to 72.96%. We notice that decision tree and random forest ensemble methods produce improved results similar to deep learning methods and it is a normal case because these techniques aggregate multiple models and predictors to provide results that are more accurate. In addition, we inferred from the experiments that families of RNN architecture achieved a high accuracy rate in comparison to the traditional machine learning classifiers. The reason for that is that RNN architectures are able to memorize information over time and have connection sequences of information that store previous blocks values. On the other hand, for binary classification, as illustrated in Figure 6 and 7, the performance of classical machine learning models decreased to 74.78% while the accuracy of deep learning models decreased to 84.50%, which is a higher value than the machine learning model's value.

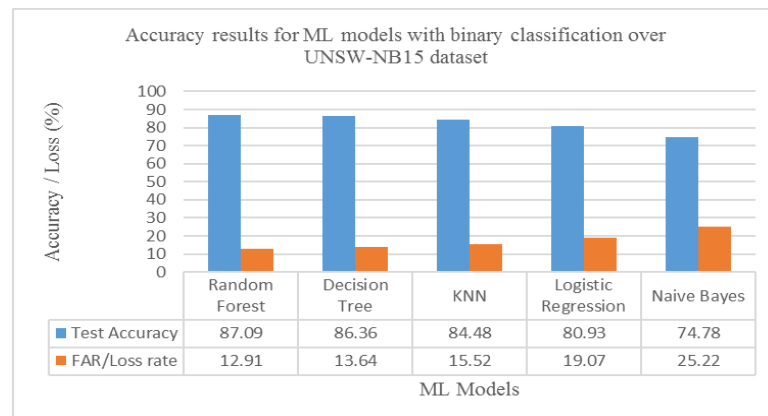


**Figure 6.** ML models performance over binary classification with 42 features

*Machine and Deep Learning-based Intrusion Detection and Comparison in Internet of Things*

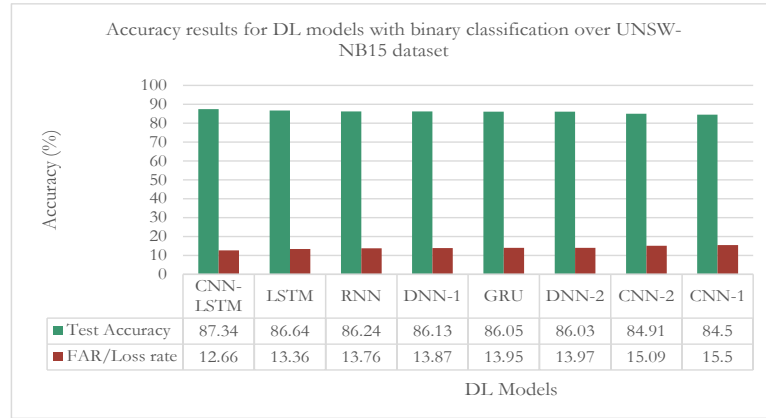


**Figure 7.** DL models performance over binary classification

The receiver operating characteristic (ROC) is a graphical representation of a binary classifier system's diagnostic ability as its discrimination threshold is varied. This curve plots two parameters: False Positive Rate (FPR) and True Positive Rate (TPR). As shown in Figure 8, we can see the variance in performances between ML and DL models for binary classification problems, the ROC curve of DL models is better than the ROC curve of ML models.

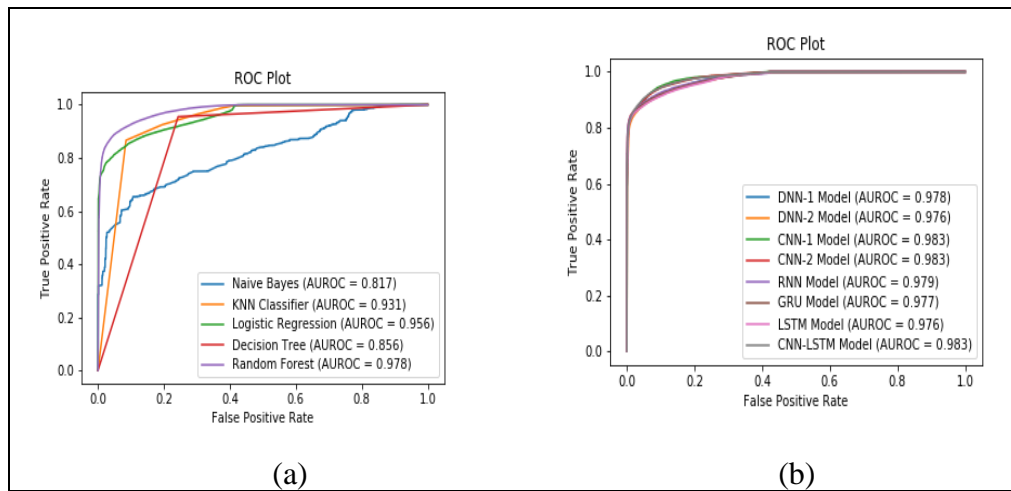


**Figure 8.** Comparison between ROC curves for classical ML models and DL models: (a) ROC curve for ML models in binary classification, (b) ROC curve for DL models in the binary classification problem.

Implementation of deep learning models depends on different hyperparameters, which are a critical component of any deep network since they enable us to optimize the network's quality.

**Table 7.** Intrusion detection results using DNN-2 DL model over multiclass classification with different number of epochs.

DNN-2 Model	Epochs	Cross Validation Results				Evaluation Results on Testing Data				
		CV Accuracy mean	CV Precision mean	CV Recall mean	CV F1 mean	Test Accuracy	Test FAR rate	Test Precision	Test Recall	Test F1
* Activation function in hidden layers: ReLU & in output layer: Softmax * Optimizer: adam * Batch size: 32	40	82.09	82.16	82.09	80.09	<u>77.17</u>	22.83	81.57	77.17	<u>78.14</u>
	50	82.06	81.68	82.06	80.32	75.58	24.42	80.29	75.58	76.59
	100	82.25	81.90	82.25	80.47	75.39	24.61	81.81	75.39	76.45
	25	81.95	81.99	81.95	79.98	75.15	24.85	80.82	75.15	76.29
	10	81.86	81.50	81.86	79.98	75.02	24.98	80.97	75.02	76.25

**Table 8.** Intrusion detection results using DNN-2 DL model over multiclass classification with different batch size.

DNN-2 Model	Batch Size	Cross Validation Results				Evaluation Results on Testing Data				
		CV Accuracy mean	CV Precision mean	CV Recall mean	CV F1 mean	Test Accuracy	Test FAR rate	Test Precision	Test Recall	Test F1
* Activation function in hidden layers: ReLU & in output layer: Softmax * Optimizer: adam * Epochs: 40	16	81.78	81.63	81.78	79.84	<u>76.80</u>	23.20	81.42	76.80	<u>77.36</u>
	32	82.05	81.67	82.05	80.06	76.49	23.51	80.77	76.49	77
	64	81.86	81.59	81.86	80.02	75.82	24.18	80.97	75.82	76.92
	48	81.83	81.58	81.83	79.89	75.74	24.26	80.62	75.74	76.31
	128	81.96	81.73	81.96	79.83	75.62	24.38	81.15	75.62	76.73

From Table 7, we can observe that epochs number 40 will be a better choice for the DNN-2 model with 77.17% test accuracy and 78.14% test F1. Because of that, we chose it and then implemented it with different batch size values (16, 32, 48, 64, 128). As shown in Table 8, it indicates that the batch size value of 16 achieves better results with 76.80% test accuracy and 77.36% test F1. Besides comparison between accuracy and different epoch numbers, and batch size values over deep learning methods, we could also use different activation functions in hidden layers, optimization algorithms,

learning rate, batch number, number of neurons, and number of hidden layers.

## **5. CONCLUSION AND RECOMMENDATIONS**

In this research, we applied the following supervised Machine Learning (ML) methods for IDS: Naïve Bayes (NB), k-Nearest-Neighbor (kNN), Logistic Regression (LR), Decision Tree (DT) and Random Forest (RF). Also, Deep Learning (DL) methodologies such as: Deep Neural Network (DNN), Convolutional Neural Network (CNN), Recurrent Neural Network (RNN), Gated Recurrent Unit (GRU), Long Short-Term Memory (LSTM), and CNN-LSTM model. Traditional machine learning methods depend heavily on feature engineering, which is often time-consuming and complex and with the complexity of the IoT structure, it is critical to develop an IDS that achieves low computational costs and reduces the amount of energy consumed. As a result, it is impractical to detect anomalies in real-time using classical machine learning models. For that in our work, we also applied deep learning methods that are used to generate non-linear combinations, where the features that have a lesser effect are automatically given a lower weight. Since our data are labeled, we employed supervised deep learning methods. We applied the Random Forest algorithm over UNSW-NB15 dataset to calculate the feature importance measure for each feature, generate reduced optimal feature vectors. We considered two schemes binary and multiclass classification configurations. We compared different models using their performance results and accuracies. We can conclude that deep learning methods exceed traditional methods with their performance in the attack detection tasks; also feature selection methods can enhance performance in some classical machine learning models.

In the future work, we can compare the experimental results of UNSW-NB15 dataset with other datasets like Bot-IoT, CIC-IDS2018, and N-BaIoT datasets or we can create our own dataset using simulation tools. We aim to be more creative in intrusion detection methods and increase accuracies using hybrid models by combining blockchain with deep learning algorithms. We think to add an intrusion prevention system (IPS) to IDS, this technology used to prevent and mitigate attacks and drop the malicious packets and threats.

*Siham AMAROUCHE, Kerem KÜÇÜK*

**CONFLICT OF INTEREST STATEMENT**

The authors declare no conflict of interest.

## **REFERENCES**

Abiodun, O. I., Jantan, A., Omolara, A. E., Dada, K. V., Mohamed, N. A., & Arshad, H. (2018). "State-of-the-art in artificial neural network applications: A survey". *Heliyon*, 4(11), pp. 1-41.

Albawi, S., Mohammed, T.A., & Al-Zawi, S. (2017). "Understanding of a convolutional neural network". In *2017 International Conference on Engineering and Technology (ICET)* (pp. 1-6).

Alsamiri, J., & Alsubhi, K. (2019). "Internet of things cyber attacks detection using machine learning". *International Journal of Advanced Computer Science and Applications*, 10(12), pp. 627-634.

Boateng, E. Y., & Abaye, D. A. (2019). "A review of the logistic regression model with emphasis on medical research". *Journal of Data Analysis and Information Processing*, 7(4), pp. 190-207.

Breiman, L. (2001). "Random Forests". *Machine Learning*, 45(1), pp. 5-32.

Chandrashekar, G., & Sahin, F. (2014). "A survey on feature selection methods". *Computers & Electrical Engineering*, 40(1), pp. 16-28.

Chomboon, K., Chujai, P., Teerarassamee, P., Kerdprasop, K., & Kerdprasop, N. (2015). "An empirical study of distance metrics for k-nearest neighbor algorithm". In *Proceedings of the 3rd International Conference on Industrial Application Engineering* (pp. 280-285).

Graves, A. (2012). "Long Short-term Memory". *Supervised Sequence Labelling with Recurrent Neural Networks* (pp. 37-45). Springer, Berlin, Heidelberg.

Hochreiter, S., & Schmidhuber, J. (1997). "Long Short-term Memory". *Neural Computation*, 9(8), pp. 1735-1780.



Jozefowicz, R., Zaremba, W., & Sutskever, I. (2015). "An empirical exploration of recurrent network architectures". F. R. Bach & D. M. Blei (Eds.), *International Conference on Machine Learning* (pp. 2342-2350). PMLR.

Kasongo, S. M., & Sun, Y. (2020). "Performance analysis of intrusion detection systems using a feature selection method on the UNSW-NB15 dataset". *Journal of Big Data*, 7(1), pp. 1-20.

Kaviani, P., & Dhotre, S. (2017). "Short survey on naive bayes algorithm". *International Journal of Advance Engineering and Research Development*, 4(11), pp. 607-611.

Khraisat, A., Gondal, I., & Vamplew, P. (2019). "Survey of intrusion detection systems: techniques, datasets and challenges". *Cybersecurity*, 2, pp. 1-20.

Manaswi, N. K. (2018). *Deep Learning with Applications Using Python: Chatbots and Face, Object, and Speech Recognition with Tensorflow and Keras*. Apress, Berkeley, CA.

Medsker, L. R., & Jain, L. C. (1999). *Recurrent Neural Networks: Design and Applications*. CRC Press.

Moustafa, N., & Slay, J. (2015). "UNSW-NB15: A comprehensive data set for network intrusion detection systems (UNSW-NB15 network data set)". In *2015 Military Communications and Information Systems Conference (MilCIS)* (pp. 1-6). Australia.

Patel, K. K., & Patel, S. M. (2016). "Internet of Things-IOT: Definition, Characteristics, Architecture, Enabling Technologies, Application & Future Challenges". *International Journal of Engineering Science and Computing*, 6(5), pp. 6122-6131.

*Machine and Deep Learning-based Intrusion Detection and Comparison in Internet of Things*

Safavian, S. R., & Landgrebe, D. (1991). "A survey of decision tree classifier methodology". *IEEE Transactions on Systems, Man, and Cybernetics*, 21(3), pp. 660-674.

Sherstinsky, A. (2020). "Fundamentals of recurrent neural network (RNN) and long short-term memory (LSTM) network". *Physica D: Nonlinear Phenomena*, 404, Article 132306. doi:10.1016/j.physd.2019.132306.

Sze, V., Chen, Y. H., Yang, T. J., & Emer, J. S. (2017). "Efficient processing of deep neural networks: A tutorial and survey". *Proceedings of the IEEE*, 105(12), pp. 2295-2329. doi:10.1109/JPROC.2017.2761740.

Van Houdt, G., Mosquera, C., & Nápoles, G. (2020). "A review on the long short-term memory model". *Artificial Intelligence Review*, 53(8), pp. 5929-5955. doi:10.1007/s10462-020-09838-1.

Vinayakumar, R., Soman, K. P., & Poornachandran, P. (2017). "Evaluation of recurrent neural network and its variants for intrusion detection system (IDS)". *International Journal of Information System Modeling and Design (IJISMD)*, 8(3), pp. 43-63.

*\*An ethical committee approval and/or legal/special permission has not been required within the scope of this study.*

**PROJECT PLANNING WITH CPM AND PERT METHODS:  
EXAMPLE OF DEFENCE INDUSTRY\***

**Beste DESTİCİOĞLU TAŞDEMİR **

*National Defence University, Alparslan Defence Sciences and National Security Institute, Department of Operations Research, Ankara, Turkey,  
bdesticioglu@kho.msu.edu.tr*

**Received: 13.04.2022**

**Accepted: 16.05.2022**

**ABSTRACT**

*Project management is the process of planning activities in the project, estimating time and cost, assigning resources, making schedules, and performing controls. Project planning methods are used in project management to make time estimations. CPM, PERT, Gantt Charts, Fuzzy CPM, Fuzzy PERT are project planning methods. The CPM method is used when the activity durations are known certainly. However, in a project implemented for the first time, the duration of activity cannot be estimated certainly. In order to take this variability into account, the PERT method, which calculates the optimistic, probable and pessimistic durations of the activities, is used. Defence industry projects are of great importance as they are related to the defence of the country. In order for defence industry projects to be successful, the projects must be planned effectively. In this study, the planning process of a project realized for the first time by a company serving in the defence industry was examined. In the study, first of all, the activities of the project, their previous activities and duration are defined. In the study, the completion time of the project was calculated using CPM and PERT methods and the results were compared. In the last part of the study, the completion time of the project was calculated under different probabilities by using the PERT method.*

**Keywords:** *Defence Industry, Project Management, CPM, PERT, Project Planning.*

**CPM VE PERT YÖNTEMLERİYLE PROJE PLANLAMA:  
SAVUNMA SANAYİ ÖRNEĞİ**

**ÖZ**

*Proje yönetimi, projedeki faaliyetlerin planlanması, zaman ve maliyet tahmininin yapılması, kaynakların atanması, programların yapılması ve kontrollerin gerçekleştirilmesi sürecidir. Proje yönetiminde zaman tahminlerinin yapılabilmesi için proje planlama yöntemlerinden faydalanılmaktadır. CPM, PERT, Gantt Şemaları, Bulanık CPM, Bulanık PERT proje planlama yöntemlerindedir. CPM yöntemi faaliyet süreleri kesin olarak bilindiğinde kullanılmaktadır. Ancak ilk kez uygulanan bir projede faaliyet süreleri kesin olarak tahmin edilememektedir. Bu değişkenliği dikkate alabilmek için ise, faaliyetlerin iyimser, olası ve kötümser süreleri hesaplama yapan PERT yöntemi kullanılmaktadır. Savunma sanayi projeleri, ülke savunması ile ilgili olduğundan büyük önem taşımaktadır. Savunma sanayi projelerinin başarıya ulaşabilmesi için, projelerin etkin bir şekilde planlanması gerekmektedir. Bu çalışmada da savunma sanayinde hizmet veren bir firmanın ilk kez gerçekleştirdiği bir projenin planlanma süreci incelenmiştir. Çalışmada ilk olarak, projenin faaliyetleri, öncüllük ilişkileri ve süreleri tanımlanmıştır. Çalışmada projenin tamamlanma zamanı CPM ve PERT yöntemleri kullanılarak hesaplanmış ve elde edilen sonuçlar karşılaştırılmıştır. Çalışmanın son bölümünde ise PERT yöntemi kullanılarak farklı olasılıklar altında projenin tamamlanma zamanı hesaplanmıştır.*

**Anahtar Kelimeler:** *Savunma Sanayi, Proje Yönetimi, CPM, PERT, Proje Planlama.*

## **1. INTRODUCTION**

The project is the set of activities created to achieve the determined targets within the specified time frame. The most confusing concept of the project concept is the operation. Although the project and the operation have many common aspects, there are points where these two concepts differ. While the project is defined as original and temporary activities; operation is defined as ongoing and repetitive activities. In this case, project can be defined as a unique service, product or a temporary attempt to achieve a specified goal. The project is the process where resources or employees come together with an organization within a certain time interval and these resources are transferred to other units after the project is completed in order to reach the determined goal (Abdel-Basset et al., 2021). Since projects consist of many activities, they must be carefully planned and completed within the specified time by acting in a coordinated manner at each stage (Gül et al., 2017).

In order for a project to be successful, it is necessary to make a good planning, to determine the relationships between the activities correctly, to predict the completion time and cost of the project, and to allocate resources accordingly. The success of the project is only possible with a successful project management. Project management can be defined as the process that ensures the effective management of the machinery, workforce, tools, information, software and other resources needed for the high quality of the project, in the shortest time possible, with minimum cost. Project management includes all stages of planning, management, organization and control of project activities in order for the project to be carried out in any sector to achieve its determined goals (Aksoy et al., 2019). Project management includes the stages of planning activities to achieve the determined goal, estimating the completion time and cost of the project, assigning resources and realizing project control (Temiz and Dursun, 2016).

Project management, considering the project as a whole, allows examining all components, making systematic arrangements within the project and carrying out activities suitable for the project. Project management enables the company to see ahead even in a project implemented for the first time (Sanchez et al., 2019). With the realization of an effective project

management, companies can estimate the completion time and cost of the project at the beginning of the project.

Planning is the first stage of project management and also forms the basis of the project. Therefore, the planning must be carried out effectively in order for the project to be successful. The planning stage is the stage in which what, when and how to do is determined, and at the same time resource allocation is carried out. Estimating the completion time of the project is the most important part of the planning phase. For the estimation of the completion time, it is first necessary to determine the priority relationships between the activities and these activities. When we look at the studies in the literature, it is seen that the Critical Path Method (CPM) and Program Evaluation and Review Method (PERT) are mostly used in estimating the durations.

Defence industry projects are among the most important factors that will increase the success of countries in the field of defence. Countries are investing heavily in defence industry projects in order to be a deterrent against their enemies by increasing their defence power. It is seen that a large share is allocated to defence industry projects within defence expenses. In order for defence industry projects to be successful and to reduce costs by using resources effectively, proper planning is required. In the creation of these plans, it is very important to define the activities, to determine the antecedent relations, and to estimate the completion time of the project by considering these relations.

As a result of the literature review, it has been determined that the researchers have been working on project planning for different sectors, and it has been seen that there is no study on project planning in the field of defence industry. Therefore, in this study, project activities were defined for a product to be produced for the first time by a company serving in the defence industry, and the project completion time was estimated. In the literature, it has been seen that CPM and PERT methods are widely used in determining the completion times of projects. However, in the projects implemented for the first time, this uncertainty should be reflected in the durations as the durations are not known clearly. For this reason, in the study, PERT method was used to determine the critical path by taking into account the optimistic, probable and pessimistic duration in order to define

*Project Planning with CPM and PERT Methods: Example of Defence Industry*

the uncertainty in question in the duration of the activities. In addition, critical paths were determined for both CPM and PERT; Project completion times were calculated with both methods.

In the study, firstly, the literature research on project planning is included. In the following, CPM and PERT methods are discussed. In the next section, the network of the project was drawn by considering the priority relations of the activities in the project. In the study, the probable completion times of the project were calculated using CPM and PERT methods and the results were interpreted. In the last part of the study, the completion time of the project was calculated for different possibilities with the PERT method.

## **2. LITERATURE REVIEW**

It is seen that there are many studies on project planning and project scheduling in the literature. In the studies in the literature, it has been determined that CPM, PERT, Fuzzy CPM and Fuzzy PERT methods are generally used in project planning. In this section, information is given about the studies carried out in recent years.

In their study, Turan and Güner (2013) used the CPM method to calculate the completion time of the green platform supply vessel project to be built for the first time in Turkey. In the study, the critical activities and critical path that took place during the project and directly affected the completion time of the project were determined. With the calculated slack, they stated how long the project could be delayed without changing the completion time.

Mazlum and Güneri (2015) used CPM and PERT methods in the scheduling of the online internet branch project. Researchers stated that there may be uncertainty in activity durations and defined activity durations using fuzzy triangle numbers. Fuzzy CPM and fuzzy PERT methods were used to calculate the completion time of the project with fuzzy activity times. In the last part of the study, they compared the results obtained with CPM, PERT, fuzzy CPM and fuzzy PERT methods.

Agyei (2015) examined the scheduling of a construction project in Ghana. In the study, the completion time of the project and the cost to be incurred were estimated by using CPM and PERT methods. At the same time, the changes that will occur on the project costs when the project is accelerated are also discussed in the study.

Temiz and Dursun (2016) used the PERT method to calculate the completion time in the port marine services automation project in their study. In the study, they also calculated the probability of completion of the project in different time periods by finding the variance values of each activity.

Gül et al. (2017) used fuzzy CPM and fuzzy PERT methods to evaluate the patient flow of the emergency department in a university hospital. Since the services provided in the emergency department contain uncertainty, they determined the duration of their activity with fuzzy numbers. In the study, factors affecting patient flow were determined. Researchers created the project network by considering the priority relations and calculated the completion time of the project.

Kholil et al. (2018) calculated the completion time of 36 house types (defined as 36 m<sup>2</sup> houses) projects with CPM and PERT methods. In the study, the results obtained by using both methods were compared and interpreted and the project was planned more efficiently.

Maulana and Kurniawan (2019) used CPM, PERT and PDM (Precedence Diagram Method) methods to determine the completion time of the social service construction project in their studies. As a result of the calculations, the shortest completion time was obtained with the PDM method. In the study, they stated that the fact that the completion of the predecessor activity was not taken into account in the beginning of an activity was effective in the fact that the PDM method was lower than the others.

In their study, Tümtürk and Tümtürk (2020) examined the planning of urban transformation building projects in İzmir Karşıyaka. In the study, they used the CPM method to calculate the completion time of the project and made cost estimation. The study also includes how much the project can be accelerated and the additional costs that this acceleration will bring.



*Project Planning with CPM and PERT Methods: Example of Defence Industry*

Gasparikova and Leitner (2021), in their study, created the evacuation planning process of people using the network analysis method. In the study, networks of processes related to crisis management and evacuation of people were created, and the completion time of the evacuation was calculated with the PERT method. In the last part of the study, the results obtained are interpreted.

Abdel-Basset et al. (2022) studied the scheduling of high-risk projects under uncertain environmental conditions. Since the activity durations are uncertain, they used fuzzy numbers to determine the durations. In the study, they calculated the completion time of the project using fuzzy CPM and fuzzy PERT methods.

In the literature review, it was seen that the researchers conducted studies on the planning and scheduling of projects in different sectors. However, it has been determined that no study has been done on the planning of the projects carried out in the defence industry before. Therefore, in this study, the planning phase of a plate project to be developed by an enterprise serving in the defence industry has been examined. In the literature review, it was determined that researchers generally use CPM and PERT methods in calculating the required completion time in the planning process of projects. Therefore, in this study, CPM and PERT methods were used to calculate the completion time of the project. In the next part of the study, CPM and PERT methods are explained.

### **3. CPM AND PERT METHODS**

The first study on project planning techniques was made by Gantt in the 1950s. Gantt developed the Gantt chart for estimating project durations. In the creation of this scheme, the completion time of the project was calculated by taking into account the antecedent relationships between the activities (Anderson et al., 2000). Although the Gantt chart shows the relationship between successive activities of the same activity, it falls short of showing the relationship between different activities. Critical Path Method (CPM) and Project Evaluation and Review Technique (PERT) were developed to show the relationship between different activities (Temiz and Dursun, 2016).

CPM and PERT are network-based methods developed for project planning, coordination and control. Both methods require the creation of the project network, taking into account the priority relations between the activities. The purpose of these methods is to create tools for planning the project. The network is the diagram in which the activities in the project and the antecedent relationships are shown by arrows and nodes. Drawing the network of the project by considering the priority relations of the activities helps in calculating the completion time of the project (Gül et al., 2017).

If the duration of the activities involved in the project is known certainly, the critical path method (CPM) can be used to determine the completion time of the project. CPM was developed by Kelly and Walker in order to calculate the downtimes caused by maintenance activities in chemical plants and to complete the project as soon as possible (Kelly and Walker, 1957). In the CPM method, the project's completion time is calculated by determining the critical activities and critical paths of the project. The critical path is the longest path between the start and end points in the project network. The activities on the critical path are called critical activities (Gül et al., 2017). In order to control the deficiencies in the project, it is of great importance to determine the critical path and critical activities of the project. Since the sum of the durations of critical activities is equal to the completion time of the project. The slightest delay that may occur in critical activities will cause disruption of the project and the amount of delay will affect the completion time of the project. If the project manager wants to make flexibility in terms of the duration of the activities, he/she can only do so through non-critical activities.

In the CPM method, it is assumed that the activity periods involved in the project are known certainly. The critical path is determined by calculating the earliest start and earliest completion times, and the latest start and latest completion times of the activities. Here first, the earliest start and earliest completion time of each activity is found. Afterwards, the earliest completion time of the last activity is equal to the latest completion time of the last activity, and the backward calculation is made. Let  $ES_j$  represent the earliest start time of activity  $j$ ,  $EF_j$  the earliest completion time of activity  $j$ , and  $t_j$  the duration of activity  $j$ . Accordingly,  $ES_j$ , earliest start time of

*Project Planning with CPM and PERT Methods: Example of Defence Industry*

activity  $j$  and  $EF_j$ , earliest completion time of activity  $j$  are calculated using Eq. 1 and Eq. 2:

$$ES_j = \max_{i < j} [EF_i] \quad (1)$$

$$EF_j = ES_i + t_j \quad (2)$$

If there are  $n$  activities in the project, the  $ES_n$  value of the  $n$ th activity gives the completion time of the project. In order to determine the critical path of the project, it is necessary to calculate the latest start and latest completion time of each activity. In order to make this calculation, first of all, the earliest completion time of the last activity,  $n$ , must be equal to the latest completion time. Afterwards, the calculation must be done backwards to the first activity. In order to make this calculation, it is necessary to calculate the latest start and latest completion times for each activity. Let  $LS_i$  represent the latest start time of activity  $i$ , and  $LF_i$  the latest completion time of activity  $i$ . Accordingly, the latest completion time of activity  $i$  is calculated by Eq. 3, and the latest start time of activity  $i$  is calculated using Eq. 4:

$$LF_i = \min_{i < j} [LF_j] \quad (3)$$

$$LS_i = LF_i - t_i \quad (4)$$

In order to determine the completion time of the project and the critical path, it is necessary to calculate the earliest start and completion times and the latest start and completion times for each activity. The path combining activities with equal earliest and latest completion times is called the critical path, and the activities in this path are called critical activities. Project completion time can be calculated by adding up the durations of critical activities on the critical path.

Project Evaluation and Review Technique (PERT) is a method used in project scheduling. The PERT method emerged as a result of the work of the United States Navy in 1958. The PERT method was used for the first time in the development process of a rocket (Çetmeli, 1982). This method is used to determine the start and end times of the activities in the project and the completion time of the project. In the PERT method, the completion time of the project is calculated by using the network diagram created

according to the priority relations between the activities. In the project planning, the first time the workers do that job, the disruptions in the supply of materials, unexpected machine downtimes, malfunctions, etc. Due to various reasons, there may be changes in the activity periods (Gencer and Türkbey, 2001). In general, PERT method is used in the planning of projects that are implemented for the first time or where the duration of the activity cannot be determined certainly. In the PERT method, the activity times are not known certainly. In this method, triple time estimation is made as optimistic time, probable time and pessimistic time. In addition, the average duration and standard deviation of each activity are calculated in the PERT method, and the probability of completion of the project in different times can be determined by using the normal distribution (Temiz and Dursun, 2016). In the PERT method, the duration of the activities conforms to the Beta distribution, and the completion time of the project conforms to the normal distribution. In the PERT method, the critical path and critical activities are calculated with the formulas used in the CPM method.

In the PERT method, the standard deviations calculated for the activities show how much deviation can occur in the activity times and these deviations enable it to be determined how much longer the project will be completed than the planned time. In the duration estimation,  $a$  is the optimistic duration,  $b$  is the pessimistic duration, and  $m$  is the probable duration, and the probable duration of the activity is calculated with the following formulation:

$$\mu = \frac{a + 4m + b}{6} \quad (5)$$

The variance and standard deviation of each activity are calculated with the Eq. 6 and Eq. 7 given below:

$$\sigma^2 = \left[ \frac{b - a}{6} \right]^2 \quad (6)$$

$$\sigma = \frac{b - a}{6} \quad (7)$$

*Project Planning with CPM and PERT Methods: Example of Defence Industry*

In the PERT method, mean times and variances are calculated for all activities. After calculating the activity times, the critical path and critical activities in the project network are determined. The completion time of the project with 50% probability is equal to the sum of the durations of the critical activities. In order to calculate the deviation in the completion time of the project, the variances of the critical activities are added and then the square root of the total is taken (Temiz and Dursun, 2016). The completion time of the project follows a normal distribution.

When there is more than one critical path in the project, the path with the largest variance is determined as the critical path. In the PERT method, Eq. 8 is used to calculate the probability of completion of the project in the specified time:

$$Z = \frac{X - \mu}{\sigma} \quad (8)$$

X= Time required to complete the project

μ= Average completion time of the project

σ= Standard deviation of the project

The probability of completion of the project within the specified time is calculated by determining the value that the value found as a result of the calculations corresponds to from the standard distribution table.

#### **4. METHODOLOGY**

CPM and PERT methods are used in scheduling projects in many sectors, from construction sector projects to production sector projects, from service sector projects to logistics sector projects. In the literature review, it has been seen that CPM and PERT methods are used in many different areas such as port project, construction project, organization of emergency services of hospitals, creation of a website. However, it has been determined that there is no study on the scheduling of defence industry projects in the literature. Therefore, in this study, CPM and PERT methods were used to calculate the completion time of the plate project to be produced by an enterprise serving in the defence industry.

The development of the defence industry is seen as an indicator of the military, economic and political power of the countries. The defence industry not only involves more risk and uncertainty than other industries, but also requires a large investment and capital (Uçakcioğlu and Eren, 2017). Therefore, time and cost management should be done carefully in the planning of defence industry projects. In this study, the scheduling and time estimation of the plate project that will be produced for the first time by an enterprise serving in the defence industry has been made. In the study, firstly, the network of the project was drawn by considering the priority relations of the activities. Afterwards, the probable completion time of the project was calculated with CPM and PERT methods. At the end of the application part, the completion time of the project is calculated for different possibilities.

Gantt Chart is widely used in calculating the completion time of projects. However, the Gantt diagram is insufficient in determining the priority relationships in the project and the critical activities of the project. Critical activities are activities that directly affect the calculation of the completion time of the project. The completion time of the project is obtained by summing the durations of the critical activities. Therefore, it is of great importance to identify the critical activities of the project. Critical activities that are so important for the project can be determined as a result of calculations made with CPM and PERT methods. In this study, considering this situation, CPM and PERT methods were used to calculate the completion time of the project.

The activities of the plate to be produced, the priority relations between the activities and the duration of the activities are given in Table 1.

*Project Planning with CPM and PERT Methods: Example of Defence Industry*

**Table 1.** Activities, priority relations and durations in the project.

Activities	Predecessor	Durations	PERT Durations		
			a	m	b
A- Creation of prescriptions	-	120	100	120	132
B- Preparation of the mixture	A	8	7	8	10
C- Waiting for the mixing sand to dry	B	10	9	10	14
D- Sifting the mix sand	C	5	4	5	6
E- Placing the press mold	A	2,5	2	2,5	4
F- Pressing	D, E	3	2	3	5
G- Quality control of the pressed product	F	2	2	2	3
H- Preparation of the pre-sinter mold	G	6	5	6	7
I- Pre-sintering	H	18	17	18	22
J- Emptying the pre-sinter furnace	I	2	1	2	3
K- Quality control of pre-sintered products	J	5	4	5	7
L- Preparation of the sinter mold	K	6	5	6	8
M- Sintering of products	L	32	30	32	40
N- Emptying the sinter furnace	M	6	5	6	7
O- Quality control of sintered products	N	7	6	7	8
P- Preparation of composite fabrics	A	8	6	8	9
R- Arrangement of products to be autoclaved	O, P	1	0,5	1	2
S- Processing of products in autoclave	R	6	5	6	7
T- Emptying the autoclave	S	2	1	2	3
U- Quality control of products	T	8	6	8	10
V- Packaging of products	U	3	2	3	5

In order to calculate the completion time of the project with CPM and PERT methods, first of all, the activities, the duration of the activities and the antecedent relationships between the activities should be defined. Afterwards, the network of the project should be created by taking into account the priority relations of the activities. In order to be able to calculate in CPM and PERT methods, the network of the project must be created. Therefore, the network diagram of the project given in Figure 1 was created

by considering the priority relationships between the activities given in Table 1.

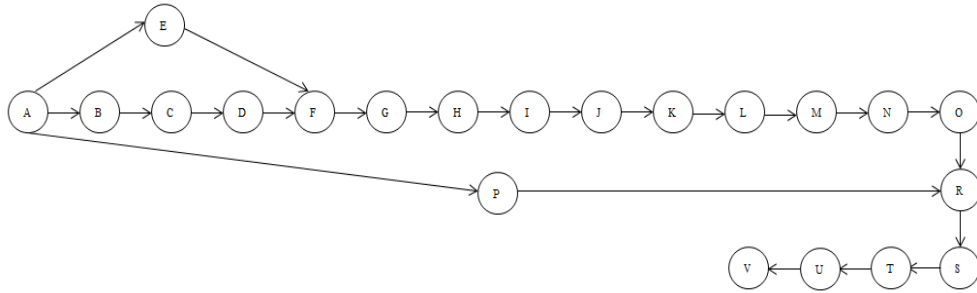


**Figure 1.** Network of the project.

#### 4.1. Calculations of CPM Method

When the activity periods of the project are deterministic, the completion time of the project can be calculated with CPM. In this calculation, firstly, the earliest start and completion times of each node and the latest start and completion times are calculated using the equations given in Eq. 1, Eq. 2, Eq. 3 and Eq. 4.

In Table 2, the earliest start and completion times and the latest start and completion times and completion times for each activity in the project are given. Critical activities in the project are also indicated in the Table 2.

As a result of the calculations, it was found that the project could be completed in 250 hours. Activities other than E and P are critical activities in the project. In other words, the duration of these activities directly affects the completion time of the project.



*Project Planning with CPM and PERT Methods: Example of Defence Industry*

**Table 2.** Results from the calculation with CPM.

Activity	Predecessor	Durations	Earliest		Latest		Note
			ES	EF	LS	LF	
A	-	120	0	120	0	120	Critical*
B	A	8	120	128	120	128	Critical*
C	B	10	128	138	128	138	Critical*
D	C	5	138	143	138	143	Critical*
E	A	2.5	120	122.5	140.5	143	
F	D; E	3	143	146	143	146	Critical*
G	F	2	146	148	146	148	Critical*
H	G	6	148	154	148	154	Critical*
I	H	18	154	172	154	172	Critical*
J	I	2	172	174	172	174	Critical*
K	J	5	174	179	174	179	Critical*
L	K	6	179	185	179	185	Critical*
M	L	32	185	217	185	217	Critical*
N	M	6	217	223	217	223	Critical*
O	N	7	223	230	223	230	Critical*
P	A	8	120	128	222	230	
R	O; P	1	230	231	230	231	Critical*
S	R	6	231	237	231	237	Critical*
T	S	2	237	239	237	239	Critical*
U	T	8	239	247	239	247	Critical*
V	U	3	247	250	247	250	Critical*

#### 4.2. Calculations of PERT Method

In real life problems, variables such as demand and time cannot be known precisely in advance, and these values change over time. For example, for a project made for the first time, the duration of a machine to be used for the first time cannot be predicted. In this case, an average processing time for the machine is determined using the information from previous projects. In the PERT method, besides the possible duration, the optimistic and pessimistic duration for the activity is also determined. PERT method is

*Beste DESTİCİOĞLU TAŞDEMİR*

used to calculate the completion time of the project by considering these three different periods. In this study, since the project will be implemented for the first time, it is thought that there are uncertainties in the activity durations and optimistic duration, probable duration and pessimistic duration are defined for each activity. Afterwards, the calculations were made with the PERT method. Table 3 was created by using the results obtained in the calculations. The table also includes the average durations and variances of the activities.

**Table 3.** Results from the calculation with PERT.

Activity	Durations			$\mu$	$\sigma^2$	Earliest		Latest		Note
	a	m	b			ES	EF	LS	LF	
A	100	120	132	118.7	28.41	0	118.7	0	118.7	Critical*
B	7	8	10	8.2	0.25	118.7	126.9	118.7	126.9	Critical*
C	9	10	14	10.5	0.69	126.9	137.4	126.9	137.4	Critical*
D	4	5	6	5	0.11	137.4	142.4	137.4	142.4	Critical*
E	2	2,5	4	2.7	0.11	118.7	121.4	139.7	142.4	
F	2	3	5	3.2	0.25	142.4	145.6	142.4	145.6	Critical*
G	2	2	3	2.2	0	145.6	147.8	145.6	147.8	Critical*
H	5	6	7	6	0.11	147.8	153.8	147.8	153.8	Critical*
I	17	18	22	18.5	0.69	153.8	172.3	153.8	172.3	Critical*
J	1	2	3	2	0.11	172.3	174.3	172.3	174.3	Critical*
K	4	5	7	5.2	0.25	174.3	179.5	174.3	179.5	Critical*
L	5	6	8	6.2	0.25	179.5	185.7	179.5	185.7	Critical*
M	30	32	40	33	2.78	185.7	218.7	185.7	218.7	Critical*
N	5	6	7	6	0.11	218.7	224.7	218.7	224.7	Critical*
O	6	7	8	7	0.11	224.7	231.7	224.7	231.7	Critical*
P	6	8	9	7.8	0.06	118.7	126.5	223.9	231.7	
R	0,5	1	2	1.1	0.33	231.7	232.8	231.7	232.8	Critical*
S	5	6	7	6	0.11	232.8	238.8	232.8	238.8	Critical*
T	1	2	3	2	0.11	238.8	240.8	238.8	240.8	Critical*
U	6	8	10	8	0.44	240.8	248.8	240.8	248.8	Critical*
V	2	3	5	3.2	0.25	248.8	252	248.8	252	Critical*

*Project Planning with CPM and PERT Methods: Example of Defence Industry*

In order to find the completion time of the project, the earliest start and latest finish times, and the latest start and latest finish times were calculated for each activity, as in the CPM method. As a result of the calculations, it was found that activities other than E and P activities are critical activities. In this case, the sum of the durations of the activities other than the E and P activities gives the completion time of the project. The time calculated by the PERT method shows the completion time of the project with 50% probability. Accordingly, the completion time of the project with 50% probability was calculated as 252 hours.

The same problem is solved using both CPM and PERT method. When the calculations for both methods are examined, it is seen that the completion times of the activities are close to each other. Table 4 was created to compare the times calculated with CPM and PERT.

**Table 4.** Comparison of results obtained with CPM and PERT.

<b>Completion Time</b>	<b>CPM</b>	<b>PERT</b>	<b>Difference</b>
Time (hour)	250	252	2

When Table 4 is examined, it is seen that the CPM method is more effective than the PERT method. While it is predicted that the project will be completed in 250 hours with the calculations made with the CPM method, it is predicted that the project will be completed within 252 hours as a result of the calculations made with the PERT. When the completion time calculated by the PERT method is compared with the completion time calculated by the CPM method, it is seen that there is a 2-hour deviation. This difference is due to the fact that three different situations are taken into account in the PERT method, as optimistic, probable and pessimistic duration for each activity. Considering the pessimistic time for activities negatively affects the results obtained by calculating the completion time of the project.

The time obtained by the PERT method gives the project completion time with 50% probability. However, no manager can carry out project planning by taking into account estimation made with 50% probability. Therefore, it is necessary to calculate the completion time of the project with higher probabilities. In the literature, it is seen that the completion time of the project is calculated with high probabilities such as 90%, 95%, 97.5% and

99%. Therefore, in this section, the completion time of the project is calculated with 90%, 95%, 97.5% and 99% probabilities.

In order to find the completion time of the project for different probabilities, it is first necessary to calculate the sum of the variances of the critical activities.

$$\sum \sigma^2 = 35.09 \quad (9)$$

In order to be able to calculate with Eq. 9, the sum of the standard deviations of the critical activities is needed. By taking the square root of the calculated variance, the standard deviation of critical activities was found to be 5.92. Table 5 was created by calculating the completion times of the project for different possibilities.

**Table 5.** Project completion time for different possibilities.

Probability	Completion Time
%50	252
%90	259.6
%95	261.7
%97.5	263.6
%99	265.8

When Table 5 is examined, it is seen that the completion time of the project increases as the probability value increases. The reason for this increase is taking into account the fact that all activities were carried out in the pessimistic period. As a result, the project will be completed in 265.8 hours with 99% probability. In this case, it is seen that there is a 15.8 hour deviation between the completion time found by the CPM method and the 99% probability completion time found by the PERT method. However, in the project planning applied for the first time, the workers doing that job for the first time, the disruptions in the supply of materials, unexpected machine downtimes, malfunctions, etc. Due to reasons, there may be changes in the operating times. With the calculations made with the PERT method, more realistic results are obtained for real life problems. Therefore, it would be

*Project Planning with CPM and PERT Methods: Example of Defence Industry*

more appropriate to plan the project according to the times obtained in the PERT method.

## **5. CONCLUSION**

Project management is the process of managing time, cost, resources, etc., in order to achieve the targeted goal in the project. The use of resources and costs at the right time and in the right place is possible by establishing an effective project management. In order for the projects to be concluded successfully and to reach the determined targets, the project must be managed successfully. Defence industry projects are of great importance for both Turkey and the whole world.

Defence industry projects are among the most important factors that will increase the success of countries in the field of defence. Countries are investing heavily in defence industry projects in order to be a deterrent against their enemies by increasing their defence power. The success of defence industry projects is of great importance for the defence of the country. Therefore, defence industry projects need to be planned and managed effectively. In the literature review, it has been determined that there are studies on the planning and scheduling of projects in different sectors, but there has been no study on the planning of projects in the defence industry sector before. Therefore, in this study, the project planning process for a newly developed project of a company working in the defence industry sector was examined.

In the study, first of all, the activities, predecessor relations and activity durations of the project were defined. The network of the project was created by taking into account the precedence relations between the activities. Afterwards, the completion times of the project were calculated using CPM and PERT methods. As a result of the calculations made with the CPM method, it was found that the project could be completed within 250 hours. As a result of the calculations made with the PERT method, it was found that the project could be completed in 252 hours with 50% probability. Afterwards, the completion times of the project were calculated under different probabilities using the PERT method. As a result of the calculations, it has been determined that the completion time of the project increases as the probability values increase.

When the calculations made with CPM and PERT methods are compared, it is seen that there is a 2-hour deviation between them. This is due to the fact that calculations are made in the CPM method under the assumption that the activity durations are deterministic, while in the PERT method, the calculations are made by considering 3 different activity periods of the activities: optimistic, pessimistic and probable duration. When the studies in the literature are examined, it is seen that better results are achieved with the calculations made with the CPM method. However, since the projects made for the first time contain uncertainty, there may be variability in the activity periods. The estimations made according to the results obtained by the PERT method, which takes into account the variability in the activity periods, are more consistent for the completion times of the projects encountered in real life. Therefore, using the PERT method in scheduling the projects for the first time and planning the project accordingly will be effective in the success of the project.

In this study, CPM and PERT methods were used to calculate the completion time of a project developed for the defence industry and the results were compared. The variability in the activity period of the project, which was carried out for the first time in the study, was taken into account with the PERT method and calculations were made. In the literature, it is seen that fuzzy CPM and fuzzy PERT methods are also used in calculating the completion time of the project in order to take into account the variability in the activity times. In future studies, the completion times of the projects can be calculated and compared between them by using fuzzy CPM and fuzzy PERT methods. Also, taking into account the assumption that the activity times are stochastic, the completion times of the project can be calculated.

*Project Planning with CPM and PERT Methods: Example of Defence  
Industry*

**CONFLICT OF INTEREST STATEMENT**

The author declares no conflict of interest.

## REFERENCES

- Abdel-Basset, M., Atef, A., Abouhawwash, M., Nam, Y., and AbdelAziz, M. N. (2022) "Network analysis for projects with high risk levels in uncertain environments". *Computers, Materials & Continua*, Vol. 70 Issue 1, pp. 1281-1296. doi:10.32604/cmc.2022.018947.
- Agyei, W. (2015). "Project planning and scheduling using PERT and CPM techniques with linear programming: case study". *International Journal of Scientific & Technology Research*, Vol. 4, Issue 8, pp. 222-227.
- Aksoy, A., Akansel, M., Atalay, C., Çamlıbel, A. M., Yaşar, D., Keseroğlu, D., and Vanlıoğlu, S. (2019). "Proje Yönetiminde Zaman ve Maliyet Odaklı Bütünleşik Planlama Yaklaşımı ve Bir Uygulama". *Journal of Entrepreneurship and Innovation Management*, Vol. 8, Issue 1, pp. 1-20.
- Anderson, D. R., Sweeney, D. J., Williams, T. A., Camm, J. D., and Cochran, J. J. (2012). *Quantitative Methods for Business*. Cengage Learning, Hampshire.
- Çetmeli, E. (1982). *Yatırım Planlamasında Kritik Yörünge ve PERT Metodları*. Teknik Kitaplar Yayınevi, İstanbul.
- Gašparíková, Z., and Leitner, B. (2021). "Application of the PERT method in planning of area evacuation of persons". *Transportation Research Procedia*, Vol. 55, pp. 1547-1554. doi:10.1016/j.trpro.2021.07.144.
- Gencer, C., and Türkbey, O. (2001). "Proje Tamamlanma Zamanının Bulunmasında İstatistiksel Analiz Yardımıyla Bulanık-PERT, Klasik-PERT ve Gerçek-Dağılım Yöntemlerinin Karşılaştırılması". *Dokuz Eylül Üniversitesi Mühendislik Fakültesi Fen ve Mühendislik Dergisi*, Vol. 3, Issue 2, pp. 29-39.
- Gül, M., Güneri, A. F., and Güneş, G. (2017). "Project management in healthcare: A case study for patient flow evaluation in an emergency room using fuzzy CPM and fuzzy PERT". *Sigma*, Vol. 8, Issue 1, pp. 41-51.
- Kelly, J. E., and Walker, M. R. (1957). The Critical Path Method. *Remington Rand and DuPont Corporation*.



*Project Planning with CPM and PERT Methods: Example of Defence Industry*

Kholil, M., Alfa, B. N., and Hariadi, M. (2018). "Scheduling of house development projects with CPM and PERT method for time efficiency (Case study: House type 36)". *IOP Conference Series: Earth and Environmental Science*, Vol. 140, No. 1, pp. 1-8. doi:10.1088/1755-1315/140/1/012010.

Maulana, A., and Kurniawan, F. (2019). "Time optimization using CPM, PERT and PDM methods in the social and department of Kelautan building development project Gresik district". *IJTI International Journal of Transportation and Infrastructure*, Vol. 2, Issue 2, pp. 57-66. doi:10.29138/ijti.v2i2.784.

Mazlum, M., and Güneri, A.F. (2015). "CPM, PERT and project management with fuzzy logic technique and implementation on a business". *Procedia-Social and Behavioral Sciences*, Vol. 210, pp. 348-357. doi:10.1016/j.sbspro.2015.11.378.

Sanchez, F., Bonjour, E., Micaelli, J. P., and Monticolo, D. (2020). "An approach based on bayesian network for improving project management maturity: An application to reduce cost overrun risks in engineering projects". *Computers in Industry*, Vol. 119, pp. 1-13. doi:10.1016/j.compind.2020.103227.

Temiz, N., and Dursun, E. (2016). "PERT Tekniği'nin Liman Deniz Hizmetleri Otomasyonu Projesine Uygulanması". *Dokuz Eylül Üniversitesi Denizcilik Fakültesi Dergisi*, Vol. 8, Issue 1, pp. 1-30. doi:10.18613/deudfd.57749.

Tümtürk, A., & Tümtürk, E. (2020). "Kritik yol metodu ile kentsel dönüşüm bina projelerinin programlanması: İzmir Karşıyaka örneği". *Dumlupınar Üniversitesi Sosyal Bilimler Dergisi*, Vol. 63, pp. 175-190.

Turan, E., and Güner, M. (2013). "A Critical Path Method Approach to a Green Platform Supply Vessel Hull Construction". *International Journal of Industrial Engineering*, Vol. 20, Issue 7/8, pp. 515-525. doi:10.23055/ijietap.2013.20.7-8.916.

Uçakcıoğlu, B., and Eren, T. (2017). "Analitik hiyerarşi prosesi ve VIKOR yöntemleri ile hava savunma sanayisinde yatırım projesi seçimi". *Harran Üniversitesi Mühendislik Dergisi*, Vol. 2, Issue 2, pp. 35-53.

## JOURNAL OF NAVAL SCIENCES AND ENGINEERING (JNSE) PUBLISHING RULES

**Submission of Papers:** Manuscripts which are submitted to the journal should not be published elsewhere or sent to be published. Authors are (preferably) requested to submit an electronic copy of their original works to the given "System Address" or one hard copy to the address and a soft copy to the "E-mail Address" which have been given below. It is necessary for the authors to submit their manuscripts together with the "Copyright Release Form". "Copyright Release Form" can be downloaded from the "Copyright Page" of JNSE's Web Page. Authors are requested to obtain the relevant documents for their studies that require "Ethics Committee Approval and/or Legal/Special Permission" and submit these approval documents to the system together with their study. The author(s) of the manuscript must declare that there are no conflicts of personal and/or financial interest within the scope of the study.

**System Address:**

<https://dergipark.org.tr/tr/pub/jnse>

**Address:**

Assoc.Prof.Dr. Fatih ERDEN  
National Defence University (Milli Savunma Üniversitesi)  
Turkish Naval Academy (Deniz Harp Okulu Dekanlığı)  
34942 Tuzla/İstanbul/Türkiye

**E-mail:** [jnse@dho.edu.tr](mailto:jnse@dho.edu.tr)

**Types of Contributions:** The journal publishes original papers, review articles, technical notes, book reviews, letters to the editor, extended reports of conferences and meetings.

**Manuscript Evaluation Process:** The Peer Review Step:

- The content and layout format of manuscript are examined, and the originality of study is checked by iThenticate Software Programme.
- The language and correlation of the English abstract with Turkish abstract are checked.
- Manuscript which has a similarity index above 40% is rejected. The author is informed about the manuscript which has a similarity index between 20% and 40% (must not contain more than 4% from a single source), which is not appropriate for the writing rules of JNSE or needs correction in English and Turkish abstracts and the author is requested to revise the manuscript within "two weeks". Otherwise, the article is considered as a retracted manuscript. The similarity percentage criteria may differ for review articles, letters to the editor, book reviews, and invited articles. Special care is taken to ensure that more than 50% of the articles in an issue are original research articles.

Our journal uses **double-blind** review, which means that both the reviewer and author identities are concealed from the reviewers, and vice versa, throughout the review process. So, the uploaded manuscript does not contain the name, address, and affiliation of author(s). The manuscript evaluation steps are as follows:

- Editor is assigned by the Editor-in-Chief.
- The relevant reviewers are assigned by the Editors.
- As a result of the reviewer's evaluation, the manuscript may be rejected, accepted or a correction for the manuscript may be requested.
- If the negative feedback is given by major number of the reviewers, the process is terminated, and the article is rejected.
- If major/minor revisions are required for the manuscript, the author has to do this revision according to the reviewers' comments in "three weeks".
- If the revision is accepted by the reviewers, the article is accepted.

The Workflow Diagram for the evaluation process can be accessed from the web page of the journal.

The articles submitted to JNSE to be published are free of article submission, processing and publication charges.

The accepted articles are published **free-of-charge** as online from the journal website and printed.

## DENİZ BİLİMLERİ VE MÜHENDİSLİĞİ DERGİSİ (DBMD) YAYIN KURALLARI

**Yazların Gönderilmesi:** Dergiye gönderilen makaleler başka bir yerde yayımlanmamış ya da yayımlanmak üzere gönderilmemiş olmalıdır. Yayımlanması istenilen yazılar (tercihen) aşağıda verilen “Sistem Adresi”nden yüklenmeli veya aşağıdaki adrese bir kopya kâğıda basılı olarak ve aynı zamanda “E-mail Adresi”ne dijital olarak gönderilmelidir. Dergimize makale gönderen yazarların makaleleriyle birlikte “Yayın Hakkı Devir Formu”nu da göndermeleri gerekmektedir. “Yayın Hakkı Devir Formu”na DBMD Web Sayfasındaki “Telif Hakkı” sayfasından erişilebilmektedir. Yazarların “Etik Kurul İzni ve/veya Yasal/Özel İzin” gerektiren çalışmaları için ilgili izin belgelerini temin etmesi ve bu izin belgelerini çalışmalarıyla birlikte sisteme yüklemeleri gerekmektedir. Yazarlar çalışmalarını gönderirken çalışma kapsamında herhangi bir kişisel ve/veya finansal çıkar çatışması olmadığını bildirmek zorundadır.

### **Sistem Adresi:**

<https://dergipark.org.tr/tr/pub/jnse>

### **Adres:**

Doç.Dr. Fatih ERDEN  
Deniz Harp Okulu Dekanlığı  
34942 Tuzla/ İstanbul/Türkiye

**E-mail:** [jnse@dho.edu.tr](mailto:jnse@dho.edu.tr)

**Yazı Türleri:** Dergide; orijinal yazılar, derlemeler, teknik notlar, kitap incelemeleri, editöre mektuplar ile konferans ve toplantıların genişletilmiş raporları yayımlanır.

**Yazların Değerlendirilme Süreci:** Makalenin Ön Kontrol Süreci:

- Makalenin içeriği ve yazım formatı incelenir ve iThenticate Programı ile benzerlik taraması yapılır.
- Makalenin İngilizce özetinin, Türkçe öz ile uygunluğu ve yazım dili kontrol edilir.
- Benzerlik oranı %40’ın üzerinde olan makale reddedilir. Benzerlik oranı %20 ile %40 arasında olan (tek bir kaynakla benzerlik %5’ten fazla olmamalıdır), yazım formatına uymayan ya da İngilizce ve Türkçe özetinde düzeltme gereken makale yazara bildirilir ve “iki hafta” içerisinde makalenin düzeltilmesi istenir. Aksi takdirde makale geri çekilmiş kabul edilir. Derleme makaleler, editöre mektuplar, kitap incelemeleri ve davetli makaleler için benzerlik yüzdesi kriterleri farklılık gösterebilir. Bir sayıdaki makalelerin %50’den fazlasının özgün araştırma makalesi olmasına özen gösterilmektedir.

Dergimiz, makale değerlendirme sürecinde **çift-kör** hakemlik sistemini kullanmaktadır. Buna göre değerlendirme sürecinde hakem ve yazarlar birbirlerinin bilgilerini görememektedir. Bu nedenle, yüklenen ön yükleme formatında yazar(lar)ın isim, adres ve bağlı olduğu kuruluş(lar) yer almamaktadır. Makale değerlendirme sürecindeki adımlar ise aşağıdaki gibidir;

- Baş editör tarafından makaleye Editör atanır.
- Editörler makale için hakemleri atar.
- Hakem değerlendirmesi sonucunda makale reddedilebilir, kabul edilebilir veya makalenin düzeltilmesi istenebilir.
- Hakem görüşlerinin çoğunluğu doğrultusunda makale reddedilmiş ise süreç sonlandırılır ve makale reddedilir.
- Makale için majör / minör düzeltme istenirse hakem görüşleri doğrultusunda yazarın gerekli düzeltmeleri en geç “üç hafta” içerisinde yapması istenir.
- Revize edilmiş makale kabul alırsa düzenleme aşamasına geçilir.

Değerlendirme sürecine ilişkin Akış Şemasına, derginin web sayfasından erişilebilir.

DBMD’ye yayımlanmak üzere gönderilen makaleler; makale gönderim, işlem ve yayın ücretinden muafır.

Kabul edilen makaleler, **ücretsiz** olarak basılı şekilde ve dergi web sayfasından çevrimiçi (online) olarak yayımlanmaktadır.

## **JOURNAL OF NAVAL SCIENCES AND ENGINEERING (JNSE) WRITING RULES**

**General:** Manuscripts must be prepared in MS Word, single-spaced with justify. Font: Times New Roman, 12 points. Margins: left 4,5 cm- right 3,5 cm, top 5 cm- bottom 7 cm, header 3,25 cm- footer 6 cm, gutter 0. Paper type: A4. Page numbers should be on the middle of bottom of page with -1-, -2-, -3- etc. format. Using footnotes is not allowed.

**Ethics Committee Approval and/or Legal/Special Permission:** The articles must state whether an ethical committee approval and/or legal/special permission is required or not. If these approvals are required, then it should be clearly presented from which institution, on what date and with which decision or number these approvals are obtained.

**Body of Text:** Follow this order when typing manuscripts: Title, Authors, Abstract, Keywords, Title (Turkish), Abstract (Turkish), Keywords (Turkish), Main Text, Appendix (if any), References.

**Title:** Title should reflect objectives of the paper clearly, be easily understandable and not exceed 15 words.

**Abstracts:** Each paper should have an abstract with 100-200 words and have a structured form, i.e. standard structure of an article (background, purpose, material and methods used, results, conclusion).

**Paper Length:** The manuscript should be minimum 2000 words or 5 pages, maximum 7000 words or 25 pages including references.

**Keywords:** Author must provide some keywords (between 3 and 5) that will be used to classify the paper.

**Unit:** International System of Unit (Système Internationale d'Unités; SI) (<https://www.britannica.com/science/International-System-of-Units>) should be used for all scientific and laboratory data.

**References:** References should be given according to the APA standard as effective from November, 2020 issue.

**Abbreviations and Acronyms:** Standard abbreviations and acronyms should be used for each related discipline. Acronyms should be identified at the first occurrence in the text. Abbreviations and acronyms may also be attached to main text as an appendix.

**Equations and Formulas:** Equations and formulas should be numbered consecutively. These numbers must be shown within parentheses being aligned to the right. In the text, equations and formulas should be referred with their numbers given in parentheses. Comprehensive formulas, not appropriate to be written in the texts, should be prepared in figures.

**Figures and Tables:** Figures and tables should be numbered consecutively. In the text referring to figures and tables should be made by typing "Figure 1." or "Table 1." etc. A suitable title should be assigned to each of them.

## DENİZ BİLİMLERİ VE MÜHENDİSLİĞİ DERGİSİ (DBMD) YAZIM KURALLARI

**Genel Bilgiler:** Yazılar; Microsoft Word'de tek satır aralığı ve iki yana yaslanarak hazırlanmalıdır. Yazı tipi: Times New Roman, 12 punto. Kenar boşlukları: sol 4,5 cm- sağ 3,5 cm- üst 5 cm- alt 7 cm- üst bilgi 3,25 cm- alt bilgi 6 cm, oluk 0. Kâğıt ölçüsü: A4. Sayfa numaraları sayfanın alt ortasında -1-, -2-, -3- vb. şeklinde yer almalıdır. Dipnot kullanılmamalıdır.

**Etik Kurul İzni ve/veya Yasal/Özel İzin:** Makalelerde etik kurul izni ve/veya yasal/özel izin alınmasının gerekip gerekmediği belirtilmiş olmalıdır. Eğer bu izinlerin alınması gerekli ise, izinlerin hangi kurumdan, hangi tarihte ve hangi karar veya sayı numarası ile alındığı açıkça sunulmalıdır.

**Yazı Yapısı:** Yazı şu sırada hazırlanmalıdır: Başlık, Yazarlar, Özet, Anahtar Kelimeler, Başlık (Türkçe), Özet (Türkçe), Anahtar Kelimeler (Türkçe), Ana Metin, Ek (varsa), Referanslar.

**Başlık:** Başlık; açık, net, anlaşılır olmalı ve 15 kelimeyi geçmemelidir.

**Öz (Abstract):** Yazı, 100-200 kelimelik, arka plan, amaç, yöntem, bulgular ve sonuçtan oluşan yapılandırılmış bir özeti içermelidir.

**Sayfa Sayısı:** Dergiye gönderilecek yazıların boyutu, kaynakça dâhil asgari 2000 kelime veya 5 sayfa, azami 7000 kelime veya 25 sayfa arasında olmalıdır.

**Anahtar Kelimeler:** Yazıyı sınıflandırmaya yarayacak, anahtar görevi yapan 3-5 kelime yer almalıdır.

**Birimler:** Yazının uluslararası alanlarda da kolay izlenebilir ve anlaşılabilir olması için Uluslararası Birim Sistemine (<https://www.britannica.com/science/International-System-of-Units>) uygun olarak hazırlanması gerekir.

**Referans:** Referanslar Kasım, 2020 sayısından itibaren geçerli olmak üzere APA standardına göre verilmelidir.

**Notasyon ve Kısaltmalar:** İlgili bilim alanının standart notasyon ve kısaltmaları kullanılmalı, yeni notasyonlar ise metin içinde ilk geçtiği yerde tanımlanmalıdır. Gerekli durumlarda, notasyon ve kısaltmalar ek olarak konulabilir.

**Denklem ve Formüller:** Denklem ve formüller ardışık olarak numaralandırılmalı ve bu numaralar sağa dayalı parantez içinde yazılmalıdır. Metin içinde denklem ve formüllere parantez içinde yazılan numaraları ile atıfta bulunulmalıdır. Metin arasında verilmesi uygun olmayan kapsamlı formüller şekil olarak hazırlanmalıdır.

**Şekiller ve Tablolar:** Şekiller ve tablolar, ardışık olarak numaralandırılmalıdır. Bunlara metin içinde "Şekil 1." veya "Tablo 1." şeklinde atıfta bulunulmalıdır. Her bir şekil ve tablo için uygun bir başlık kullanılmalıdır.

## Ethical Principles and Publication Policy

Journal of Naval Sciences and Engineering (hereafter JNSE) is a peer reviewed, international, inter-disciplinary journal in science and technology, which is published semi-annually in November and April since 2003. JNSE is committed to provide a platform where highest standards of publication ethics are the key aspect of the editorial and peer-review processes.

The editorial process for a manuscript to the JNSE consists of a double-blind review, which means that both the reviewer and author identities are concealed from the reviewers, and vice versa, throughout the review process. If the manuscript is accepted in the review stage of the Editorial Process then, the submission goes through the editing stage, which consists of the processes of copyediting, language control, reference control, layout and proofreading. Reviewed articles are treated confidentially in JNSE.

Papers submitted to JNSE are screened for plagiarism regarding the criteria specified on the [Publishing Rules](#) page with plagiarism detection tool. In case that the editors become aware of proven scientific misconduct, they can take the necessary steps. The editors have the right to retract an article whether submitted to JNSE or published in JNSE.

Following the completion of the editing stage, the manuscript is then scheduled for publication in an issue of the JNSE. The articles which are submitted to JNSE to be published are free of article submission, processing and publication charges. The accepted articles are published free-of-charge as online from the journal website and printed. The articles that are accepted to appear in the journal are made freely available to the public via the journal's website. The journal is also being printed by National Defence University Turkish Naval Academy Printing House on demand.

JNSE has editors and an editorial board which consists of academic members from at least five different universities. JNSE has an open access policy which means that all contents are freely available without charge to the user or his/her institution. Users are allowed to read, download, copy, distribute, print, search, or link to the full texts of the articles, or use them for any other lawful research purposes.

Publication ethics of the JNSE are mainly based on the guidelines and recommendations which are published by the Committee on Publication Ethics (COPE), World Federation of Engineering Organizations (WFEO), Council of Science Editors (CSE) and Elsevier's Publishing Ethics for Editors statements.

The duties and responsibilities of all parties in the publishing process including editors, authors and others are defined below.

### **The Responsibilities of the Authors:**

- Authors are responsible for the scientific, contextual, and linguistic aspects of the articles which are published in the journal. The views expressed or implied in this publication, unless otherwise noted, should not be interpreted as official positions of the Institution.
- Authors should follow the "Author Guidelines" in JNSE's web page on DergiPark.
- Authors should conduct their researches in an ethical and responsible manner and follow all relevant legislation.
- Authors should take collective responsibility for their work and for the content of their publications.
- Authors should check their publications carefully at all stages to ensure that methods and findings are reported accurately.
- Authors must represent the work of others accurately in citations, quotations and references.
- Authors should carefully check calculations, data presentations, typescripts/submissions and proofs.
- Authors should present their conclusions and results honestly and without fabrication, falsification or inappropriate data manipulation. Research images should not be modified in a misleading way.
- Authors should describe their methods to present their findings clearly and unambiguously.
- Authors accept that the publisher of JNSE holds and retains the copyright of the published articles.
- Authors are responsible to obtain permission to include images, figures, etc. to appear in the article.

- In multi-authored publications -unless otherwise stated- author rankings are made according to their contributions.
- Authors should alert the editor promptly if they discover an error in any submitted.
- Authors should follow the publication requirements regarding that the submitted work is original and has not been published elsewhere in any language.
- Authors should work with the editor or publisher to correct their work promptly if errors are discovered after publication.
- If the work involves chemicals, procedures or equipment that have any unusual hazards inherent in their use, the authors must clearly identify these in the manuscript.
- If the work involves the use of animals or human participants, the authors should ensure that all procedures were performed in compliance with relevant laws and institutional guidelines and that the appropriate institutional committee(s) has approved them; the manuscript should contain a statement to this effect.
- Authors should also include a statement in the manuscript that informed consent was obtained for experimentation with human participants. Because the privacy rights of human participants must always be preserved. It is important that authors have an explicit statement explaining that informed consent has been obtained from human participants and the participants' rights have been observed.
- Authors have the responsibility of responding to the reviewers' comments promptly and cooperatively, in a point-by-point manner.

#### **The Responsibilities of the Reviewers:**

- Peer review process has two fundamental purposes as follow: The first purpose is to decide whether the relevant article can be published in JNSE or not and the second purpose is to contribute to the improvement of the weaknesses of the related article before the publication.
- The peer review process for an article to the JNSE consists of a double-blind review, which means that both the reviewer and author identities are concealed from the reviewers, and vice versa, throughout the review process. Reviewed articles are treated confidentially in JNSE.
- Reviewers must respect the confidentiality of peer review process.
- Reviewers must refrain from using the knowledge that they have obtained during the peer review process for their own or others' interests.
- Reviewers should definitely be in contact with the JNSE if they suspect about the identity of the author(s) during the review process and if they think that this knowledge may raise potential competition or conflict of interest.
- Reviewers should notify the JNSE in case of any suspicion regarding the potential competition or conflict of interest during the review process.
- Reviewers should accept to review the studies in which they have the required expertise to conduct an appropriate appraisal, they can comply with the confidentiality of the double-blind review system and that they can keep the details about the peer review process in confidential.
- Reviewers should be in contact with the JNSE in order to demand some missing documents, following the examination of the article, supplementary files and ancillary materials.
- Reviewers should act with the awareness that they are the most basic determinants of the academic quality of the articles to be published in the journal and they should review the article with the responsibility to increase academic quality.
- Reviewers should be in contact with the JNSE editors if they detect any irregularities with respect to the Ethical Principles and Publication Policy.
- Reviewers should review the articles within the time that has been allowed. If they can not review the article within a reasonable time-frame, then they should notify the journal as soon as possible.
- Reviewers should report their opinions and suggestions in terms of acceptance / revision / rejection for the manuscript in the peer review process through the Referee Review Form which is provided by JNSE.
- In case of rejection, reviewers should demonstrate the deficient and defective issues about the manuscript in a clear and concrete manner in the provided Referee Review Form.
- Review reports should be prepared and submitted in accordance with the format and content of the Referee Review Form which is provided by JNSE.
- Review reports should be fair, objective, original and prudent manner.
- Review reports should contain constructive criticism and suggestions about the relevant article.

**The Responsibilities of the Editors:**

-Editors are responsible of enhancing the quality of the journal and supporting the authors in their effort to produce high quality research. Under no conditions do they allow plagiarism or scientific misconduct.

-Editors ensure that all submissions go through a double-blind review and other editorial procedures. All submissions are subject to a double-blind peer-review process and an editorial decision based on objective judgment.

-Each submission is assessed by the editor for suitability in the JNSE and then, sent to the at least two expert reviewers.

-Editors are responsible for seeking reviewers who do not have conflict of interest with the authors. A double-blind review assists the editor in making editorial decisions.

-Editors ensure that all the submitted studies have passed initial screening, plagiarism check, review and editing. In case the editors become aware of alleged or proven scientific misconduct, they can take the necessary steps. The editors have the right to retract an article. The editors are willing to publish errata, retractions or apologies when needed.





## Etik İlkeler ve Yayın Politikası

Deniz Bilimleri ve Mühendisliği Dergisi (Bundan sonra DBMD olarak anılacaktır.); uluslararası düzeyde, hakemli, çok disiplinli, Nisan ve Kasım aylarında olmak üzere 2003 yılından bu yana yılda iki kez yayınlanan, bilim ve teknoloji dergisidir. DBMD yayın etiğinde en yüksek standartların, editöryal ve hakemlik süreçlerinin kilit unsuru olarak değerlendirildiği bir platform sunmayı taahhüt etmektedir.

DBMD'ne gönderilen her bir makale için değerlendirme sürecinde çift-kör hakemlik sistemi uygulanmaktadır. Buna göre, değerlendirme süreci boyunca hakem ve yazarlar birbirlerinin bilgilerini görememektedir. Dergiye gönderilen çalışmaların yazar-hakem ve hakem-yazar açısından süreçlerinde gizlilik esastır. DBMD'ne gönderilen makalelerin değerlendirme sürecindeki inceleme aşamasında kabul edilmeleri halinde, ilgili makaleler için düzenleme aşamasına geçilmektedir. Düzenleme aşamasında, ilgili makaleler yazım formatı ve dilbilgisel yönlerden incelenir. Makalelerin sayfalar üzerindeki biçimi ve yerleşimleri kontrol edilip düzenlenir. Ayrıca referans kontrolü yapılır. DBMD'nde kontrol edilen ve düzenlenen makaleler gizli tutulmaktadır.

DBMD'ne gönderilen makaleler, [Yayın Kuralları](#) sayfasında belirtilen kriterlere ilişkin, intihal tespit programı aracılığıyla kontrol edilir. Editörler, kanıtlanmış bir bilimsel kötü kullanımdan ya da usulsüzlükten haberdar olurlarsa bu konuda gerekli adımları atabilirler. Bu anlamda, Editörler gerekli durumlarda DBMD'ne gönderilen ya da DBMD'nde yayınlanmış makaleleri geri çekme hakkına sahiptir.

Düzenleme aşamasının başarılı olarak sonuçlanmasını takiben, ilgili makaleler DBMD'nin bir sayısında yayınlanmak üzere saklı tutulur ve kayıt altına alınır. DBMD'ne yayınlanmak üzere gönderilen makaleler; yazılı materyal gönderme, işleme ve yayınlama süreçlerindeki tüm ücretlerden muaf tutulmaktadır. DBMD'nde yayınlanmak üzere kabul edilen makaleler, derginin internet sitesinden çevrimiçi olarak ücretsiz bir şekilde yayınlanır ve basılır. Dergide yayınlanması kabul edilen çalışmalar, derginin web sitesinden açık erişim ile erişilebilir kılınmıştır. Dergi ayrıca, Milli Savunma Üniversitesi, Deniz Harp Okulu Matbaası tarafından basılmaktadır.

DBMD; editörü ve en az beş değişik üniversitenin öğretim üyelerinden oluşmuş danışman grubu ile açık erişim politikasını benimsemektedir. Buna göre, tüm içerikler ücretsiz olarak kullanıcılar veya kurumlar için ulaşılabilir. Kullanıcıların DBMD bünyesindeki makalelerin tam metinlerini okuma, indirme, kopyalama, dağıtma, yazdırma, arama veya bunlara bağlantı verme ve diğer yasal araştırma amaçları için kullanma hakları saklı tutulmaktadır.

DBMD'nin yayın etiği, temel olarak Yayın Etiği Komitesi (COPE), Dünya Mühendislik Kuruluşları Federasyonu (WFEO), Bilim Kurulu Editörleri (CSE) ve Elsevier'in Editörler için Yayın Etiği açıklamaları kapsamında yayınlanmış yönergelere ve önerilere dayanmaktadır.

Editörler, yazarlar ve diğer taraflar da dâhil edilebilecek şekilde yayın sürecindeki görev ve sorumluluklar aşağıdaki gibi tanımlanmıştır.

### **Yazarların Sorumlulukları:**

-Yazarlar, dergide yayınlanan makalelerinin bilimsel, bağlamsal ve dilsel yönlerinden sorumlu tutulmaktadır. Dergide ifade edilen veya ima edilen görüşler, aksi belirtilmediği sürece, Enstitünün resmi görüşü olarak yorumlanamaz ve yansıtılamaz.

-Yazarlar çalışmalarında, DBMD'nin DergiPark internet sayfasında yer alan "Yazım Kuralları"na dikkate almalıdır.

-Yazarlar araştırmalarını etik ve sorumlu bir şekilde yürütmeli ve ilgili tüm mevzuatları takip etmelidir.

-Yazarlar çalışmalarını ve yayınlarının içeriği için ortak sorumluluk almalıdır.

-Yazarlar, yöntemlerin ve bulguların doğru bir şekilde raporlandığından emin olmak için yayınlarını her aşamada dikkatlice kontrol etmelidir.

-Yazarlar, başkalarına ait çalışmalarını dolaylı alıntı, doğrudan alıntı ve referanslar ile doğru bir şekilde göstermelidir. Yazarlar, makalelerindeki fikirlerin şekillendirilmesinde etkili ya da bilgilendirici olmuş her türlü kaynağa referans vermelidir.

-Yazarlar çalışmalarındaki hesaplamaları, ispatları, veri sunumlarını ve yazı tiplerini dikkatlice kontrol etmelidir.

- Yazarlar çalışmalarının sonuçlarını dürüstçe; uydurma, çarpıtma, tahrifat veya uygunsuz manipülasyona yer vermeden sunmalıdır. Çalışmalardaki görsel kaynaklar yanıltıcı bir şekilde değiştirilmemelidir.
- Yazarlar, çalışmalarındaki bulguları açık ve net bir şekilde sunmak için araştırma yöntemlerini tanımlamalı ve paylaşmalıdır.
- Yazarlar, yayınlanmış makalelerinin telif haklarını DBMD yayıncısına devrettiklerini kabul etmektedir.
- Yazarlar çalışmalarına çeşitli görsel kaynakları, figürleri, şekilleri vb. dahil etmek için gerekli izinleri almakla yükümlüdür. İlgili çalışmada yer alması gereken resim, şekil vb. anlatımı destekleyici materyaller için gerekli kişilerden ya da kurumlardan izin alınması yazarın sorumluluğundadır.
- Çok yazarlı yayınlarda -aksi belirtilmedikçe- yazar sıralamaları sunulan katkılara göre yapılmalıdır.
- Yazarlar gönderdikleri çalışmada herhangi bir hata tespit ederlerse bu konuda derhal editörü uyarmalıdır.
- Yazarlar dergiye gönderdikleri makalelerin başka bir yerde yayımlanmamış ya da yayımlanmak üzere gönderilmemiş olmaları ile ilgili DBMD'nin DergiPark internet sayfasında yer alan "Yayın Kuralları"na dikkate alınmalıdır.
- Yazarlar, ilgili çalışmalarını DBMD'nde yayımlandıktan sonra hata tespit ederlerse bu konuda gerekli düzeltmelerin yapılabilmesi amacıyla derhal editör veya yayıncı ile iletişime geçip onlar ile birlikte çalışmalıdır.
- İlgili çalışmada, doğası gereği kullanımlarında olağandışı tehlikeler barındıran çeşitli kimyasallar veya ekipmanlardan yararlanılmış ise yazarların tüm bunları çalışmasında açıkça belirtmesi ve tanımlaması gerekmektedir.
- İnsanlar ve hayvanların katılımını gerektiren çalışmalar için, yazarlar tüm sürecin ilgili yasalara ve kurumsal yönergelere uygun olarak gerçekleştirildiğinden emin olmalıdır ve ilgili komitelerden etik onay alındığını çalışmalarında açık bir şekilde ifade edip belgelendirmelidir.
- İnsanların katılımını gerektiren çalışmalar için, yazarlar kurumsal etik kurul onayı almakla yükümlüdürler. Yazarlar, katılımcıların süreç ile ilgili olarak bilgilendirildiklerini ve bu anlamda, katılımcılardan gerekli izinlerin alındığını bildirmek ve belgelemek zorundadır. Yazarlar, katılımcıların haklarının gözetildiğini açıklayan açık bildirim sunmalıdır. Ayrıca bu süreçte, katılımcıların gizlilik hakları her zaman korunmalıdır.
- Yazarlar, hakemlerin değerlendirmelerini, yorumlarını ve eleştirilerini zamanında ve işbirliği içerisinde dikkate alınmalıdır ve bu konuda, gerekli güncellemeleri yapmalıdır.

#### **Hakemlerin Sorumlulukları:**

- Hakem değerlendirme sürecinin iki temel amacı vardır: İlk amaç, ilgili makalenin DBMD'nde yayınlanıp yayınlanamayacağına karar vermektir ve ikinci amaç, yayından önce ilgili makalenin eksik yönlerinin geliştirilmesine katkıda bulunmaktır.
- DBMD'ne gönderilen her bir makale için değerlendirme sürecinde çift-kör hakemlik sistemi uygulanmaktadır. Buna göre, değerlendirme süreci boyunca hakem ve yazarlar birbirlerinin bilgilerini görememektedir. Dergiye gönderilen çalışmaların yazar-hakem ve hakem-yazar açısından süreçlerinde gizlilik esastır.
- Hakemler, değerlendirme sürecinin gizliliğine saygı göstermelidir.
- Hakemler, değerlendirme sürecinde elde ettikleri bilgileri kendilerinin veya başkalarının çıkarları için kullanmaktan kaçınmalıdır.
- Hakemler, değerlendirme sürecinde yazar(lar)ın kimliğinden şüphe etmeleri ve bu bilginin herhangi bir potansiyel rekabet veya çıkar çatışması yaratacağını düşünmeleri halinde mutlaka DBMD ile iletişime geçmelidir.
- Hakemler, değerlendirme sürecinde şüphe ettikleri potansiyel rekabet veya çıkar çatışması durumlarını DBMD'ne bildirmelidir.
- Hakemler, uygun bir değerlendirme yapabilmek için gereken uzmanlığa sahip oldukları, çift-kör hakemlik sisteminin gizliliğine riayet edebilecekleri ve değerlendirme süreci ile ilgili detayları gizli tutabilecekleri çalışmaların hakemliğini kabul etmelidir.
- Hakemler makaleyi, ek dosyaları ve yardımcı materyalleri incelemelerini takiben bazı eksik belgelere ihtiyaç duymaları halinde bunları talep etmek üzere DBMD ile iletişime geçmelidir.
- Hakemler dergide yayınlanacak makalelerin akademik kalitesinin en temel tespit edicisi olduklarının bilinciyle davranmalı ve akademik kaliteyi artırma sorumluluğuyla inceleme yapmalıdır.
- Hakemler, Etik İlkeler ve Yayın Politikası ile ilgili herhangi bir usulsüzlük tespit etmeleri halinde DBMD editörleri ile irtibata geçmelidir.

- Hakemler, kendilerine tanınan süre içerisinde makaleleri değerlendirmelidir. Şayet uygun bir zaman içerisinde değerlendirme yapamayacaklarsa, bu durumu en kısa zamanda DBMD'ne bildirmelidirler.
- Hakemler, değerlendirme sürecindeki çalışma için kabul etme / yeniden gözden geçirme / reddetme şeklindeki önerilerini DBMD tarafından sağlanan Hakem Değerlendirme Formu aracılığıyla bildirmelidir.
- Sonucu reddetme şeklinde olan değerlendirmeler için hakemler, ilgili çalışmaya dair eksik ve kusurlu hususları Hakem Değerlendirme Formu'nda açık ve somut bir şekilde ortaya koymalıdır.
- Hakem değerlendirme raporlarının, DBMD tarafından sağlanan Hakem Değerlendirme Formu'na uygun biçimde ve içerikte hazırlanması ve gönderilmesi gerekmektedir.
- Hakem değerlendirme raporları adil, objektif, özgün ve ölçülü olmalıdır.
- Hakem değerlendirme raporları, ilgili makale ile ilgili yapıcı eleştiriler ve tavsiyeler içermelidir.

#### **Editörlerin Sorumlulukları:**

- Editörler, derginin bilimsel kalitesini arttırmak ve yazarları bilimsel kalitesi yüksek araştırmalar üretmek için desteklemek ile sorumludur. Hiçbir koşulda, intihal ya da bilimsel kötüye kullanıma izin verilmemektedir.
- Editörler, dergiye gönderilen her çalışmanın çift-kör hakemlik sürecine ve diğer editoryal süreçlere tabi olmasını sağlamaktadır. DBMD'ne gönderilen her çalışma, çift-kör hakemlik sürecine ve nesnel değerlendirmeye dayalı editör kararına bağlı tutulmaktadır.
- DBMD'ne gönderilen her bir çalışma, uygunlukları açısından editör tarafından değerlendirilir ve daha sonrasında, incelenmesi ve değerlendirilmesi amacıyla en az iki uzman hakeme gönderilir.
- Editörler, yazarlar ile çıkar çatışması olmayan hakemleri, çalışmayı değerlendirmek üzere atamakla sorumludur. Çift-kör hakemlik süreci, editör için değerlendirme ve düzenleme aşamalarında katkı sağlamaktadır.
- Editörler, DBMD'ne gönderilen tüm çalışmaların ön kontrol, tarama, intihal kontrolü, değerlendirme ve düzenleme aşamalarından geçmesini sağlar. Editörler iddia edilen veya kanıtlanmış bilimsel kötü kullanımdan haberdar olurlarsa makaleyi geri çekebilirler. Editörler, gerekli durumlarda gönderilen çalışmayı düzeltme, geri çekme veya çalışma hakkında özür yayınlama hakkına sahiptir.

NATIONAL DEFENCE UNIVERSITY  
TURKISH NAVAL ACADEMY  
JOURNAL OF NAVAL SCIENCES AND ENGINEERING

VOLUME: 18 NUMBER: 2 NOVEMBER 2022 ISSN: 1304-2025

---

CONTENTS / İÇİNDEKİLER

*EDITORIAL*

**Foreword (Önsöz)** 155-157  
*Fatih ERDEN*

*Electrical-Electronics Engineering / Elektrik-Elektronik Mühendisliği*

*RESEARCH ARTICLE*

**A New Receiver Design for Spatial Modulation Systems** 159-178  
(Uzaysal Modülasyon Sistemleri için Yeni Bir Alıcı Tasarımı)  
*Gökhan ALTIN*

*Electrical-Electronics Engineering / Elektrik-Elektronik Mühendisliği*

*RESEARCH ARTICLE*

**Mechanical Gyroscope-based Roll Motion Reduction of Marine Vehicles:  
An Educational Setup** 179-204  
(Mekanik Jiroskop ile Deniz Araçlarında Yalpa Hareketinin Sönümlendirilmesi:  
Bir Eğitim Seti Tasarımı)  
*Şefik CİNAL, İlyas EMİNOĞLU*

*Electrical-Electronics Engineering / Elektrik-Elektronik Mühendisliği*

*RESEARCH ARTICLE*

**The Effect of FOV Angle on a RSSI-based Visible Light Positioning System** 205-230  
(Bir RSSI Tabanlı Görünür Işık Konum Belirleme Sistemi Üzerine FOV Açısının Etkisi)  
*Özlem AKGÜN*

*Electrical-Electronics Engineering / Elektrik-Elektronik Mühendisliği*

*RESEARCH & REVIEW ARTICLE*

**An Extension of the Last Work of Oleg A. Tretyakov:  
A Novel Format of the Wave Equation in SI Units** 231-250  
(Oleg A. Tretyakov'un Son Çalışmasının Bir Uzantısı:  
SI Birim Sisteminde Yeni Bir Dalga Denklemi Formatı)  
*Fatih ERDEN, Ahmet Arda ÇOŞAN*

---

MİLLİ SAVUNMA ÜNİVERSİTESİ  
DENİZ HARP OKULU DEKANLIĞI  
DENİZ BİLİMLERİ VE MÜHENDİSLİĞİ DERGİSİ

CİLT: 18

SAYI: 2

KASIM 2022

ISSN: 1304-2025

NATIONAL DEFENCE UNIVERSITY  
TURKISH NAVAL ACADEMY  
JOURNAL OF NAVAL SCIENCES AND ENGINEERING

VOLUME: 18      NUMBER: 2      NOVEMBER 2022      ISSN: 1304-2025

---

CONTENTS / İÇİNDEKİLER

- Naval Architecture and Marine Engineering / Gemi İnşaatı ve Gemi Makineleri Mühendisliği*  
*RESEARCH ARTICLE*
- Investigation of the Effect of the Flow Regulators on the Flow Around a Generic Submarine Sail** 251-279  
(Akış Düzenleyicilerin Bir Jenerik Denizaltı Yelkeni Etrafındaki Akışa Etkisinin İncelenmesi)  
*Gökay SEVGİ, Barış BARLAS, Uğur Oral ÜNAL*
- Oceanography and Hydrography / Oşinografi ve Hidrografi*  
*RESEARCH ARTICLE*
- Bathymetric Analysis of Lystad Bay, Horseshoe Island by Using High Resolution Multibeam Echosounder Data** 281-303  
(Yüksek Çözünürlüklü Çok Bimli İskandil Verileri ile Horseshoe Adası, Lystad Körfezi'nin Batimetrik Analizi)  
*Emre TÜKENMEZ, Emre GÜLHER, Özgür KAYA, H. Fatih POLAT*
- Computer Engineering / Bilgisayar Mühendisliği*  
*RESEARCH ARTICLE*
- An Evaluation on Weapon Target Assignment Problem** 305-332  
(Silah Hedef Atama Problemi Üzerine Bir Değerlendirme)  
*Tolga ÖNEL, Elif BOZKAYA*
- Computer Engineering / Bilgisayar Mühendisliği*  
*RESEARCH ARTICLE*
- Machine and Deep Learning-based Intrusion Detection and Comparison in Internet of Things** 333-361  
(Makine ve Derin Öğrenme Yöntemleri ile Nesnelerin İnterneti için Saldırı Tespitinin Karşılaştırılması)  
*Siham AMAROUCHE, Kerem KÜÇÜK*
- Industrial Engineering / Endüstri Mühendisliği*  
*RESEARCH ARTICLE*
- Project Planning with CPM and PERT Methods: Example of Defence Industry** 363-385  
(CPM ve PERT Yöntemleriyle Proje Planlama: Savunma Sanayi Örneği)  
*Beste DESTİCİOĞLU TAŞDEMİR*
- 

MİLLİ SAVUNMA ÜNİVERSİTESİ  
DENİZ HARP OKULU DEKANLIĞI  
DENİZ BİLİMLERİ VE MÜHENDİSLİĞİ DERGİSİ

CİLT: 18      SAYI: 2      KASIM 2022      ISSN: 1304-2025